



Pathological mechanisms of serious and neglected zoonotic retinal infections

Dr Genevieve Frances Oliver

BHB, MBChB, MOphth, FRANZCO

THESIS SUBMITTED TO FLINDERS UNIVERSITY FOR THE DEGREE OF

Doctor of Philosophy

COLLEGE OF MEDICINE & PUBLIC HEALTH

MAY 2021

TABLE OF CONTENTS

LIST OF FIGURES	x
LIST OF TABLES	xii
DECLARATION	xiv
ACKNOWLEDGEMENTS	xv
ABBREVIATIONS	xvii
ABSTRACT	xxiii
THESIS OUTCOMES	xxvi
PREFACE	xxix
CHAPTER 1	1
Introduction	1
1.1 Introduction	1
1.2 Zoonotic infectious diseases.....	2
1.3 Retinal structure and function	7
1.3.1 Retinal cell populations.....	9
1.3.2 Immunological conditions of the posterior eye.....	12
1.3.3 Clinical imaging of the posterior eye	18
1.4 Ocular toxoplasmosis.....	21
1.4.1 <i>Toxoplasma gondii</i>	21
1.4.2 Toxoplasmosis	22
1.4.3 Clinical features of ocular toxoplasmosis.....	24
1.4.4 Visual outcomes of ocular toxoplasmosis.....	25
1.4.5 Pathology of ocular toxoplasmosis	26
1.5 Dengue retinopathy.....	33
1.4.1 Dengue virus	33

1.5.1	Clinical manifestations of dengue retinopathy.....	37
1.5.2	Pathogenesis of dengue retinopathy.....	38
1.6	Post-Ebola uveitis.....	41
1.4.1	Ebola virus.....	41
1.6.1	Ebola Virus Disease	42
1.6.2	Clinical manifestations of post-Ebola uveitis	45
1.6.3	Pathogenesis of post-Ebola uveitis	47
1.6.4	Summary of mechanisms of zoonotic retinal infections.....	51
1.7	Aims of the thesis.....	54
CHAPTER 2.....		56
Materials and Methods.....		56
2.1	Spectral-domain optical coherence tomography study.....	59
2.1.1	Patient selection and human ethics statement	59
2.1.2	Ophthalmic examination and diagnosis.....	59
2.1.3	Optical coherence tomographic imaging and interpretation	60
2.1.4	Treatment and follow-up schedule.....	61
2.2	Laboratory biosafety.....	62
2.3	Chemicals and reagents.....	62
2.3.1	Buffers and solutions	62
2.3.1.1	<i>Phosphate-buffered saline</i>	<i>62</i>
2.3.1.2	<i>Tris base, acetic acid and EDTA buffer</i>	<i>63</i>
2.3.1.3	<i>Dulbecco's Modified Eagle Medium.....</i>	<i>63</i>
2.3.1.4	<i>Luria Bertani broth.....</i>	<i>63</i>
2.3.2	Antibodies	64
2.4	Eukaryotic cells.....	68
2.4.1	Cell lines and culture medium.....	68
2.4.1.1	<i>ARPE-19 cell line and medium</i>	<i>68</i>

2.4.1.2	<i>MIO-M1 cell line and medium</i>	68
2.4.1.3	<i>Vero cell line and medium</i>	68
2.4.1.4	<i>C6/36 cell line and medium</i>	69
2.4.2	Primary human retinal cells	69
2.4.2.1	<i>Primary human ocular cell isolation</i>	69
2.4.2.2	<i>Primary human Müller cell characterisation</i>	69
2.4.3	Cell culture techniques	71
2.4.3.1	<i>Cell maintenance</i>	71
2.4.3.2	<i>Cell monolayer dissociation</i>	71
2.4.3.3	<i>Cell counting</i>	71
2.4.3.4	<i>Freezing cells</i>	72
2.4.3.5	<i>Thawing cells from cryopreservation</i>	72
2.4.3.6	<i>Mycoplasma testing</i>	73
2.5	Viruses	74
2.5.1	Virus strains.....	74
2.5.2	Viral infections	76
2.5.3	Plaque assays	77
2.5.4	Immunostaining	78
2.5.5	Interferon-beta immunoassay	79
2.6	Reverse transcription-polymerase chain reaction.....	79
2.6.1	RNA Extraction	79
2.6.2	Complementary DNA synthesis	80
2.6.3	Oligonucleotides and primers.....	81
2.6.4	Gradient polymerase chain reaction.....	81
2.6.5	Quantitative real-time polymerase chain reaction.....	81
2.6.6	Data analysis	82
2.7	Western blotting	82
2.7.1	Preparation of cell lysate	82
2.7.2	Protein quantitation.....	83
2.7.3	Protein separation by gel electrophoresis.....	84
2.7.4	Gel transfer	85
2.7.5	Antibody staining	85

2.8	Restriction enzyme-based subcloning	86
2.8.1	Sub-cloning new plasmids.....	86
2.8.1.1	<i>Creation of no-vector plasmid</i>	86
2.8.1.2	<i>Creation of pCAGGS-FLAG-VP35 plasmid</i>	88
2.8.2	Subcloning techniques	88
2.8.2.1	<i>Double restriction endonuclease digestion</i>	88
2.8.2.2	<i>DNA separation by electrophoresis</i>	92
2.8.2.3	<i>DNA purification</i>	92
2.8.2.4	<i>DNA quantification</i>	93
2.8.2.5	<i>DNA ligation</i>	93
2.8.3	Preparation of competent cells.....	94
2.8.3.1	<i>Preparation of agar plates</i>	94
2.8.3.2	<i>Transformation of competent cells</i>	94
2.8.3.3	<i>Growth of plasmid-expressing bacteria</i>	95
2.8.3.4	<i>Plasmid harvest by maxipreparation</i>	95
2.8.4	Sequencing.....	95
2.9	Cell transfection with VP35 plasmid and Poly I:C.....	96
2.10	Microscopy.....	97
2.10.1	Cell photography and image processing.....	97
2.11	Bioinformatics.....	98
2.11.1	RNA sequencing	98
2.11.2	Data processing and differential expression analysis	98
2.11.3	Target predictions for microRNA	99
2.11.4	Pathway and network analyses.....	100
2.12	Statistical analyses.....	100
CHAPTER 3	102
	Tissue changes in active toxoplasmic retinochoroiditis by spectral-domain optical coherence tomography.....	102
3.1	Introduction	103

3.2	Results.....	104
3.2.1	Participant demographics	104
3.2.2	Clinical characteristics of toxoplasmic retinochoroiditis	107
3.2.3	Spectral-domain optical coherence tomography findings at presentation	109
3.2.3.1	<i>Retinal findings at presentation by spectral-domain optical coherence tomography</i>	<i>109</i>
3.2.3.2	<i>Macular changes at presentation by spectral-domain optical coherence tomography.....</i>	<i>116</i>
3.2.3.3	<i>Vitreous signs at presentation by spectral-domain optical coherence tomography.....</i>	<i>116</i>
3.2.3.4	<i>Retinal pigment epithelial and choroidal findings at presentation by spectral-domain optical coherence tomography.....</i>	<i>119</i>
3.2.4	Tissue changes by spectral-domain optical coherence tomography during follow-up	121
3.2.5	Features of retinal necrosis by spectral-domain optical coherence tomography	121
3.2.6	Visual outcomes associated with spectral-domain optical coherence tomography features of toxoplasmic retinochoroiditis	126
3.3	Discussion	130
CHAPTER 4		142
Dengue virus infection of human retinal Müller glial cells		142
4.1	Introduction	143
4.2	Results.....	146
4.2.1	Susceptibility of the MIO-M1 human Müller cell line to infection with dengue virus.....	146
4.2.1.1	<i>Type I interferon response in dengue virus-infected MIO-M1 human Müller cells</i>	<i>151</i>
4.2.1.2	<i>Immune responses of MIO-M1 human Müller cells to infection with dengue virus.....</i>	<i>152</i>
4.2.2	Müller cell infection with field isolates of dengue virus	156
4.2.2.1	<i>Infection of MIO-M1 human Müller cells with DENV field isolates.....</i>	<i>156</i>
4.2.3	Responses to dengue infection in primary Müller cells.....	163
4.2.3.1	<i>Infection of primary human Müller cells with DENV.....</i>	<i>163</i>
4.3	Discussion	175
CHAPTER 5		184

Computational predictions of the biological effects of microRNA in <i>Ebola virus</i>-infected human retinal pigment epithelial cells	184
5.1 Introduction	185
5.2 Results.....	189
5.2.1 Small RNA dataset preparation by deep sequencing.....	189
5.2.2 Differential expression of microRNA.....	189
5.2.3 Gene target prediction of differentially expressed microRNA.....	194
5.2.4 Pathway analysis of gene targets of microRNA	196
5.2.5 Network analysis of miRNA-gene target interactions.....	199
5.3 Discussion	204
CHAPTER 6	212
Ebola viral protein 35 and the type I interferon response in human retinal pigment epithelial cells.....	212
6.1 Introduction	213
6.2 Results.....	214
6.2.1 Restriction digest-based plasmid subcloning.....	214
6.2.2 Confirmation of plasmid structure.....	220
6.2.3 Confirmation of plasmid protein expression	220
6.2.4 Interferon- β expression in retinal pigment epithelial cells after treatment with Poly I:C.....	221
6.2.4.1 <i>Primary human retinal pigment epithelial cell isolates</i>	224
6.2.5 Impact of Ebola protein 35 on interferon- β expression in retinal pigment epithelial cells.....	228
6.3 Discussion	236
CHAPTER 7	241
Discussion	241

Appendix A: Spectral-domain optical coherence tomography data collection sheet	
.....	250
Appendix B: Manufacturer headquarters	253
Appendix C: Primary cell isolation	256
Appendix D: Primer sequences used for quantitative reverse transcription	
polymerase chain reaction	259
Appendix E: Viral quantification	262
Appendix F: Statistical analyses in Chapter 4	263
Appendix G: pCAGGS-FLAG-VP35 sequencing	272
REFERENCES	274

LIST OF FIGURES

Figure 1.1: Anatomy of the human eye.....	8
Figure 1.2 : Neural cells of the human retina.....	11
Figure 1.3: Inner and outer blood-retinal barriers.....	15
Figure 1.4: Spectral-domain optical coherence tomography of the normal human macula	20
Figure 1.5: Dengue viral proteins	35
Figure 1.6: Replication cycle of flaviviruses.....	36
Figure 1.7: Filovirus genome and life cycle	44
Figure 2.1: Template plasmid maps.....	87
Figure 2.2: No-vector plasmid.....	89
Figure 2.3: pCAGGS-FLAG-VP35 plasmid.....	91
Figure 3.1: Study selection criteria	105
Figure 3.2: Active recurrent toxoplasmic retinochoroiditis at presentation.....	108
Figure 3.3: Pathological changes in eyes with active toxoplasmic retinochoroiditis by spectral-domain optical coherence tomography	115
Figure 3.4: Response to treatment	123
Figure 3.5: Evolution of retinal necrosis in toxoplasmic retinochoroiditis.....	128
Figure 3.6: Retinal pigment epithelial thickening.....	138
Figure 4.1: The Müller cell	145
Figure 4.2: Infection of MIO-M1 human Müller cells with dengue virus	149
Figure 4.3: Infection of human Müller cells with Mon601.....	150

Figure 4.4: Type I interferon response to DENV infection in MIO-M1 human Müller cells	154
Figure 4.5: Immune response to dengue virus infection in MIO-M1 human Müller cells	155
Figure 4.6: MIO-M1 human Müller cell infection with DENV field isolates	158
Figure 4.7: Viral RNA level of DENV-infected MIO-M1 human Müller cells	159
Figure 4.8: Molecular responses of MIO-M1 human Müller cells infected with DENV field isolates	162
Figure 4.9: Human primary Müller cells	164
Figure 4.10: Expression of Müller cell markers in primary human Müller cell isolates .	166
Figure 4.11: Infection of primary human Müller cell infection with DENV	168
Figure 4.12: Primary Müller cell infection with DENV field isolates.....	169
Figure 4.13: Responses of primary human Müller cell isolates to infection with DENV.	173
Figure 5.1: Processing and function of miRNA.....	188
Figure 5.2: Multi-dimensional scaling.....	192
Figure 5.3: Pathway analysis of miRNA gene targets	198
Figure 5.4: Host miRNA-gene target interactions	201
Figure 6.1: Construction of the pCAGGS-VP35 expression plasmid	217
Figure 6.2: Sub-cloning DNA products.....	219
Figure 6.3: Western blots of protein lysate from transfected ARPE-19 cells	223
Figure 6.4: Treatment of ARPE-19 cells with Poly I:C.....	225
Figure 6.5: Poly I:C-induced IFN- β expression in ARPE-19 cells	226
Figure 6.6: Stimulation of VP35-expressing ARPE-19 cells with Poly I:C	231
Figure 6.7: Cell toxicity after pCAGGS vector transfection and Poly I:C stimulation.....	233
Figure 6.8: IFN- β production in VP35-expressing retinal pigment epithelial cells.....	235

LIST OF TABLES

Table 1.1: Zoonotic infections of the retina.....	6
Table 1.2: Histopathological signs of retinal tissue destruction in toxoplasmic retinochoroiditis	30
Table 2.1: Primary antibodies	65
Table 2.2: Control antibodies	66
Table 2.3: Secondary antibodies	67
Table 2.4: Dengue virus field isolates	75
Table 3.1: Participant and disease characteristics	106
Table 3.2: Retinal findings at the toxoplasmic retinochoroiditis lesion by spectral-domain optical coherence tomography at presentation	110
Table 3.3: Retinal changes adjacent to the toxoplasmic retinochoroiditis lesion by spectral-domain optical coherence tomography at presentation.....	112
Table 3.4: Macular features by spectral-domain optical coherence tomography at presentation with active toxoplasmic retinochoroiditis	117
Table 3.5: Vitreous signs in active toxoplasmic retinochoroiditis by spectral-domain optical coherence tomography at presentation	118
Table 3.6: Retinal pigment epithelial and choroidal findings in active toxoplasmic retinochoroiditis by spectral-domain optical coherence tomography at presentation.....	120
Table 3.7: Retinal features of active toxoplasmic retinochoroiditis during follow-up....	124
Table 3.8: Visual acuity and spectral-domain optical coherence tomography features..	129
Table 4.1: Primary human Müller cell donors	165
Table 4.2: Two-way ANOVA of immune responses to DENV infection in Müller cells.....	174

Table 5.1: Trimming statistics.....	191
Table 5.2: Differential expression of human miRNA.....	193
Table 5.3: Ebola virus-derived miRNA	195
Table 5.4: Network connections.....	202
Table 6.1: Primary human retinal pigment epithelial cell isolates	227

DECLARATION

I certify that this thesis does not incorporate without acknowledgment any material previously submitted for a degree or diploma in any university; and that to the best of my knowledge and belief it does not contain any material previously published or written by another person except where due reference is made in the text.

Genevieve Oliver

ACKNOWLEDGEMENTS

Every PhD has a beginning.

Mine began a few years after laughing at the suggestion I undertake one. But curiosity encountered opportunity, and the rest is thesis. This PhD would not exist were it not for my principal supervisor, clinician scientist Professor Justine Smith. Her conscientious supervision, academic rigour and unwavering support have equipped me with foundational skills I will use for the rest of my career, and I remain in awe of her expertise, professionalism, and passion for research. I also thank A/Professor Jill Carr, my associate supervisor, for her wisdom, logic, and extensive virology experience. I gratefully acknowledge the hospitality and support of my adjunct supervisors, Dr Glenn Marsh at CSIRO Australian Centre for Disease Preparedness in Geelong, Victoria, and Dr João Furtado at the University of São Paulo Ribeirão Preto Medical School in Brazil. For precious feedback and transformative encouragement, I thank Australia's doyenne of ophthalmic research, Emeritus Professor Keryn Williams.

I acknowledge and thank all members past and present of the Eye & Vision Health and Carr Laboratories for their friendship and support. I am utterly grateful to resident cell culture whisperer, Dr Yuefang Ma, and the Eye & Vision Health Lab Manager-cum-Oracle, Liam Ashander. My sincere gratitude also to Janet Matthews for sparking joy in times of administration, to Abby Dawson for all those viruses, and to Drs Alix Farrall, Binoy Appukuttan and Mandy Lumsden for molecular biology grade genius. Particular thanks to Andrew Stempel and Dr Elise Rochet for benevolent answers to embarrassing questions. I am indebted to fellow PhD student Ayla Orang for those masterclasses in the dark art of bioinformatics, and to Nusha Chegeni in Proteomics for overseeing my best westerns. I thank all in the Ophthalmology

Department, including clinic and theatre staff, and remain ever grateful for the collegial support and perpetual encouragement of Dr Stewart Lake.

I would have struggled to undertake a PhD and preserve a surgical career without institutional support. I thank Associate Professor Richard Mills, clinical director of Ophthalmology at Flinders Medical Centre, for fostering a culture that supports research and for actively supporting me as a clinician. I thank the College of Medicine & Public Health for the Student Travel and Publication awards. I thank Professor Tara Brabazon and Professor Paul Ward for engendering humanity in the Research by Higher Degree environment at Flinders University. I thank European Molecular Biology Laboratory Australia for the opportunity to attend their PhD course. I thank Avant Mutual for their support of clinician scientists through the Doctor-In-Training Research Scholarship, and the Royal Australian and New Zealand College of Ophthalmologists for the RANZCO Allergan Industry Scholarship.

I thank Australian Federal and State Government for support in the form of the South Australian Department of Environment and Water Minister's Humane Research Scholarship, the Australian Government Research Training Scholarship, and the National Health and Medical Research Council Postgraduate Scholarship (PGS1150282).

The bulk of these chapters were written in the shadow of a pandemic and under level 4 lockdown in New Zealand. I remain indebted to the good people who helped me rapidly vacate Australia, and the enthusiastic welcome committee on the far side of the Tasman. I would not have completed, nor survived, this PhD without the love and encouragement of family and friends.

Here's to you.

ABBREVIATIONS

AIDS	acquired immunodeficiency syndrome
AlphaLISA®	amplified luminescent proximity homogeneous assay
ANOVA	analysis of variance
AQP4	aquaporin 4
ARPE-19	adult retinal pigment epithelial cell line-19
ATCC	American Type Culture Collection
BA	beta-actin
BCVA	best-corrected visual acuity
BME	Basal Medium Eagle
bp	base pairs
BSA	bovine serum albumin
C6/36	cell line from <i>Aedes albopictus</i> larvae
cat.	catalogue number
CD4	cluster of differentiation 4
cDNA	complementary deoxyribonucleic acid
CI	confidence interval
CMV	cytomegalovirus
CN	cranial nerve
CO ₂	carbon dioxide
Cq	quantification cycle
CRAL-BP	cellular retinaldehyde-binding protein
CTLA2 α	cytotoxic T-lymphocyte associated antigen 2 alpha
CV	coefficient of variation
DALYs	disability-adjusted life years
DAPI	4',6-diamidino-2-phenylindole
DENV	dengue virus
DENV1	dengue virus, serotype 1
DENV2	dengue virus, serotype 2
df	degrees of freedom

dH ₂ O	distilled water
DMEM	Dulbecco's modified Eagle medium
DNA	deoxyribonucleic acid
dsRNA	double-stranded ribonucleic acid
E	envelope protein
EBOV	<i>Zaire ebolavirus</i>
EBV	Epstein-Barr virus
EDI	enhanced-depth imaging
EDTA	ethylenediaminetetraacetic acid
EIF2AK2	eukaryotic translation initiation factor 2-alpha kinase 2
ELISA	enzyme-linked immunosorbent assay
ELM	external limiting membrane
EV	extracellular vesicle
EVD	Ebola virus disease
F	F statistic
F12	Ham's nutrient mixture F-12
FASL	Fas ligand
FBS	fetal bovine serum
<i>g</i>	standard gravity
GAPDH	glyceraldehyde-3-phosphate dehydrogenase
GFAP	glial fibrillary acidic protein
GS	glutamine synthetase
H ₂ O	water
HEPES	N-2-hydroxyethylpiperazine-N-2-ethane sulfonic acid
HIV	human immunodeficiency virus
hpi	hours post-inoculation
HREC	human retinal endothelial cell
HRP	horseradish peroxidase
IFITM1	interferon-induced transmembrane protein 1
IFN	interferon
Ig	immunoglobulin
IGF1	insulin-like growth factor 1
IL-10	interleukin-10

IL-1 β	interleukin-1 beta
IL-6	interleukin-6
ILM	internal limiting membrane
IRF-3	interferon regulatory factor-3
IRF-7	interferon regulatory factor-7
ISG15	interferon-stimulated gene 15
KEGG	Kyoto Encyclopedia of Genes and Genomes
LB	Luria Bertani
LRRK2	leucine-rich repeat kinase 2
M value	expression stability measure
MDA5	melanoma differentiation-associated antigen 5
MEM	minimum essential medium Eagle
MIO-M1	Moorfields / Institute of Ophthalmology-Müller 1
miRNA	micro RNA
MOI	multiplicity of infection
mRNA	messenger RNA
N	population size
n	sample size
NEAA	non-essential amino acid
NF	nuclease-free
NF- κ B	nuclear factor kappa-light-chain-enhancer of activated B cells
NGS	normal goat serum
NS	non-structural
nt	nucleotide
OCT	optical coherence tomography
PACT	protein activator of the IFN-induced protein kinase
PBS	phosphate-buffered saline (Dulbecco's)
PBS-T	phosphate-buffered saline with 0.1% Tween® 20 detergent
pCAGGS	plasmid with CMV-IE/beta-Actin/beta-Globin promoter
PCR	polymerase chain reaction
PD-1	programmed cell death protein-1
PD-L	programmed death-ligand
PEDF	pigment epithelial-derived factor

PFA	paraformaldehyde
pfu	plaque-forming units
Poly I:C	polyriboinosinic:polyribocytidylic acid
PPIA	peptidylprolyl isomerase A
prM	precursor membrane
PRR	pattern recognition receptor
PVDF	polyvinylidene difluoride
rcf	relative centrifugal force
RIG-I	retinoic acid-inducible gene-I
RIPA	radioimmunoprecipitation assay
RNA	ribonucleic acid
RNASeq	ribonucleic acid sequencing
RPE	retinal pigment epithelium
RPLP0	ribosomal protein lateral stalk subunit P0
RSAD2	radical S-adenosyl methionine domain-containing 2
RT	room temperature
RT-qPCR	quantitative reverse transcription polymerase chain reaction
RT-PCR	reverse transcription polymerase chain reaction
SD	standard deviation
SD-OCT	spectral domain optical coherence tomography
SOC	super optimal broth with catabolite repression
sRNA-Seq	small RNA sequencing
TAE	Tris/acetic acid/ethylenediaminetetraacetic acid (EDTA)
TBP	thymine adenine thymine adenine (TATA)-binding protein
TD-OCT	time-domain optical coherence tomography
TE	Tris-ethylenediaminetetraacetic acid (EDTA)
TGF- β	Transforming growth factor-beta
TIFF	tagged file image format
TLR3	toll-like receptor 3
TNF- α	tumour necrosis factor-alpha
TRC	toxoplasmic retinochoroiditis
Tris	tris(hydroxymethyl)aminomethane
TRITC	tetramethylrhodamine isothiocyanate

TSP-1	thrombospondin-1
UV	ultraviolet
v.	version
v/v	concentration by volume/volume
VA	visual acuity
VEGF	vascular endothelial growth factor
viperin	virus inhibitory protein, endoplasmic reticulum-associated, IFN-inducible
VP35	viral protein 35
VP40	viral protein 40
w/v	concentration by weight/volume
ZIKV	Zika virus

STATISTICAL SIGNIFICANCE

*	$p < 0.05$
**	$p < 0.01$
***	$p < 0.001$
****	$p < 0.0001$

GREEK ALPHABET

α	alpha
β	beta
γ	gamma
κ	kappa

STANDARD INTERNATIONAL UNITS OF MEASURE

A	ampere
°C	degrees Celsius
Da	Dalton
g	gram
h	hour
L	litre
M	molarity, moles per litre
m	metre
min	minute
mol	mole
s	second
V	volt

INDICATORS OF MAGNITUDE

M	mega-	$\times 10^6$
k	kilo-	$\times 10^3$
m	mili-	$\times 10^{-3}$
μ	micro-	$\times 10^{-6}$
n	nano-	$\times 10^{-9}$
p	pico-	$\times 10^{-12}$

ABSTRACT

Zoonotic diseases form the bulk of emerging infections, and are responsible for epidemics and pandemics that impact global health and security. Many of these pathogens cause ocular disease, and retinal involvement often results in visual impairment. The retina is a complex tissue that has limited capacity to regenerate. It performs a critical sensory function, converting the visual image into a neural signal in the initial stages of visual processing. This thesis studied three important zoonoses that involve the retina: *Toxoplasma gondii*, dengue virus (DENV), and Ebola virus. The ubiquitous parasite *T. gondii* has infected one third of the human population, and retinal involvement results in tissue destruction with resultant visual impairment. The cat is the definitive host, and mammals and birds are intermediate hosts. Each of the four serotypes of DENV, a mosquito-borne epidemic *flavivirus*, causes a serious tropical disease. The features of retinal involvement in dengue infection are diverse and are poorly understood. The largest Ebola epidemics have been caused by Ebola virus spill-over from the bat population. Survivors develop a multisystem syndrome that includes infectious ocular pathology and serious visual sequelae.

This thesis advances the body of knowledge of retinal infections on many fronts. Spectral-domain optical coherence tomography (SD-OCT) is considered a standard tool in clinical ophthalmology that renders *in vivo*, real-time data on tissue architecture. Through the largest study of toxoplasmic retinochoroiditis by SD-OCT, this work presents a thorough portrayal of the spectrum of the tissue-level changes that occur as a result of infection. The investigation identified signs that were characteristic of the disease and/or indicated poor visual prognosis. The presence of retinal hyporeflective spaces or signal voids, likely

representing liquefactive necrosis of the retina, was identified as an SD-OCT sign associated with visual acuity of worse than 20/200 (defined as legal blindness in Australia and other industrialised nations, including the United States). This observation is expected to be useful to the practising ophthalmologist.

This thesis also presents the first published work on human Müller cells in DENV infection, and provides first details of the molecular responses to DENV. Müller cells are a specialized glial cell unique to the retina. They form part of the blood-retinal barrier, contact most other retinal cell populations, and provide critical physiological support to neurons. To understand the response of human Müller cells to infection in dengue, the MIO-M1 human Müller cell line and primary human Müller cell isolates were infected with multiple DENV strains of DENV1 and DENV2 serotypes, and antiviral, inflammatory and immunomodulatory responses after DENV infection were evaluated. Müller cells mounted an inflammatory response to DENV infection that was characterised by upregulation of pro-inflammatory cytokines, and the response varied by viral strain, with DENV2 inducing stronger responses. Curiously, a lack of a type I interferon response to infection was demonstrated in MIO-M1 cells, but not primary human Müller isolates, which this thesis is the first to report.

The pathogenesis of post-Ebola uveitis is poorly understood. Viral persistence in the eye, despite clinical recovery, has been demonstrated, and pigmented retinal scars in survivors implicate involvement of retinal pigment epithelial cells. To understand the potential involvement of microRNA (miRNA) signalling in EBOV infection of human retinal pigment epithelial cells, bioinformatic processes were utilized to predict pathways and networks based on miRNA expression in the ARPE-19 human retinal pigment epithelial cell line following infection with EBOV. Bioinformatic analysis of miRNA-driven

pathways in EBOV-infected ARPE-19 cells identified leucine-rich repeat kinase (LRRK) 2, a protein associated with neuroinflammation, as the most highly connected molecule in miRNA signalling networks that were active in EBOV-infected retinal pigment epithelial cells. Mitogen-activated protein kinases (MAPK) 13 and 7 were also highly involved in EBOV infection and are associated with neuroinflammation. Central to the response to EBOV infection, miR-190a and miR-101 may facilitate EBOV survival in retinal pigment epithelium through prevention of apoptosis.

To examine the effect of the EBOV protein, VP35, on the type I interferon (IFN) antiviral response by human retinal pigment epithelial cells, a plasmid expressing VP35 was transfected into the ARPE-19 cell line and primary cell isolates. Expression of VP35 inhibited IFN- β production in some primary human retinal pigment epithelial cell isolates, indicating that this viral protein plays a key role in subversion of the host cell, and this interaction varies across individuals. These mechanistic studies of the interplay between EBOV and the type I IFN response in retinal pigment epithelial cells represent first-in-field experiments.

The overall aim of this thesis was to identify and address unanswered questions relating to the mechanisms of retinal pathology caused by three serious human pathogens that are transmitted by animals: *T. gondii*, DENV and EBOV. Various aspects of the host cellular and/or molecular response to an infection with each of these three pathogens were addressed in this thesis. The work has demonstrated a range of indicators of retinal tissue damage and provides a foundation for further mechanistic research and potential therapeutic opportunities to reduce infection-mediated tissue damage and resultant visual impairment in zoonotic retinal infections.

THESIS OUTCOMES

PUBLICATIONS ARISING DIRECTLY FROM THIS THESIS

Oliver GF, Orang AV, Appukuttan B, Marri S, Michael MZ, Marsh GA, Smith JR. Expression of microRNA in human retinal pigment epithelial cells following infection with Zaire ebolavirus. BMC Res Notes. 2019 Oct 1;12(1):639.

ADDITIONAL PUBLICATIONS RELATED TO THIS THESIS

Oliver GF, Carr JM, Smith JR. Emerging Infectious Uveitis: Chikungunya, Dengue, Zika, Ebola. Clin Exp Ophthalmol. 2019 Apr;47(3):372-380.

ADDITIONAL PUBLICATIONS DURING PHD CANDIDATURE

Oliver GF, Stathis RM, Furtado JM, Arantes TE, McCluskey PJ, Matthews JM; International Ocular Syphilis Study Group, Smith JR. Current Ophthalmology Practice Patterns for Syphilitic Uveitis. Br J Ophthalmol. 2019 Nov;103(11):1645-1649.

ORAL PRESENTATIONS RELATED TO THIS THESIS

Oliver GF, Orang AV, Appukuttan B, Michael MZ, Marsh GA, Smith JR. Expression of microRNA by Human Retinal Pigment Epithelial Cells in Response to Infection with Ebola Virus. In: 9th Australasian Virology Society Scientific Meeting; 2017 Dec 5-8; Stamford Grand Adelaide Hotel, Adelaide, South Australia: Oral and poster presentation.

Oliver GF. Emerging viral uveitis. Royal Australian and New Zealand College of Ophthalmologists 50th Annual Scientific Congress; 2018; Adelaide, South Australia, Australia.

Oliver GF, Vieira BR, Araújo M, Arruda S, Carr JM, Furtado JM, Smith JR. In vivo retinal imaging of ocular toxoplasmosis in human patients. Australian Society for Parasitology Annual Conference; 2019; Adelaide, Australia.

Oliver GF. Spectral Domain Optical Coherence Tomography in Active Toxoplasmic Retinochoroiditis. Royal Australian and New Zealand College of Ophthalmologists 51st Annual Scientific Congress; 2019; Sydney, Australia. (Ophthalmic Research Institute of Australia Best Paper Award).

POSTER PRESENTATIONS RELATED TO THIS THESIS

Oliver GF, Granado GB, Ma Y, Ashander LM, Appukuttan B, Carr JM, Smith JR. Type I interferon responses of human iris pigment epithelial cells to infection with flaviviruses. In: ComBio2017; 2017 Oct 2-5; Adelaide Convention Centre, Adelaide, South Australia: Poster POS-THU-154.

AWARDS IN SUPPORT OF THIS THESIS

- Australian Government Research Training Scholarship (2017-2020)
- Avant Doctor-In-Training Research Scholarship (2017)
- Flinders University Faculty of Medicine, Nursing & Health Science Student Travel Award (2017)
- European Molecular Biology Laboratory Australia PhD Course (2017)
- Flinders University Three-Minute Thesis Finalist (2017)
- Eye & Vision Collaborators Day, Flinders University, winner Three-Minute Thesis competition (2017)
- Royal Australian and New Zealand College of Ophthalmologists / Allergan Scholarship (2017)
- National Health and Medical Research Council Postgraduate Scholarship (2018-2020)
- Flinders Medical Centre Clinicians Special Purpose Trust Scholarship (2018-2020, relinquished for National Health and Medical Research Council Scholarship)
- Flinders University College of Medicine & Public Health Research Higher Degree Student Publication Award (2018)
- The Minister's Humane Research Scholarship, South Australian Department of Environment and Water (2019-2020)

PREFACE

The material presented in this doctoral thesis represents my own original work, with the exception of:

- Clinical data used in the spectral-domain optical coherence study of ocular toxoplasmosis: collected as part of a clinical cohort study, and designed and executed by Dr João Furtado and colleagues at the University of São Paulo Ribeirão Preto Medical School, Brazil, and in collaboration with Prof. Justine Smith (Chapter 3).
- Production and titering of dengue virus: Ms Abby Dawson (Chapter 4).
- Isolation of primary human retinal Müller cells (Chapter 4) and retinal pigment epithelial cells (Chapter 6): Dr Yuefang Ma.
- Original dataset of differentially-expressed microRNA (Chapter 5) used in bioinformatics study of Ebola eye infection: generated through experimental work undertaken by Dr Glenn Marsh and Prof. Justine Smith and colleagues at CSIRO and Flinders University.

CHAPTER 1

Introduction

1.1	Introduction	1
1.2	Zoonotic infectious diseases.....	2
1.3	Retinal structure and function	7
1.3.1	Retinal cell populations	9
1.3.2	Immunological conditions of the posterior eye.....	12
1.3.3	Clinical imaging of the posterior eye	18
1.4	Ocular toxoplasmosis.....	21
1.4.1	<i>Toxoplasma gondii</i>	21
1.4.2	Toxoplasmosis	22
1.4.3	Clinical features of ocular toxoplasmosis	24
1.4.4	Visual outcomes of ocular toxoplasmosis	25
1.4.5	Pathology of ocular toxoplasmosis.....	26
1.5	Dengue retinopathy.....	33
1.4.1	Dengue virus.....	33
1.5.1	Clinical manifestations of dengue retinopathy.....	37
1.5.2	Pathogenesis of dengue retinopathy.....	38
1.6	Post-Ebola uveitis.....	41

1.4.1	Ebola virus.....	41
1.6.1	Ebola Virus Disease.....	42
1.6.2	Clinical manifestations of post-Ebola uveitis.....	45
1.6.3	Pathogenesis of post-Ebola uveitis.....	47
1.6.4	Summary of mechanisms of zoonotic retinal infections	51
1.7	Aims of the thesis.....	54

1.1 INTRODUCTION

Human infectious diseases that arise from animal reservoirs are complex, diverse, and incompletely understood.¹ A large proportion of these zoonoses affect the retina, which may result in visual impairment. Tissue damage can occur as the consequence of direct infection, or from infection-related immune responses of the host, and is determined by a range of factors.² The pathogenic mechanisms of retinal damage in such zoonotic infections are poorly understood. These diseases often occur in tropical regions and low- and middle-income countries where research capacity is limited. Some pathogens require high-level biosafety infrastructure, which restricts the pool of scientists able to research these diseases. A significant obstacle to all research involving the retina is the lack of human retinal tissue, as the risk-to-benefit ratio of obtaining a retinal biopsy is usually too high to justify a potentially blinding procedure. Thus, indirect means of measuring and monitoring retinal tissue changes must be employed to further our knowledge in this area.

In work described in this thesis, a range of methods and tools were used to study zoonotic retinal diseases caused by three pathogens: dengue virus, Ebola virus and the obligate intracellular parasite, *Toxoplasma gondii*. Cell culture techniques were employed to study the effect of dengue virus infection in human Müller cells. The interactions of Ebola virus and retinal pigment epithelial cells were interrogated using cell culture and bioinformatics processes, specifically, the effect of Ebola protein VP35 on the type I interferon response in human retinal pigment epithelial cells, and the retinal pigment epithelial cell response to Ebola virus infection through predictions of molecular targets of small non-coding RNA. Retinal tissue changes in ocular toxoplasmosis were evaluated

using spectral-domain optical coherence tomography in a large cohort of individuals with active infection. Biological markers of retinal pathology were identified, and help to bridge gaps in our understanding of the mechanisms by which these zoonoses affect the retina.

1.2 ZOOONOTIC INFECTIOUS DISEASES

Zoonoses are responsible for the majority of infectious and emerging diseases, and some of the most devastating epidemics and pandemics in human history.³⁻⁶ Unlike the viruses that cause polio, smallpox and measles, these pathogens spread between animal reservoirs and infect humans, making them extraordinarily difficult to eliminate. The coronavirus disease of 2019 (COVID-19) pandemic, caused by severe acute respiratory syndrome coronavirus 2 (SARS-CoV-2), has brought into sharp focus the wicked complexity of factors that drive disease transmission, as well as the catastrophic consequences to global health and security. In 2005, the World Health Organization defined those extraordinary events that endanger international public health as “Public Health Emergencies of International Concern” (PHEICs).⁷ Five of the six PHEICs declared since then have been zoonotic infectious diseases: the H1N1 swine ‘flu pandemic (2009), the Zika virus epidemic in the Americas and Asia-Pacific (2015-2016), the Ebola virus epidemics in West Africa (2014-2016), and the Democratic Republic of Congo (2018-), and the COVID-19 pandemic (2019-).

One large group of zoonoses are the arthropod-borne (“arbo-“) viruses. Flaviviruses are single-stranded RNA arboviruses that are transmitted between mammalian and avian hosts, and pose a global threat to public health.⁸⁻¹⁰ Dengue virus (DENV), a mosquito-

borne epidemic *flavivirus*, causes a serious tropical disease – dengue – and is the most common human disease-causing arbovirus in the world, infecting an estimated 400 million globally.¹¹⁻¹³ The geographic spread of DENV mirrors that of its *Aedes* mosquito vectors. Today, over half the global population is at risk of infection, but modeling forecasts this will rise to 80% in 2080.¹⁴ In addition to DENV, *Aedes* mosquitoes can transmit other febrile disease-causing zoonotic viruses: yellow fever virus, chikungunya virus, West Nile virus, and Zika virus.¹⁵ Yellow fever virus is a single-stranded RNA flavivirus considered endemic to Africa and America, causing a febrile illness with eponymous jaundice,¹⁶ and responsible for 80,000 vaccine-preventable fatalities annually.¹⁷

Arboviruses are capable of causing unpredictable outbreaks. Zika virus was widespread in Africa for approximately 50 years,¹⁸ causing a mild self-limiting febrile illness,¹⁹ before an epidemic of rash, arthralgia and conjunctivitis occurred in the West Pacific in 2007.²⁰ An outbreak of infection in French Polynesia in 2013²¹ was associated with a spike in Guillain-Barre syndrome.²¹ In 2015, Zika virus infection was diagnosed in febrile individuals in Brazil, where it caused over 1.7 million infections and at least 3,000 definite cases of microcephaly.²²⁻²⁶ Another flavivirus, West Nile virus, has infected an estimated 3 million people in North America, and is associated with a mild viral illness in most, but meningitis and encephalitis in a minority of individuals.^{16, 27} Chikungunya virus is endemic in tropical regions, and causes a febrile illness, characteristic arthralgia, and in severe cases, encephalitis.²⁸ A single mutation allowed it to infect a new *Aedes* mosquito and cause an epidemic involving 266,000 people.²⁹ All of these arboviruses are globally significant pathogens, and all can cause ophthalmic complications.³⁰

Some of the deadliest zoonotic viruses are found in bat reservoirs. The only mammals capable of free flight, bats represent 20% of extant mammalian species and demonstrate genetic diversity second only to rodents.³¹ The exceptional biology that allows them to act as a viral reservoir is largely unstudied. The fruit bat is assumed to be the reservoir for Ebola virus, which since its discovery in 1976 has caused 23 separate outbreaks of Ebola virus disease (EVD) that have spilled into the human population.³² The largest Ebola epidemics were caused by the *Zaire ebolavirus* species (EBOV). The 2014-2016 epidemic in west Africa infected 28,000 individuals and had a case-fatality rate of 40%, and the ongoing 2018 epidemic in the Democratic Republic of Congo has infected over 3,500 individuals and has a case-fatality rate of 66%.³³ Survivors of EVD develop a multisystem syndrome that includes ocular complications, and live virus has been isolated from immune-privileged sites including the eye.³⁴⁻³⁶

The parasite *Toxoplasma gondii* can infect virtually every species of mammal and bird.³⁷ The definitive host is the cat, and one third of the human population shows evidence of infection.³⁸ Seroprevalence studies of anti-*T. gondii* antibodies in humans show remarkable variation across geography,³⁹⁻⁵⁷ age,⁵⁸ gender,⁵⁹ and socioeconomic status.⁵³ In the last 50 years, researchers in Western countries have documented a decrease in *T. gondii* seroprevalence over time.^{41, 54, 60} The presence of anti-*T. gondii* immunoglobulin (Ig)G antibodies indicates prior infection, and this status is significant in women of childbearing age as – with rare exception - antibodies confer protection against vertical transmission of toxoplasmosis from mother to child.⁶¹ Immunocompetent adults form the largest group of affected individuals, and become infected through: ingestion of oocysts in soil-contaminated produce, in contaminated filter feeders and shellfish, and directly from cat faeces; from consumption of tissue cysts in undercooked meat; or due to

movement of free tachyzoites across the placenta.^{37, 54, 62, 63} The main complication of toxoplasmosis is retinochoroiditis, which causes profound retinal tissue destruction and is associated with blindness in one quarter of eyes.⁶⁴

Zoonotic diseases form the bulk of emerging infections and are responsible for epidemics and pandemics that impact global health and security. Many of these pathogens cause ocular complications (Table 1.1), and infection of the retina often results in visual impairment.

Table 1.1: Zoonotic infections of the retina

Pathogen	Type	Primary host	Transmission	Retinal complications	References
West Nile virus	Flavivirus	Birds	Culex and Aedes mosquitoes	Multifocal chorioretinitis	16, 27, 65
Zika virus	Flavivirus	Primates	Aedes mosquitoes, vertical and sexual transmission	Congenital zika syndrome, posterior uveitis	30, 66, 67
Yellow fever	Flavivirus	Primates	Aedes mosquitoes	Retinopathy, maculopathy	30, 68, 69
Chikungunya	Alphavirus	Primates	Aedes mosquitoes	Retinitis, choroiditis, vasculitis, cystoid macular oedema, acute macular neuroretinopathy	30, 70
Dengue virus	Flavivirus	Primates	Aedes mosquitoes	Retinochoroiditis, maculopathy, foveolitis, haemorrhagic retinopathy, vasculitis	30, 70
Ebola virus	Filovirus	Fruit bats	Direct contact	Posterior and panuveitis, pigmented retinal scars	70
<i>Toxoplasma gondii</i>	Parasite	Cat	Oocysts, tissue cysts, vertical transmission	Retinochoroiditis	71

1.3 RETINAL STRUCTURE AND FUNCTION

The retina is a complex tissue that converts the visual image into a neural signal in the initial stages of visual processing. In humans, the healthy retina ranges from 150 to 320 μm in thickness and forms the innermost layer of the eye, containing at least 60 distinct types of neurons that are meticulously arranged to maximize visual resolution.^{72, 73} The retina performs a critical sensory function and has limited capacity to regenerate. Thus, damage in the form of infection causes loss of vision that is often permanent. The anterior segment of the eye consists of the cornea, iris and crystalline lens, which together serve to focus the visual image onto the retinal plane (Figure 1.1). Aqueous humour and vitreous gel fill the anterior and posterior segments respectively, and provide optically empty media which minimize light scatter. The neural retina is supported by a polarized monolayer of pigmented epithelial cells known as the retinal pigment epithelium (RPE), which lies between the retina and the choroid, a highly-pigmented layer of vascularized loose connective tissue.^{73, 74} The macula is a 6 mm-diameter area of the central retina that is bounded by the optic disc and vascular arcades, and is responsible for the central visual field. Structural and functional specializations at the centre of this area, the fovea, enable the highest resolution of vision.

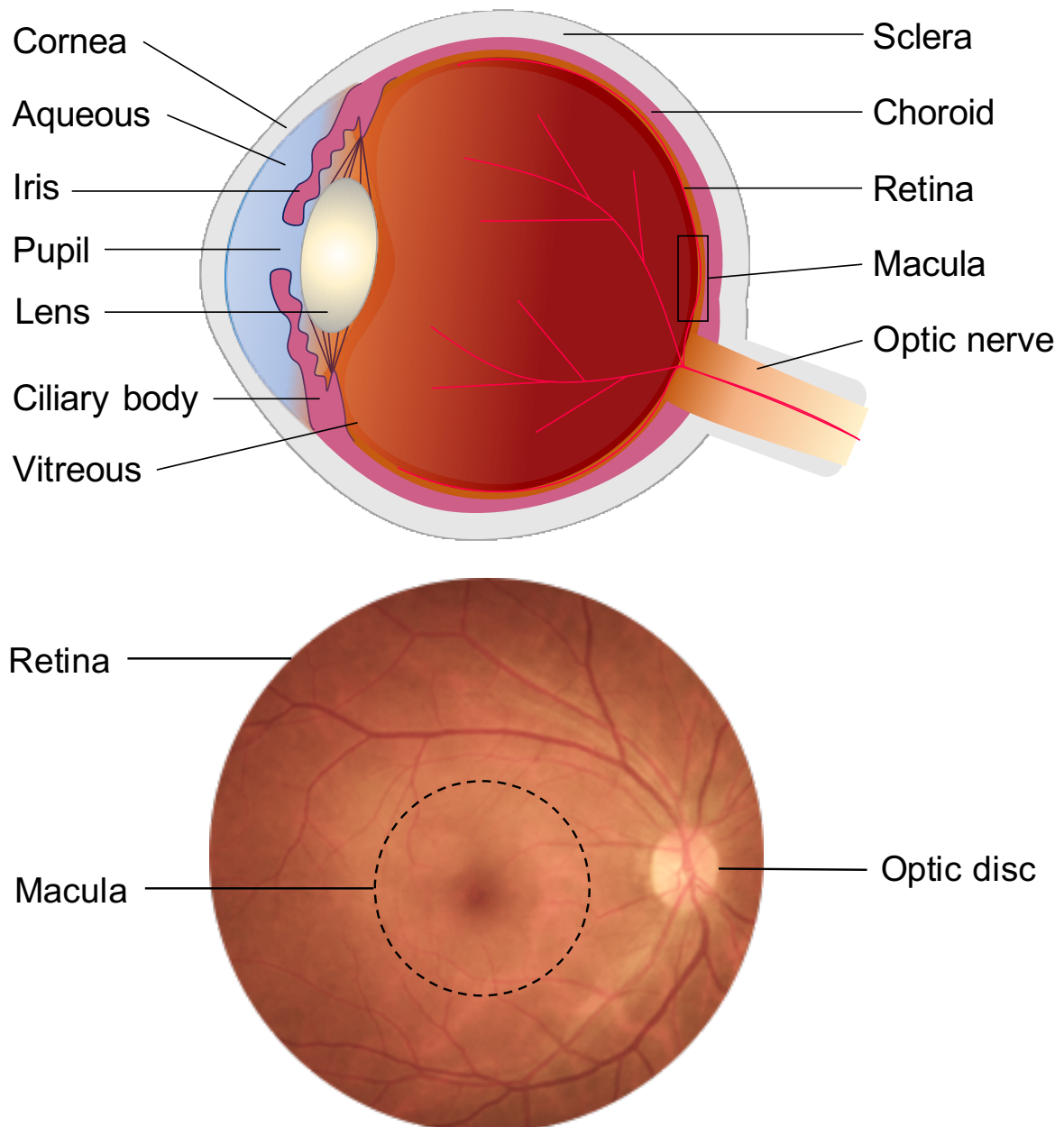


Figure 1.1: Anatomy of the human eye

Cross-sectional cartoon of basic eye structures (top). The crystalline lens separates the anterior and posterior segments of the eye. The anterior segment is filled with aqueous humour, while the posterior segment is filled with vitreous gel. The macula is positioned at the posterior pole of the eye, adjacent to the optic nerve head, known as the optic disc. Colour fundus photograph of the right posterior pole (bottom), demonstrating macula and optic disc.

1.3.1 Retinal cell populations

Five major classes of neurons comprise the retina, and distinct layers characterize the cross-sectional profile of this tissue. The cell bodies are arranged in three layers that are interspersed by two plexiform layers where synaptic junctions are located. The outermost layer of the retina is formed by 100 million rod and 5 million cone photoreceptors which transduce light into an electrochemical signal and are intimately associated with the underlying RPE.⁷² Three types of interneurons – bipolar, amacrine and horizontal cells – process the visual signal in parallel and converge on 1.5 million ganglion cells, which leave the eye via the optic disc. In cross-section, and moving outwards from the posterior vitreous (or hyaloid) face, the retinal layers comprise: internal limiting membrane, retinal nerve fibre layer, ganglion cell layer, inner plexiform layer, inner nuclear layer (containing bipolar, Müller, horizontal and amacrine cell bodies), outer plexiform layer, outer nuclear layer (photoreceptor cell bodies), external limiting membrane, photoreceptor inner and outer segments, and RPE. The inner segments of the photoreceptors comprise an inner myoid and an outer ellipsoid region, the latter of which contains an abundance of mitochondria, while the tips of the outer segments are enveloped by retinal pigment epithelial cells (Figure 1.2).

Non-neural cells provide functional and structural support as part of the retinal matrix. Microglia – specialized macrophages – are distributed in the two plexiform layers and among the ganglion cells, and are the most abundant immune cell in the retina.⁷³ They perform immune surveillance, phagocytosis, and synaptic maintenance. Macroglia – astrocytes and Müller cells – regulate retinal homeostasis. Müller cells are involved in

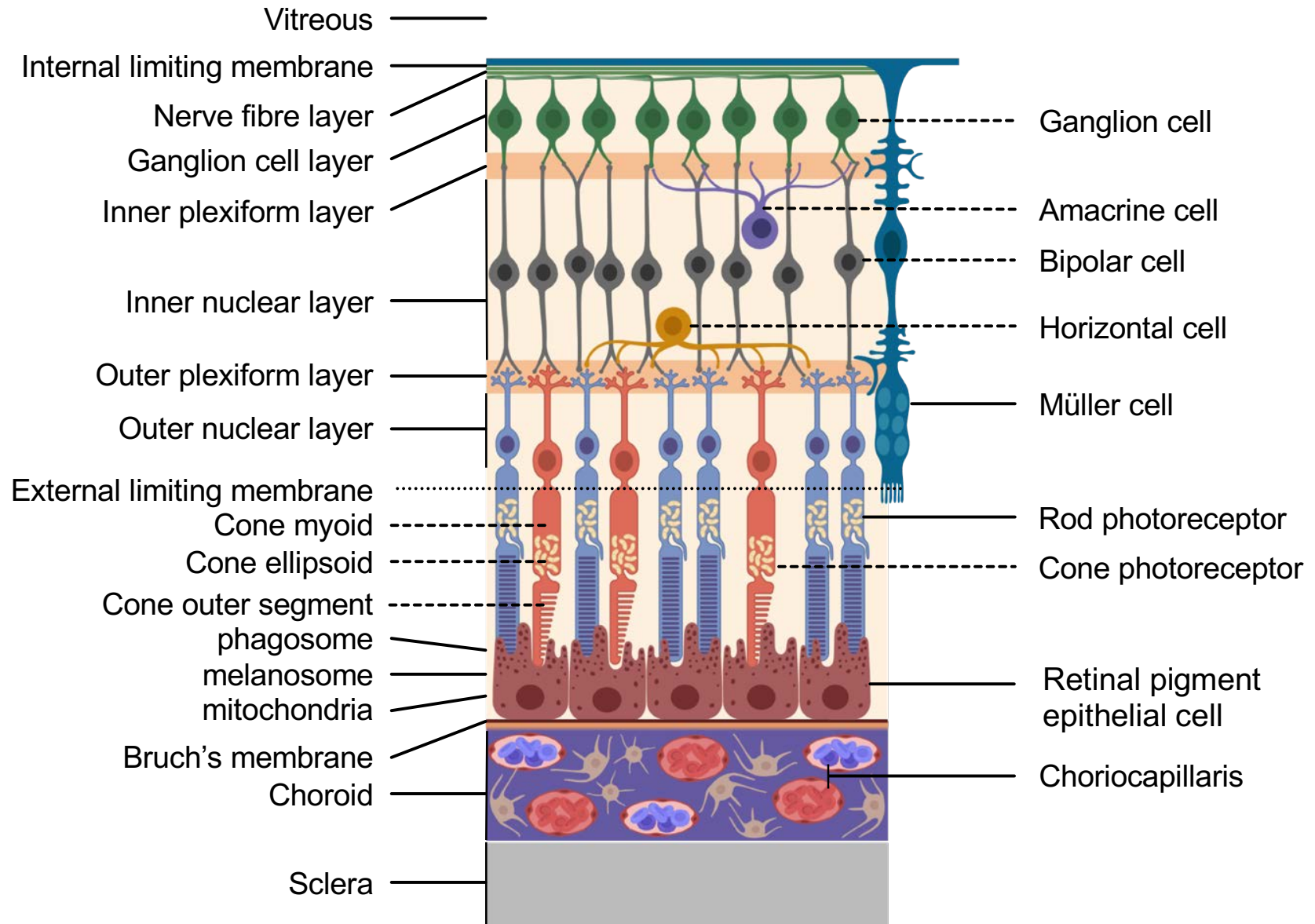


Figure 1.2 : Neural cells of the human retina

The inner retina extends from the internal limiting membrane to the outer plexiform layer and is supplied by the arterioles from the central retinal artery. Müller cells extend from the internal limiting membrane (which is formed by their footplates) to the external limiting membrane, and their cell bodies lie within the inner nuclear layer. The outer retina includes rod and cone photoreceptors, Müller cell processes and retinal pigment epithelium, and is supplied by the choriocapillaris. Image created in BioRender.com.

neurotransmitter recycling, clearance of CO₂ and waste products, maintenance of pH, fluid homeostasis, and potassium buffering.⁷⁵ Müller cells are radially orientated – extending from the external to the internal limiting membrane - and support retinal architecture, guide light to the photoreceptors, and contact the vitreous cavity, subretinal space, vascular network and virtually every cell in the retina. The RPE is closely apposed to the photoreceptor layer, and each retinal pigment epithelial cell serves about 30 photoreceptors.⁷⁴ These cells are metabolically coupled in a relationship that is critical for visual functioning. The outer segments at the tips of photoreceptors are shed in a diurnal cycle and phagocytosed by retinal pigment epithelial cells, which transport and process retinoids, while melanin, abundant in RPE, absorbs scattered light to enhance visual acuity.⁷⁶ The basement membrane of the RPE is continuous with Bruch's membrane, which forms a type of sub-endothelial matrix to the subjacent fenestrated choriocapillaris of the choroid.

1.3.2 Immunological conditions of the posterior eye

The eye comprises multiple specialized post-mitotic, terminally-differentiated cell subsets that have poor regenerative capacity. This makes the organ vulnerable to injury. The ability to modulate immune-mediated inflammation allows the eye to minimize any collateral damage to preserve tissue integrity, and thus vision.⁷⁷ Ocular immune privilege describes the anatomical barriers and molecular and cellular immunoregulatory mechanisms that achieve this.⁷⁸

A combination of anatomical and immunological defences protect vision-processing cell populations within the eye.⁷⁹ The blood-retinal-barrier (BRB) forms the primary

boundary that isolates retinal tissue from the systemic circulation (Figure 1.3). The inner BRB is formed by endothelial cells within retinal arterioles, venules and capillaries, that are supported by pericytes and astrocytes. These non-fenestrated endothelial cells restrict the passage of macromolecules and leukocytes.⁷⁸ The outer BRB is formed by the RPE and allows transcellular transport of molecules from the choriocapillaris to the photoreceptors.⁸⁰ Tight junctions play a critical role in maintaining the barrier function and are located between retinal pigment epithelial cells and retinal endothelial cells.

A second component of ocular immune privilege protects vision-processing cell populations from the harmful effects of inflammation. The regional immune system within the eye is controlled by parenchymal cells which include microglia, retinal pigment epithelial cells that line the interior aspect of the BRB. These cells modulate the immunological inflammatory response through the release of soluble or membrane-bound products. Key molecules secreted by retinal pigment epithelial cells include: transforming growth factor-beta (TGF- β), thrombospondin-1 (TSP-1), cytotoxic T-lymphocyte associated antigen 2 alpha (CTLA2 α), programmed-death-ligand 1 (PD-L1), galectin 1, pigment epithelial-derived factor (PEDF), and retinoic acid.⁷⁹ Additional immunological modifications serve to protect the ocular environment. Perivascular microglial populations perform immune surveillance, and in contrast to other nucleated cell populations, ocular cells express few major histocompatibility complex molecules on their surface.^{75, 78}

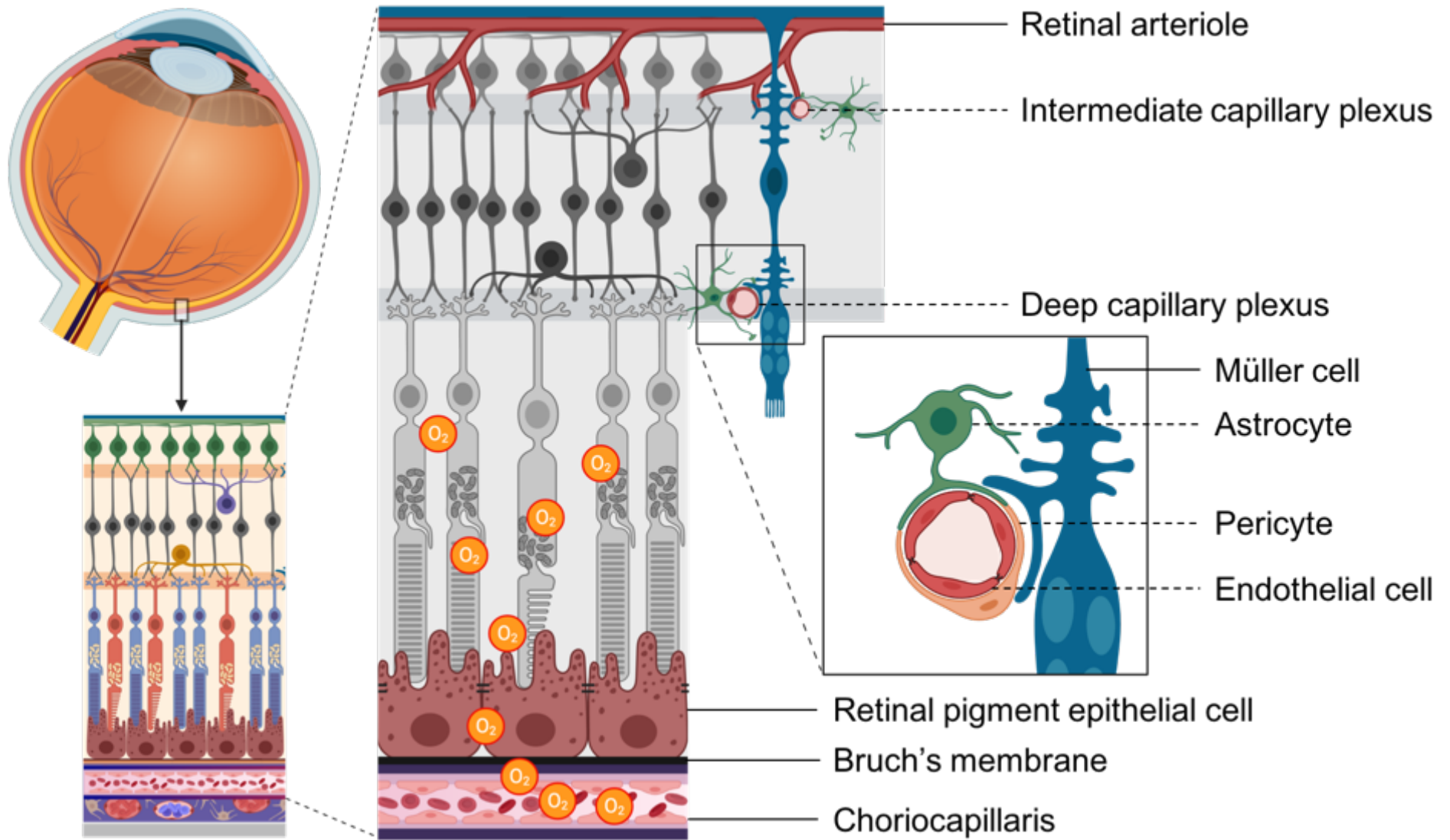


Figure 1.3: Inner and outer blood-retinal barriers

The retina is isolated from the systemic circulation by barrier systems that regulate ion, water and molecule movement. The blood–retinal barrier (BRB) has two components: the inner BRB is formed by tight junctions that seal neighbouring capillary endothelial cells and the outer BRB has tight junctions that restrict paracellular trafficking between retinal pigment epithelial cells. Figure constructed at BioRender.com

Immune privilege can be vetoed if the eye perceives a microbial threat.⁸¹ The early warning network of the immune system is served by pattern recognition receptors that surveil the intra- and extracellular environment to detect molecular signs of infection. These so-called PAMPs and DAMPs (pathogen- and damage-associated molecular patterns, respectively) initiate pathogen-specific signalling pathways. Toll-like receptors (TLRs) are important pattern recognition receptors for both viral and parasitic infections. In addition, the RIG-I-like receptors, retinoic acid-inducible gene 1 (RIG-1) and melanoma differentiation factor 5 (MDA5), are key components of the antiviral response.^{82, 83}

Stimulated pattern recognition receptors block viral replication through multiple pathways. Products of viral replication – especially double-stranded (ds)RNA – are potent PAMPs that initiate a cascade of signalling events and lead to inhibition of viral messenger RNA translation, degradation of viral RNA by the endonuclease RNaseL, production of cytokines including type I interferons (IFNs), and chemokines, and the induction of apoptosis.^{84, 85} These pathways drive the cell to an antiviral state and modulate the adaptive immune response.⁸⁶

Eukaryotic pathogens do not express the same antigenic markers of bacteria and viruses, but unique protozoan molecular signatures, as well as indirect signals of parasitic infection, stimulate both PAMPs and DAMPs.⁸⁷ Human cells infected with *T. gondii* produce the soluble mediator, S100 calcium binding protein A11 (S100A11), which is a DAMP that stimulates receptors for advanced glycation end-products (RAGE)-dependent production of C-C motif chemokine ligand 2 (CCL2), a major chemokine and inductor of the monocyte-mediated immune response.⁸⁸ The innate response to parasitic infection is incompletely understood, but TLRs play an important role in the early response to infection.

Toll-like receptors are membrane-bound pattern recognition receptors constitutively expressed in multiple cell types. They are located on the cell surface or within the endosomal compartment.⁸⁹ Humans possess ten TLRs, which each recognizes a unique signature of molecular patterns.⁸⁴ Research involving murine models of toxoplasmosis show that TLRs 11 and 12 are key receptors in parasitic infections, but these TLRs do not exist in humans.⁸⁷ While human TLRs 3, 7, 8 and 9 show ligand similarity to murine TLRs 11 and 12, a number of TLRs have been implicated in human infection.⁹⁰ Activated by parasite RNA, TLR 3 initiates the type I IFN response, while TLR 9 contributes to the pro-inflammatory phenotype of ocular toxoplasmosis.⁹¹ Protection against congenital toxoplasmosis is associated with single nucleotide polymorphisms of TLRs 4 and 9, while TLRs 2 and 4 contribute to *T. gondii* recognition and host protection.⁹¹ Toxoplasma-infected macrophages, dendritic cells and plasmacytoid dendritic cells produce interleukin (IL)-12, which stimulates the release of IFN- γ , an initiator of signal transducer and activator of transcription 1 (STAT1) signalling, to modulate the production of pro- and anti-inflammatory molecules.⁹²

Human ocular cell populations show differential expression of TLRs. Primary human retinal pigment epithelial cells express all TLRs except TLR 8, and show abundant expression of TLR 3, which when stimulated by dsRNA, causes production of IFN β and pro-inflammatory cytokines.⁹³ Primary human retinal endothelial and human choroidal cells express most TLRs.⁹⁴ The human Müller cell line MIO-M1⁹⁵ expresses all 10 TLRs, and agonist challenge of TLRs 2, 3, 4, 7 and 9 induces transcription of inflammatory mediators.⁹⁶ Identification of TLR expression in multiple cell types of the macaque neural retina was recently undertaken.⁹⁷ For technical reasons, only TLRs 4 to 7 were tested, and the retina was not stimulated with TLR agonists before fixing and staining, but expression

of TLR protein was identified in ganglion (TLRs 4 through 7), Müller (TLRs 4 and 7), amacrine and bipolar cells (TLRs 4, 6 and 7). Curiously, microglia, pericytes, endothelial cells and astrocytes did not constitutively express TLRs 4 to 7 in the resting state.

The cell cytosol contains RNA sensors, RIG-I and MDA5, which are activated by dsRNA products of viral replication, and engage in signalling that leads to the production of type I IFN and inflammatory mediators – in particular, the IL-1 family of cytokines.⁸⁶ Interferon-stimulated genes (ISGs) produced in this pathway include protein kinase R (PKR), and 2'5'-oligoadenylate synthetase. These enzymes are stimulated by dsRNA. By phosphorylating and inactivating eukaryotic initiation factor (eIF)-2a, PKR blocks viral messenger RNA translation and triggers apoptosis. Viral degradation is initiated by 2'-5'-oligoadenylate synthetase activation of the latent endonuclease RNaseL.

Multiple intracellular sensors recognize molecular patterns indicating damage or infection, which initiate complex signalling pathways to protect the cell from invasion. These mechanisms also generate potent inflammatory responses intended to eliminate the invading pathogen, but with the potential to cause significant tissue damage.

1.3.3 Clinical imaging of the posterior eye

Pathological changes in tissue can be assessed by histopathology. This technique requires a tissue biopsy, and is usually unjustifiable in the case of retinal disease due to its unacceptable risk-to-benefit ratio. Thus, pathological information must be inferred by indirect means. Optical coherence tomography (OCT) is a non-invasive, real-time, *in vivo* imaging technique that utilizes the principle of low coherence interferometry to construct cross-sectional images of biological tissue from backscattered light (Figure 1.4).⁹⁸ Since

its first description in 1991,⁹⁹ refinements to light source, signal acquisition and data processing systems have seen generations of commercially-available OCT systems for ophthalmic use. Replacement of the movable reference beam mirror with a spectrometer has enabled Fourier analysis of reflected light, markedly reducing image acquisition time, improving resolution, and heralding the leap from so-called time-domain to spectral-domain OCT (SD-OCT).¹⁰⁰ Since the earliest OCT images of the human macula were published in 1993,¹⁰¹ image acquisition time has improved from 400 to 20,000 axial scans per second, and axial resolution has improved from 7-10 μm to 3-5 μm , two orders of magnitude greater than that of conventional ultrasound.¹⁰²

Retinal OCT imaging technology is in constant development. Swept-source OCT is a commercially available system that delivers complex volume rendering and high-resolution three-dimensional imaging of the retina. Image acquisition time is markedly decreased as a result of a tunable laser light source and a photodetector rather than a spectrometer to measure the interference spectrum. Longer wavelength light - 1050 nm compared to 840 nm for SD-OCT - enables better penetration through media opacities, increased depth imaging down to the sclera, and reduced light scattering, allowing visualization through oil and gas.¹⁰³ Megahertz OCT has recently been developed, and utilizes mode-locking of the laser light source to enable swept-source OCT imaging at exceptional speeds, achieving over 20 million axial scans per second.¹⁰⁴ OCT angiography utilizes alterations in the phase of reflected consecutive B-scans to image the retinal vasculature, obviating the need for dyes such as fluorescein.¹⁰⁵ Technology utilizing adaptive optics that reduce the higher order aberrations of optical systems have pushed the limits of resolution and enable evaluation of retinal cellular physiology, documenting

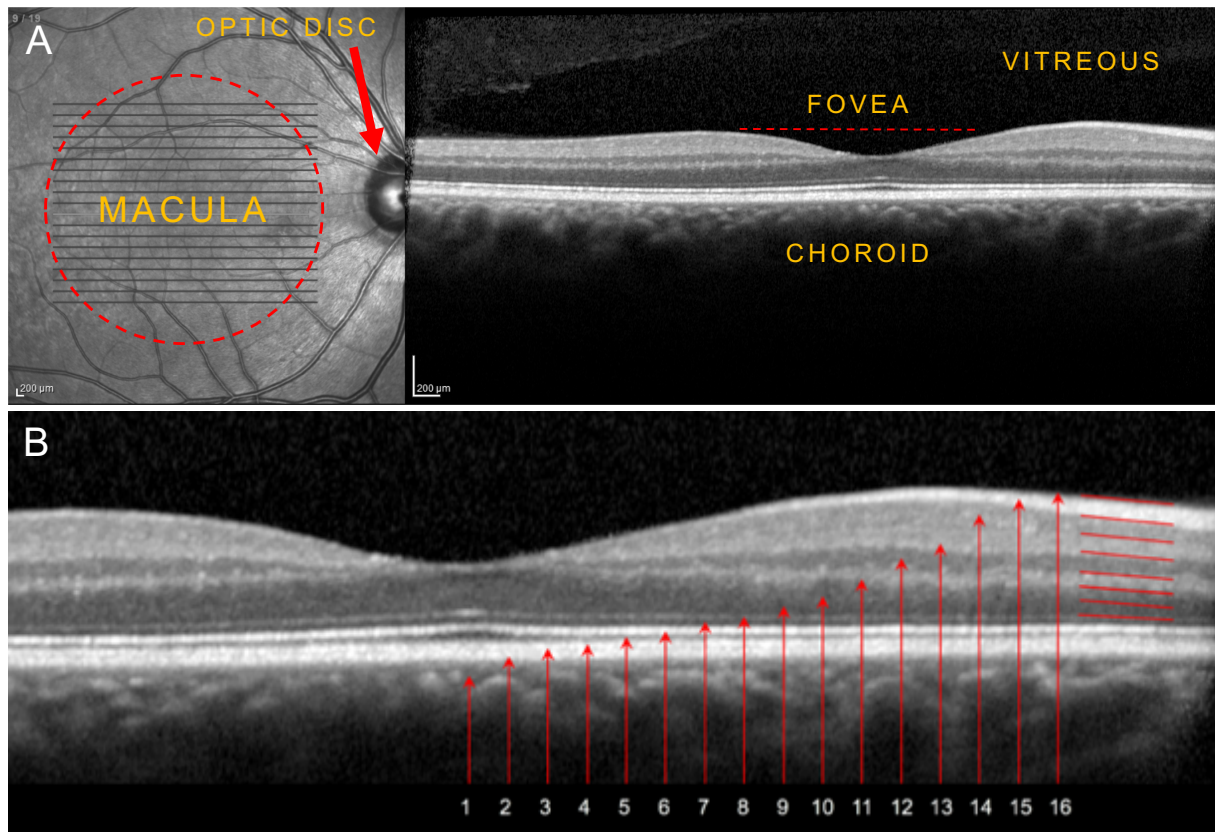


Figure 1.4: Spectral-domain optical coherence tomography of the normal human macula

Heidelberg SPECTRALIS SD-OCT of the normal right human macula, with near infrared image (left) for clinical correlation. (1) Choriocapillaris, (2) Mitochondrial zone of the RPE, (3) Melanosome zone of the RPE, (4) Phagosome zone of the RPE, (5) Cone outer segments, (6) Cone ellipsoids, (7) Cone myoids, (8) External limiting membrane, (9) Outer nuclear layer, (10) Henle fibre layer [macula only], (11) Outer plexiform layer, (12) Inner nuclear layer (13) Inner plexiform layer, (14) Ganglion cell layer, (15) Nerve fibre layer, (16) Internal limiting membrane. Retinal bands as per Cuenca et al, 2018.¹⁰⁶ **Abbreviations:** RPE = retinal pigment epithelium; SD-OCT spectral-domain optical coherence tomography.

fluctuations in cell size, blood velocity, and identification of subcellular organelles.¹⁰⁷

These developments show promising opportunities for research that will expand our understanding of disease mechanisms within the retina.

1.4 OCULAR TOXOPLASMOSIS

1.4.1 *Toxoplasma gondii*

Toxoplasma gondii is an apicomplexan obligate intracellular protozoan, and arguably the most successful parasite in the world.¹⁰⁸ It is capable of infecting any nucleated eukaryotic cell, and has been found in an extensive range of members of the animal kingdom, including birds, marsupials and marine mammals.³⁷ Three forms of the parasite are infectious: metabolically-active tachyzoites, dormant bradyzoites, which form tissue cysts within host cells, and sporulated oocysts, which are found in cat faeces.

The cat – any felid – is the primary or definitive host, being the only animal in which the parasite has a sexual replication cycle.¹⁰⁹ A cat is most likely to become infected after ingestion of a tissue cyst containing bradyzoites.¹¹⁰ Within the cat gut, bradyzoites transform into tachyzoites and schizonts, which undergo rounds of asexual division before producing unsporulated oocysts within the gut epithelium by sexual reproduction.¹¹⁰ Infection in cats is usually subclinical.¹⁰⁹ Most cats shed oocysts only once in their lives, and an infected domestic cat can shed up to 5 million oocysts over a period of two weeks.¹¹¹ Depending on environmental conditions, oocysts undergo sporulation within 5 days of excretion to become infective.¹¹² Sporulated oocysts are

hardy, can survive extremes of temperature and humidity, and are still viable after 28 days at 40 °C.⁶³

Any mammal or bird that supports parasite replication is considered a secondary host, and this group includes humans. Infection in animals can be fatal, and toxoplasmosis is a common cause of abortion in ruminants.¹¹⁰ Intermediate hosts become infected through oocyst-contaminated feed or water, vertically by tachyzoites that cross the placenta, or through ingestion of tissue cysts in the tissue of other secondary hosts. Bradyzoites within tissue cysts transform into tachyzoites and divide by asexual reproduction, which can occur within any nucleated eukaryotic cell. Encysted parasite is usually found in any nucleated intermediate host cell, although brain, retina or muscle tissue is preferred. Cysts are assumed to persist in these tissues for the life of the intermediate host, conferring protective immunity against reinfection.⁶¹

1.4.2 Toxoplasmosis

Adults and children who contract postnatal *T. gondii* infection typically have a low-grade or subclinical disease that is likely influenced by parasite load, virulence and host genetics.¹¹¹ Toxoplasmosis causes a mild and non-specific illness, characterized by cervical lymphadenopathy, headache, myalgia and fever. Severe multi-organ involvement can occur in immunocompromised individuals and rarely, severe clinical syndromes in otherwise healthy individuals have been linked to virulent strains and outbreaks in South America.⁵⁴

Toxoplasmosis infection is confirmed by the presence of anti-*T. gondii* IgM antibodies, which appear 7-14 days after infection, peak at two months, and are usually negative after

eight months, but may persist for two years.^{113, 114} A late marker of infection, IgG, rises 14-21 days post-infection, and persists at a low titre for life, indicating past infection.¹¹⁴ In the last 50 years, researchers in many western countries have documented a decrease in *T. gondii* seroprevalence over time,^{41, 54, 60} but not in Australia, where recent estimates indicate a high seroprevalence of 66%.⁵⁸ The presence of IgG antibodies is significant in women of childbearing age as – with rare exception – they confer protection against vertical transmission of toxoplasmosis from mother to child.⁶¹ The global seroprevalence of IgG in pregnant women is 33%, and ranges from 45% in the Americas to 11% in the Western Pacific region.¹¹⁵

The most common consequence of toxoplasmosis is retinochoroiditis, which can occur at any time, but is most likely within a year of systemic infection. An outbreak of toxoplasmosis affecting 100 people in Canada caused retinochoroiditis in 19 individuals, and occurred on average 6 weeks after symptom onset (range 2-12 weeks).¹¹⁶ Similarly, after a large outbreak in Santa Isabel do Ivaí in Southern Brazil, 290 of 454 individuals who became seropositive for anti-*T. gondii* IgM antibodies were examined, and 11.4% had signs of retinal inflammation when first examined within 4 months of the start of the outbreak.¹¹⁷

The global prevalence of toxoplasmic retinochoroiditis (TRC) shows striking geographic variation. In the United States, an estimated 2% of seropositive individuals have TRC.¹¹⁸ In South America, the infection is at least ten times more common than in the United States,⁵⁴ and parts of Southern Brazil have an 18% prevalence of TRC in the general population.¹¹⁹ A large cross-sectional study in Germany found a prevalence of TRC lesions in 0.2% of the population,¹²⁰ while investigators in Ghana reported a TRC prevalence of 2.3%.¹²¹ A study of referrals to a tertiary uveitis service in the US has noted an overall

decrease in the prevalence of TRC over a 40-year period, and an increase in the proportion of Hispanics presenting with the disease, reflecting higher seroprevalence in this population.¹²²

1.4.3 Clinical features of ocular toxoplasmosis

The necrotizing retinitis caused by *T. gondii* classically presents as a “satellite lesion” of well-circumscribed, dense, creamy-white retinochoroiditis adjacent to a pigmented chorioretinal scar.¹²³ Overlying vitritis can give the appearance of a “headlight in the fog”. In presentations such as these, the diagnosis is straightforward. Necrotizing retinochoroiditis tends to resolve to form a discrete round or oval area of retinochoroidal atrophy with pigmented borders.¹¹⁷ Complications of toxoplasmic retinochoroiditis (TRC) include persistent vitreous opacities, epiretinal membrane, vitreomacular traction and retinal detachment.¹²⁴ Multiple studies have confirmed the finding that TRC is more aggressive in the older population, likely due to reduced cell-mediated immunity. Individuals infected with human immunodeficiency virus (HIV) and suffering from acquired immunodeficiency syndrome (AIDS) are at high risk of TRC, which can be atypical and particularly aggressive.^{125, 126}

In the presence of a characteristic lesion, further testing can include serology, but often is not required.¹²⁷ The aims of treatment of active TRC are to reduce parasite load and prevent inflammatory complications and thus vision loss. No treatment has been shown to kill tissue cysts.¹²⁸ A 2016 Cochrane review found insufficient evidence to support the use of antibiotics to reduce visual impairment in TRC, and weak evidence that treatment reduces the risk of TRC recurrence.¹²⁹ A separate Cochrane review of the use of adjunctive oral corticosteroid therapy could not find any trials that were eligible for inclusion.¹³⁰

Nevertheless, a lack of evidence of benefit does not equate to a lack of benefit, and despite these findings, experts still advocate treatment.¹³¹

1.4.4 Visual outcomes of ocular toxoplasmosis

The visual sequelae of TRC can be serious. Large cohort studies involving adults with active disease found legal blindness (visual acuity worse than 20/200) occurred in at least one eye of 17-24% of participants.^{64, 124} This was most likely due to macular location of the lesion or retinal detachment.⁶⁴ Bilateral blindness was rare, involving only 1-1.6% of participants. A retrospective review of 233 patients attending a tertiary uveitis centre included 159 with active disease and 74 with inactive disease.¹³² Investigators found that young age was the highest predictor of macular involvement, which in turn was the highest predictor of vision loss. At presentation, two-thirds (67%) of those with active disease had a visual acuity of 20/40 or worse, while only 47% of those with inactive lesions had this level of visual acuity. Investigators showed that intraocular inflammation, followed by macular involvement, were the main reasons for poor vision in active disease, and for those with inactive disease, macular scar formation and amblyopia caused vision loss. A retrospective study of 48 patients attending a tertiary uveitis referral centre in Australia reported that the majority of patients (32/48, 67%) recovered visual acuity to 20/30 or better, while a smaller proportion (7/48, 15%) developed severe vision loss (20/200 or worse).¹³³

Visual acuity provides a measure of macular function, but does not account for peripheral retinal function, and 25-40% of individuals with TRC have lesions exclusively outside the vascular arcades.^{64, 124} A study of 61 individuals with quiescent TRC found evidence of visual field damage in 94% of eyes, despite only 41% having reduced visual acuity.¹³⁴

Investigators found that when measuring visual function by field loss, 65% of eyes had moderately severe impairment, compared to only 28% when evaluated by visual acuity. Thus, functional damage associated with TRC can be extensive when evaluated by visual field testing.

1.4.5 Pathology of ocular toxoplasmosis

Our understanding of the tissue changes in TRC has been gleaned largely from histopathological specimens of enucleated eyes. These usually involve cases of advanced disease in the context of immunocompromise or masquerade, and are not commonly reported. The largest case series detailed 53 enucleated globes from healthy adults and was published across two papers in 1952.^{135, 136} Most individuals carried a diagnosis of ocular tuberculosis and their blind, painful eyes showed end-stage disease. More recently, a series of 10 enucleated globes from 10 immunocompetent subjects was published.¹³⁷ Cause of death and reasons for enucleation were not provided, nor were clinical details about the ocular toxoplasmosis, but were presumably cases of active TRC. Extensive areas of retinal necrosis were characterized by the presence of *T. gondii* cysts. The choroid was thickened and showed granulomatous inflammation, with infiltration of B and T lymphocytes and macrophages.

In a series of eight individuals with HIV/AIDs and ocular toxoplasmosis, two individuals had accompanying histopathological specimens that were reported.¹²⁵ The first, a 44 year-old female, underwent an eye wall biopsy, which demonstrated segmental retinal necrosis, lymphocytic infiltration, and tachyzoites and tissue cysts within areas of necrosis. Parasite was also identified in perivascular clusters and within the choroid, which was infiltrated with plasma cells and eosinophils. The second case involved a 28

year-old male who presented with bilateral TRC and died from toxoplasmic encephalitis, which involved extensive necrosis of his brain. Post-mortem examination indicated bilateral peripapillary retinal necrosis and optic nerve extension with infarction on the left, and widespread tachyzoites extending to the cut end of both optic nerves. Tissue cysts were mostly in the nerve fibre and ganglion cell layers but some were seen within inner nuclear and outer plexiform layers. Retinal pigment epithelial cells were necrotic or densely infiltrated with tachyzoites. The choroid demonstrated signs of marked chronic inflammation, and tachyzoites were rarely identified in this tissue. Concomitant and separate areas of cytomegalovirus retinitis were seen in the right eye.

While few series detailing histopathological findings in TRC have been published, sporadic cases have been reported, in the literature and are summarized in Table 1.2. A total of 24 patients (17 male) ranging from 20 to 76 years old are presented. Healthy individuals usually had falsely-negative *T. gondii* serology or severe disease that was not responsive to treatment, while others carried a diagnosis of HIV/AIDs, cancer or hepatitis C. Pathological specimens comprised enucleated globes (9 cases), vitreous biopsies (6 cases), chorioretinal biopsies (5 cases), post-mortem enucleation (3 cases), and eyewall biopsy (1 case).

In these cases, tissue cysts were found in the vitreous, at the vitreoretinal interface, within necrotic retina, at the edge of necrotic retina, in normal retinal tissue, the RPE, and occasionally the choroid. Free tachyzoites were seen throughout the retina and in the vitreous. Subretinal aspirates contained proteinaceous fluid, tissue cysts and eosinophils. The choroid demonstrated granulomatous inflammation, cellular infiltration and in extreme cases, necrosis. The sclera was rarely involved, but occasionally contained tissue cysts, neutrophils and macrophages, which were also seen in the vitreous, vitreoretinal

interface, overlying areas of vasculitis, in the outer retina, and RPE. The pathology described in these cases represented end-stage disease with extensive retinal destruction in blind, painful eyes.

One healthy 46 year-old male in this series died incidentally, during an episode of active TRC in his left eye.¹³⁸ Histopathological examination of his right eye, which contained old TRC scars, found no tissue cysts. The left eye contained a focus of necrotic retina and associated tissue cysts. No cysts were seen within any retinal scars. The choroid was thickened and infiltrated with inflammatory cells, and the sclera was uninvolved. This one case report, published in 1964, is one of the few that document histopathological changes in acute TRC presenting in a healthy individual.

The ultrastructural changes in *T. gondii*-infected cells harbouring bradyzoites have been characterized.¹¹² Tachyzoites infect the host cell and establish themselves within a thin membrane known as a parasitophorous vacuole, where they continue to replicate before lysing the cell and invading neighbouring cells in a pattern that results in tissue destruction.¹³⁹ Some tachyzoites convert to the bradyzoite stage through activation of the transcription factor BDF1, a master switch that controls *T. gondii* differentiation.¹⁴⁰ The vacuole then undergoes reversible ultrastructural modifications into a tissue cyst that protects the parasite from immune recognition and digestive enzymes.¹³⁹ The density of bradyzoites packed within this cyst is variable and dynamic,¹⁴¹ and thus its size can vary greatly.¹¹² Host cell mitochondria associate with the parasitophorous vacuole, creating a peculiar rearrangement of organelles that has been the subject of much research.¹⁴² Encysted bradyzoites measure 20 to 100 μm in the human brain,¹⁴³ and 20 to 40 μm in the human retina.^{144, 145} Published histopathology largely describes the TRC lesions of immunosuppressed individuals with extensive disease. In these patients, encysted

parasite is found within necrotic retina,^{125, 145-154} but has also been identified in the vitreous,¹⁵⁵⁻¹⁵⁸ the subretinal space,^{159, 160}, the choroid,^{161, 162} the optic nerve head,¹⁴⁴ and the sclera.¹⁶³ A post-mortem study of a healthy individual who incidentally died during an episode of active TRC found cysts within necrotic retina and some cysts in normal adjacent retina, but did not identify which layer of the (normal) retina these were found. Curiously, uninvolved scars in this individual's eye were also examined for cysts, but none were identified.¹³⁸

Our ability to understand the pathology of TRC is limited by a lack of retinal tissue specimens in the early stage of disease. Spectral-domain OCT is considered a standard tool in clinical ophthalmology that renders *in vivo*, real-time data on tissue architecture. However, studies evaluating tissue changes in TRC by SD-OCT are limited. The largest case series to date studied 24 eyes and noted signs of tissue alterations including posterior hyaloid thickening, and retinal hyperreflectivity, disorganisation and thickening.¹⁶⁴ Tissue changes that aid diagnosis or indicate prognosis are largely unstudied, and research in this area is warranted in order to fully understand the early stages of this disease.

Table 1.2: Histopathological signs of retinal tissue destruction in toxoplasmic retinochoroiditis

Patient	Clinical details	Ocular diagnosis	Specimen	Findings
54 M ¹⁵⁹	Hepatitis C, systemic corticosteroid Tg IgM negative	TRC	Vitreous biopsy	Vitreous cytology, immunostaining, PCR all negative for Tg; subretinal aspirate showed Tg cysts.
66 M ¹⁴⁷	B cell lymphoma	Blind painful eye	Enucleated globe	Choroidal inflammatory infiltrate; Tg cysts in necrotic retina; Bruch's membrane necrotic.
53 M ¹⁴⁸	Undiagnosed disseminated SCC	Bilateral PU and retinal necrosis	Postmortem enucleation	Numerous Tg cysts in necrotic retina.
38 F ¹⁵⁶	HIV / AIDS	Bilateral PU and retinal necrosis	Vitreous biopsy after 3 PCR-negative AC taps	Vitreous cytology showed Tg cysts; same size as other vitreous cells.
37 M ¹⁶¹	Treated colonic carcinoma	Amelanotic choroidal lesion	Chorioretinal biopsy	Tg cysts within choroidal granuloma and fibroglial tissue.
75 M ¹⁵⁵	Hepatitis C Tg IgM negative	Necrotizing retinitis	Vitreous biopsy	Vitreous cytology showed encysted BZs in vitreous, 20 – 40 µm diameter.
29 M ¹⁶⁵	HIV / AIDS	Panophthalmitis, orbital cellulitis	Enucleated globe	Tg cysts throughout all layers of retina and RPE.
32 M ¹⁵⁷	HIV / AIDS	Bilateral TRC	Vitreous biopsy	Tg cysts passaged and isolated from mouse.
20 M ¹⁶⁶	Healthy; congenital toxoplasmosis	Blind phthical eye	Enucleated globe	Extensive retinal necrosis with secondary gliosis; no acute inflammation, and no Tg seen, but biopsy passaged and cysts isolated from mouse.

Patient	Clinical details	Ocular diagnosis	Specimen	Findings
67 F ¹⁴⁹	Healthy	TRC not responding to treatment	Chorioretinal biopsy after 2 negative vitreous taps	Tg cysts within necrotic retina.
30 M ¹⁶²	Healthy, malaria	Chronic TRC, PU, RD, blind eye	Enucleated globe	Tg passaged and isolated from animals; necrotic retina containing Tg cysts; some in subadjacent choroid.
73 F ¹⁴⁶	Waldenström gammaglobulinaemia	TRC (false negative Tg serology)	Chorioretinal biopsy	Granulomatous inflammatory cell infiltrate in choroid; necrotic retina; numerous Tg cysts.
19 M ¹⁵⁸	Healthy Tg IgG and IgM negative	TRC, PU, RD	Vitreous biopsy	IgG+ vitreous sample; encysted BZ and free TZ in vitreous.
43 M ¹⁶³	HIV / AIDS	Panophthalmitis	Full thickness eye wall biopsy	Necrotic retina, with Tg cysts and TZ; necrotic RPE; choroid and sclera infiltrated with neutrophils and macrophages.
34 M ¹⁶³	HIV / AIDS	Panophthalmitis, orbital cellulitis	Enucleated globe Orbital biopsy	Extensive intraocular necrosis; Tg cysts within necrotic retina, and some in sclera; no Tg seen in orbital biopsy.
35 F ¹⁵⁰ 59 M	HIV, CD4 count 41 HIV, CD4 count 400	Panophthalmitis	Enucleated globe	Encysted Tg present.
61 F ¹⁵⁰	Hypogammaglobulinaemia Steroid treatment	TRC (false negative Tg serology)	Retinal biopsy	Encysted Tg in retina.
58 F ¹⁴⁴	Presumed sarcoidosis Long-term systemic and ocular corticosteroid treatment	TRC, PU, paravascular necrosis	Postmortem enucleation	Cysts 20-40 µm (5-30 BZ) in necrotic retina, RPE, normal retina; free TZ at edge of necrosis and rarely in normal retina; choroidal infiltration.

Patient	Clinical details	Ocular diagnosis	Specimen	Findings
71 M ¹⁶⁰	Corticosteroid treatment	TRC, PU	Retinal biopsy, previous negative vitreous biopsy	Normal retinal tissue; subretinal aspirate contained encysted BZ.
29 F ¹⁶⁰	Corticosteroid and TB treatment	TRC	Vitreous biopsy	Vitreous positive for anti-Tg IgM and IgG; encysted Tg in vitreous.
38 M ¹⁵¹	IVDU, likely AIDS (not tested)	Primary disease TRC, PU	Enucleated globe	Macrophages on ILM, outer retina, choroid; necrotic retina, RPE, free TZ, and cysts in retina; PR and CC destruction, with proliferation of RPE.
76 M ¹⁵²	Healthy	Bilateral TRC, blind painful eye	Enucleated globe	Coagulative necrosis; Tg cysts and TZ throughout retina; necrosis of RPE; diffuse granulomatous inflammation in choroid.
46 M ¹³⁸	Healthy	Active TRC	Post-mortem enucleation (died during active TRC)	RE: no cysts; LE: cysts in necrotic retina, with normal adjacent retina; no cysts in scars; choroid thickened and infiltrated; sclera uninvolved.

Abbreviations: AC = anterior chamber, AIDS = acquired immunodeficiency syndrome, BZ = bradyzoites, CC = choriocapillaris, EM = electron microscopy, F = female, HIV = human immunodeficiency virus, Ig = immunoglobulin, ILM = internal limiting membrane, IVDU = intravenous drug user, LE = left eye, M = male, ON = optic nerve, PCR = polymerase chain reaction, PU = posterior uveitis, RD = retinal detachment, RE = right eye, RPE = retinal pigment epithelium, SCC = squamous cell carcinoma, SRS = subretinal space, Tg = *Toxoplasma gondii*, TRC = toxoplasmic retinochoroiditis, TZ = tachyzoites.

1.5 DENGUE RETINOPATHY

1.6.1 Dengue virus

In the world of viruses, dengue (DENV, *Flavivirus* genus, *Flaviridae* family) is relatively small, with a diameter of only 50 nm.¹⁶⁷ Its icosahedral shape is almost spherical and formed by 90 envelope (E) glycoprotein dimers that surround a lipid bilayer.¹⁶⁸ This houses an 11 kb single-stranded positive-sense RNA genome that is wrapped in nucleocapsid.¹⁶⁹ The three structural proteins - capsid (C), precursor to membrane (prM) and E - serve to protect the viral genome and facilitate entry into the host cell. There are seven non-structural (NS) proteins and these perform multiple functions: NS1 and 2A coordinate viral replication and assembly, NS2B cofactors with NS3 which has helicase and protease functions, NS4A and 4B are involved in membrane reorganization, and NS5 has polymerase and methyltransferase properties, and is involved in RNA synthesis.¹⁷⁰⁻

174

Using receptor-mediated endocytosis to enter cells, DENV binds the C-type lectin CD209 antigen receptor on its principal target, the dendritic cell, but uses multiple other molecules, including phosphatidylserine receptors, to gain entry to other cells.¹⁷⁵ Within the endosome, pH-dependent fusion allows release of viral RNA into the cytoplasm. The genome is positive-sense RNA, and thus ready for translation into one single polyprotein that is subsequently cleaved by host and viral proteases to produce ten proteins (Figure 1.5). The replication strategy of DENV is to hijack the endoplasmic reticulum, which it remodels to create invaginations that protect it from host recognition and allow efficient viral genome replication, protein synthesis, and virion production.¹⁷⁶ Assembled virions

are taxied through an increasingly acidic trans-Golgi network before being released from the cells through exocytosis as mature virus particles (Figure 1.6).⁸

Classification of the illness caused by DENV infection has been simplified to dengue, dengue with warning signs, and severe dengue.¹⁷⁷ Up to a week after the bite of an infected *Aedes aegypti* mosquito, individuals develop fever, rash, myalgia and arthralgia that can last for seven days before defervescence. A critical 48-hour phase follows, during which vascular permeability syndrome and metabolic derangements may occur, which can be fatal. While most people recover after a week, convalescence may be complicated by liver, brain and cardiac involvement, post-viral fatigue, and arthralgia.¹¹ Treatment is supportive as there are no antiviral drugs effective against dengue. With appropriate clinical management, mortality should be near zero, but reported deaths have increased over the last decade, and the average case-fatality rate is between 1-2.5%.^{178, 179} Reasons for the increase in age-standardized death rates include climate, biological, and socioeconomic factors, and the highest death rates are seen in South Asia.¹⁸⁰ Serological investigations confirm DENV infection through reverse transcription polymerase chain reaction (RT-PCR) of viral RNA during early infection, IgM antibodies after day 3 of infection, and IgG antibodies indicating past exposure to DENV.¹⁷⁷

Dengue exists as four serotypes (DENV1, DENV2, DENV3, DENV4) that are all capable of epidemic spread.¹⁸¹ Infection confers lifelong immunity to that serotype, but subsequent infection with a different serotype may cause severe disease.^{182, 183} Repeat infections carry the risk of antibody-dependent enhancement, whereby antibodies generated from a previous infection do not effectively neutralize the newly infecting virus, and instead facilitate entry into and infection of immune cells.¹⁸⁴ This can lead to a fulminant infection

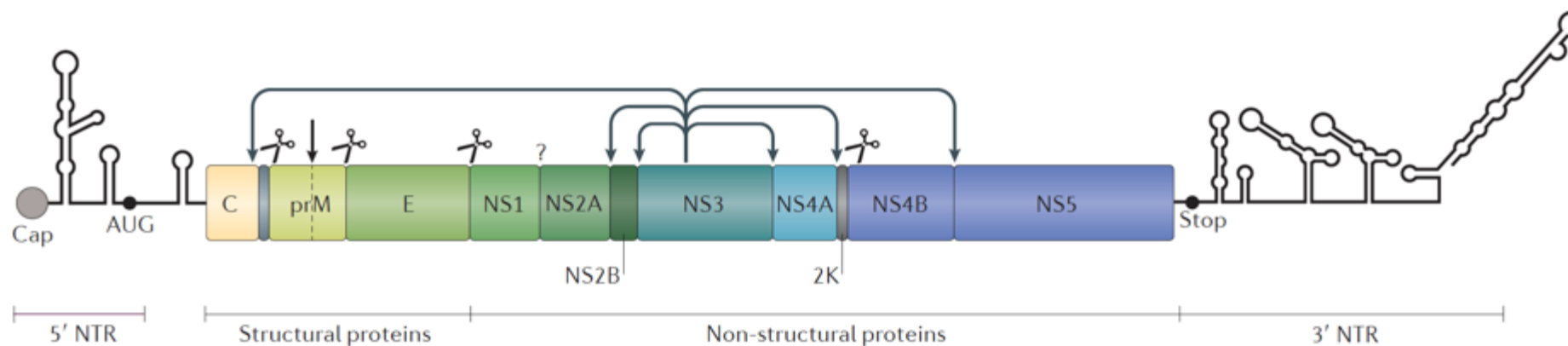


Figure 1.5: Dengue viral proteins

The translated DENV polyprotein is cut by cellular peptidases (scissors), furin protease (short arrow), viral protease (long arrows), and as-yet unknown proteases (?). Structural proteins: capsid protein (C), precursor to membrane (prM), envelope (E). Non-structural proteins: (NS)1-5. Used with permission from Springer Nature: Nature Microbiology (Neufeldt CJ, Cortese M, Acosta EG, Bartenschlager R. Rewiring cellular networks by members of the Flaviviridae family. *Nat Rev Microbiol*).¹⁸⁵ Copyright (2018). **Abbreviations:** C = capsid, DENV = dengue virus, E = envelope, NS = non-structural, NTR = non-translated region, prM = precursor to membrane.

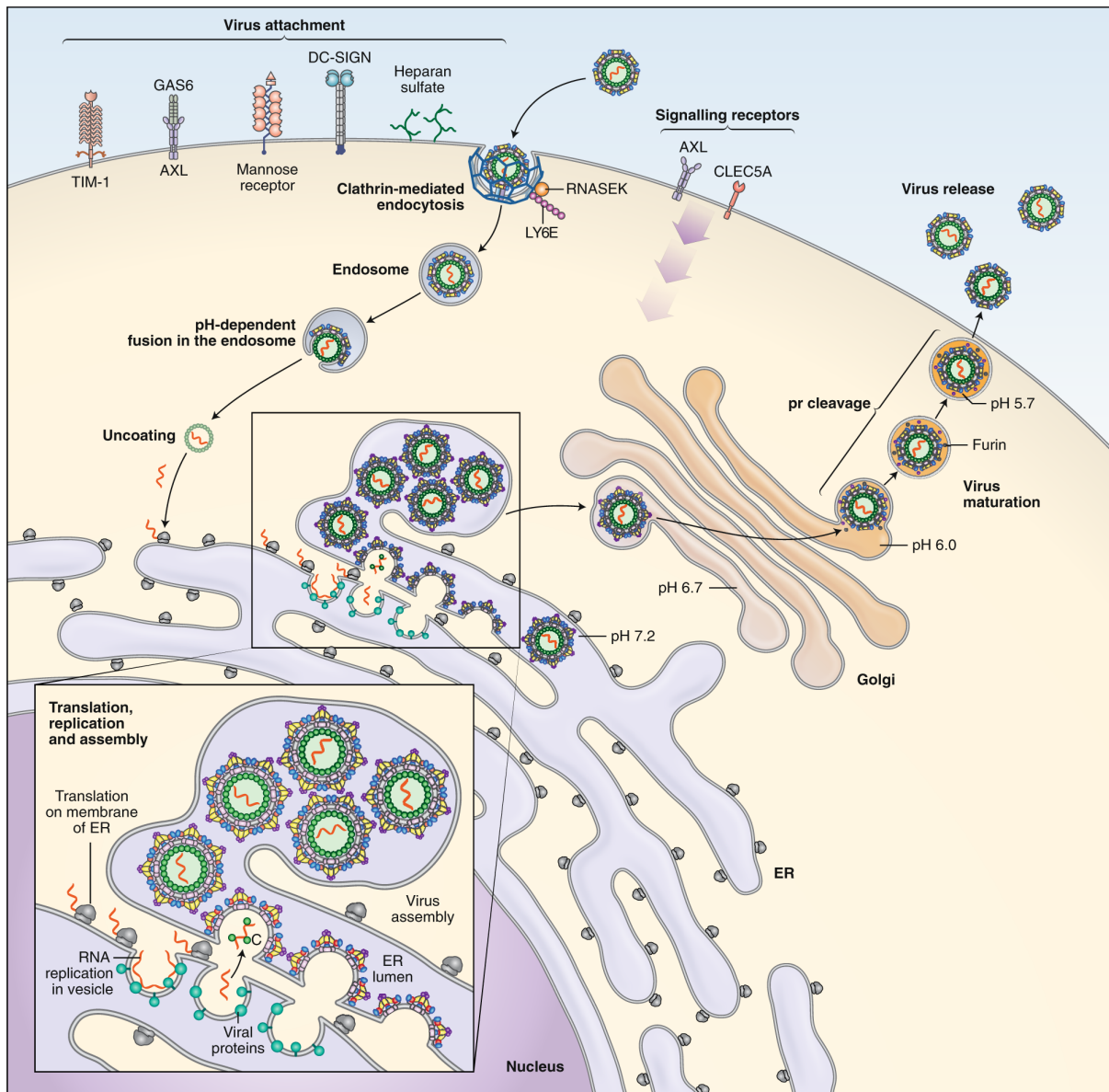


Figure 1.6: Replication cycle of flaviviruses

Flaviviruses attach to cell surface molecules, and interact with signalling receptors to modulate immune responses. The virus enters via clathrin-dependent endocytosis, a transport pathway designed for large molecules. Endosome fusion at low pH enables cytoplasmic release. Positive-sense single-stranded RNA virus proceeds directly to the ribosome for translation. Non-structural viral proteins modify the ER to allow efficient replication and virion assembly that is shielded from immune surveillance. Virus particles traverse the ER as they are formed and mature within the Golgi apparatus before trafficking out of the cell. Used with permission from Springer Nature: [Nature Microbiology](#) (Pierson, T.C., Diamond, M.S. The continued threat of emerging flaviviruses. *Nat Microbiol*).⁸ Copyright (2020). **Abbreviations:** ER = endoplasmic reticulum; RNA = ribonucleic acid.

and severe dengue.^{182, 183} For this reason, the development of an effective vaccine has been extraordinarily difficult. The only licensed dengue vaccine placed seronegative children at higher risk of hospitalisation with severe dengue, and is now only recommended for those with evidence of prior dengue infection, or those at least 9 years of age who live in areas that have high rates of dengue seroprevalence.¹⁸⁶

1.5.1 Clinical manifestations of dengue retinopathy

Infection with DENV is associated with a wide range of ocular phenotypes, and ocular complications have long been associated with DENV.¹⁸⁷⁻¹⁹⁰ Retinopathy is the most common complication, and involves the macula in the majority of cases.¹⁹¹⁻¹⁹⁴ Cross-sectional studies performed during epidemics provide the best estimates of prevalence. DENV1 was largely responsible for the 2005 epidemic in Singapore, and during this time nearly 200 hospital inpatients with dengue were examined.¹⁹³ Excluding those in intensive care, maculopathy was found in 10% of seropositive inpatients. Affected individuals had a mean complement C3 level lower than those without maculopathy, tended to be young adults, and were either asymptomatic or had ignored their symptoms.¹⁹³ A smaller cross-sectional study during the 2007 Singapore epidemic that largely involved the DENV2 serotype, found no maculopathy or eye symptoms in DENV-positive inpatients.¹⁹⁴ These inpatients tended to be older, and had milder liver impairment compared to the 2005 cohort, suggesting that maculopathy and ocular complications may be related to serotype or virulence.

The features of dengue-related maculopathy were addressed in a study using time-domain OCT.¹⁹⁵ Visual outcomes and macular changes were detailed in 74 eyes of 41 patients. Visual changes tended to coincide with the nadir of thrombocytopenia, about 7

days after onset of systemic symptoms. Three phenotypes of maculopathy were described: diffuse retinal thickening (type 1), which had favourable visual outcomes; cystic macular oedema (type 2), and foveolitis (type 3), characterized by outer retinal thickening and hyper-reflectivity on OCT. Foveolitis, described as a yellow or orange subretinal dot, is widely associated with, and characteristic of, dengue maculopathy.¹⁹²

While retinal haemorrhages are a common association with dengue, unusual presentations include vasculitis, acute posterior multifocal placoid pigment epitheliopathy, acute zonal occult outer retinopathy, acute macular neuroretinopathy, foveolitis and retinochoroiditis.¹⁹⁶⁻²⁰³ The visual prognosis of these manifestations varies. For maculopathy, visual acuity improved to better than 20/40 in 80 percent of eyes at 2 years, but all eyes with foveolitis retained visual field defects.¹⁹⁵ Persistent scotomas in the presence of good visual acuity are also a feature of acute macular neuroretinopathy, and reflect ischaemic damage to the outer retina.^{197, 204}

1.5.2 Pathogenesis of dengue retinopathy

Little is known about the mechanisms of dengue retinopathy. Published studies largely focus on cellular components of the BRB, which are permissive to infection with DENV.^{205,}
²⁰⁶ A study comparing primary human retinal endothelial cells, retinal pigment epithelial cells and the cell line ARPE-19 demonstrated that DENV-infected retinal pigment epithelial cells generated a stronger type I IFN response compared to endothelial cells, and that endothelial cells demonstrated increased expression of cell adhesion molecules in response to infection.²⁰⁵ The barrier function of infected RPE was reduced, but endothelial cell monolayers showed similar results to uninfected controls, with concomitant expression of tight and adherens junction transcripts. This experiment used

Mon601, a recombinant laboratory-based DENV2 isolate, and comparison with a DENV2 isolate from an infected human generated similar results.

Another study addressed the differential response of endothelial cell populations to infection with DENV.²⁰⁷ Human microvascular endothelial cells from skin, lung, brain and retina were subjected to infection with DENV serotypes 1 through 4. The presence of junctional proteins was identified by western blot, and inflammatory cytokines, chemokines and adhesion molecules were detected by flow cytometry. Investigators demonstrated that vascular permeability varied by endothelial cell population and viral serotype. In retinal endothelial cells, cytokine production in DENV1 infection was highly increased, while C-C motif chemokine ligand 5 (CCL5) was the most abundant cytokine produced. Retinal endothelial infection caused loss of barrier function through reduced intercellular adhesion and increased cell membrane permeability. Across the virus serotypes, DENV1 caused an immediate reduction in cell membrane permeability, followed by increased permeability, whereas the opposite pattern was seen with infection with DENV serotypes 2-4.

These data indicate that barrier function of the outer BRB is impaired with DENV infection, and that infected retinal pigment epithelial cells generate a robust antiviral response. The endothelial cell layer of the inner BRB appears to be more resilient in terms of its ability to maintain intercellular connections. Compromise of the outer BRB during infection exposes the outer retina to direct invasion by the virus, plus potentially harmful fluid shifts and leakage of intravascular components into retinal tissue.

Transcriptome profiling of retinal pigment epithelial cells infected with Zika, dengue and other flaviviruses demonstrated differential molecular gene expression signatures.²⁰⁶ Zika virus and DENV both induced expression of ATP-binding cassette sub-family G

member 1, a membrane transporter of cholesterol and a modulator of innate immune responses in macrophages, and suppression of this gene reduced infectivity of Zika virus. Infected cells also upregulated tumour necrosis factor (TNF) ligand superfamily member 13B, a cytokine and potent B cell activator, but at lower levels in DENV-infected cells. Similar patterns of suppression were seen for aldehyde dehydrogenase 5 family member A1, a mitochondrial enzyme implicated in neurological diseases, and choroideremia-like Rab escort protein, which mediates intracellular trafficking.

A study of murine Müller cells in Zika virus infection that used DENV as a control demonstrated that this cell population was easily infectible with DENV, and that p38 mitogen-activated protein kinase is a critical molecule in the cellular response to infection and induces the expression of chemokine (C-X-C motif) ligand 1, C-C motif chemokine ligand 2, chemokine (C-C motif) ligand 7, and vascular endothelial growth factor.²⁰⁸ Müller cell infection resulted in pro-inflammatory responses that were stronger with Zika virus infection compared to DENV, indicating distinct but overlapping cellular responses to infection between the two flaviviruses.²⁰⁸

Advances in retinal imaging provide some clues as to the pathogenesis of dengue maculopathy. A recent series evaluated dengue maculopathy in 32 eyes of 16 individuals using multimodal imaging.²⁰⁹ All participants had demonstrable vitreous cells, and outer plexiform and outer nuclear layer hyperreflectivity on swept-source OCT, with deep capillary plexus flow deficit on OCT angiography. Fundus photography showed a grey-white foveal reflex. In most cases, fluorescein angiography appeared normal, and disruption of the outer retinal hyperreflective bands (external limiting membrane, ellipsoid zone, phagosome zone of RPE) was noted. At follow-up, all eyes showed outer plexiform thinning and deep capillary plexus flow deficit. These signs point to outer

retinal damage caused by both ischaemia and inflammation, likely in the form of immune complex deposition in the watershed zones of the deep capillary plexus of the retina. Similar OCT changes can be seen in acute macular neuroretinopathy, which is associated with dengue and other viral infections, and caused by ischaemia at the level of the deep capillary plexus.¹⁹⁶⁻¹⁹⁹

Taken together, research indicates that multiple ocular cell populations are susceptible to infection with DENV, that retinal pigment epithelial cells forming the outer BRB mount a stronger antiviral response than retinal endothelial cells, and that infected RPE demonstrates more dysfunction to its barrier properties than endothelial cells of the inner blood-retinal barrier. Müller cells are also permissive to infection and mount an anti-inflammatory response. Ischaemic damage to the outer retina due to occlusion of tiny capillaries in the deep capillary plexus results in persistent scotomas. The macular oedema seen in DENV infection may be due to host inflammatory responses to the virus, ischaemia and dysfunction of critical components of the blood-retinal barrier, direct infection of cells involved in retinal fluid homeostasis, or a combination of these processes.

1.6 POST-EBOLA UVEITIS

1.6.1 Ebola virus

The *Ebolavirus* genus forms part of the *Filoviridae* family of the *Mononegavirales* order: enveloped, non-segmented, negative-polarity RNA viruses.²¹⁰ These viruses infect primates, bats, swine and possibly fish.²¹¹ Six antigenically-distinct viral species have

been identified: *Zaire*, *Sudan*, *Tai Forest*, *Bombali*, *Reston* and *Bundibugyo ebolavirus*.²¹¹ All species except *Reston* and *Bombali ebolavirus* cause disease in humans.^{212, 213} *Zaire ebolavirus* (EBOV) is responsible for the majority of epidemics of EVD in humans.^{32, 214}

Named for their filamentous form (Latin *filum*, thread), filoviruses are extremely large. They have a diameter of 98 nm and a variable length that can extend beyond 20 µm. Filovirus genomes are 15-19 kb long and encode seven genes: nucleoprotein (NP), viral protein (VP)24, VP30, VP35, VP40, glycoprotein (GP) and large protein (L) (Figure 1.7A).²¹¹ The virus is polypliodal, harbouring multiple copies of its RNA genome within an extremely long virus. Due to its size, the virus must be assumed into the cell via micropinocytosis. Through a process of “apoptotic mimicry”, the virus coats itself with lipid found in the inner leaflet of cell membranes, which host cells recognize as a sign of apoptosis and a cue to phagocytose the virus.²¹⁵ The genome is then released into the cytoplasm in a pH-dependent process (Figure 1.7B). The L protein functions as an RNA-dependent RNA polymerase enzyme. Replication of the viral genome requires L, NP and VP35 proteins, which, with VP30, transcribe the negative-sense genome into mRNA. Virion assembly and release is driven by VP40, which with VP35 and VP24 also functions to antagonize type 1 IFN signalling.²¹⁶

1.6.1 Ebola Virus Disease

Ebola virus disease is a haemorrhagic illness caused by infection with Ebola virus species in humans. After an incubation period of up to three weeks, fever, sore throat, headache, myalgia and fatigue are characteristic. Diarrhoea, vomiting, rash and bleeding complications follow. Recovery or deterioration occurs a few weeks later. Hepatic,

Figure 1.7: Filovirus genome and life cycle

(A). Ebola viruses encode a negative-sense single-stranded RNA genome that has characteristically long 3' and 5' non-coding sequences surrounding seven genes encoding: NP, VP24, VP30, VP35, VP40, GP and L. Filoviruses have unusually long non-coding regions at the 5' and 3' ends of their mRNAs. (B). Filoviruses attach to cell surface molecules through interactions with the viral surface GP, and enter the cell via clathrin-dependent endocytosis, a transport pathway designed for large molecules. Progressive reduction of the endosomal pH as the virus trafficks through the cell causes a conformational change which releases viral contents into the cytoplasm. The negative-sense RNA genome then undergoes transcription into mRNA and replication of the virus genome. Viral proteins are translated and particles are assembled at the plasma membrane before release of virions by budding. Used with permission from Springer Nature: [Nature Reviews Microbiology](#) (Messaoudi, I., Amarasinghe, G. & Basler, C. Filovirus pathogenesis and immune evasion: insights from Ebola virus and Marburg virus. *Nat Rev Microbiol*).²¹⁰ Copyright (2015). **Abbreviations:** GP = glycoprotein; L = large protein; mRNA = messenger ribonucleic acid; NP = nucleoprotein; VP = viral protein.

respiratory and renal impairment is common, and death is associated with systemic shock, and electrolyte, metabolic and coagulation derangements. Suspected, probable, and definite case definitions of EVD vary, depending on the physical location of the individual and whether it occurs in the context of an outbreak, but high fever, bloody diarrhoea and haematuria are classic signs.²¹⁷ Laboratory detection of serum anti-EBOV IgM antibodies or EBOV RNA by RT-PCR and/or the isolation of EBOV confirm the diagnosis.

A range of experimental antiviral drugs have been administered to patients,²¹⁸ including convalescent serum and monoclonal antibody cocktails, but clinical trials of these have failed to prove efficacy.^{219, 220} The mainstay of treatment is supportive and involves fluid rehydration. A vaccine expressing EBOV surface glycoprotein in a recombinant vesicular stomatitis virus vector was implemented in three phase II/III trials across West Africa in 2015 in a randomized, unblinded, ring-vaccination trial without placebo.²²¹ No participants developed EVD, but oligoarthritis, dermatitis and vasculitis occurred in some participants, motivating the development of other recombinant vaccines.²²² The case-fatality rates of EVD vary markedly and range from 40-90% in outbreaks.²¹⁸ Those who survive experience fatigue, myalgia, arthralgia, gastric pain, auditory and psychiatric sequelae, as well as uveitis, in what is known as post-EVD syndrome.²²³⁻²²⁵

1.6.2 Clinical manifestations of post-Ebola uveitis

The association of uveitis with EVD was widely recognized with the case of a US physician repatriated from Sierra Leone in 2014 with EVD.²²⁶ He survived multiorgan failure and nine weeks after resolution of viraemia, presented with photophobia and a foreign body sensation. He had no intraocular inflammation at that point but was noted to have

multiple pigmented chorioretinal scars with hypopigmented haloes scattered in his retinal periphery. A diagnosis of inactive chorioretinitis was made. One month later, he presented with iris heterochromia and a unilateral hypertensive anterior uveitis that progressed despite intensive topical treatment. Due to his worsening inflammation, an anterior chamber paracentesis was performed and EBOV RNA was confirmed by quantitative reverse transcription polymerase chain reaction (RT-qPCR). He deteriorated, developed scleritis and panuveitis, and was treated with systemic corticosteroids and an experimental antiviral drug. Three months after the onset of inflammation, his uveitis resolved, the heterochromia reversed, and vision in that eye returned to 20/15.

Rates of uveitis in survivors of the West Africa outbreak vary, affecting up to a third of survivors, who present on average 3 to 8 weeks post-discharge from the Ebola treatment unit.²²⁷⁻²²⁹ Risk factors for developing uveitis include a high viral load whilst in the treatment unit, presumed conjunctivitis during the acute phase of disease, and older age.²²⁸⁻²³⁰ In one study, uveitis was ten times more likely if survivors had displayed red eyes during their acute disease.²²⁹ Length of Ebola treatment unit stay and systemic symptoms (hair loss, hearing impairment, arthralgia, arthritis) were not associated with the development of uveitis.³⁴

Post-Ebola uveitis was most often unilateral but was bilateral in up to a third of cases.²²⁸ Anatomic location was anterior in almost half of cases, while posterior or panuveitis occurred in about a quarter of cases respectively.^{227, 228} Retinal pigment epithelial scars with hypopigmented borders were more common in survivors who developed uveitis.³⁴ The visual prognosis of EVD survivors was unfavourable, and those who developed uveitis had significantly worse vision than those who did not. In one study of 96 survivors,

nearly 40% of those with uveitis were blind (visual acuity worse than 20/400).³⁴ White cataract was associated with hypotony in EVD survivors, surgery in these eyes increased the risk of progression to phthisis bulbi.²³¹ The persistence of virus in ocular fluid was not permanent, as is the case for other immune-privileged sites. At median 19 and 34 months post EVD, all 50 survivors tested negative for EBOV RNA in aqueous and vitreous samples, respectively.

1.6.3 Pathogenesis of post-Ebola uveitis

The pathogenesis of post-Ebola uveitis is poorly understood. Biosafety level 4 laboratory requirements mean that only a very small pool of researchers are able to work with EBOV, and as such, little has been done in this space. Ocular examination during the acute phase of EVD, and histopathological studies of human ocular tissue have not been reported. Case reports of ocular involvement after recovery from EVD in macaques have been published. A series of six macaques that recovered from EVD and survived longer than expected, had signs of EBOV infection with viral antigen in the epithelium, stroma and endothelium of the cornea, as well as in the brain, pancreas, thyroid and lung – sites that are not primary targets of the virus.²³² Another report detailed necropsy of a macaque that had an apparent recovery from EVD before developing unilateral scleritis, conjunctivitis, peri-optic neuritis and multi-organ involvement.²³³ An example of extended persistence was seen in the case of a 39 year-old EVD survivor who developed meningoencephalitis with live EBOV isolated from cerebrospinal fluid, 9 months after discharge from the treatment unit.²³⁴ These cases demonstrate viral persistence despite clinical recovery, with reservoirs in organs that have privileged immunity.

The identification of pigmented retinal scars before the onset of florid uveitis with replicating virus in an EVD survivor pointed to the RPE as a potential reservoir of EBOV in the eye.³⁵ Researchers demonstrated that the human retinal pigment epithelial cell line, ARPE-19, supported productive EBOV infection, and bioinformatic analysis of the host transcriptome of these infected cells implicated a strong type I IFN response.²³⁵ The finding that infected retinal pigment epithelial cells still produced IFN- β in spite of EBOV infection was unexpected, given the profound type I IFN suppression seen in other cell populations infected with EBOV, such as dendritic cells and mononuclear phagocytes.^{217,}

236

Persistent and asymptomatic EBOV infection was investigated through research involving non-human primate participants of EBOV therapeutic trials.²³⁷ Animals were humanely euthanized according to clinical criteria, and could be separated into three groups: those that died during acute, lethal EVD; survivors that deteriorated early, and demonstrable EVD survivors. By *in situ* hybridization of archived histological specimens, CD68-positive cells containing EBOV RNA were identified in the vitreous, internal limiting membrane, uveal tract, and surrounding retinal vessels of survivors, implicating macrophages as a niche for EBOV persistence.²³⁷ Non-human primate survivors also showed signs of reactive gliosis in Müller cells that extended into the inner and outer nuclear layers of the retina, indicating active chronic repair mechanisms.

Primates that had been euthanized during acute lethal EVD had no sign of EBOV RNA in parenchymal ocular tissue, but genomic RNA indicated extraocular infection involving the meninges. In addition to these sites, those primates that survived longer than expected showed EBOV RNA in sclera and connective tissue, and in one case, also had EBOV RNA in the vitreous.²³⁷ These results suggested to investigators that the route of EBOV infection

may occur initially via the optic nerve meninges before adjacent spread. Moreover, those who survived had more time to clear the virus from these tissues, leaving only intraocular reservoirs of EBOV. Optic nerve spread of EBOV was speculated as a route of viral migration by investigators who documented peripapillary retinal lesions that were sharply angulated, pale grey, respected the horizontal raphe, and spared the fovea in 14 human EVD survivors.²³⁸

The same researchers also published a study of EVD survivors examined on two occasions an average of 12 months apart. They documented the expansion and regression of “dark without pressure” retinal lesions in 10 of 57 (18%) survivors.²³⁹ None of these individuals showed signs of intraocular inflammation. “Dark without pressure” is not a sign specific to EVD and has been described in other conditions,^{240, 241} including as a “shadow sign” that disappears over time and lies anterior to congenital hypertrophy of the RPE lesions in young pigmented myopic individuals.²⁴² Imaging of dark-without-pressure areas shows changes at the level of the outer retina, demonstrating hyporefectivity of the ellipsoid layer on SD-OCT.²⁴³ In EVD survivors, these lesions may reflect virus-induced subclinical inflammation. A study of cytomegalovirus (CMV) retinitis in an immunocompetent murine model elegantly demonstrated that after infection of immunocompetent hosts, CMV was absent from the retina, and retinal OCT was normal, yet evidence of ongoing and sustained inflammation was proven by immunohistology and flow cytometry.²⁴⁴ White cataract is associated with EVD,^{245, 246} and may be an overt manifestation of chronic low-grade inflammation.²⁴⁷

Marburg virus, a filovirus closely related to EBOV, produces a similar disease phenotype to EVD.^{210, 248-250} Reports of post-convalescent uveitis with viral isolation from the anterior chamber date back to the 1970s.^{251, 252} Recently published research into Marburg

virus disease mechanisms in the macaque model demonstrated viral persistence in immune-privileged sites, including the eye.²⁵³ Investigators probed histological specimens by immunohistochemistry for Marburg virus VP40 and GP proteins, and viral RNA, by *in situ* hybridisation. All six macaques showed evidence of uveal involvement with widespread infiltration of infected macrophages, which were seen as iris perivascular infiltrates (in 3/6 macaques) and uveal emboli (in 5/6 macaques). Viral RNA and antigens were detected in iris stroma, ciliary body epithelium and/or ciliary body stromal fibroblasts in all macaques, throughout the trabecular meshwork in half the animals, and RNA was found in the vitreous of all macaques. Curiously, two animals showed viral genomic RNA in discrete patches located in the inner nuclear layer of the retina, encompassing the first report of filovirus infiltration of the neural retina. These macaques were euthanised at a relatively early stage of disease, and demonstrated involvement of the uveal tract, retina and vitreous early in the course of disease.

In summary, histopathology of ocular tissue from non-human primates demonstrates that in the acute phase of EBOV infection, intraocular tissue is infiltrated with infected macrophages, and evidence of viral infection is found throughout the vitreous, choroid, and within the retina. Signs of repair include the formation of reactive gliosis involving Müller cells, and late in the disease course, virus is cleared from extraocular compartments, leaving reservoir populations that include macrophages.^{237, 253} Pigmented retinal scars in human survivors point to retinal involvement in the acute phase, and migratory outer retinal changes may indicate subclinical outer retinal inflammation.³⁴ Viral reservoirs associated with post-convalescent uveitis are presumably cleared, as EVD survivors who attend for cataract surgery show no evidence of viral RNA on ocular fluid testing, and cataract surgery itself does not induce further uveitis.²⁴⁵

1.6.4 Summary of mechanisms of zoonotic retinal infections

Zoonotic diseases form the bulk of emerging infections and are responsible for epidemics and pandemics that impact global health and security. Many of these pathogens cause ocular complications, and infection of the retina often results in visual impairment. The pathophysiology of infection in retinal tissue is poorly understood for a number of reasons, including the biosafety requirements of research with dangerous pathogens, the fact that these infections disproportionately affect lower income countries with limited research capacity, and the inherent challenges involved in the study of retinal disease due to a lack of tissue specimens. In consequence, indirect means of studying tissue alterations in the context of infection must be sought.

Dengue is a flavivirus that represents an important class of epidemic vector-borne zoonoses. In spite of growing prevalence of this infection in humans, the mechanisms of retinal complications are largely unstudied. Maculopathy occurs in up to 10% of those hospitalised with dengue,¹⁹³ and characteristic changes include foveolitis and macular oedema.¹⁹⁵ Ocular cell populations that comprise the inner and outer BRBs have been shown to be infectable with DENV, and infected retinal pigment epithelial cells mount a strong type I IFN response.²⁰⁵ Infected retinal endothelial cells increase their expression of cell adhesion molecules, which mediate leukocyte trafficking into the retina.^{205, 254} Disruption of BRB function occurs after infection with DENV, and this is more apparent with retinal pigment epithelial cell monolayers compared to retinal endothelium,²⁰⁵ and endothelial barrier dysfunction varies by viral serotype.²⁰⁷ Little is known about other retinal cell populations in the context of dengue maculopathy. Murine Müller cells infected with DENV as a control for experiments on Zika virus are permissive to infection and mount an anti-inflammatory response of lower magnitude than with Zika virus

infection.²⁰⁸ Taken together, components of the blood-retinal barrier are targets of DENV, and infection stimulates production of inflammatory and anti-viral molecules, and compromises the vascular barrier function.

Despite a century of research, outbreaks and sporadic cases of toxoplasmosis and toxoplasmic retinochoroiditis continue to occur,²⁵⁵ and there is still no treatment that eliminates encysted parasite from tissue.^{71, 110} Our understanding of disease mechanisms of *T. gondii* infection of the retina is far from complete. Knowledge gaps include understanding which individuals are at risk of infection, why recurrences occur, and the mechanisms of retinal infection and recurrence.^{118, 131} Clinical tools for evaluating the retina such as SD-OCT are now part of standard practice, yet little is known about early tissue changes in toxoplasmic retinochoroiditis. The largest series OCT changes involved 24 individuals,¹⁶⁴ but the characteristics of retinal tissue changes, and signs that indicate prognosis in acute disease are unstudied.

Ebola is a deadly virus that continues to cause epidemics from repeated spill over into the human population.²¹⁷ A significant proportion of survivors develop ocular complications in the convalescent phase, and this carries a high burden of disability due to involvement of the retina.^{32, 34, 256, 257} Viral persistence has been demonstrated in immune-privileged organs including the eye,³⁵ and involvement of ocular tissue early in the course of disease is seen in both EBOV and Marburg virus infection of non-human primates.^{237, 253} Ocular tissue in these animals show widespread ocular infiltration of infected macrophages, while viral RNA is commonly found in the vitreous and vitreoretinal interface, and rarely, within the inner nuclear layer of the retina early in the disease process.^{237, 253} Human survivors show a spectrum of retinal scars, white cataract, and uveitis, demonstrating profound inflammatory responses to EBOV infection.^{34, 238, 246} Studies of a human retinal

pigment epithelial cell line indicate that these cells mount a robust type I inflammatory response while supporting concomitant productive infection with EBOV, a combination of responses not seen in other cell populations.²³⁵

1.7 AIMS OF THE THESIS

The overall aim of the work described in this thesis was to identify and address unanswered questions relating to the mechanisms of retinal involvement in diseases caused by three zoonoses: *T. gondii*, DENV and EBOV. Using translational research methods that include cell culture and molecular biology techniques, bioinformatic processes, and clinical imaging tools, these knowledge gaps were addressed. It was anticipated that the ultimate result of this work would be better understanding of the processes of infection with these pathogens in the retina. Specifically, the objectives of the work presented in this thesis were:

- To demonstrate the pathological changes of retinal tissue in active toxoplasmic retinochoroiditis by *in vivo* imaging using SD-OCT.
- To identify signs of retinal tissue damage on SD-OCT that indicate visual prognosis in a large patient cohort with active disease.
- To understand whether human Müller cells are permissive to infection with DENV.
- To interrogate the responses of primary human Müller cells and a human Müller cell line to infection with different DENV strains and serotypes.
- To investigate the impact of EBOV VP35 on the type I IFN response of human retinal pigment epithelial cells.

- To further understand the role of the retinal pigment epithelial cell in post-Ebola uveitis through interrogation of RNA sequencing and bioinformatics *in silico* predictions of molecular targets of EBOV-infected retinal pigment epithelial cells.

CHAPTER 2

Materials and Methods

2.1	Spectral-domain optical coherence tomography study.....	59
2.1.1	Patient selection and human ethics statement.....	59
2.1.2	Ophthalmic examination and diagnosis	59
2.1.3	Optical coherence tomographic imaging and interpretation.....	60
2.1.4	Treatment and follow-up schedule	61
2.2	Laboratory biosafety.....	62
2.3	Chemicals and reagents.....	62
2.3.1	Buffers and solutions.....	62
2.3.1.1	<i>Phosphate-buffered saline</i>	62
2.3.1.2	<i>Tris base, acetic acid and EDTA buffer</i>	63
2.3.1.3	<i>Dulbecco's Modified Eagle Medium</i>	63
2.3.1.4	<i>Luria Bertani broth</i>	63
2.3.2	Antibodies.....	64
2.4	Eukaryotic cells.....	68
2.4.1	Cell lines and culture medium	68
2.4.1.1	<i>ARPE-19 cell line and medium</i>	68
2.4.1.2	<i>MIO-M1 cell line and medium</i>	68
2.4.1.3	<i>Vero cell line and medium</i>	68
2.4.1.4	<i>C6/36 cell line and medium</i>	69

2.4.2	Primary human retinal cells.....	69
2.4.2.1	<i>Primary human ocular cell isolation</i>	69
2.4.2.2	<i>Primary human Müller cell characterisation</i>	69
2.4.3	Cell culture techniques	71
2.4.3.1	<i>Cell maintenance</i>	71
2.4.3.2	<i>Cell monolayer dissociation</i>	71
2.4.3.3	<i>Cell counting</i>	71
2.4.3.4	<i>Freezing cells</i>	72
2.4.3.5	<i>Thawing cells from cryopreservation</i>	72
2.4.3.6	<i>Mycoplasma testing</i>	73
2.5	Viruses	74
2.5.1	Virus strains	74
2.5.2	Viral infections.....	76
2.5.3	Plaque assays.....	77
2.5.4	Immunostaining.....	78
2.5.5	Interferon-beta immunoassay.....	79
2.6	Reverse transcription-polymerase chain reaction.....	79
2.6.1	RNA Extraction.....	79
2.6.2	Complementary DNA synthesis.....	80
2.6.3	Oligonucleotides and primers.....	81
2.6.4	Gradient polymerase chain reaction	81
2.6.5	Quantitative real-time polymerase chain reaction	81
2.6.6	Data analysis.....	82
2.7	Western blotting.....	82
2.7.1	Preparation of cell lysate.....	82
2.7.2	Protein quantitation	83
2.7.3	Protein separation by gel electrophoresis.....	84
2.7.4	Gel transfer	85
2.7.5	Antibody staining.....	85
2.8	Restriction enzyme-based subcloning.....	86

2.8.1	Sub-cloning new plasmids	86
2.8.1.1	<i>Creation of no-vector plasmid</i>	86
2.8.1.2	<i>Creation of pCAGGS-FLAG-VP35 plasmid</i>	88
2.8.2	Subcloning techniques.....	88
2.8.2.1	<i>Double restriction endonuclease digestion</i>	88
2.8.2.2	<i>DNA separation by electrophoresis</i>	92
2.8.2.3	<i>DNA purification</i>	92
2.8.2.4	<i>DNA quantification</i>	93
2.8.2.5	<i>DNA ligation</i>	93
2.8.3	Preparation of competent cells	94
2.8.3.1	<i>Preparation of agar plates</i>	94
2.8.3.2	<i>Transformation of competent cells</i>	94
2.8.3.3	<i>Growth of plasmid-expressing bacteria</i>	95
2.8.3.4	<i>Plasmid harvest by maxipreparation</i>	95
2.8.4	Sequencing	95
2.9	Cell transfection with VP35 plasmid and Poly I:C.....	96
2.10	Microscopy.....	97
2.10.1	Cell photography and image processing.....	97
2.11	Bioinformatics.....	98
2.11.1	RNA sequencing.....	98
2.11.2	Data processing and differential expression analysis.....	98
2.11.3	Target predictions for microRNA.....	99
2.11.4	Pathway and network analyses	100
2.12	Statistical analyses	100

2.1 SPECTRAL-DOMAIN OPTICAL COHERENCE TOMOGRAPHY STUDY

2.1.1 Patient selection and human ethics statement

From January 14th 2015 to November 16th 2017, consecutive patients diagnosed with toxoplasmic retinochoroiditis (TRC) and aged over 12 years were prospectively recruited at the Uveitis Clinic at Ribeirão Preto General Hospital. This tertiary referral clinic serves a population of approximately 1.7 million people in the State of São Paulo, Brazil, where the seroprevalence of toxoplasmosis is approximately 60%.²⁵⁸ The Ethics Committee in Human Research at Ribeirão Preto General Hospital, São Paulo, Brazil, approved this study (protocol number: 46015415.2.0000.5440).

2.1.2 Ophthalmic examination and diagnosis

Patients had a complete ophthalmic examination, including measurement of best-corrected Snellen visual acuity and dilated fundus examination. Toxoplasmic retinochoroiditis was classified by clinical and serological criteria. Lesions were grouped into primary (active retinochoroiditis without chorioretinal scarring), recurrent (active retinochoroiditis with chorioretinal scarring) and inactive (chorioretinal scarring alone). Chorioretinal scars were variably pigmented, and active disease was indicated by retinal whitening, vitritis, and vitreous haze.²⁵⁹ Only individuals with active TRC were included in this study, and any patient with co-existing, unrelated retinal pathology was excluded.

Active TRC was defined as a focus of retinochoroiditis with a positive serological test for *Toxoplasma gondii* immunoglobulin (Ig)G.¹³¹ Serological testing for *T. gondii* IgM and human immunodeficiency virus (HIV) IgG was also performed, and additional HIV tests included enzyme-linked immunosorbent assay and western blot. When the diagnosis was uncertain, aqueous and vitreous humour was tested for *T. gondii* DNA by PCR. Individuals who were HIV-positive had serological testing for syphilis. Documented medical history locating the time of infection was required to classify TRC as congenital or postnatally acquired. Zone of disease was designated by location of the posterior edge of the lesion, per Holland et al.²⁶⁰ Zone 1 lesions extended to within 3000 µm of the fovea and/or 1500 µm from the optic disc margin. Zone 2 lesions were located between zone 1 and the equator. Zone 3 lesions were positioned anterior to the equator, and were excluded as SD-OCT in this location was not possible.

2.1.3 Optical coherence tomographic imaging and interpretation

The posterior pole and lesion were imaged by colour photography and SD-OCT, as permitted by media clarity. Spectral-domain OCT scans were acquired using the Spectralis® HRA+OCT (Heidelberg Engineering) and analysed with Eye Explorer software (Heidelberg Engineering, v.6.9.4.0). Automatic real time mode was selected, with 24 frames per location, using volume scans of the macula and lesion (20 x 15 degree area formed by 19 B-scans, each separated by 242 µm), single slice acquisition and in some cases, single-slice enhanced-depth imaging (EDI).

An SD-OCT scan was considered gradable if features at the vitreoretinal interface could be resolved. Patients whose presentation scans were not gradable were excluded from

the study. Vitreous, posterior hyaloid, neural retina, retinal pigment epithelium and choroid were individually assessed. Measurements included: macular central subfield volume (1000 μm diameter), maximum lesion thickness (in the centre of the lesion, from internal limiting membrane to base of the RPE, less subretinal fluid if present), and choroidal thickness under the maximum lesion thickness. The choroid was considered thickened if it measured at least 300 μm on EDI. Images were graded by a single clinician, who was a fellowship-trained vitreoretinal surgeon. The data collection sheet is displayed in Appendix A.

One eye per patient was analysed. If both eyes had active lesions, the eye with the most posterior lesion was selected for analysis. If bilaterally active disease was symmetrical, the right eye was selected for analysis. Comparisons were made between clinical subgroups: by type of infection (primary versus recurrent), location (zone 1 versus zone 2), *T. gondii* IgM status, and HIV status.

2.1.4 Treatment and follow-up schedule

Patients with active TRC were offered treatment. Drug regimens included a course (6-7 weeks) of oral trimethoprim and sulfamethoxazole (160/800 mg twice daily) or oral sulfadiazine (1 g 4-times daily) and pyrimethamine (25 mg daily), plus oral prednisolone (40 mg daily for two weeks, with a 4-week taper). Intravitreal and intravenous anti-parasitic drugs or corticosteroids were not used. Unless the clinical situation required earlier review, patients were re-evaluated at 2 and 6-8 weeks after presentation. In selected cases, SD-OCT of the lesion and/or macula was repeated during follow-up.

2.2 LABORATORY BIOSAFETY

Safety and containment aspects of work with microorganisms were governed by the Australian and New Zealand Standard 2243.3 '*Safety in Laboratories - Part 3: Microbiological Safety and Containment*'.²⁶¹ All experiments were conducted under Biosafety Level 2 conditions and using appropriate personal protective equipment. The work with DENV and the work with expression plasmids was approved by the Flinders University Institutional Biosafety Committee (dealing numbers: 2011-10, 2013-04, 2014-06)

2.3 CHEMICALS AND REAGENTS

Specialist chemicals are listed throughout the text, with manufacturer headquarters listed in Appendix B. Commonly used buffers and solutions made in-house are listed below.

2.3.1 Buffers and solutions

2.3.1.1 PHOSPHATE-BUFFERED SALINE

Sterile Dulbecco's calcium- and magnesium-free phosphate-buffered saline (PBS) with (Thermo Fisher, cat. 14190-250) was used for cell culture procedures. Non-sterile PBS was used for immunolabelling and was made in-house according to the following recipe. For 1 L of 10X PBS, 80 g NaCl, 2 g KCl, 14.4 g Na₂HPO₄ and 2.4 g KH₂PO₄ were mixed to 1 L with deionised (d)H₂O and adjusted to pH 7.4 to 7.6. To make 1X PBS, 10X PBS was diluted 1:9 in dH₂O.

2.3.1.2 TRIS BASE, ACETIC ACID AND EDTA BUFFER

Tris base, acetic acid and ethylenediaminetetraacetic acid (EDTA), known as TAE buffer, was prepared by making a 50X master mix. To 900 mL dH₂O, 242 g tris(hydroxymethyl)aminomethane (Tris) base (VWR, cat. 28808.294), 57 mL glacial (100%) acetic acid (Sigma-Aldrich, cat. 320099) and 18.5 g EDTA was added, and volume adjusted to 1 L with dH₂O. The 50X buffer was diluted 1:49 with dH₂O to make 1x TAE buffer.

2.3.1.3 DULBECCO'S MODIFIED EAGLE MEDIUM

To prepare Dulbecco's Modified Eagle Medium, (DMEM) 13.4 g endotoxin-free DMEM powder (Gibco, cat. 12100-103) was diluted in 900 mL of sterile-filtered H₂O (Sigma-Aldrich, cat. W3500) in glassware before adding 3.7 g sodium bicarbonate and bringing the volume to 1000 mL with sterile-filtered H₂O. The medium was then filtered by negative-pressure using a Nalgene™ filter (Thermo Fisher Scientific) into two 500 mL bottles.

2.3.1.4 LURIA BERTANI BROTH

To prepare the starter culture, 5 g Luria Bertani (LB) broth (Miller's modification, containing NaCl) powder (Sigma-Aldrich, cat. 12795-027) was dissolved in dH₂O to a volume of 200 mL, transferred to a 500 mL glass bottle, and sterilized at 121 °C for 15 minutes without a drying step. After 30 min, and under sterile conditions, ampicillin powder was added to the broth to a concentration of 50 µg/mL and used as a starting culture.

2.3.2 Antibodies

Sources and concentrations of antibodies used for human Müller cell immunolabelling are listed in Tables 2.1, 2.2 and 2.3.

Table 2.1: Primary antibodies

Target	Supplier	Catalogue Number	Description	Working Concentration	Research Resource Identifier
Vimentin	Merck Millipore	MAB3400	Monoclonal mouse IgG1	5 µg/mL	AB_94843
Glutamine synthetase	Sigma-Aldrich	G2781	Polyclonal rabbit IgG	15 µg/mL	AB_259853
Glial fibrillary acidic protein	R&D Systems	AF2594	Polyclonal sheep IgG	10 µg/mL	AB_2109656
FLAG®	Sigma-Aldrich	F3165	Monoclonal mouse IgG1	5 µg/mL	AB_259529
VP35	Kerafast	EMS702	Monoclonal mouse IgG2a	2 µg/mL	-

Abbreviations: Ig = immunoglobulin, VP = viral protein.

Table 2.2: Control antibodies

Description	Supplier	Catalogue number	Working Concentration	Research Resource Identifier
Sheep IgG	R&D Systems	5-001-A	10 µg/mL	AB_10141430
Monoclonal mouse IgG1K (MOPC-21)	BD Bioscience	554121	5 µg/mL	AB_395252
Rabbit IgG	Sigma-Aldrich	I5006	2 µg/mL	AB_1163659

Abbreviations: Ig = immunoglobulin.

Table 2.3: Secondary antibodies

Description	Supplier	Catalogue Number	Working Concentration	Research Resource Identifier
Alexfluor® 488 goat anti-rabbit IgG (H+L)	Thermo Fisher Scientific	A-11008	0.5 µg/mL	AB_143165
Alexfluor® 488 goat anti-mouse IgG (H+L)	Thermo Fisher Scientific	A11005	0.5 µg/mL	AB_2534073
Alexfluor® 594 donkey anti-sheep IgG (H+L)	Thermo Fisher Scientific	A110-16	0.5 µg/mL	AB_2534083
Donkey anti-mouse horseradish peroxidase, IgG (H+L)	Thermo Fisher Scientific	A16011	1:3000	AB_2534685

Abbreviations: H+L = heavy and light, Ig = immunoglobulin.

2.4 EUKARYOTIC CELLS

2.4.1 Cell lines and culture medium

2.4.1.1 ARPE-19 CELL LINE AND MEDIUM

The human adult retinal pigment epithelial cell line, ARPE-19 (American Type Culture Collection (ATCC), cat. CRL-2302) was first isolated from spontaneously-immortalised retinal pigment epithelial cells of a 19 year-old male eye donor.²⁶² The cells were cultured in a 1:1 DMEM: Ham's F-12 nutrient mixture (F12, Thermo Fisher Scientific, cat. 11765-054) and 10% foetal bovine serum (FBS, Bovogen, cat. SFBS-AU), and incubated at 37 °C and 5% CO₂ (MCO-19AIC, Panasonic).

2.4.1.2 MIO-M1 CELL LINE AND MEDIUM

The human Müller cell line, MIO-M1 line (Moorfields Institute of Ophthalmology – Müller 1) was originally isolated from spontaneously-immortalised Müller cells from the retina of a 68 year-old female⁹⁵ and is generously gifted for this work by G. Astrid Limb, PhD and Sir Peng Khaw, PhD, University College London, London, United Kingdom. Cells were cultured in DMEM and 10% FBS.

2.4.1.3 VERO CELL LINE AND MEDIUM

Vero cells (ATCC, cat. CCL-81) were previously isolated from the kidney of a healthy African green monkey.²⁶³ Vero cells were cultured in DMEM plus 10% FBS, and required alternative media for different stages of the plaque assay (see section 2.6.1.1).

2.4.1.4 C6/36 CELL LINE AND MEDIUM

The mosquito C6/36 cells (ATCC, cat. RL-1660) were isolated from *Aedes albopictus* larvae and used to propagate viral stocks.²⁶⁴ When growing, C6/36 cells were cultured in basal medium Eagle (BME, Gibco, cat. 21010-046) plus 1 mM sodium pyruvate (Thermo Fisher Scientific, cat. 11360-070), 2 mM L-glutamine (Thermo Fisher Scientific, cat. 25030081) plus non-essential amino acid (NEAA, Thermo Fisher, cat. M7145) and 10% FBS. When infected, C6/36 cells required a lower proportion of FBS (7.5%). Cells were incubated at 28 °C and 5% CO₂.

2.4.2 Primary human retinal cells

2.4.2.1 PRIMARY HUMAN OCULAR CELL ISOLATION

Primary human ocular cell isolation was performed by Dr Yuefang Ma on donor eyecups sourced from the Eye Bank of South Australia, Bedford Park, SA, and these methods are described in Appendix C. This work complied with the National Statement on Ethical Conduct in Human Research (2015)²⁶⁵ and the Australian Code for the Responsible Conduct of Research (2018).²⁶⁶ Experiments were conducted with the approval of the Southern Adelaide Clinical Human Research Ethics Committee (SAC HREC EC00188) to use human eye tissue to study diseases that involve the retina or choroid (protocol number: 175.13).

2.4.2.2 PRIMARY HUMAN MÜLLER CELL CHARACTERISATION

Primary Müller cells were plated to at 1×10^4 cells per well in 96-well plates (Sigma-Aldrich, cat. CLS3795) and allowed to adhere. Medium was removed and cells were washed with PBS, then fixed with 4% paraformaldehyde (PFA, Sigma-Aldrich, cat. P6148)

in PBS (pH 6.9 at RT) for 10 min. After fixation and further washing, cells were incubated in blocking buffer (2% bovine serum albumin (BSA, Sigma-Aldrich, cat. A2058-5G) and 0.05% Triton™ X-100 (Sigma-Aldrich, cat. X100) in PBS) for 1 hour with gentle agitation (EOM5, Raytek) at RT. Cells were then incubated overnight at 4 °C with one primary antibody diluted in blocking buffer (Table 2.1): vimentin, glutamine synthetase, glial fibrillary acidic protein, and appropriate negative control antibody (Table 2.2).

The following day, wells were washed three times with 0.1% Tween™ (Sigma-Aldrich, cat. P1379) in PBS for 5 minutes and RT before incubation for 1 hour with gentle agitation, and protected from light. An appropriate secondary fluorescein-conjugated antibody was used, and diluted in blocking buffer: Alexfluor® 488 goat anti-rabbit IgG, Alexfluor® 488 goat anti-mouse IgG, Alexfluor® 594 donkey anti-sheep IgG (Table 2.3). Antibody was then removed, and cells were washed three times with 0.1% Tween in PBS for 5 minutes each time. To stain cell nuclei, cells were incubated with 0.1 µg/mL 4',6-diamidino-2-phenylindole (DAPI, Sigma-Aldrich, cat. D9542) in PBS at RT for 2 min. Wells were washed and covered with PBS prior to image capture under a fluorescence microscope. Filters appropriate to the wavelength of the respective secondary antibody were used (488 nm = green, 594 nm = red, 461 nm = blue).

2.4.3 Cell culture techniques

2.4.3.1 CELL MAINTENANCE

Cells were checked daily, and medium changed twice weekly. When cells became confluent, cell monolayers were dissociated and sub-cultured for use in experiments, or frozen.

2.4.3.2 CELL MONOLAYER DISSOCIATION

Confluent cell monolayers in a T75 flask (Sigma-Aldrich, cat. CLS430641U) were visualised through a microscope before dissociation with trypsin. Medium was aspirated with a serological pipette, and cells were washed with PBS thrice before adding 0.5 mL trypsin (Thermo Fisher Scientific, cat. 25200056). Cells were incubated for 5 minutes at 37 °C and checked again under a microscope (IX53, Olympus) to ensure they were floating free. Trypsin was quenched by adding 1 mL pre-warmed serum-containing medium. Cell suspension was transferred to a tube and centrifuged at a relative centrifugal force of 280 $\times g$ and RT for 5 minutes on the Allegra X-12R Centrifuge (Beckman Coulter). Supernatant was discarded, and pelleted cells were resuspended with pre-warmed medium to a pre-determined volume.

2.4.3.3 CELL COUNTING

If indicated, cells were counted on the TC20™ Automated Cell Counter (Bio-Rad) by mixing 20 μL of cell suspension with 20 μL of 0.4% trypan blue (Thermo Fisher Scientific, cat. 15250061), and adding this to a counting chamber (Bio-Rad, cat. 1450011). Four chambers were filled and each chamber counted three times, and cell count was averaged.

The automated cell counter had been validated with manual cell counting using Hausser Scientific™ Levy™ Hemacytometer (Thermo Fisher Scientific, cat. 0267155A).

2.4.3.4 FREEZING CELLS

Cryogenic storage vials (Sigma-Aldrich, cat. CLS430487) were used, and a freezing cylinder was prepared by adding isopropanol (VWR, cat. 20842.33) to Mr Frosty™ Freezing Container (Thermo Fisher Scientific). Appropriate cell culture medium was used to make 10% dimethyl sulfoxide (DMSO, Sigma-Aldrich, cat. D2650), and then chilled to 4 °C alongside the cryovials and Mr Frosty™ cylinder. Cell monolayers were dissociated with trypsin (see section 2.5.3.2), and the cell pellet was resuspended in 1 mL of 10% DMSO in cell-appropriate medium. Each cryovial was filled with 0.5 mL of cell suspension before transferring to Mr Frosty™ cylinder for incubation at -80 °C. The following day, cryovials were transferred to liquid nitrogen storage, wearing appropriate personal protective equipment.

2.4.3.5 THAWING CELLS FROM CRYOPRESERVATION

To raise cells from liquid nitrogen storage, appropriate cell culture medium was incubated at 37 °C. Cryovials were retrieved from liquid nitrogen storage, transported on ice, incubated for 1 minute in the dry bead bath, wiped with 70% (v/v) ethanol (VWR, cat. VWRC83813.440), and transferred to a 15 mL tube with 10 mL of warm medium. Cells were pelleted by centrifugation at 280 x *g* and RT for 5 minutes on the Allegra X-12R Centrifuge (Beckman Coulter). Supernatant containing DMSO was discarded, and 3 mL warm medium used to gently resuspend cells using a serological pipette (Sigma-Aldrich, cat. CLS4488). Cells were transferred to a T75 flask and checked under the microscope before incubating at 37°C and 5% CO₂ in an incubator.

2.4.3.6 MYCOPLASMA TESTING

Mycoplasma species are intracellular prokaryotes that can contaminate tissue culture and may impact cell biology and gene expression.²⁶⁷ Cultured cells were routinely tested for *Mycoplasma* contamination by qPCR of culture medium at the time of freezing, and after isolation of primary cells. Given their slow growth and the length of time spent in culture conditions, primary Müller cells were also tested every 2 to 3 weeks. Genomic DNA was isolated from growth medium using the PureLink™ Genomic DNA Mini Kit (Invitrogen, cat. K1820-01) and following the manufacturer's instructions. Samples were prepared for PCR in a UV-decontaminated BioAir Aura PCR cabinet (Adelab Scientific), and each PCR well contained: 2 µL of cDNA, at 1:10 dilution in nuclease-free (NF) H₂O (2.5 ng); 1.5 µL each of forward and reverse *Mycoplasma* primers (Appendix D) at 10 µM; 11 µL of nuclease-free (NF) H₂O; and 4 µL of iQ SYBR Green Supermix (Bio-Rad, cat. 170-8884). Samples were tested in triplicate with a 'no template' negative control well, replacing cDNA with 2 µL of NF H₂O. Plates were sealed and centrifuged for 1 minute at RT at 280 x *g* on the Allegra X-12R Centrifuge (Beckman Coulter).

The qPCR was performed using the Bio-Rad CFX Connect Real-Time PCR Detection System Thermocycler (Bio-Rad) and CFX Connect Software (Bio-Rad, v.3.1.1517.0823). Amplification consisted of: a pre-cycling hold at 95 °C for 5 min; then 40 cycles of: 30 seconds at 94 °C (denaturation); 1 minute at 60 °C (annealing); 30 seconds at 72 °C (extension); and a post-extension hold at 72 °C for 1 second. A melting curve was produced by a 1-second hold at 0.5 °C increments from 70 °C and 95 °C. Only cell isolates that were negative for *Mycoplasma* were used for experiments.

2.5 VIRUSES

2.5.1 Virus strains

Six DENV strains were sourced from the National Environment Agency of the Environmental Health Institute of Singapore under a Material Transfer Agreement (EHI-132), representing DENV1 and DENV2 isolated from individuals hospitalised during the 2004-2005 and 2007 epidemics in Singapore (Table 2.4), and propagated in C6/36 mosquito cells. A seventh strain, the full-length, infectious recombinant DENV2, Mon601, was first cloned from a mouse brain-adapted New Guinea C isolate,²⁶⁸ and viral RNA was transfected into baby hamster kidney BKH-21 fibroblasts before amplification in C6/36 mosquito cells. Tropism of Mon601 for human primary ocular cells and ocular cell lines has been previously demonstrated.²⁰⁵ Viral strains were propagated and quantified by Ms Abby Dawson (Appendix E).

Table 2.4: Dengue virus field isolates

Six serotype 1 and 2 DENV strains that had been isolated from individuals with dengue during epidemics in Singapore were used in these experiments.

Name	Year isolated	Serotype	GenBank ID
EHI0393Y04	2004	DENV1	EU069606.1
EHI0418Y05	2005	DENV1	EU069594.1
EHI0377Y04	2004	DENV2	JN851123.1
EHI0578Y05	2005	DENV2	JN851126.1
EHI0043Y07	2007	DENV1	GQ357691.1
EHI0169Y07	2007	DENV1	GQ357690.1

2.5.2 Viral infections

At least one day before viral infections, host cells were seeded into 12-well dishes to 90% confluence (Sigma-Aldrich, cat. CLS3513), including additional wells for counting in order to calculate infective viral load. On the day of infection, cell monolayers from additional wells were dissociated with trypsin for counting (2.5.3.3) to permit calculations for multiplicity of infection (MOI). To inactivate virus for experimental controls, Mon601 stocks were retrieved from -80 °C storage and quickly thawed before incubating in a heat block set at 80 °C for 20 min. At the time of infection, other viral stocks were transferred to an incubator for 5 minutes to rapidly thaw at 37 °C. Viral quantity was calculated by multiplying cell count by 5x(Mon601 pfu) for a MOI of 5, and by 1x(Mon601 pfu) for an MOI of 1. Virus was applied at minimum volume possible, where necessary and diluted with DMEM to achieve uniform concentration across the viruses.

Depending on downstream application, cells were plated into either 12-well or 96-well plates (Sigma-Aldrich, cat. CLS3599). At the start of the experiment, medium was discarded from cell monolayers, and suspension of virus or fresh DMEM alone were added. Plates were incubated with tipping every 15 minutes to prevent monolayers from drying out. After 90 min, supernatant was removed and monolayers washed with pre-warmed medium then replaced with medium. If indicated, supernatant was collected and centrifuged at an rcf of 3900 x *g* for 5 minutes in the 22R Microcentrifuge (Beckman Coulter, cat. 368831) before storing at -80 °C for future use.

Cells were checked under the microscope, photographed, and incubated. Every 24 hours post-inoculation (hpi), cells were checked under the microscope, and if indicated, supernatant removed and replaced with fresh medium. At the end of the experiment, cells

infected in 96-well plates were fixed for staining (see section 2.6.2), and cell monolayers in 12-well plates were homogenised with TRIzol™ (Invitrogen, cat. 15596-018) for later RNA extraction (see section 2.7.1).

A pilot experiment that involved incubating isolated primary Müller cells from one donor with Mon601 and EHI0578Y05 at an MOI of 5 for the standard 90 minutes indicated poor infection of virus by RT-qPCR of the cellular RNA extract. Further experiments with these cells were conducted with a longer viral incubation period. For these infections, cell monolayers were infected with DENV at minimum volume according to the most dilute viral stock, with intermittent rocking, and after 4 hours, 1 mL medium was added to each well without removing supernatant.

2.5.3 Plaque assays

Plaque assays were performed to quantify Mon601 virus and to measure viral load in culture supernatant of infected cells in preliminary infections. Vero cells were seeded into 6-well culture plates (Sigma-Aldrich, cat. CLS3516) the day before plaque assay, with one plate per experimental sample to be tested. Each well was plated with 3×10^5 cells into 3 mL of complete Vero medium (1X DMEM and 10 mM HEPES (Thermo Fisher Scientific, cat. 15630080) plus 10% FBS), and incubated overnight.

Supernatant with virus to be assayed was thawed quickly, and DMEM was added to samples in serial 1:9 dilutions to 10^{-6} . Positive control samples were diluted to 10^{-5} , and one negative control was used and contained only DMEM. Medium was removed from monolayers, and cells were washed in PBS, then 300 μ L of diluted sample was added to the appropriate well,. Plates were incubated for 90 minutes with intermittent rocking

every 15 minutes to avoid monolayers drying out. Meanwhile, 0.7% SeaKem agarose (Lonza, cat. 50014) was melted, and aliquoted and incubated at 56 °C for at least 30 min.

After 90 min, all medium was removed. Each well was overlaid with 3 mL of a 1:1 mix of 0.7% SeaKem agarose and complete 2X DMEM: (2X DMEM (Thermo Fisher Scientific, cat. 12100046), 2X L-Glutamine, 10 mM HEPES, 7.5% NaHCO₃ and 10% FBS). Plates were allowed to set at RT for 1 hour before incubating for 5 days.

To overlay cells with neutral red, 13 mL SeaKem agarose was warmed to 56 °C and added to 13 mL complete 2 X DMEM containing a 1:9 dilution of neutral red (Sigma-Aldrich, cat. n4638-5G). Each well was covered with 2 mL agarose and neutral red solution and allowed to set for 1 hour. Plates were inverted and incubated, and read against positive controls once plaques were visible.

2.5.4 Immunostaining

At harvest, cells were checked under a microscope. Medium was removed and cells were washed twice with PBS and fixed for 15 minutes with 4% PFA in PBS. Medium was removed, and monolayers were rinsed in PBS. Plates were covered and stored at 4 °C in PBS for later immunolabelling.

Paraformaldehyde-fixed cell monolayers were washed twice in PBS and permeabilized for 20 minutes in 0.05% Triton™ X-100 (Sigma-Aldrich, cat. X100) in PBS at RT. Monolayers were then washed three times in PBS before blocking in PBS with 4% normal goat serum (NGS, Abacus ALS, cat. VES1000) and 4% BSA for 30 minutes with agitation. Antibodies were mixed with PBS and 2% NGS as diluent, and primary antibodies were: J2 Mouse anti-dsRNA IgG2 κ and control antibody Mouse IgG2 κ isotype (Tables 2.1 and

2.2). Plates were incubated with primary antibodies overnight at 4 °C. Monolayers were washed thrice with PBS. The secondary antibody Alexa Fluor® 488 Goat anti-Mouse (Table 2.3). Plates were incubated at RT and protected from light for 45 min. Cells were then washed 5 times with PBS, and fixed for 10 minutes with 4% PFA in PBS. Cells were washed with PBS twice, incubated at RT with 0.1 µg/mL DAPI, then washed a further two times in PBS. Finally, monolayers were mounted in SlowFade® Gold (Thermo Fisher Scientific, cat. S36939) and protected from light before image capture.

2.5.5 Interferon-beta immunoassay

Secreted IFN-β in culture supernatants from DENV-infected MIO-M1 cells was measured by amplified luminescent proximity homogeneous assay (Alpha)-linked immunosorbent assay (LISA) by the Cell Screen SA high-throughput screening core facility at Flinders University. Using the ProxiPlate™-384 Plus AlphaLISA kit (PerkinElmer, cat. 6008280), undiluted samples were assayed in triplicates of 2 µL in each 20 µL assay, and IFN-β protein concentration in each sample was calculated by comparison with 12 human IFN-β standards, with a lower detection limit of 9.6 pg/mL.

2.6 REVERSE TRANSCRIPTION-POLYMERASE CHAIN REACTION

2.6.1 RNA extraction

Cell homogenate was incubated for 5 minutes to permit complete dissociation of nucleoproteins. Per 1 mL of TRIzol™ reagent used for cell lysis, 0.2 mL chloroform was

added, vortexed, before incubation at RT for 3 min. Samples were centrifuged for 15 minutes at 12,000 x *g* at 4 °C. Aqueous supernatant was transferred to a new tube, and 10 µg RNase-free glycogen (Thermo Fisher Scientific, cat. R0551) was added as a carrier to the aqueous phase to allow visualisation of the precipitate. Per 1 mL of TRIzol™ reagent, 0.5 mL isopropanol was added and samples incubated for 10 minutes before centrifugation for 10 minutes at 12,000 x *g* at 4 °C. Supernatant was discarded and RNA pellet resuspended in 1 mL 75% (v/v) ethanol per 1 mL of TRIzol™ reagent used for lysis. Samples were briefly vortexed then centrifuged for 5 minutes at 7,500 x *g* at 4 °C. Supernatant was discarded and RNA pellet air dried for 10 minutes before resuspension in 20 µL RNase-free H₂O. Samples were incubated in a heat block set at 55 °C for 15 min. Quality, purity and concentration of RNA was measured using the NanoDrop 2000 spectrophotometer (Thermo Fisher Scientific).

2.6.2 Complementary DNA synthesis

Complementary DNA (cDNA) was synthesized via reverse transcription using 5X iScript Reverse Transcription Supermix (containing reaction buffer, iScript Moloney Murine Leukemia Virus reverse transcriptase, RNase inhibitor, deoxyribonucleotide triphosphates, oligo (deoxythymine) primer, MgCl₂, and stabilizers; Bio-Rad, cat. 170-8841) to yield 20 µL of cDNA for every 250 ng of RNA template. Reverse transcription master mix was prepared in a UV-decontaminated PCR cabinet (BioAir Aura, Adelaab) and processed in the Bio-Rad T100 Thermocycler under the following conditions: priming for 5 minutes at 25 °C, reverse transcription for 30 minutes at 42 °C, reverse transcription inactivation for 5 minutes at 85 °C. Complementary DNA was aliquoted, and working stocks were diluted to 1:10 with NF H₂O and stored at -20 °C for later use.

2.6.3 Oligonucleotides and primers

Oligonucleotide primers were sourced from GeneWorks or Sigma-Aldrich (Appendix D). Lyophilized primers were dissolved in Tris-EDTA buffer (10 mM Tris-HCl, 1 mM disodium EDTA, pH 8.0, Sigma-Aldrich, cat. 93283) to provide a stock solution of 100 μ M and were stored at -20 °C. Aliquots of 10 mM primer were made with NF H₂O and stored at -20 °C.

2.6.4 Gradient polymerase chain reaction

Amplification of VP35 with ligation primers was achieved with the HotStar HiFidelity Polymerase Kit (Qiagen, cat. 202602). Each 25 μ L PCR reaction contained: 2.5 μ L 10X CoralLoad concentrate, 0.5 μ L 10 mM dNTP, 1 μ L forward and 1 μ L reverse primers (each 20 μ M), 0.5 μ L REDTaq® DNA polymerase (Qiagen, cat. D4309), 0.5 μ L template DNA, and 19 μ L NF H₂O. The gradient PCR protocol was run on the Bio-Rad T100 Thermocycler (Bio-Rad), and conditions were: 96 °C for 3 min, then 40 cycles of : (denaturation at 96 °C for 5 seconds, annealing at 68 to 58 °C (across 8 temperatures) for 1 second, extension at 72 °C for 30 seconds); then 72 °C for 1 minute before holding at 15 °C.

2.6.5 Quantitative real-time polymerase chain reaction

Quantitative real-time PCR was used to quantify expression of molecular transcripts. Samples were prepared in a UV-decontaminated PCR cabinet (BioAir Aura, Adalab), and each 20 μ L PCR well contained: 2 μ L of cDNA at 1:10 dilution in NF H₂O (2.5 ng); 1.5 μ L each of forward and reverse primers at 10 μ M; 11 μ L of NF H₂O, and 4 μ L of iQ SYBR Green Supermix. Plates included two replicates per sample, and a 'no template' negative control

well, replacing cDNA with 2 μ L of NF H₂O. Plates were sealed and centrifuged for 1 minute at RT at an 280 x *g* in the Allegra X-12R Centrifuge (Beckman Coulter). The qPCR was performed using the Bio-Rad CFX Connect Real-Time PCR Detection System Thermocycler and CFX Connect Software (v.3.1.1517.0823). Amplification consisted of: a pre-cycling hold at 95 °C for 5 min; then 40 cycles of: 30 seconds at 95 °C (denaturation), 30 seconds at 59 °C (annealing), 30 seconds at 72 °C (extension); and a post-extension hold at 75 °C for 1 second. A melt curve was generated from a 1-second hold at 0.5 °C increments from 70 °C to 95 °C, before a hold for 5 minute at 15 °C.

2.6.6 Data analysis

A single fluorescence peak was produced for each primer set. The cycle threshold was measured, with quantification cycle (C_q) determination mode set to regression. Relative expression was determined and normalized to stable reference genes, with CV (coefficient of variation) and M values (expression stability measurement) less than or equal to 0.25 and 0.5 respectively. Standard curves, produced with serially diluted product, confirmed PCR efficiency of 85% or greater. Size of PCR product was confirmed by electrophoresis on a 1% agarose gel.

2.7 WESTERN BLOTTING

2.7.1 Preparation of cell lysate

Western blotting was performed to separate and identify proteins expressed in human retinal pigment epithelial transfectants. To isolate protein from cell monolayers in 6-well

plates, the following steps were performed on ice, using ice-cold reagents. Medium was removed from monolayers and replaced with 1 mL PBS to each well. Wells were gently scraped with a Corning® cell scraper (Sigma-Aldrich, cat. CLS3010) and homogenate transferred by pipette into a microcentrifuge tube. An additional 500 µL PBS was used to remove remaining cells from the well before vortex mixing the homogenate for 5 min. The cell suspension was then centrifugated at 16,000 x *g* and 4 °C for 5 min. Supernatant was discarded, and the cell pellet was resuspended in 100 µL of a 1:25 solution of cOmplete™ Protease Inhibitor Cocktail x25 (Roche Life Science, cat. 4693116001) and radioimmunoprecipitation assay (RIPA) buffer (150 mM NaCl, 1.0% octylphenoxy poly(ethyleneoxy)ethanol, 0.5% sodium deoxycholate, 0.1% sodium dodecyl sulfate, 50 mM Tris, pH 8.0; Sigma-Aldrich, cat. R0278). To complete cell lysis, microfuge tubes were incubated on ice for 20 min. Cell debris was pelleted by centrifugation at 16,000 x *g* and 4 °C for 20 min. Supernatant containing protein lysate was immediately aliquoted for storage at -20 °C.

2.7.2 Protein quantitation

Fluorescence-based quantitation of protein homogenate was performed using the EZQ™ Protein Quantitation Kit (Bio-Rad). First, protein standards were prepared by making serial dilutions of the 10 mg/mL ovalbumin stock solution (2 mg/mL, 1 mg/mL, 0.5 mg/mL, 0.2 mg/mL, 0.1 mg/mL, 0.05 mg/mL, 0.02 mg/mL, blank RIPA buffer). Standards were spotted alongside experimental samples onto assay paper included in the kit. To remove contaminants, assay paper was incubated with methanol (Sigma-Aldrich, cat. 494437) at RT and with gentle agitation for 5 min. Methanol was discarded and assay paper dried on low heat with the Hoefer™ Easy Breeze™ Gel Dryer (Thermo Fisher

Scientific). Next, assay paper was incubated in 35 mL of EZQ® protein quantitation reagent (Bio-Rad) for 30 minutes under cover and with gentle agitation at RT. Reagent was discarded and assay paper rinsed with 40 mL of buffer (10% methanol and 7% acetic acid in dH₂O) before incubation with agitation for 2 min. This step was performed thrice. Wet assay paper was placed into the Bio-Rad Gel Doc™ EZ Imager, and fluorescence was imaged on a SYPRO Ruby® protocol with automatic exposure. The Tagged Image File Format document was then analysed using Image Lab™ v6.0 software (Bio-Rad). A standard curve was generated using protein standards and from this, protein concentrations of experimental samples were generated, and values with the lowest coefficient of variation were used.

2.7.3 Protein separation by gel electrophoresis

Loading buffer was prepared by adding 4 µL of 1 M dithiothreitol (Thermo Fisher Scientific, cat. 1610611) to 100 µL of 4x Laemmli Sample Buffer (62.5 mM Tris-HCl, pH 6.8, 10% glycerol, 1% lithium dodecyl sulfate, 0.005% Bromophenol Blue; Bio-Rad, cat. 161-0747). Next, 5 µL of this solution was added to 20 µg of protein sample, and volume made to 20 µL with dH₂O. Samples were heated at 95 °C for 5 minutes before a short centrifugation to pellet insoluble product. Samples were loaded into a 4–20% Stainfree Mini-PROTEAN® TGX™ Precast Polyacrylamide Gel (Bio-Rad, cat. 4561093), alongside Precision Plus Protein™ Dual Color molecular weight standards (Bio-Rad, cat. 1610394). Electrophoresis was performed using 10x Tris/Glycine/sodium dodecyl sulphate running buffer (Bio-Rad, cat. 1610772), diluted with dH₂O and electrophoresed at 200 V for approximately 30 min. The gel was then imaged using the Gel Doc™ EZ imager (Bio-Rad).

2.7.4 Gel transfer

Pre-cut polyvinylidene difluoride (PVDF) membranes were soaked in methanol for 1 minute with agitation, and then rinsed and soaked with transfer buffer (40 mL 5X Transfer Buffer (Bio-Rad, cat 1704275), 40 mL ethanol, 120 mL dH₂O) for at least 5 min. The PVDF membrane was then sandwiched between the gel and pre-soaked blotting pads in the Trans-Blot® Turbo™ Transfer System with RTA Midi LF PVDF Transfer Kit; (Bio-Rad, cat. 1704275), gently flattened to remove excess fluid, and electrotransferred using a mixed molecular weight protocol (1.3 A, 25 V) for 7 min.

2.7.5 Antibody staining

After transfer was complete, the blotting pads and gel were removed from the membrane. Small holes were punched in the membrane to indicate marker bands before incubation for 1 hour with agitation in blocking buffer (5% low-fat milk in 1X phosphate-buffered saline with 0.1% Tween® 20 detergent, PBS-T, pH 7.4). Blocking solution was discarded, and the membrane was washed once with wash buffer (1x PBS-T). Wash buffer was discarded, and the membrane was incubated in primary antibody diluted in 5% low-fat milk powder solution in 1x PBS-T. Primary antibodies (Table 2.1) were mouse anti-VP35 1:100 or mouse monoclonal anti-FLAG® M2 antibody at 1:6000. The membrane was covered and incubated at 4 °C overnight with agitation. The following day, the membrane was washed thrice with wash buffer for 10 minutes each time. The secondary antibody was diluted 1:30,000 with 0.1% low-fat milk powder solution in 1x PBS-T and applied to the membrane, which was then covered and incubated at RT for 1 hour with agitation. Secondary antibodies used were donkey anti-mouse horseradish peroxidase (Table 2.3).

The membrane was again subjected to three 10 minutes washes with wash buffer before rinsing with dH₂O. Clarity Western Enhanced Chemiluminescence Substrate components (Bio-Rad) were mixed 1:1, and applied to the membrane before incubated and protected from light at RT for 5 min, before imaging on ChemiDoc MP Imaging system (Bio-Rad).

2.8 RESTRICTION ENZYME-BASED SUBCLONING

In order to measure the effect of EBOV VP35 protein expression in human cells, restriction-based subcloning was performed to create a plasmid expressing the EBOV VP35 gene and a FLAG reporter. The pCAGGS-FLAG-VP35 plasmid was created from two plasmids generously provided by Dr Glenn Marsh, CSIRO Australian Centre for Disease Preparedness (Figure 2.1).

2.8.1 Sub-cloning new plasmids

2.8.1.1 CREATION OF NO-VECTOR PLASMID

A pCAGGS plasmid backbone was created by removing the VP40 gene insert from the pCAGGS-FLAG-VP40 plasmid (Figure 2.1A) through restriction endonuclease digestion with XbaI (located at 1623 nucleotides)(New England BioLabs, cat. R0145T) and NheI (located at 2760 nucleotides) (New England BioLabs, cat. R3131S) (see section 2.9.2.1), before separation by agarose gel electrophoresis and ligation of the pCAGGS backbone to generate a “no insert” plasmid (Figure 2.2).

2.8.1.2 CREATION OF PCAGGS-FLAG-VP35 PLASMID

To create a VP35-expressing plasmid with reporter FLAG tag, the VP40 gene in the pCAGGS-FLAG-VP40 plasmid (Figure 2.1A) was replaced with VP35. First, VP35 was amplified from its pCAGGS plasmid (Figure 2.1B) using ligation-mediated gradient PCR (see section 2.7.4) with linker primers encoding the NotI and NheI restriction sites (Figure 2.2). Products were size-separated on a 1% agarose gel, and yielded 1 kb bands (see section 2.9.2.2), which were excised under long-wave UV illumination, purified (see section 2.9.2.3), quantified (see section 2.9.2.4), digested with NotI and NheI restriction endonucleases (see section 2.9.2.1), and further purified and quantified. Restriction endonucleases NotI and NheI were also used to cleave VP40 from pCAGGS-FLAG-VP40, before ligation of VP35 and p-CAGGS-FLAG-VP40 (see section 2.9.2.5).

2.8.2 Subcloning techniques

2.8.2.1 DOUBLE RESTRICTION ENDONUCLEASE DIGESTION

Double digestion was prepared on ice, with 1 µg of DNA plasmid template added to 10 units of each restriction enzyme, 5 µL of 10X CutSmart® Buffer (50 mM Potassium Acetate, 20 mM Tris-acetate, 10 mM Magnesium Acetate, 100 µg/mL BSA, pH 7.9 at 25 °C) (New England BioLabs, cat. B7204S), and made to 50 µL with NF (NF) H₂O (New England BioLabs, cat. B1500S). The mixture was incubated for 2 hours at 37 °C in the T100 Thermal Cycler (Bio-Rad).

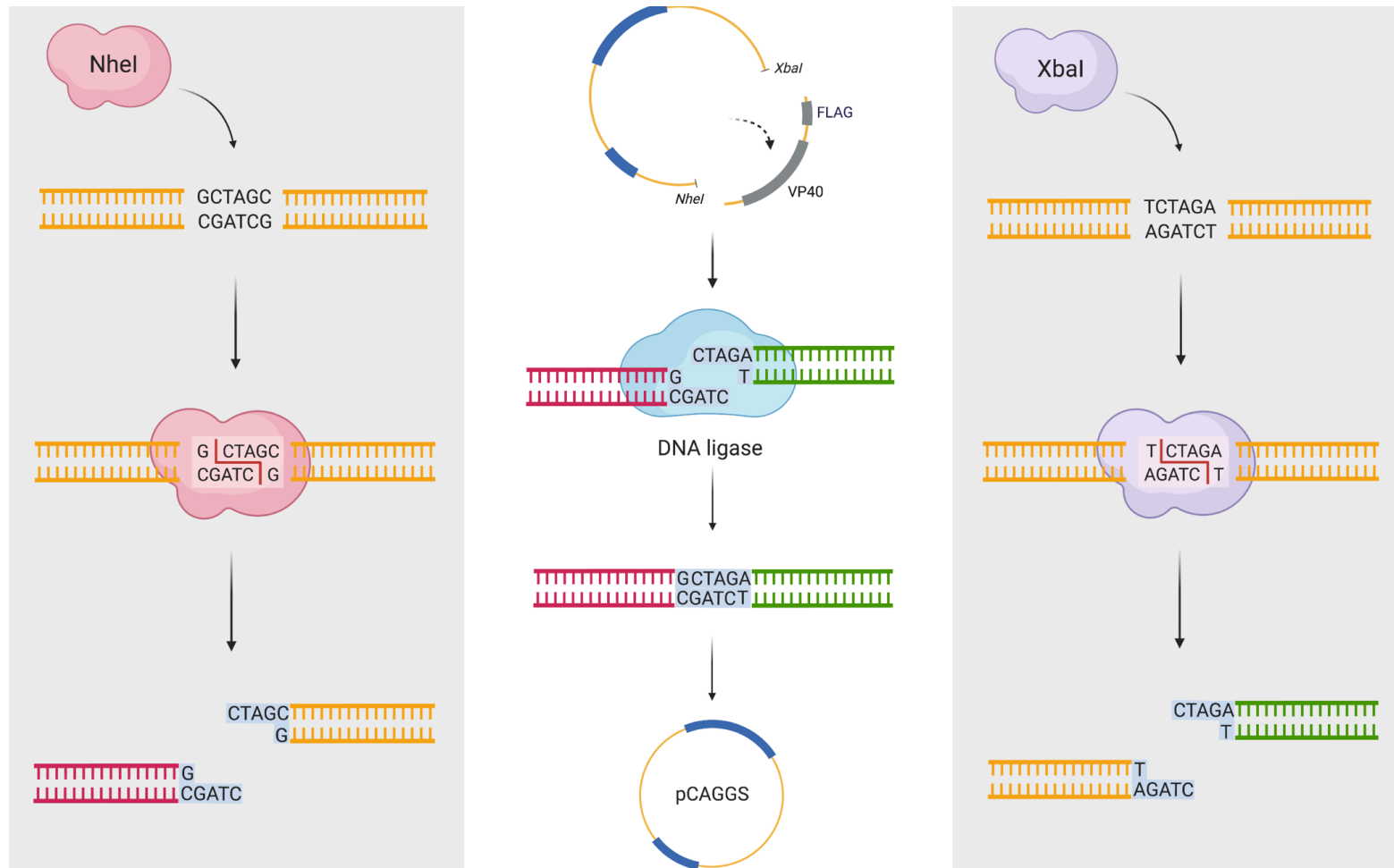
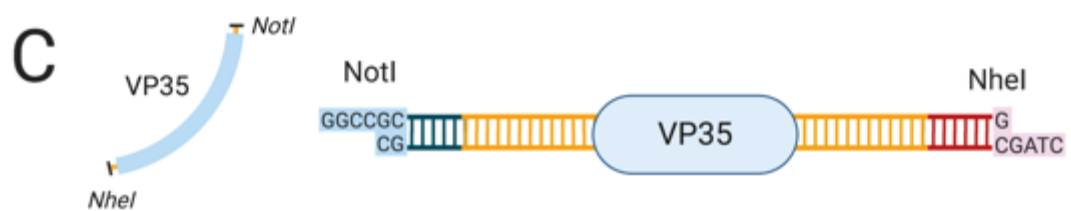
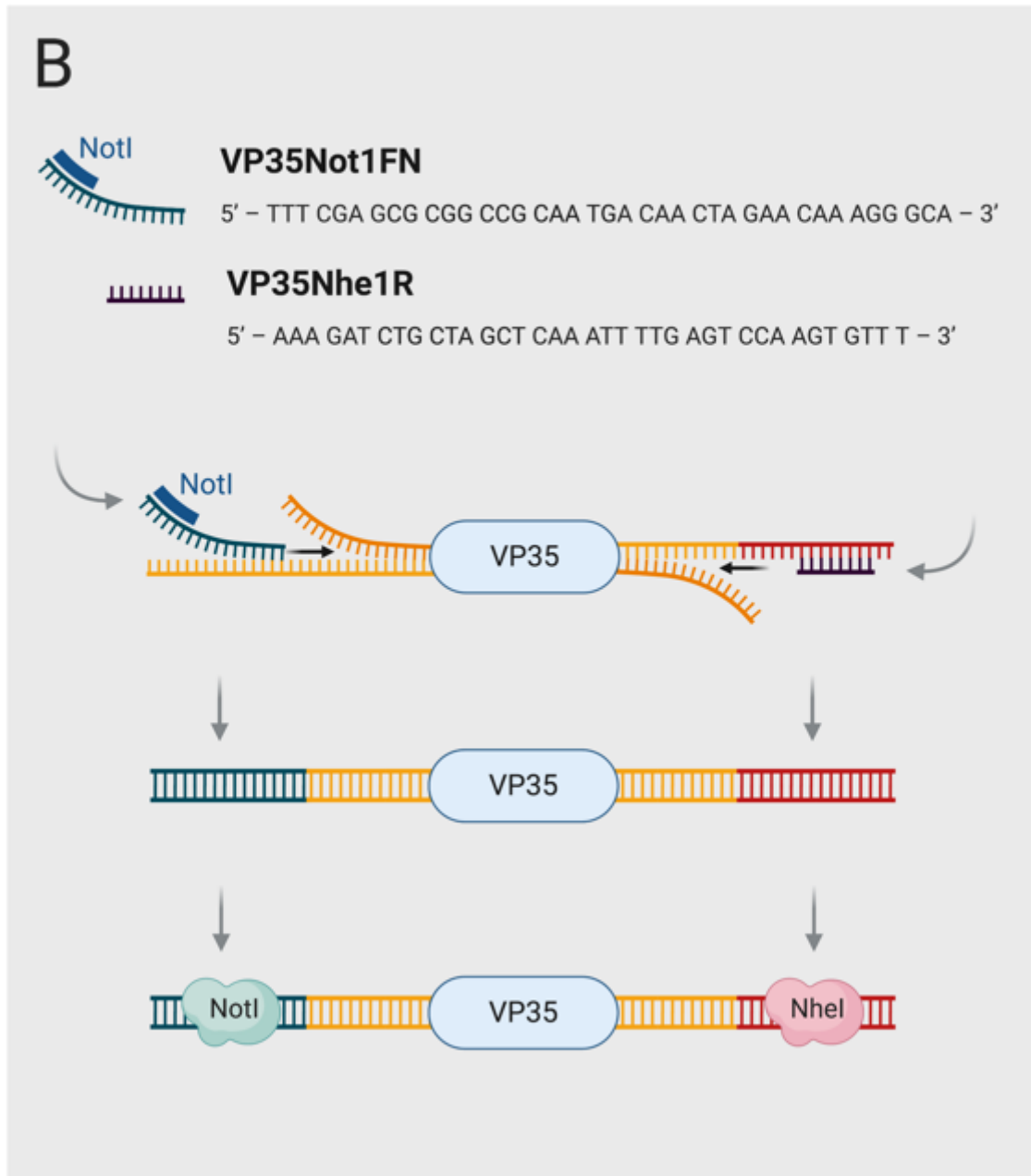
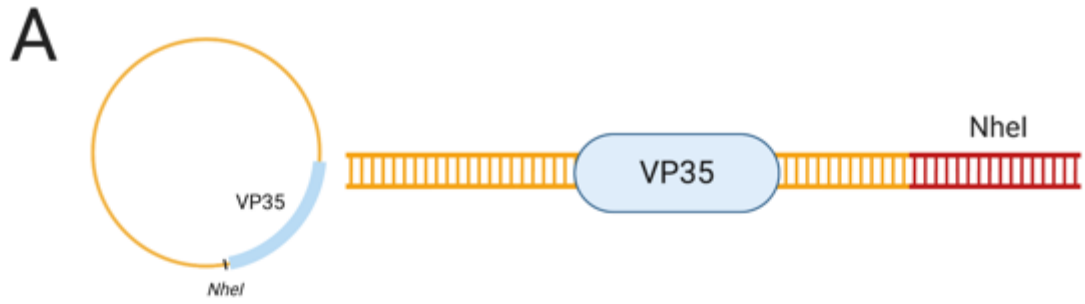


Figure 2.2: No-vector plasmid

The pCAGGS no-insert plasmid was created by using restriction endonucleases NheI and XbaI to excise the FLAG-VP40 component, and complementary ends were ligated with DNA ligase.



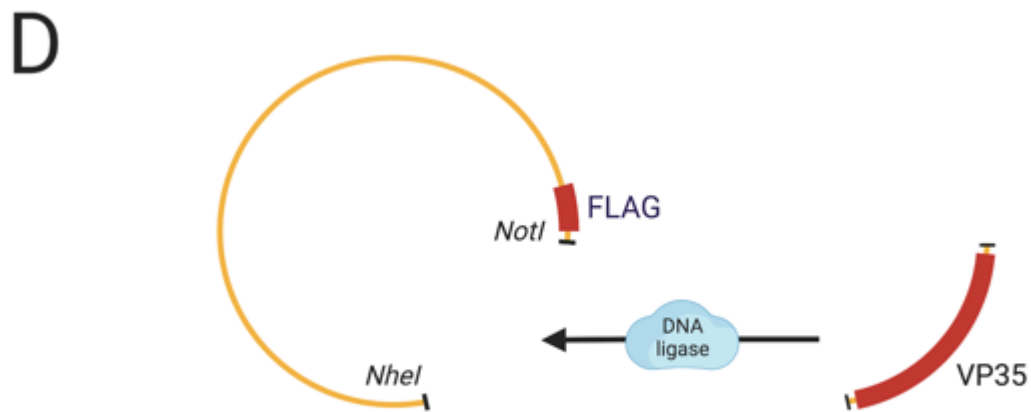


Figure 2.3: pCAGGS-FLAG-VP35 plasmid

A pCAGGS plasmid expressing FLAG and VP35 was created. (A) The original pCAGGS-VP35 plasmid did not contain restriction endonuclease NotI, so (B) the VP35 insert was amplified by PCR-ligation to encode NotI, then double-digested by restriction endonucleases NotI and NheI to create (C) complementary ends, which were (D) inserted into the pCAGGS-FLAG backbone using DNA ligase. Figure constructed at BioRender.com

2.8.2.2 DNA SEPARATION BY ELECTROPHORESIS

Restriction endonuclease products were separated on size by electrophoresis. A 1% agarose gel was made by mixing 1.5 g SeaKem® ME agarose powder with 150 mL TAE buffer (see section 2.4.1.2) and heating until dissolved before adding 15 µL SYBR Safe DNA gel stain (X10,000 concentrate, Invitrogen, cat. S33102) was added, and the flask was gently swirled until thoroughly mixed. The solution was poured into a gel casting tray with 15 combs (Bio-Rad), allowed to cool, placed in the electrophoresis tank (Bio-Rad) and covered with TAE buffer. Neat DNA product was combined with gel loading dye (New England BioLabs, cat. B7021S) and loaded into wells, flanked by marker wells that contained 6 µL of DNA molecular weight ladder (GelPilot 1 kb Plus Ladder, Qiagen, cat. 239095). The gel was run for approximately 35 minutes at 100 V, until the dye had migrated to the bottom of the gel, and then imaged on the Invitrogen™ Safe Imager™ 2.0 Blue-Light Transilluminator (Invitrogen) with a 470 nm filter and Canon Rebel XSi digital single lens reflex camera (Canon). Images were processed using Canon EOS Utility (v.2.14) and Canon Digital Photo Professional (v.3.14) software.

2.8.2.3 DNA PURIFICATION

Under UV visualization, the single DNA band representing linearized product of appropriate size was excised from the agarose gel. Extraction of DNA from agarose gel was performed using the GenElute Gel Extraction Kit (Sigma-Aldrich, cat. NA1111) and following the manufacturer's instructions. First, three gel volumes of Gel Solubilization Solution (Sigma-Aldrich, cat. G8668) were added to the DNA gel fragment and incubated at 55 °C for 10 minutes with intermittent vortex mixing. One gel volume of isopropanol was added and the solution mixed until homogenous.

Binding columns (Sigma-Aldrich, cat. C6863) were prepared by adding 500 μL of Column Preparation Solution (Sigma-Aldrich, cat. C2112) to each column, before centrifugation at 16,000 $\times g$ and RT for 1 min, and before discarding the eluate. The solubilized gel solution was loaded into the binding column in 700 μL aliquots and centrifuged each time at 16,000 $\times g$ and RT for 1 minute before discarding eluate. This was repeated once with diluted Wash Solution (Sigma-Aldrich, cat. W2139) before repeat centrifugation at 16,000 $\times g$ and RT for 1 minute to ensure complete removal of residual Wash Solution. The binding column was transferred to a fresh collection tube (Sigma-Aldrich, cat. T7813), and 50 μL of Elution Solution (10 mM Tris-HCl, pH 9.0; Sigma-Aldrich, cat. E9027), pre-heated to 65 $^{\circ}\text{C}$, was applied to the centre of the membrane before incubating at RT for 1 min. The column was then centrifuged at 16,000 $\times g$ and RT for 1 min, and the eluate collected.

2.8.2.4 DNA QUANTIFICATION

Quality, purity and concentration of eluate was measured using the NanoDrop 2000 spectrophotometer (Thermo Fisher Scientific), aiming for a ratio of absorbance at (A260-A320)/(A280-A320) between 1.8 and 2.0.

2.8.2.5 DNA LIGATION

In a 0.2 mL tube on ice, 50 ng of plasmid DNA was added to 1 μL of T4 DNA ligase (400 units, New England BioLabs, cat. M0202S), 2 μL of 10x T4 DNA buffer (New England BioLabs, cat. B0202S) and NF H₂O, to a total volume of 20 μL before incubation for 10 minutes at RT, followed by 10 minutes at 65 $^{\circ}\text{C}$ in the Bio-Rad T100™ Thermal Cycler (Thermo Fisher Scientific), and final chilling on ice.

2.8.3 Preparation of competent cells

2.8.3.1 PREPARATION OF AGAR PLATES

To make agar plates, 2.5 g of LB broth powder was dissolved in dH₂O to a volume of 100 mL and added to a 250 mL glass bottle. The broth was sterilized in a 2540 Autoclave (Tuttnauer) at 121 °C for 15 minutes without a drying step. Under a butane burner, hot agar was poured into two plates (25 mL each), before adding ampicillin powder (Sigma-Aldrich, cat. A5354) to the remaining agar to make a concentration of 50 µg/mL. Plates were allowed to cool for 30 minutes before covering with lids, sealing with Parafilm (Sigma-Aldrich, cat. P7793), and inverting and storing at 4 °C.

2.8.3.2 TRANSFORMATION OF COMPETENT CELLS

To generate multiple copies of the cloned DNA plasmid, the construct was transformed into *Escherichia coli*, which was then cultured in broth. One 50 µL vial of chemically-competent *E. coli* (One Shot STB13, Invitrogen, cat. C737303) was thawed on ice for 20 min, then heat-shocked by placing in a 42 °C water bath for 45 seconds, before adding 400 µL of Super Optimal broth with Catabolite repression medium (Thermo Fisher Scientific, cat. 15544034), and incubating at 37 °C and moderate agitation at an rcf of 1 x *g* in the Incu-Shaker™ (Benchmark Scientific). After 1 hour, 150 µL of *E. coli* suspension was pipetted into the centre of two agar plates, one containing ampicillin. The suspension was evenly spread across the agar before inverting and incubating at 37 °C overnight in a MyTempMini incubator (H2200, Benchmark Scientific). The next day, agar plates were checked. Using sterile technique, a single colony was harvested from agar containing ampicillin using a cooled, sterile flame loop. The colony was streaked onto a new ampicillin-positive agar plate before inverting and incubating at 37 °C overnight.

2.8.3.3 GROWTH OF PLASMID-EXPRESSING BACTERIA

A single colony was selected from the ampicillin-positive agar plate with a cooled, sterile flame loop, and transferred to 4 mL of LB broth (section 2.4.1.2) in a 15 mL tube. This starter culture was capped and incubated overnight at 37 °C and moderate agitation at an rcf of 1 x *g*. The next day, 150 µL of starter culture was added to 150 mL of 37 °C broth prepared the previous day, and incubated in aluminium foil-capped Erlenmeyer flasks overnight at 37 °C and moderate agitation at an rcf of 1 x *g*.

2.8.3.4 PLASMID HARVEST BY MAXIPREPARATION

Plasmid DNA was extracted from *E. coli* using the GenElute HP Endotoxin-Free Plasmid Maxiprep Kit (Sigma-Aldrich, cat. NA041), according to manufacturer's instructions. Bacterial cells were harvested by centrifugation of culture broth at 5,000 x *g* for 10 minutes at RT. Resuspended cells were lysed and neutralised, and genomic DNA was precipitated and removed by vacuum filtration through a binding column. Plasmid lysate was then washed to remove nucleic acid-binding protein, desalted by elution, and plasmid DNA was precipitated, purified and resuspended in endotoxin-free H₂O. Purity and concentration of plasmid DNA were determined by spectrophotometric analysis using the NanoDrop 2000 spectrophotometer (Thermo Fisher Scientific), aiming for a ratio of absorbance at A₂₆₀-A₃₂₀)/(A₂₈₀-A₃₂₀) between 1.8 and 2.0.

2.8.4 Sequencing

Sequencing was performed at the Flinders Sequencing Facility in SA Pathology, South Australia. Viral PCR and plasmid product sequences were confirmed using the basic local

alignment search tool (BLAST) at the National Center for Biotechnology Information (NCBI) website^{269, 270} to confirm alignment with consensus sequences.

2.9 CELL TRANSFECTION WITH VP35 PLASMID AND POLY I:C

Preliminary studies were performed to determine the kinetics of IFN- β production in retinal pigment epithelial cells after administration of synthetic pattern recognition receptor agonist, polyriboinosinic:polyribocytidylic acid (Poly I:C), and also to determine whether a transfection reagent was required for Poly I:C to be effective in these cells. Monolayers of ARPE-19 cells were seeded into 12-well plates to 90% confluence the day before transfection. Conditions included Poly I:C alone, Poly I:C with transfection reagent Lipofectamine 2000™ (Thermo Fisher Scientific, cat. 11668-027), and unmanipulated cells, with 3 replicates per condition, and two time points: 1 and 4 hours post-transfection. A 1:1 mixture of high- (InvivoGen, cat. tlr1-picr) and low-molecular weight rhodamine-tagged Poly I:C (InvivoGen Life Research, cat. tlr1-piwr) was diluted with Opti-MEM reduced serum medium (Thermo Fisher Scientific, cat. 31985070) to yield a Poly I:C concentration of 2 $\mu\text{g}/\text{mL}$, and a total of 200 μL was applied to each well. Lipofectamine was added at 4 μL per well as per manufacturer's directions. Brightfield and fluorescence imaging was performed at the start of the experiment, and 1 hour and 4 hours post-transfection, with a barrier filter allowing 620 nm wavelength Rhodamine peak emission, and the UC50 Camera (Olympus) and cellSens Imaging Software (Olympus, v.1.11). At 1 and 4 hours post transfection, cell monolayers were homogenised with TRIzol™ for RNA

extraction, cDNA synthesis and RT-qPCR of IFN- β , expressed relative to stable reference genes.

To measure IFN- β production in Poly I:C-stimulated human retinal pigment epithelial cells expressing VP35, cells were first transfected with plasmids. Cells were seeded to confluency in 12 of 24-well plates. The following day, monolayers were transfected with either a pCAGGS plasmid or a pCAGGS-FLAG-VP35 plasmid with 2 μ L Lipofectamine 2000™ transfection reagent per well, according to the manufacturer's instructions. At 48 hours post-transfection, wells of cells were Lipofectamine 2000™-transfected with 1:1 high- and low-molecular weight Rhodamine-tagged Poly I:C (InvivoGen Life Research). At 4 hours post-transfection, cells were photographed and monolayers homogenised with TRIzol™ for RNA extraction, cDNA synthesis and RT-qPCR of IFN- β .

2.10 MICROSCOPY

2.10.1 Cell photography and image processing

Photographs of plated cells were taken with exposure and magnification for each well matched with respective control, in brightfield mode or with narrow-pass emission filters appropriate to the fluorescence wavelength of secondary antibodies. Digital images were saved in 16-bit tagged file image format (TIFF), and fluorescent images were manually merged using Adobe Photoshop CC (Adobe, v.19.1.6), with uniform adjustments across samples to image brightness as necessary.

2.11 BIOINFORMATICS

2.11.1 RNA sequencing

Next-generation RNA sequencing of EBOV-infected retinal pigment epithelial cells was performed by the Flinders Genomics Facility, South Australia. Total RNA was sourced from previous work done in the laboratory,²³⁵ in which ARPE-19 cells were infected in triplicate with EBOV at a MOI of 5 or mock-infected for 24 hours. In brief, from 1 µg of total RNA extracted with TRIzol™ reagent, small RNA was selectively enriched through sequential adapter ligation to 3' and 5' ends of RNA fragments using the TruSeq Small RNA Library Preparation Kit (Illumina). Single-stranded cDNA was synthesized by reverse transcription, and separately amplified with polymerase chain reaction using one of 48 primers containing index sequences (11 cycles). Using the Pippin Prep DNA Size Selection System (Sage Science), amplified cDNA constructs were purified from 3% agarose gel to isolate a library of small clone fragments. The library was sequenced on Illumina NextSeq 500, using NextSeq 75-cycle High Output Kits (Illumina), with the PhiX Control v3 library (Illumina) as sequencing control.

2.11.2 Data processing and differential expression analysis

Short reads were filtered for adapters and reads of low quality using Cutadapt (v.1.8)²⁷¹ with error rate of 0.2 and minimum length of 18 bp, aligned against GENCODE human genome reference assembly GRCh38.p3 using Burrows Wheeler Aligner²⁷², and assigned to miRBase (v.21) annotations using HTSeq (v.0.6.1p2).^{273, 274} Data were filtered for

targets with a minimum of 10 counts in at least 50% of samples. After normalization, differentially expressed miRNAs between EBOV- and mock-infected ARPE-19 cells were identified using the DESeq2 statistical package (v.3.2).²⁷⁵ Reads were screened for complete matches to published EBOV miRNA sequences, allowing for 3 mismatches.²⁷⁶ Raw data from a previous RNA sequencing study of the total RNA transcriptome of EBOV-infected ARPE-19 cells²³⁵ were processed in the same statistical pipeline used for human miRNAs, to identify genes that were differentially regulated with adjusted p-value 0.05 or less and log₂ fold-change 1 or greater, and were deposited at the National Center for Biotechnology Information's Gene Expression Omnibus,^{277, 278} and are accessible through Gene Expression Omnibus Series accession number GSE100839.²⁷⁹ Data processing and differential expression analysis were performed at the Flinders Genomics Facility.

2.11.3 Target predictions for microRNA

Computational predictions of the targets of differentially expressed human miRNAs (defined by adjusted p-value less than 0.001 and log₂ fold-change greater than 1) were performed using three public databases with different algorithms: Diana microT CDS v.5.0,^{280, 281} filtering with a threshold of 0.95; TargetScan v.7.1,²⁸² sorting on a total context score less than 0.15; and miRDB v.5.0,²⁸³ with a target threshold greater than 85. The human miRNAs were also input into two public online repositories of experimentally-validated data on molecular interactions: miRecords (release 2013)²⁸⁴ and miRTarBase v.7.0,²⁸⁵ set to 'strong evidence'.

2.11.4 Pathway and network analyses

Gene ontology²⁸⁶ and pathway analyses were performed using the open-source bioinformatics platform, Cytoscape (v.3.4.0),²⁸⁷ and the ClueGO (v.2.3.3) application,²⁸⁸ to identify enriched biological processes and molecular functions, and Kyoto Encyclopedia of Genes and Genomes (KEGG) pathways.²⁸⁹ Using the STRING Action dataset (v.9) within the CluePedia application (v.1.3.3)^{290, 291} and collating miRNA-gene pairs, a miRNA-based network was constructed from miRNA-predicted gene target lists, miRNA-validated target gene lists, and the differentially expressed gene list; interactions were demonstrated based on degree, to identify the most highly-connected genes and miRNAs. An inverse correlation was required between expression of a miRNA and its target gene in these analyses.

2.12 STATISTICAL ANALYSES

Statistical analysis was performed in GraphPad Prism (GraphPad Software; v.7.04). Results were expressed as mean and standard deviation, and confidence intervals were calculated to demonstrate the estimated population mean. Statistically significant differences were defined by a p-value or alpha less than 0.05. Comparisons between two independent conditions with assumed normal distribution were by unpaired two-tailed Student's t-tests. For unpaired non-parametric data, Mann-Whitney U test was used. For analysis of data with two independent categorical variables, statistical significance was determined using Fisher's exact test.

Comparisons across multiple independent conditions with assumed normal distribution were by analysis of variance (ANOVA). In the case of one categorical independent variable, a one-way ANOVA was performed, and where two categorical independent variables were analysed, a two-way ANOVA was performed. When data involved longitudinal measurements, repeated measures ANOVA was used. When differences between conditions or interactions reached statistical significance (ie. p-value less than 0.05), post-hoc analyses (Sidak, Tukey's or Bonferroni multiple comparisons test) were performed, and determined which groups differed from each other. The F-statistic, degrees of freedom and exact p-values were reported for each factor or interaction.

CHAPTER 3

Tissue changes in active toxoplasmic retinochoroiditis by spectral-domain optical coherence tomography

3.1	Introduction	103
3.2	Results.....	104
3.2.1	Participant demographics.....	104
3.2.2	Clinical characteristics of toxoplasmic retinochoroiditis	107
3.2.3	Spectral-domain optical coherence tomography findings at presentation.....	109
3.2.3.1	<i>Retinal findings at presentation by spectral-domain optical coherence tomography.....</i>	<i>109</i>
3.2.3.2	<i>Macular changes at presentation by spectral-domain optical coherence tomography .</i>	<i>116</i>
3.2.3.3	<i>Vitreous signs at presentation by spectral-domain optical coherence tomography</i>	<i>116</i>
3.2.3.4	<i>Retinal pigment epithelial and choroidal findings at presentation by spectral-domain optical coherence tomography</i>	<i>119</i>
3.2.4	Tissue changes by spectral-domain optical coherence tomography during follow-up.....	121
3.2.5	Features of retinal necrosis by spectral-domain optical coherence tomography.....	121
3.2.6	Visual outcomes associated with spectral-domain optical coherence tomography features of toxoplasmic retinochoroiditis.....	126
3.3	Discussion.....	130

3.1 INTRODUCTION

In immunocompetent adults, toxoplasmic retinochoroiditis (TRC) is the major manifestation of infection with the parasite, *Toxoplasma gondii*.³⁸ Ocular disease is characterized by a necrotizing retinitis with inflammation in the vitreous and choroid in the acute phase, leading to a variably-pigmented retinochoroidal scar.²⁵⁹ Visual sequelae are serious: in a study of 154 consecutive patients with active TRC, blindness was manifest in at least one eye in 24% of participants.⁶⁴

Spectral-domain optical coherence tomography (SD-OCT) is a well-established modality for imaging the ultrastructure of the retina, and has an axial resolution approaching 3 μm .¹⁰⁰ A limited number of studies have used SD-OCT to identify tissue changes in TRC. In the largest cohort study to date, 24 eyes of 24 patients with active TRC were examined, and common SD-OCT signs included posterior hyaloid thickening, and retinal hyperreflectivity, thickening and disorganisation.²⁹² Smaller studies have examined both active and healed lesions, and TRC-associated macular oedema and choroidal thickening.^{164, 293-297} Common retinal diseases such as age-related macular degeneration and diabetic macular oedema rely heavily on SD-OCT signs as diagnostic²⁹⁸ or monitoring²⁹⁹ biomarkers, yet SD-OCT signs that aid diagnosis or indicate prognosis in TRC have not been reported.

Herein, SD-OCT was used to identify the tissue changes of TRC, to better understand pathophysiology. In an area of Brazil with a high prevalence of toxoplasmosis, SD-OCT was used prospectively to examine patients with TRC who presented to a tertiary referral uveitis practice over a 34-month period. The aims of this study were to define tissue

alterations in TRC as visualised by SD-OCT, to identify signs of TRC on SD-OCT that predicted visual outcome, and to establish differences between clinical situations, defined by retinal location, primary versus recurrent ocular disease, and based on *T. gondii* and HIV serology.

3.2 RESULTS

3.2.1 Participant demographics

Consecutive patients attending the Uveitis Clinic at Ribeirão Preto General Hospital in Southeast Brazil with TRC, and aged over 12 years, were prospectively recruited. From a total of 262 subjects (344 eyes) with TRC, 90 individuals (90 eyes) qualified for inclusion in this study (Figure 3.1). Mean age at presentation was 37 years (median, 33 years; range, 12 to 84 years), and 44 participants (49%) were male (Table 3.1). A total of 8 of 90 participants (9%) had bilateral TRC, and only one eye (the eye with the most posterior lesion, or if symmetrical, the right eye) was included in this study. In 10 patients, ocular fluid testing was undertaken to confirm the diagnosis. Aqueous humour samples of 7 individuals were positive for *T. gondii* by qPCR, and the remaining 3 individuals had *T. gondii* confirmation by qPCR of vitreous biopsy. For 90% of persons (n = 81), the timing of ocular infection was unknown. Of the 9 individuals who knew the timing of their infection, 1 had confirmed congenital disease by review with an ophthalmologist, and 8 had previously documented negative *T. gondii* serology or ophthalmic examination, indicating recently-acquired infection. Those with active TRC who were excluded were similar by age, gender and HIV status to those who were included.

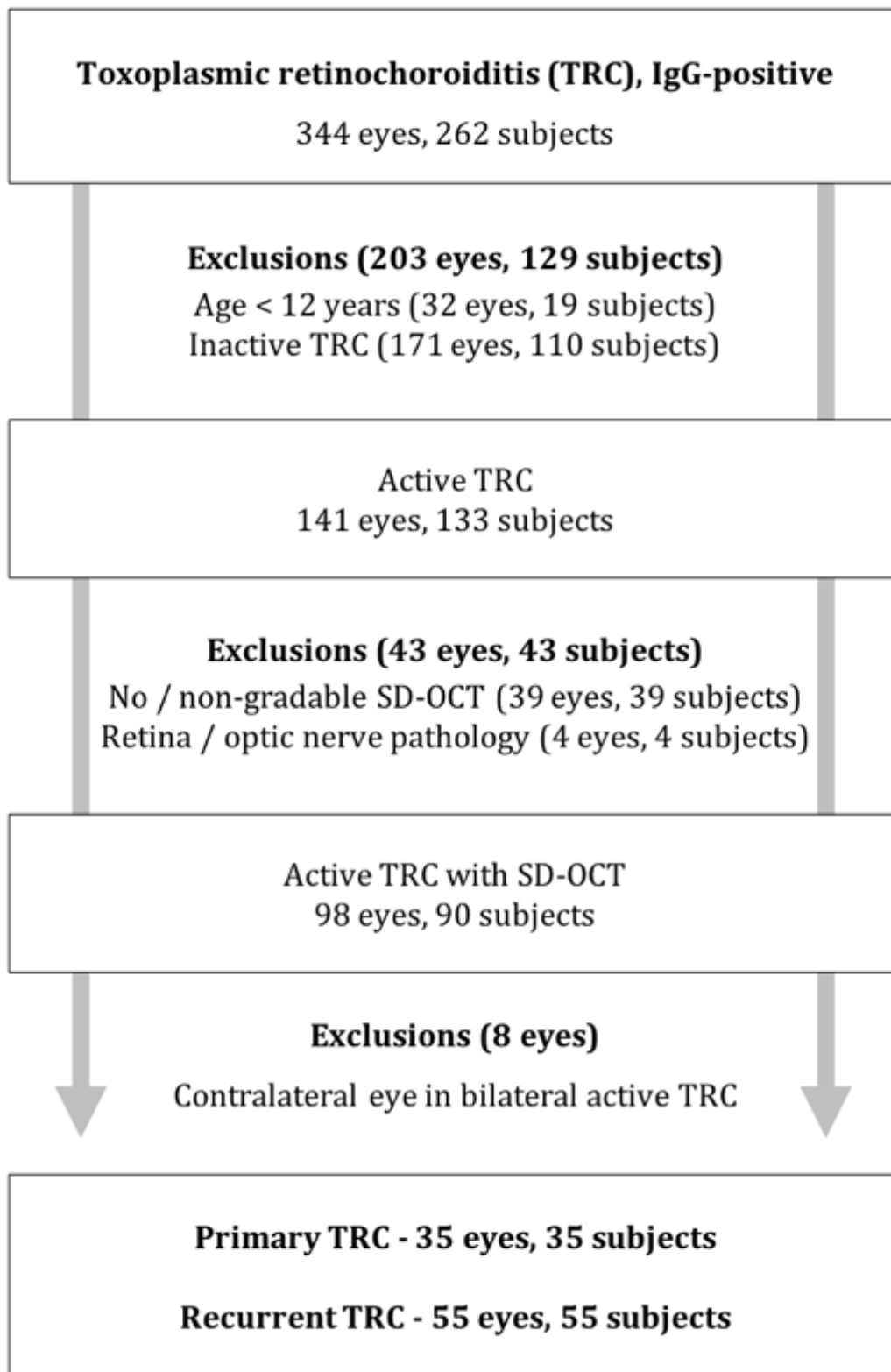


Figure 3.1: Study selection criteria

From 262 consecutive patients presenting to a tertiary-referral uveitis clinic, a final cohort of 90 eyes of 90 subjects with active *T. gondii* immunoglobulin (Ig)G-positive toxoplasmic retinochoroiditis (TRC), as imaged by Heidelberg Spectralis® SD-OCT, were included.

Table 3.1: Participant and disease characteristics

Category	Characteristic	Total (%) or median (range)
Age (years)		33.4 (12-84)
Sex	Male	44 (49)
Race	White	46 (51)
	Mulatto	13 (14)
	Black	31 (34)
Time of infection	Congenital	1 (1)
	Postnatally acquired	8 (9)
	Mode unknown	81 (90)
Laterality	Bilateral disease	8 (9)
	Right eye	49 (54)
Retinal location*	Zone 1	30 (33)
	Zone 2	60 (67)
Disease type	Primary	35 (39)
	Recurrent active	55 (61)
Ocular fluid testing	Anterior chamber paracentesis	6 (7)
	Vitreous biopsy	3 (3)
Baseline VA	BCVA \geq 20/40	33 (37)
	20/200 < BCVA < 20/40	26 (29)
	BCVA \leq 20/200	31 (34)
Serology	<i>T. gondii</i> IgM-positive	14 (16)
	<i>T. gondii</i> IgG-positive	90 (100)
	HIV IgG-positive	8 (9)
Treatment	Trimethoprim + sulfamethoxazole	63 (70)
	Sulfadiazine + pyrimethamine	12 (13)
	Oral prednisolone	77 (85)
	No treatment	6 (7)

Abbreviations: BCVA = best corrected visual acuity; Ig = immunoglobulin, SD = standard deviation, VA = visual acuity. **Location:** Zone 1 = up to 3000 μ m from fovea or 1500 μ m from disc margin; Zone 2 = between equator and zone 1.

3.2.2 Clinical characteristics of toxoplasmic retinochoroiditis

Participants underwent a full ophthalmic examination, and had active disease, which was indicated by retinal whitening, vitritis, and vitreous haze.²⁵⁹ Recurrent TRC (Figure 3.2) was defined as a focus of retinochoroiditis in an individual with variably pigmented chorioretinal scarring in either eye and a positive serological test for *T. gondii* IgG. Of 90 participants, 55 (61%) had recurrent TRC, while 35 (39%) presented with primary ocular disease, indicated by a focus of retinitis and positive *T. gondii* IgG serology in the absence of pigmented retinal scars in either eye. Lesions were located in zone 1 (within 3000 μm of the fovea or within 1500 μm of the optic disc margin) in 30 eyes (33%) and zone 2 (between the equator and zone 1) in 60 eyes (67%). Those with active TRC who were excluded were similar by age, gender and HIV status. Of all eyes with TRC, and in the absence of other retinal disease, the proportion of lesions that did not have an SD-OCT scan was 33% (15 of 45 eyes) for zone 1 lesions, and 39% (44 of 114 eyes) for zone 2 lesions. Fourteen people (16%) were *T. gondii* IgM-positive, indicating recently-acquired disease. Eight participants (9%) had evidence of HIV infection. The cluster of differentiation 4 (CD4) count was known in 7 of these individuals and ranged from 45 to 935 cells/ μL (mean = 262 cells/ μL). No study participant had positive syphilis serology. Most participants were treated with trimethoprim and sulfamethoxazole (n = 63, 70%), or sulfadiazine and pyrimethamine (n = 12, 13%), plus oral prednisolone (n = 77, 85%). The mean duration of follow-up was 12.9 months (range 1-30).

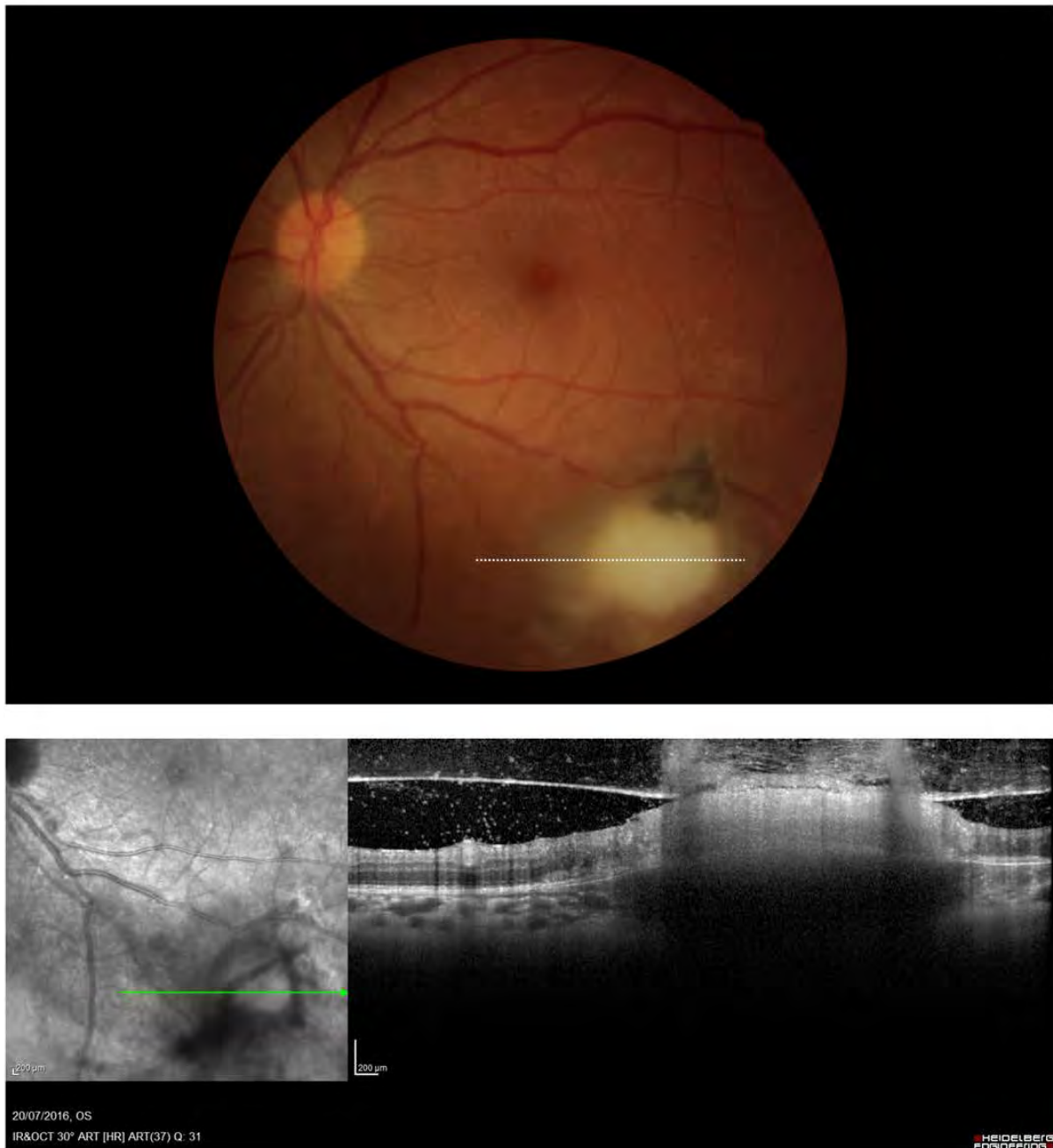


Figure 3.2: Active recurrent toxoplasmic retinochoroiditis at presentation

Representative images of the posterior segment of the eye from an individual presenting to a tertiary-referral uveitis clinic with zone 2 recurrent *T. gondii* IgG-positive TRC, studied by Heidelberg Spectralis® spectral-domain optical coherence tomography (SD-OCT) (below right). Colour fundus photograph (above) and near infrared image (below left) for clinical correlation. SD-OCT demonstrating hyperreflective dots in the vitreous and sub-hyaloid space, thickened posterior hyaloid with partial posterior vitreous detachment, full-thickness retinal hyperreflectivity in the centre of the lesion with adjacent retinal disorganisation, bowing of the retinal pigment epithelial-Bruchs complex, and choroidal thickening with hyporefectivity. **Abbreviations:** IG = immunoglobulin, TRC = toxoplasmic retinochoroiditis.

3.2.3 Spectral-domain optical coherence tomography findings at presentation

3.2.3.1 RETINAL FINDINGS AT PRESENTATION BY SPECTRAL-DOMAIN OPTICAL COHERENCE TOMOGRAPHY

The posterior pole and lesion were imaged by colour photography and SD-OCT, as permitted by media clarity. At presentation, the majority of SD-OCT tissue changes at the TRC lesion involved the retina, and findings are displayed in Table 3.2. Retinal thickening relative to adjacent uninvolved retina was seen in two-thirds of cases ($n = 46/71$, 65%). This was more common for zone 1 TRC (within 3000 μm of the fovea or 1500 μm of the optic disc margin), which was on average 201 μm thicker than zone 2 (between equator and zone 1) lesions ($p < 0.01$). Retinal hyperreflectivity (Figure 3.2) – defined as full-thickness hyperreflectivity, with the normally hyporeflexive inner nuclear and outer nuclear layers being hyperreflective – was a presenting feature in 43 of 70 lesions (61%), and was more likely in zone 1 lesions or with primary disease ($p < 0.05$). Disorganisation of retinal layers was evident in 16 of 71 lesions (23%), and noted more often in zone 2 or recurrent disease ($p < 0.05$). Intraretinal hyperreflective dots were seen in 7 of 70 lesions (10%). Tissue changes adjacent to the focus of TRC were demonstrated by SD-OCT, in the form of intraretinal and subretinal fluid, and hyperreflective dots in the retina, all of which were more likely to be seen in primary ocular TRC than recurrent disease ($p < 0.05$) (Table 3.3).

Table 3.2: Retinal findings at the toxoplasmic retinochoroiditis lesion by spectral-domain optical coherence tomography at presentation

Tissue changes on SD-OCT were compared by location, ocular infection, *T. gondii* serology and HIV infection in 90 eyes of 90 subjects presenting with acute TRC. Denominator indicates number of gradable scans. P-values were calculated using Fisher's exact test or Mann-Whitney U test (* $p < 0.05$, ** $p < 0.01$).

SD-OCT changes at TRC lesion	Total		Location*				Ocular infection				T. gondii serology				HIV infection			
	N	%	n	%	n	%	n	%	n	%	n	%	n	%	n	%	n	%
Thickened	46/71	65	24/28**	86	22/43**	51	23/31	74	23/40	58	10/14	71	36/57	63	3/7	43	43/64	67
Full-thickness hyperreflectivity	43/70	61	22/29*	76	21/41*	51	23/30*	77	20/40*	50	9/14	65	34/56	61	3/6	50	40/64	63
Disorganisation of layers	16/71	23	3/29*	10	13/42*	31	3/30*	10	13/41*	32	3/14	21	13/57	23	2/6	33	14/65	22
Optic disc involvement	9/73	12	9/29	31	N/A		8/31**	26	1/42**	2	0/14	0	9/59	15	1/7	14	8/66	12
Hyperreflective dots	7/70	10	3/29	10	4/41	10	3/30	10	4/40	10	1/14	7	6/56	11	0/6	0	7/64	11
Outer retinal cystic spaces	7/73	10	3/29	10	4/44	9	3/31	10	4/42	10	2/14	14	5/59	8	0/7	0	7/66	19
Signal void	4/71	6	2/29	7	2/42	5	1/30	3	3/41	7	1/14	7	3/57	5	1/6	17	3/65	5
Perivascular dots	4/73	5	1/29	3	3/44	7	2/31	6	2/42	5	0/14	0	4/59	7	1/7	14	3/66	5

SD-OCT changes at TRC lesion	Total		Location*				Ocular infection				T. gondii serology				HIV infection			
	N	%	n	%	n	%	n	%	n	%	n	%	n	%	n	%	n	%
RETINA																		
Round outer plexiform bodies	2/73	3	0/29	0	2/44	5	2/31	6	0/42	0	2/14*	14	0/59*	0	1/7	14	1/66	2
Intra- or subretinal fluid	2/68	3	0/28	0	2/40	5	1/31	3	1/37	3	0/15	0	2/53	4	1/8	13	1/60	2
TRC lesion height on SD-OCT	Mean		Location*				Ocular infection				T. gondii serology				HIV infection			
Mean lesion height (μm) \pm SD	434 \pm 202		565 \pm 179 **		364 \pm 173 **		491 \pm 219		382 \pm 165		463 \pm 179		424 \pm 205		406 \pm 213		435 \pm 199	

Abbreviations: HIV = human immunodeficiency virus, Ig = immunoglobulin, SD = standard deviation, SD-OCT = spectral-domain optical coherence tomography TRC = toxoplasmic retinochoroiditis. **Location:** Zone 1 = up to 3000 μm from fovea or 1500 μm from disc margin; Zone 2 = between equator and zone 1.

Table 3.3: Retinal changes adjacent to the toxoplasmic retinochoroiditis lesion by spectral-domain optical coherence tomography at presentation

Tissue changes adjacent to TRC lesion were compared by location, ocular infection, *T. gondii* serology and HIV infection in 90 eyes of 90 subjects presenting with acute TRC. Denominator indicates number of gradable scans. P-values were calculated using Fisher's exact test (* p < 0.05).

SD-OCT changes adjacent to TRC lesion	Total	Location*				Ocular infection				T. gondii serology				HIV infection				
		Zone 1		Zone 2		Primary		Recurrent		IgM +		IgM -		HIV +		HIV -		
ADJACENT RETINA	N	%	n	%	n	%	n	%	n	%	n	%	n	%	n	%	n	%
Subretinal or intraretinal fluid	11/73	15	6/29	21	5/44	11	8/31*	26	3/42*	7	1/14	7	10/59	17	1/7	14	10/66	15
Hyperreflective intraretinal dots	9/73	12	5/29	17	4/44	9	7/31*	23	2/42*	5	2/14	14	7/59	12	1/7	14	6/66	9
Disorganized lamination	8/73	11	2/29	7	6/44	14	5/31	16	3/42	7	2/14	14	6/59	10	0/7	0	8/66	12

Abbreviations: HIV = human immunodeficiency virus, Ig = immunoglobulin, SD-OCT = spectral-domain optical coherence tomography TRC = toxoplasmic retinochoroiditis. ***Location:** Zone 1 = up to 3000 µm from fovea or 1500 µm from disc margin; Zone 2 = between equator and zone 1.

A wide range of findings in the retina at the time subjects presented with TRC were documented by SD-OCT, and representative images are displayed in Figure 3.3. Intraretinal fluid in the form of large cystic spaces in the outer retina (Figures 3.3J and 3.3M) was present in 7 of 73 lesions (10%). Retinal changes adjacent to the lesion included disorganisation of retinal layers (Figures 3.4 and 3.5) in 8 of 73 eyes (11%), subretinal (Figure 3.3K) or intraretinal fluid (Figure 3.3N) in 11 of 73 eyes (15%), and hyperreflective intraretinal dots in 9 of 73 eyes (12%). Optic disc involvement (Figure 3.3A, $n = 9/73$, 12%) was more common in primary disease ($p < 0.01$), which also was associated with adjacent subretinal or intraretinal fluid ($p < 0.05$). Signal void within the retina, extending between the internal limiting membrane and RPE (Figure 3.6B) was noted in 4 of 71 lesions (6%). Novel retinal findings included perivascular hyperreflective dots (Figures 3.3A and 3.3C, $n = 4/73$, 5%), round outer plexiform bodies (Figure 3.3L, $n = 2/73$, 3%) and a “ribbon-like” outer nuclear layer (Figure 3.3E), defined by hyporefectivity of the outer nuclear layer and hyperreflectivity of the inner nuclear layer ($n = 1/73$, 1%). Round bodies in the outer plexiform layer were the only retinal or choroidal sign associated with *T. gondii* IgM-positive TRC ($p < 0.05$), and there were no differences between retinal or choroidal signs in HIV-positive versus -negative patients.

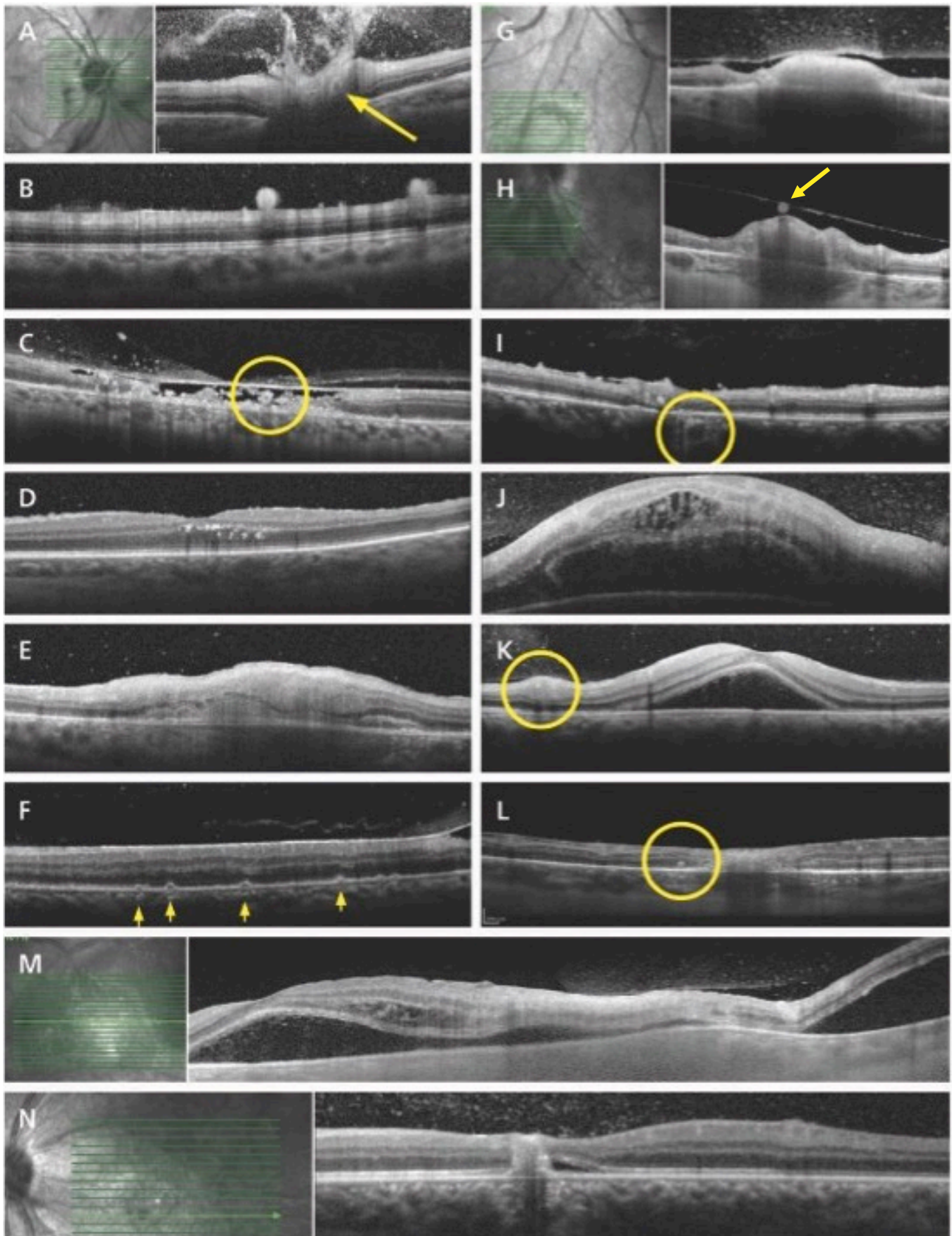


Figure 3.3: Pathological changes in eyes with active toxoplasmic retinochoroiditis by spectral-domain optical coherence tomography

(A). Hyperreflective dots in the vitreous cavity overlying the optic disc (zone 1, primary, *T. gondii* IgM-negative); note perivascular hyperreflectivity (arrow); (B). Large hyperreflective deposits at vitreoretinal interface (zone 2, recurrent, *T. gondii* IgM-negative); (C). Hyperreflective vessel (circled) within area of retinal void, (HIV-positive, zone 2, recurrent, *T. gondii* IgM-negative); (D). Intraretinal hyperreflective dots in outer plexiform and outer nuclear layer (zone 2, primary, *T. gondii* IgM-positive); (E). “Ribbon” appearance of hyporeflexive outer nuclear layer and hyperreflective inner nuclear layer within full-thickness retinal hyperreflectivity (zone 1, recurrent, *T. gondii* IgM-negative); (F). Small retinal pigment epithelial detachments (arrows), (HIV-positive, zone 2, recurrent, *T. gondii* IgM-negative); (G). Hyperreflective dots in the vitreous cavity, thickened posterior hyaloid with partial posterior vitreous detachment; retinal thickening with full-thickness hyperreflectivity and adjacent disorganisation of retinal layers and thickening of RPE; choroidal hyporeflexivity and thickening (zone 2, primary, *T. gondii* IgM-negative); (H). Large hyperreflective deposit (arrow) on posterior hyaloid face (zone 2, recurrent, *T. gondii* IgM-negative); note thickened hyperreflective retina with choroidal hyporeflexivity and thickening; (I). Prominent hyperreflective dots surrounding choroidal vessel (circled) and internal limiting membrane, and disorganisation of retinal layers (zone 2, recurrent, *T. gondii* IgM-negative); (J). Gross macular thickening with hyperreflective dots and intraretinal fluid in the outer plexiform and outer nuclear layers (“huge outer retinal cystoid spaces”), subretinal fluid and bowing of RPE-Bruch’s membrane complex (zone 1, primary, *T. gondii* IgM-negative); (K). Subfoveal fluid and hyperreflective dots in the vitreous cavity overlying a vessel (circled), (zone 2, primary, *T. gondii* IgM-negative); (L). Round body in outer nuclear layer (circled, 80 μ m), with adjacent retinal hyperreflectivity and disorganisation of retinal layers (zone 2, primary, *T. gondii* IgM-positive); (M). Subfoveal fluid containing hyperreflective dots, outer plexiform and outer nuclear layer fluid with hyperreflective dots, retinal hyperreflectivity, bowing of RPE-Bruch’s membrane complex, overlying hyperreflective dots in the vitreous cavity and partial separation of posterior hyaloid (zone 2, primary, *T. gondii* IgM-negative); (N). Hyperreflective dots in the vitreous cavity, disorganisation of retinal layers, thickening of RPE with subjacent choroidal hyporeflexivity and adjacent subfoveal fluid (zone 1, recurrent, *T. gondii* IgM-negative). **Abbreviations:** HIV = human immunodeficiency virus, Ig = immunoglobulin, RPE = retinal pigment epithelium, SD-OCT = spectral-domain optical coherence tomography TRC = toxoplasmic retinochoroiditis. **Location:** Zone 1 = up to 3000 μ m from fovea or 1500 μ m from disc margin; Zone 2 = between equator and zone 1.

3.2.3.2 MACULAR CHANGES AT PRESENTATION BY SPECTRAL-DOMAIN OPTICAL COHERENCE TOMOGRAPHY

The macula is the area of retina located at the posterior pole of the eye that is responsible for processing the central field of vision. Pathological changes at the macula were evident by SD-OCT in 64 of 86 eyes (74%) at presentation, and are outlined in Table 3.4. Zone 1 lesions were associated with hyperreflective dots at the vitreoretinal interface (Figures 3.2, 3.3A, 3.3G, 3.3N, 3.5; n = 6/29, 21%), full-thickness retinal hyperreflectivity (n = 5/29, 17%), and submacular choroidal thickening $\geq 300 \mu\text{m}$ (n = 6/29, 21%) ($p < 0.01$) at the macula. Intraretinal hyperreflective dots (Figure 3.3D; n = 8/29, 28%) and retinal voids (Figures 3.6B to 3.6D; n = 3/29, 10%) were also associated with zone 1 TRC ($p < 0.05$). Active TRC in zone 2 was associated with an abnormal macular SD-OCT scan in 22 of 57 eyes (39%). Macular oedema was seen in 19 of 86 eyes (22%), irrespective of the zone of the lesion (Figure 3.2A-C). Epiretinal membrane was observed in 10 of 86 eyes (12%), but vitreomacular traction was an uncommon presenting feature (n = 3/86, 3%).

3.2.3.3 VITREOUS SIGNS AT PRESENTATION BY SPECTRAL-DOMAIN OPTICAL COHERENCE TOMOGRAPHY

Pathological changes in the vitreous during active TRC that were documented by SD-OCT are presented in Table 3.5. At first presentation, hyperreflective dots in the vitreous were noted in 80% of eyes (n = 64/80). This change was not associated with TRC location, disease type, *T. gondii* IgM positivity or serologic evidence of HIV infection. The posterior hyaloid was attached at the lesion in 70 of 80 eyes (88%), and this was more common in primary TRC ($p < 0.05$). A partial posterior vitreous detachment (Figures 3.2 and 3.3G) was noted in 13 of 80 eyes (16%), and occurred more often in zone 2 TRC ($p < 0.05$). There were no signs of complete posterior vitreous detachment in any eye by SD-OCT.

Table 3.4: Macular features by spectral-domain optical coherence tomography at presentation with active toxoplasmic retinochoroiditis

Macular findings on SD-OCT in active TRC at presentation for 86 eyes (86 patients). P-values calculated using Fisher's exact or Student's t-test (* p < 0.05, ** p < 0.01, *** p < 0.001).

SD-OCT feature at the macula	Total (%)	TRC in zone 1 N = 29 (%)	TRC in zone 2 N = 57 (%)	p-value
Normal appearance	22 (26)	0 (0)	22 (39)	< 0.001***
Hyperreflective dots at vitreoretinal interface	6 (7)	6 (21)	0 (0)	< 0.01**
Vitreomacular traction	3 (3)	0 (0)	3 (5)	0.55
Epiretinal membrane	10 (12)	1 (3)	9 (16)	0.15
Full-thickness retinal hyperreflectivity	5 (6)	5 (17)	0 (0)	< 0.01**
Hyperreflective dots retina	13 (15)	8 (28)	5 (9)	< 0.05*
Macular oedema	19 (22)	8 (28)	11 (19)	0.42
Retinal void	3 (3)	3 (10)	0 (0)	< 0.05*
Subretinal fibrosis	1 (1)	1 (3)	0 (0)	0.34
Retinal pigment epithelial thickening	2 (2)	0 (0)	2 (4)	0.55
Choroidal thickening $\geq 300 \mu\text{m}$	7 (8)	6 (21)	1 (2)	< 0.01**
Central 1 mm diameter macular volume (mm^3) \pm SD	0.28 \pm 0.11 (N=76)	0.29 \pm 0.14 (n=23)	0.27 \pm 0.10 (n=53)	0.47

Abbreviations: SD-OCT = spectral-domain optical coherence tomography, TRC = toxoplasmic retinochoroiditis. ***Location:** Zone 1 = within 3000 μm of the fovea or 1500 μm of the optic disc margin; Zone 2 = between equator and zone 1.

Table 3.5: Vitreous signs in active toxoplasmic retinochoroiditis by spectral-domain optical coherence tomography at presentation

Alterations in the vitreous overlying active TRC by SD-OCT were compared by location, ocular infection, *T. gondii* serology and HIV infection in 90 eyes of 90 subjects at presentation. Denominator indicates number of gradable scans. P-values were calculated using Fisher's exact test (* p < 0.05).

TRC lesion at presentation by SD-OCT	Total		Location				Ocular infection				T. gondii serology				HIV infection			
	N	%	Zone 1		Zone 2		Primary		Recurrent		IgM +		IgM -		HIV +		HIV -	
OVERLYING VITREOUS	N	%	n	%	n	%	n	%	n	%	n	%	n	%	n	%	n	%
Posterior hyaloid attached	70/80	88	26/29	90	44/51	86	31/32*	97	39/48*	81	14/15	93	56/65	86	6/8	75	64/72	89
Hyperreflective dots	64/80	80	22/29	76	42/51	82	25/32	78	39/48	81	9/15	60	55/65	85	8/8	100	56/72	78
Deposits \geq 25 μ m	29/80	36	8/29	28	21/51	41	14/32	44	15/48	31	6/15	40	23/65	35	5/8	63	24/72	33
Posterior hyaloid thickening	28/80	35	9/29	31	19/51	37	10/32	31	18/48	38	3/15	20	25/65	38	3/8	38	25/72	35
Normal appearance	16/80	20	7/29	24	9/51	18	7/32	22	9/48	19	6/15	40	10/65	15	0/8	0	16/72	35
Partial posterior vitreous detachment	13/80	16	1/29*	3	12/51*	24	4/32	13	9/48	19	2/15	13	11/65	17	1/8	13	12/72	17
Vitreoschisis	2/80	3	1/29	3	1/51	2	2/32	6	0/48	0	1/15	7	1/65	2	1/8	13	1/72	1
Traction adjacent to lesion	1/80	1	0/29	0	1/51	2	0/32	0	1/48	2	0/15	0	1/65	2	0/8	0	1/72	1
Epiretinal membrane at lesion	4/80	5	0/29	0	4/51	8	1/32	3	3/48	6	1/15	7	3/65	5	0/8	0	4/72	6

Abbreviations: HIV = human immunodeficiency virus, Ig = immunoglobulin, SD-OCT = spectral-domain optical coherence tomography, TRC = toxoplasmic retinochoroiditis. ***Location:** Zone 1 = up to 3000 μ m from fovea or 1500 μ m from disc margin; Zone 2 = between equator and zone 1.

Posterior hyaloid thickening (Figures 3.2 and 3.3G) and large hyperreflective deposits at the vitreoretinal interface (Figures 3.3B and 3.3H) were present in approximately one third of eyes ($n = 28/80$ and $29/80$, respectively) at presentation, and an epiretinal membrane was present across 4 of 80 lesions (5%).

3.2.3.4 RETINAL PIGMENT EPITHELIAL AND CHOROIDAL FINDINGS AT PRESENTATION BY SPECTRAL-DOMAIN OPTICAL COHERENCE TOMOGRAPHY

Clinical characteristics of TRC include variably pigmented retinal pigment epithelial scarring and choroidal inflammation. Pathological changes of the RPE and choroid that were identified by SD-OCT are displayed in Table 3.6. At presentation, the RPE at the TRC lesion was identifiable in 26 SD-OCT scans, and showed thickening in half of these (Figures 3.3N, 3.5, 3.6B to 3.6F). Atrophic retinal pigment epithelial changes (Figure 3.5) were evident in 9 of 26 eyes (35%). Small pigment epithelial detachments (Figure 3.3F) were present in one patient with concurrent HIV infection and a CD4 count of 235 cells/ μ L. Choroidal hyporeflectivity (Figure 3.2) was a common feature, present in 25 of 41 eyes at presentation (61%), with bowing of the retinal-RPE-Bruch's membrane complex (Figure 3.2, $n = 6/73$, 8%). Forty of 90 patients had an SD-OCT scan with EDI at presentation, and the choroid was thickened in 55% of these scans (Figures 3.2, 3.3G and 3.3H, $n = 22/40$). Choroidal perivascular hyperreflective dots (Figure 3.3I) were identified in 4 of 73 eyes (5%), and were likely prominent due to the effect of overlying retinal and retinal pigment epithelial atrophy.

Table 3.6: Retinal pigment epithelial and choroidal findings in active toxoplasmic retinochoroiditis by spectral-domain optical coherence tomography at presentation

Alterations in the RPE and choroid in active TRC by SD-OCT were compared by location, ocular infection, *T. gondii* serology and HIV infection in 90 eyes of 90 subjects at presentation. Denominator indicates number of gradable scans. P-values were calculated using Fisher's exact test (* p < 0.05).

TRC lesion at presentation by SD-OCT	Total		Location				Ocular infection				<i>T. gondii</i> serology				HIV infection			
	N	%	Zone 1		Zone 2		Primary		Recurrent		IgM +		IgM -		HIV +		HIV -	
RPE and choroid	N	%	n	%	n	%	n	%	n	%	n	%	n	%	n	%	n	%
Retinal pigment epithelial thickening or detachment	14/26	54	6/8	75	8/18	44	4/8	50	10/18	56	2/3	67	12/23	52	2/3	67	12/23	52
Retinal pigment epithelial atrophy	9/26	35	2/8	25	7/18	39	3/8	38	6/18	33	1/3	33	8/23	35	1/3	33	8/23	35
Bowing of retina-RPE-Bruchs membrane	6/73	8	1/29	3	5/44	11	1/31	3	5/42	12	0/14	0	6/59	10	1/7	14	5/66	8
Choroidal hyporeflectivity	25/41	61	8/11	73	17/30	57	9/14	64	16/27	59	5/8	63	20/33	61	2/4	50	23/37	62
Choroidal hyperreflectivity	7/41	17	0/11	0	7/30	23	2/14	14	5/27	19	1/8	13	6/33	18	1/4	25	6/37	16
Choroid \geq 300 μ m thick	22/40	55	6/11	55	16/29	55	5/12	42	17/28	61	3/6	50	19/34	56	2/5	40	20/35	57
Adjacent perivascular dots	4/73	5	1/29	3	3/44	7	2/31	6	2/42	5	2/14	14	2/59	3	1/7	14	3/66	5

Abbreviations: HIV = human immunodeficiency virus, Ig = immunoglobulin, RPE = retinal pigment epithelium, SD-OCT = spectral-domain optical coherence tomography, TRC = toxoplasmic retinochoroiditis. ***Location:** Zone 1 = up to 3000 μ m from fovea or 1500 μ m from disc margin; Zone 2 = between equator and zone 1.

3.2.4 Tissue changes by spectral-domain optical coherence tomography during follow-up

The eye of 15 patients, followed for at least 8 weeks without recurrence, had additional SD-OCT imaging of the lesion and/or macula during follow-up. Figure 3.4 illustrates a representative TRC lesion on treatment, demonstrating representative signs on SD-OCT. Common tissue changes (Table 3.7) included disorganised retinal layers (n = 11/15, 73%) and posterior hyaloid thickening (n = 8/15, 53%). Involved retina often became thinned relative to adjacent tissue (n = 6/15, 40%), while the RPE became thickened at (n = 6/15 eyes, 40%) or adjacent to (n = 3/15 eyes, 20%) the lesion. Of those with macular epiretinal membrane at presentation (10 eyes), vitreomacular traction was evident in one eye, and the posterior hyaloid continued to separate with subsequent visits in 3 eyes. There were no signs of complete posterior vitreous detachment in this group.

3.2.5 Features of retinal necrosis by spectral-domain optical coherence tomography

Two types of retinal destruction were visualised by SD-OCT. The most common form presented with full-thickness retinal hyperreflectivity and thickening, and a well-demarcated border to adjacent normal-appearing retina, with underlying choroidal hyporefectivity, and hyperreflective dots in the vitreous (Figure 3.2). Over time, active TRC lesions progressively thinned, and became disorganised and less hyperreflective (Figure 3.4). Less commonly, retinal destruction presented as signal voids within the neural retina, with preservation of the RPE and internal limiting membrane (Figures 3.5A to 3.5F). As these retinal voids regressed, relatively fewer hyperreflective dots were evident in the vitreous, and void spaces were slowly replaced by disorganised retinal tissue in follow-up.

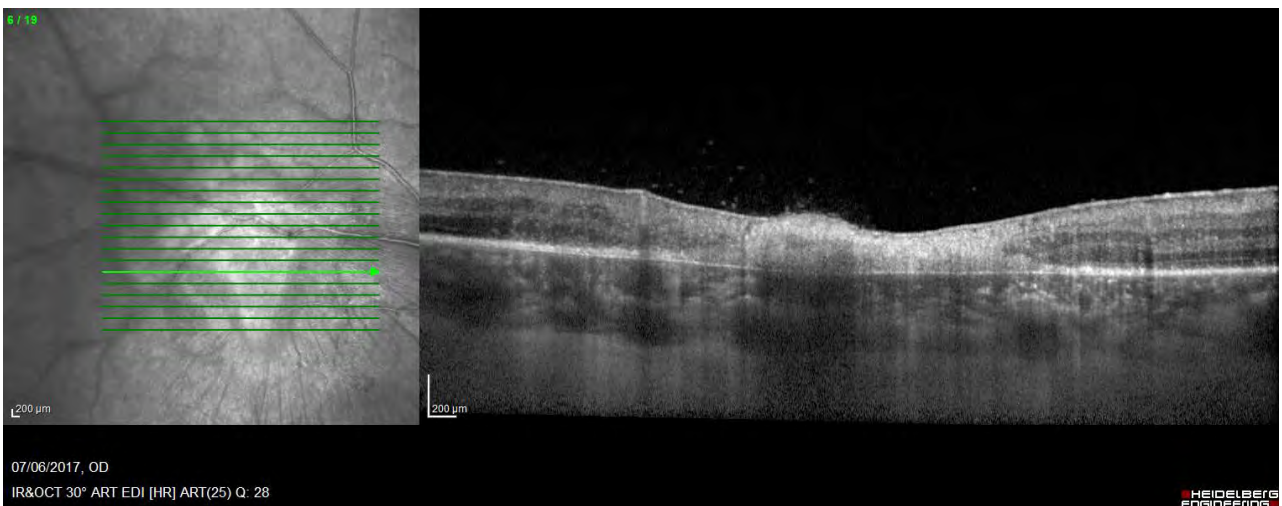


Figure 3.4: Response to treatment

Representative images from an individual at follow-up in a tertiary-referral uveitis clinic after 5 days on antibiotic therapy. The patient had primary *T. gondii* IgG-positive TRC, studied with Heidelberg Spectralis® SD-OCT of the posterior segment of the eye (below right). Colour fundus photograph (above) and near infrared image (below left) for clinical correlation. SD-OCT demonstrating minimal vitreous hyperreflective dots, epiretinal membrane, full-thickness retinal hyperreflectivity in the centre of the lesion, with relative thinning and adjacent disorganized retinal layers and sublesional choroidal shadowing.. **Abbreviations:** Ig = immunoglobulin, SD-OCT = spectral-domain optical coherence tomography, TRC = toxoplasmic retinochoroiditis.

Table 3.7: Retinal features of active toxoplasmic retinochoroiditis during follow-up

Posterior segment features (including macular signs) on SD-OCT that were observed during follow-up of active TRC in 15 eyes of 15 patients (SD-OCT of the lesion) or 23 eyes of 23 patients (SD-OCT of the macula), who were followed for at least 8 weeks and did not have a recurrence during follow-up.

LESION	N	%
Hyaloid thickening	8/15	53
Epiretinal membrane	4/15	27
Expanded posterior vitreous detachment	3/15	20
Intra- or subretinal fluid	0/15	0
Lamination - disorganised	11/15	73
Retinal hyperreflectivity	3/15	20
Retinal signal void	2/15	13
Relatively thinned retina	6/15	40
Relatively thickened retina	2/15	13
Retinal pigment epithelial thickening	6/15	40
Retinal pigment epithelial atrophy	2/15	13
Adjacent retinal pigment epithelial thickening	3/15	20
Adjacent retinal pigment epithelial atrophy	2/15	13
Choroidal shadowing or hyporefectivity	3/15	20
Choroidal hyperreflectivity	3/15	20

MACULA	N	%
Epiretinal membrane	10/23	43
Intraretinal fluid	0/23	0
Retinal hyperreflectivity	0/23	0
Retinal signal void	3/23	13
Subretinal fluid	3/23	13
Vitreomacular traction	1/23	4
Subretinal hyperreflectivity	1/23	4

Abbreviations: SD-OCT = spectral-domain optical coherence tomography, TRC = toxoplasmic retinochoroiditis.

3.2.6 Visual outcomes associated with spectral-domain optical coherence tomography features of toxoplasmic retinochoroiditis

In order to ascertain a potential association of visual outcome with tissue changes by SD-OCT, all features of active TRC by SD-OCT were compared to best-corrected visual acuity at resolution in eyes followed for at least 8 weeks ($n = 47$). Selected results are displayed in Table 3.8 and pertain to tissue changes at presentation, tissue changes at the lesion, and include individuals who had central (zone 1) or peripheral (zone 2) lesions. At presentation, vitreous signs representing inflammatory changes on SD-OCT included hyperreflective dots, large deposits ($n = 15/47$, 32%), and posterior hyaloid thickening ($n = 21/47$, 45%). These were not shown to be associated with poor visual outcomes (visual acuity of 20/200 or worse). Similarly, the presence of intra-or subretinal fluid at the macula ($n = 9/47$, 29%), and macular epiretinal membrane ($n = 15/47$, 32%) did not predict visual outcome. The only SD-OCT finding associated with visual outcome was retinal signal voids at the TRC lesion, which was unusual in eyes achieving visual acuities of 20/40 or better ($n = 1/25$, 3%, $p < 0.01$), and present in half of eyes retaining visual acuities of 20/200 or worse ($n = 7/14$, $p < 0.01$).

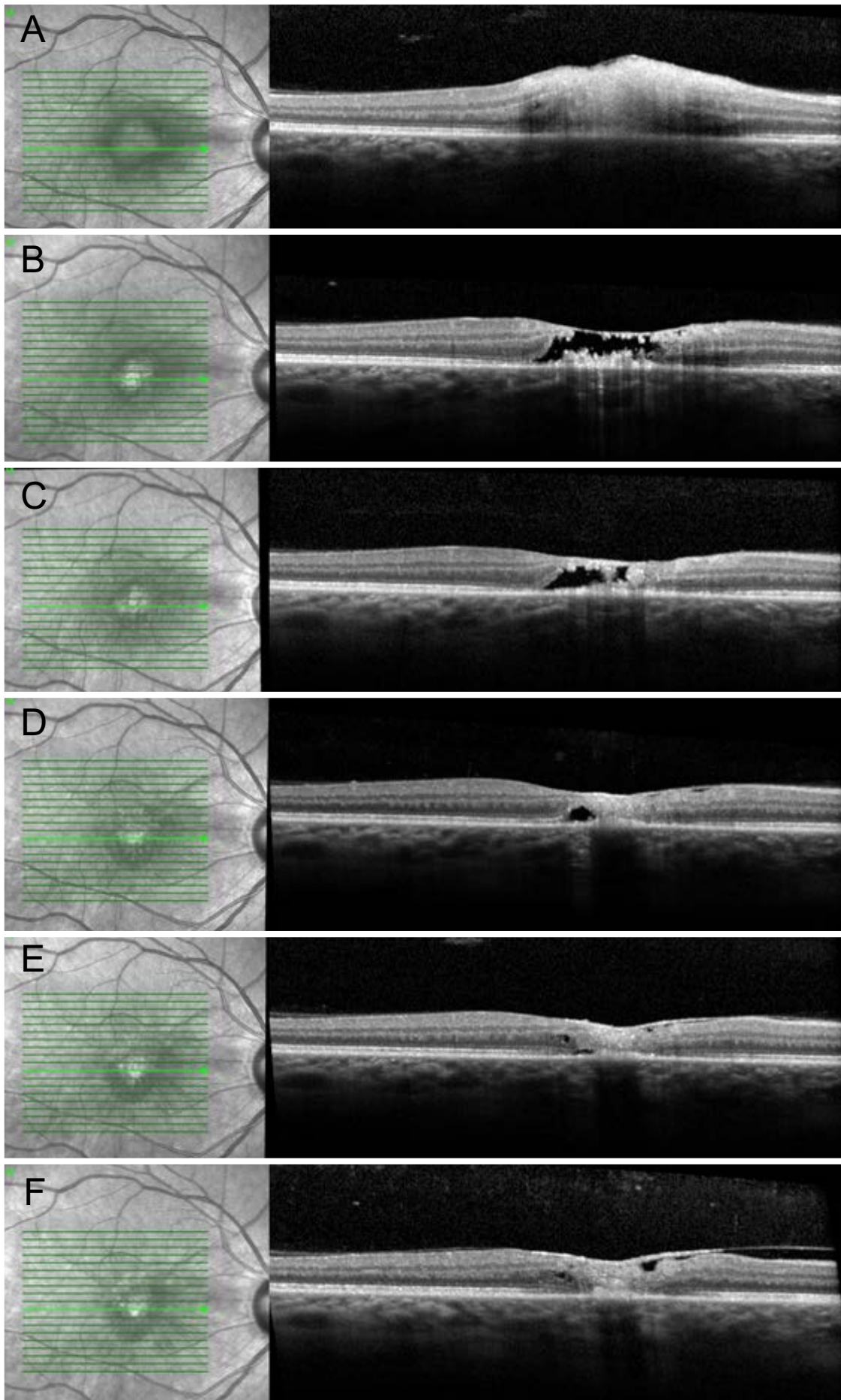


Figure 3.5: Evolution of retinal necrosis in toxoplasmic retinochoroiditis

SD-OCT scan of right macula in a patient presenting with zone 1, primary *T. gondii* IgM-positive TRC. (A). At presentation, demonstrating full-thickness retinal hyperreflectivity, thickening and disorganisation of retinal layers. Note lack of hyperreflective dots in the vitreous cavity; (B). At 7 days post-presentation. Liquefactive retinal necrosis demonstrated by large signal void within the retina, and preservation of the internal limiting membrane, and retinal pigment epithelial thickening; (C). At 2 weeks after presentation, the area of signal void was smaller; (D). Week 5 after presentation, disorganised retinal tissue and retinal pigment epithelial thickening; (E). Nine weeks after presentation, retinal signal void is replaced with granular disorganised tissue; (F). At 4 months post-presentation, showing partial separation of the posterior hyaloid, epiretinal membrane formation, disorganised retinal tissue, thickened RPE and focal choroidal hyporefectivity. **Abbreviations:** Ig = immunoglobulin, SD-OCT = spectral-domain optical coherence tomography, TRC = toxoplasmic retinochoroiditis. **Location:** Zone 1 = up to 3000 μm from fovea or 1500 μm from disc margin; Zone 2 = between equator and zone 1.

Table 3.8: Visual acuity and spectral-domain optical coherence tomography features

Visual outcomes in active TRC for 47 eyes of 47 patients. Subjects were followed for at least 8 weeks and did not have a recurrence on SD-OCT at any time during the follow-up period. Comparisons were made between eyes with good visual acuity (20/40 or better) and eyes with poor visual acuity (20/200 or worse). The p-values were calculated using Fisher's exact test (** p < 0.01).

SD-OCT feature during active TRC	Best corrected visual acuity at resolution					
	Total		< 20/40		> 20/200	
	N	%	n	%	n	%
Hyperreflective dots in vitreous at presentation	32/47	68	24/25	96	8/14	57
Deposits \geq 25 μ m in vitreous at presentation	15/47	32	6/25	24	6/14	43
Posterior hyaloid thickening at lesion at presentation	21/47	45	13/25	52	7/14	50
Retinal void at lesion at any time	8/47	17	1/25 **	4	7/14 **	50
Intra- or subretinal fluid at macula at any time	9/47	29	3/25	12	3/14	21
Macular epiretinal membrane	15/47	32	6/25	24	6/14	43

Abbreviations: SD-OCT = spectral-domain optical coherence tomography, TRC = toxoplasmic retinochoroiditis.

3.3 DISCUSSION

In this large cohort of patients presenting with TRC, diagnostic and prognostic signs of posterior segment tissue changes by SD-OCT were detailed, and the spectrum of signs of this retinal infection were presented. Common signs of active TRC included a thickened fully-hyperreflective retina with choroidal thickening and hyporefectivity, hyperreflective dots in the vitreous, and posterior hyaloid thickening. These changes were often accompanied by adjacent disorganisation of retinal layers. Over time, the retina thinned and became less hyperreflective, but did not return to a normal appearance. The RPE either thickened or became atrophic, causing secondary choroidal hyporefectivity or hyperreflectivity, respectively. Thickening of the choroid was marked in some cases (Figure 3.2), reflecting inflammatory changes secondary to the parasitic infection.

Retinal oedema was not a characteristic feature of active TRC in this series. Subretinal or intraretinal fluid, usually adjacent to the lesion, was observed in approximately 15% of eyes presenting with active TRC, and was more common in primary disease. Hyperreflective dots, also visible in the subretinal fluid, most likely represent inflammatory cells (Figure 3.3K and 3.3M).³⁰⁰ Published SD-OCT studies have identified subretinal fluid in as many as one-quarter of patients.²⁹² Two studies from the same group documented intraretinal and subretinal fluid in SD-OCT scans of TRC, although the authors did not explore clinical associations.^{294, 295} An unusual presentation of outer retinal oedema – “huge outer retinal cystic spaces”²⁹⁵ – was identified in 10% of lesions in our series (Figure 3.3J). This form of retinal oedema usually occurs at the macula, affects the outer plexiform, outer nuclear and photoreceptor layers, and is accompanied by subretinal fluid. Macular oedema was a presenting SD-OCT sign in approximately 20% of eyes; this was equally frequent in zone 1 and zone 2 lesions. Macular epiretinal membrane was noted during follow-up in 40% of eyes in our series.

Vitritis is a common clinical feature of TRC, and this was represented as hyperreflective dots in the vitreous cavity on SD-OCT. Small hyperreflective dots have been observed in the vitreous and retina of eyes with active TRC, as well as eyes with other forms of posterior uveitis, and are a size consistent with that of inflammatory cells, demonstrating regression as the inflammatory process resolves.³⁰⁰ Large hyperreflective deposits (over 25 μm) were seen in the vitreous of one-third of eyes at presentation. This feature has been noted in both viral and parasitic retinal necrosis, and absorption of these deposits into the retina has been documented with both time-domain OCT and SD-OCT.^{164, 301-303} Thus, the deposits may represent clumps of inflammatory cells.¹⁶⁰ In one report of an individual with severe TRC, the authors found clusters of macrophages attached to the posterior hyaloid and internal limiting membrane in the enucleated globe.¹⁵¹

Choroidal involvement in active TRC on SD-OCT was striking at times, and demonstrated the extent to which the choroid may be affected in what is primarily a retinal infection. The choroid cannot be directly visualized, and choroidal imaging is difficult due to the overlying retina and RPE which mask signal with many imaging tools. Angiography that utilizes indocyanine green dye does allow visualisation of the choroidal vasculature, and demonstrates choroidal involvement in TRC that usually extends beyond visible retinal lesions, but it does not provide cross-sectional information.³⁰⁴ In this work, choroidal involvement was indicated through a number of signs on SD-OCT: choroidal thickening, “bowing” of the RPE-Bruchs complex, and choroidal hyporeflectivity, which was presumed to represent choroidal shadowing from the overlying thickened retina in the majority of cases. A range of signs were taken to indicate choroidal involvement as no one sign was universally present in all cases. There are limitations with all these proxies for choroidal involvement. Choroidal thickening was arbitrarily designated as over 300 μm , which potentially missed thickening in zone 2 lesions, as the choroid is much thinner peripherally.³⁰⁵ In addition, the influence of age on choroidal thickness

was not taken into account.³⁰⁵ The ideal mode for imaging the choroid is enhanced depth imaging on SD-OCT,³⁰⁶ and not every participant had an SD-OCT in this modality. However, gross thickening was evident where obvious “bowing” of the RPE-Bruchs complex was observed (Figure 3.2). While the primary pathology of TRC is in the retina, choroidal involvement has long been documented in histopathological studies. Case reports detailing histopathology of enucleated or post-mortem eyes of immunocompromised individuals with TRC demonstrate secondary choroidal inflammatory changes, and one post-mortem enucleation of an immunocompetent male who incidentally died at the time of an episode of TRC showed a thickened choroid that was diffusely infiltrated with plasma cells and lymphocytes.¹³⁸ The unusual case of a chorioretinal biopsy of an amelanotic mass in a 37 year-old man with a history of treated bowel cancer demonstrated *T. gondii* bradyzoites within a focus of granulomatous inflammation.¹⁶¹

Features of TRC lesions were compared by location, and some differences were found between zone 1 and zone 2 lesions. The retina is thicker at the macula, and, unsurprisingly, zone 1 TRC lesions were relatively thicker than zone 2 lesions. That full thickness retinal hyperreflectivity was more likely in zone 1 lesions than peripheral lesions is not unexpected, as individuals with zone 1 lesions are more likely to present earlier as they often have symptoms sooner. It is interesting to note that macular oedema was also observed in zone 2 lesions, and macular epiretinal membrane was also a consequence of zone 2 disease, indicating that zone 2 TRC is not a benign disease, and underscoring the importance of treating this patient group. In addition, retinal signal voids, regardless of location, were associated with poor visual outcomes. Further evidence that peripheral TRC is serious was demonstrated in a study that found impaired macular function - despite normal architecture by SD-OCT - in eyes with zone 2 and 3 TRC.³⁰⁷ It is important to consider that transcriptional differences within cell populations at the macular and in the periphery have been identified, and may be a factor in pathophysiology.³⁰⁸

Müller cells are the primary host cell for *T. gondii*,³⁰⁹ and phenotypic and metabolic diversity in this cell population³¹⁰ may contribute to identifiable differences between macular and peripheral pathology in TRC. A well-documented report of a large cohort of individuals affected by an outbreak of toxoplasmosis found that retinal lesions were more likely to be necrotic when located at the macula.³¹¹

The presence of small round outer nuclear hyperreflective bodies (approximately 80 μm , Figure 3L) was a novel SD-OCT observation not previously reported in active TRC, and which was present in eyes of two *T. gondii* IgM-positive patients. These bodies might represent encysted parasites, although histopathological reports indicate cysts are most commonly found in the ganglion cell layer. We otherwise found no distinction between SD-OCT features of *T. gondii* IgM-positive versus -negative TRC. Differences between IgM-positive and -negative disease have been speculated, and while a recent paper described IgM-positive TRC as more likely to present in older individuals with macular lesions and carried a higher risk of rhegmatogenous retinal detachment,³¹² this is a largely unstudied area. A small report of enucleated globes with TRC found that IgM serology did not distinguish pathological features, including extension of necrosis and number of cysts.¹³⁷ Further research in this area is needed. Aggressive TRC has been associated with acquired immunodeficiency syndrome.¹²⁵ Our study suggested SD-OCT signs were not impacted by HIV infection status, although small retinal pigment epithelial detachments and retinal perivascular hyperreflective dots were identified in one eye of an HIV-positive patient and in no other cases. Despite a normal CD4 count, those who are HIV-positive display immune system dysfunction.³¹³ Only one participant in this study had a CD4-positive T cell count below 200 cells/ μl , precluding comparisons within this group.

It is a rare privilege to be able to correlate SD-OCT findings in retinal disease with histology due to the lack of tissue specimens, and some diseases imaged by SD-OCT may never have histopathological correlation.³¹⁴ While SD-OCT has been referred to as an “optical biopsy”, it is

important to note that histopathology demonstrates *ex vivo* chemical staining of tissue, while SD-OCT measures the optical scattering of *in vivo* tissue. Correlation of histopathology with SD-OCT findings in the normal human retina have been published,³¹⁴ but there are no studies that correlate ocular histopathology with SD-OCT in TRC. The necrotising retinitis that clinically defines active TRC represents tissue destruction and collateral inflammation related to the proliferation of *T. gondii*.¹³⁷ Coagulative necrosis, characterised by preservation of tissue architecture after cell death, is seen in pathological processes causing ischaemia and in cerebral toxoplasmosis.^{143, 315} On SD-OCT, coagulative necrosis is represented as retinal thickening and hyperreflectivity, due to cellular swelling and thus increased backscattering.³¹⁶ Similar SD-OCT changes can be seen in retinal ischaemia due to retinal arterial occlusion, with retinal thickening and hyperreflectivity being observed in the acute phase.³¹⁷

The hallmark of necrosis is breakdown of the plasma membrane of the cell.³¹⁸ Lysis of the cell and its organelles, transforming tissue into a liquefied mass of protein, reduces optical scattering as the mismatch between the refractive indices of cellular components is reduced.³¹⁶ This was elegantly presented in a study of tumour spheroids, whereby optical attenuation on SD-OCT was demonstrated to correlate accurately with areas of necrosis on histology.³¹⁹ In the current study, 5% of eyes at presentation demonstrated areflective spaces or signal voids within the retina on SD-OCT (Figure 3.5B). Similar signal voids have been identified by SD-OCT in other cases of TRC, and in retinal necrosis due to other aetiologies.^{320, 321} Without histopathological correlation, one can only speculate that this represents liquefactive necrosis, the consequence of heavy parasite proliferation with massive cell lysis and profound tissue destruction, causing an optical signal void. Over the course of TRC, retinal voids were observed in 17% of eyes, and were predictive of a poor visual outcome.

As this study was planned, it was hypothesized that encysted bradyzoites could be identified by SD-OCT. Cyst distribution in mouse models of both congenital and acquired TRC indicate

bradyzoites within Müller and ganglion cells and localized to the ganglion cell layer and inner plexiform layer of the retina.^{322, 323} Histopathological correlation with SD-OCT in TRC is unstudied. Whether encysted bradyzoites can be identified is unknown, and depends on the optical density of the cell and that of surrounding tissue. The most hyperreflective bands in the normal retina on SD-OCT are tightly packed with either mitochondria or lysosomes,¹⁰⁶ as these are the organelles most likely to scatter light.³²⁴ The optical density of infected cells is likely high, due to the concentration of mitochondria and their association with bradyzoites. Whether these presumably hyperreflective cells are identifiable will depend on the relative optical density of adjacent structures. Cells within the vitreous are a readily identifiable sign of posterior uveitis on SD-OCT, and presumed inflammatory cells are visible within the retina,³⁰⁰ but cannot be resolved in hyperreflective necrotic retina, where there is no mismatch between the scattering properties of adjacent structures. Lack of a positive control will also make identification of suspected cysts difficult, and correlation of TRC by SD-OCT and histopathology in an animal model is required before identification of cysts in humans can be achieved with confidence. As intriguing as the hunt may be, identifying tissue cysts in human retina is beyond the limits of current clinical technology.

This work found no signs on SD-OCT that were universal or specific to TRC. While other aetiologies of infectious retinitis generate similar signs on SD-OCT, with thickened hyperreflective retina in the acute phase,³²⁵ several features of necrotising retinitis in other diseases were not seen in this series of TRC. Studies of cytomegalovirus retinitis by SD-OCT have identified vertical hyperreflective strips in the retina, which were speculated to be infected Müller cells.³²¹ In the current work, care was taken to seek this change, but it was not identified on SD-OCT scans from any patient. Longitudinal documentation of cytomegalovirus retinitis by SD-OCT demonstrated vertical, then horizontal, spread of necrosis (retinal hyperreflectivity) in the early stage, followed by retinal thickening and in the late stage,

thinning of the retina.³²⁶ The early stages of acute retinal necrosis were identified by SD-OCT and showed hyperreflectivity and thickening of the inner plexiform layer initially, with vertical extension and the development of retinal signal voids similar to the voids seen in this study.³²⁷ Signs on SD-OCT that are more indicative of TRC involve the choroid and RPE, as demonstrated in Figure 3.6.

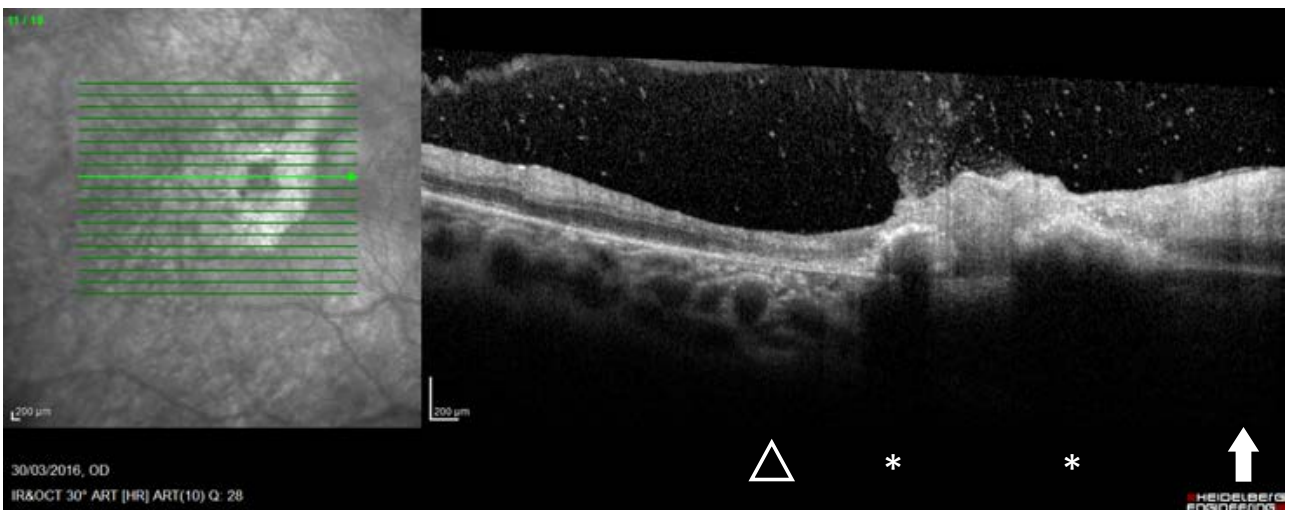


Figure 3.6: Retinal pigment epithelial thickening

Representative images from this work of an individual presenting to a tertiary-referral uveitis clinic with recurrent *T. gondii* IgG-positive TRC, studied with Heidelberg Spectralis® SD-OCT of the posterior segment of the eye (below right). Colour fundus photograph (above) and near infrared image (below left) for clinical correlation. SD-OCT demonstrating hyperreflective dots in the vitreous, retinal hyperreflectivity and thickening (above arrow), and prominent retinal pigment epithelial hyperreflectivity, elevation and thickening (above asterisks) corresponding to pigmented scar. Retina adjacent to scar (above triangle) is thinned and disorganized. Photograph reprinted with publisher's permission under [Creative Commons Attribution 4.0 International License](#) from [Lie, S.; Vieira, B.R.; Arruda, S.; Simões, M.; Ashander, L.M.; Furtado, J.M.; Smith, J.R. Molecular Basis of The Retinal Pigment Epithelial Changes That Characterize The Ocular Lesion in Toxoplasmosis. *Microorganisms* 2019, 7, 405.](#)

Abbreviations: Ig = immunoglobulin, SD-OCT = spectral-domain optical coherence tomography, TRC = toxoplasmic retinochoroiditis.

In terms of quality assessment, one previous study of SD-OCT in TRC reported that 71% of OCT scans were gradable, which is comparable to our rate of 68%.²⁹² However, in contrast to that and other studies, this work identified a relatively low prevalence of pathological changes. As one example, rates of hyaloid thickening were 90-95% in other studies,^{164, 292} compared to just 35% in this work. In addition, this study recorded lower rates of large hyperreflective deposits and focal hyaloid attachment than were identified by other investigators (i.e. 50-60% versus 36%, and 50% versus 16%, respectively).^{292, 302} Importantly, this patient group was considerably larger than any other studied to date. In addition, there was likely little referral bias in this work. Over 75% of the population uses public healthcare in Brazil,³²⁸ thus the Uveitis Service at Ribeirão Preto General Hospital serves a comprehensive patient population. Therefore rates of tissue changes by SD-OCT in individuals presenting with active TRC are likely to reflect those presented in this study.

There are a number of limitations of this work that should be highlighted. Methodological limitations include exclusions due to a lack of SD-OCT scan despite attendance at follow-up appointments, and a lack of clinical correlation in the form of fundus photographs for all participants. Photographic correlation would allow interpretation of particular SD-OCT signs such as small pigment epithelial detachments, subretinal scarring, and retinal haemorrhage. Ancillary imaging of the retina could provide further correlation: fundus autofluorescence may indicate occult RPE lesions that were not obvious on SD-OCT imaging; indocyanine green imaging could be used to identify choroidal infiltrates and correlate with SD-OCT signs. Technical issues include an SD-OCT scanning protocol that did not utilize narrow frame separation, which may have improved image quality. At limited times during the study period, the SD-OCT machine was undergoing maintenance

or repairs, and thus was not available for scanning patients. Another limitation of this work is that data on symptom duration were not collected, which means tissue changes by SD-OCT could not be correlated to symptom onset. However, the aims of this work were to evaluate patients from their first presentation to the uveitis service, rather than by their recollection of their symptoms, and to identify tissue pathology by SD-OCT in the real-world clinic setting, and correlate it to clinical and functional outcomes.

The continuous evolution of ocular imaging technology is pushing the boundaries of retinal visualisation and providing opportunities to better understand *in vivo* pathophysiology of TRC in humans. Technology utilising adaptive optics to reduce the higher order aberrations of optical systems extends the limits of resolution beyond what is currently possible with SD-OCT, and enables evaluation of retinal cellular physiology, documenting fluctuations in cell size, blood velocity, and identification of subcellular organelles.¹⁰⁷ While technology in some instances cannot replace animal models of disease, these tools allow further insight into the mechanisms of TRC. Infections of the retina are destructive.

This work presents the largest prospective cohort of individuals with active TRC studied by SD-OCT. A spectrum of SD-OCT signs were identified that characterize the extent of involvement of the retina, choroid and vitreous, the severity of retinal necrosis, and the evolution of tissue remodelling over time in active TRC. No sign was universal to all individuals with TRC, and all signs identified in patients with active TRC have been observed in other forms of infectious and non-infectious uveitis.^{302, 325, 329} Macular pathology in the form of macular oedema and epiretinal membrane is a feature of both zone 1 and zone 2 disease. SD-OCT features of infection do not vary by IgM-positive or-negative disease, and coexistent HIV infection does not distinguish pathological features.

Over the course of TRC, retinal voids were observed in 17% of eyes and were predictive of a poor visual outcome, providing a useful sign for the treating clinician.

CHAPTER 4

Dengue virus infection of human retinal Müller glial cells

4.1	Introduction	143
4.2	Results.....	146
4.2.1	Susceptibility of the MIO-M1 human Müller cell line to infection with dengue virus.....	146
4.2.1.1	<i>Type I interferon response in dengue virus-infected MIO-M1 human Müller cells</i>	<i>151</i>
4.2.1.2	<i>Immune responses of MIO-M1 human Müller cells to infection with dengue virus.....</i>	<i>152</i>
4.2.2	Müller cell infection with field isolates of dengue virus	156
4.2.2.1	<i>Infection of MIO-M1 human Müller cells with DENV field isolates</i>	<i>156</i>
4.2.3	Responses to dengue infection in primary Müller cells.....	163
4.2.3.1	<i>Infection of primary human Müller cells with DENV.....</i>	<i>163</i>
4.3	Discussion	175

4.1 INTRODUCTION

Ocular involvement in dengue virus (DENV) infection was reported as early as the 19th century,^{187-190, 330} but only in the last few decades has retinopathy been recognised as a significant complication.^{331, 332} The extent to which the retina is involved was revealed after a cross-sectional study during an epidemic found a 10% prevalence of maculopathy in those hospitalised with dengue.¹⁹³ Viral serotype may be a factor in the development of retinopathy, as the same study was repeated during an epidemic 2 years later, and showed no maculopathy was identified in anyone admitted to hospital with dengue.¹⁹⁴

Published studies investigating dengue retinopathy focus largely on the cellular components of the BRB. Prior work has showed that human retinal pigment epithelial cells and retinal endothelial cells support DENV infection, and mount a type I IFN and inflammatory response *in vitro*.²⁰⁵ Other research has demonstrated a differential response of endothelial cell subpopulations to infection with DENV, and suggested that vascular endothelial permeability may vary by cell site and viral serotype.²⁰⁷ Comparison with Zika (ZIKV), a closely-related flavivirus, revealed that the two viruses induce distinct but overlapping responses from human primary retinal pigment epithelial cells, with less inflammation in dengue infection.²⁰⁶ Other human retinal cell populations have not been examined in dengue retinopathy or in response to DENV infection.

Müller cells are specialized glial cells unique to the retina. They are radially oriented with cell bodies located in the inner nuclear layer, and processes that span the retinal thickness from internal limiting membrane to external limiting membrane (Figure 4.1).³³³ Müller cells interact with all major anatomical compartments of the posterior segment of the eye, and provide

scaffolding that is critical to meticulous retinal organisation.³³⁴ Müller cell processes associate with the synaptic connections of retinal neurons, blood vessels, the interphotoreceptor matrix of the subretinal space, and the vitreous gel. Approximately five million Müller cells are distributed across the human retina, each forming the central axis of a column of neurons, which contain one cone per Müller cell, and comprise the basic functional unit of visual processing.^{75, 334}

Through their interaction with retinal capillaries, Müller cells form part of the inner BRB. They mediate neurovascular exchanges, recycle neurotransmitters and cater for the extreme energy and oxygen requirements of inner retinal neurons.^{335, 336} Müller cells play a crucial role in fluid homeostasis, and are implicated in a wide range of ischaemic, degenerative and metabolic diseases that result in macular oedema.³³⁷ The Müller cell has no homologue in the CNS, and has been shown to perform highly specialized functions, including that of a clock that controls circadian molecular expression within the retina.³³⁸ The role of the Müller cell in dengue retinopathy is largely unknown, but there are compelling reasons why this cell warrants further study.

Given its anatomical location, Müller cells are intimately involved with all other cell types of the neural retina. They are susceptible to infection with other flaviviruses, including ZIKV,^{208, 339} and support infection of the apicomplexan parasite *Toxoplasma gondii*,³⁴⁰ which infects human Müller cells in preference to neuronal retinal cell populations.³⁰⁹ Müller cells are targets for lentiviral³⁴¹ and adeno-associated viral vectors,³⁴² and also interact with extracellular pathogens such as in bacterial endophthalmitis, where they mediate early innate immune responses through expression of toll-like receptors and inflammatory mediators, and are capable of phagocytosis.^{96, 343, 344}

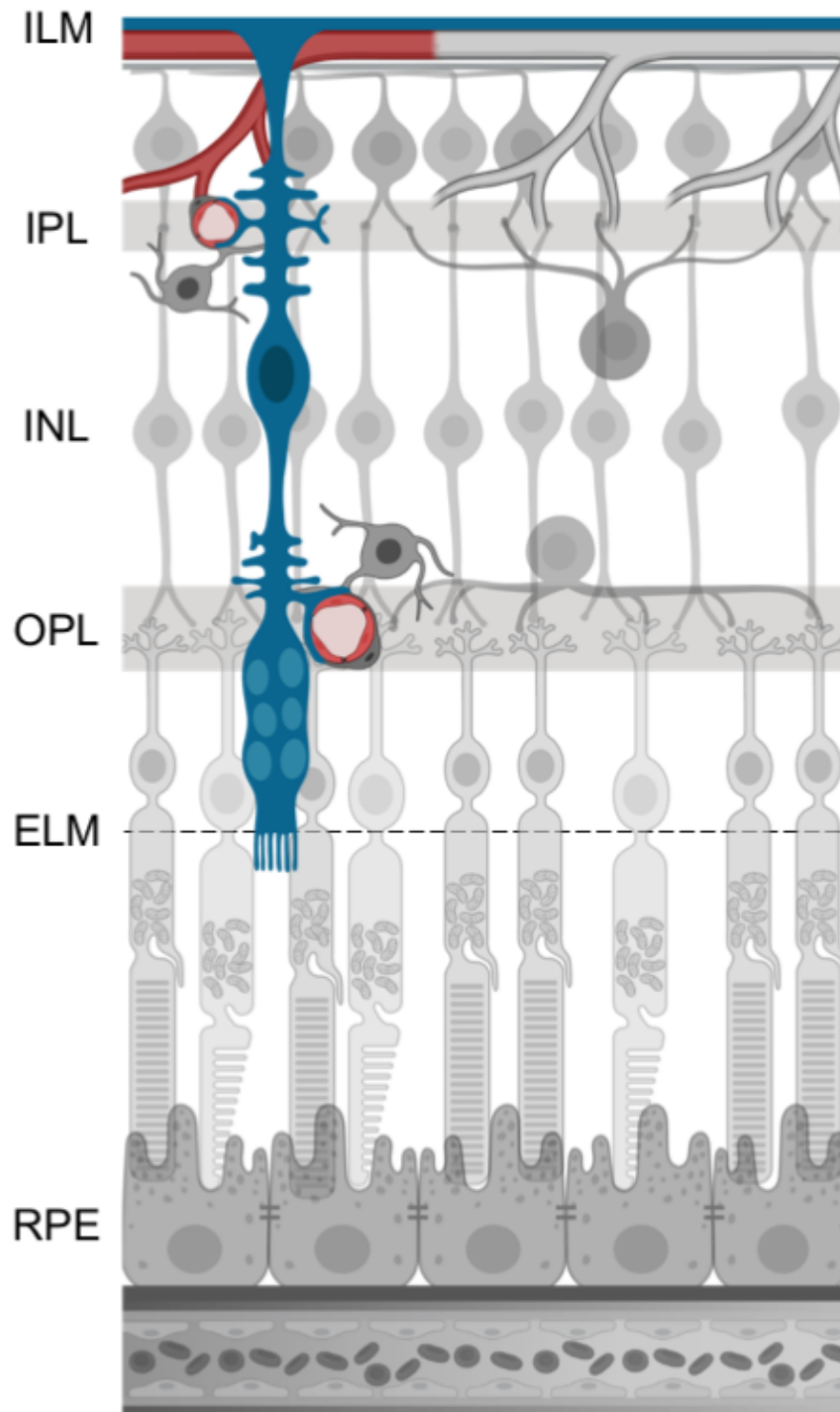


Figure 4.1: The Müller cell

Müller cells (blue) are specialized glial cells unique to the retina. They form the internal (ILM) and external (ELM) limiting membranes of the retina and their cell bodies lie within the inner nuclear layer (INL). They form synaptic connections with most retinal cell populations, and contact capillary networks in the inner plexiform (IPL) and outer plexiform layers (OPL) as part of the inner BRB. The retinal pigment epithelium (RPE) forms the outer BRB. Figure constructed at BioRender.com

The work in this chapter was designed to establish the susceptibility of the human retinal Müller cell to infection with DENV and identify characteristics of the Müller cell response to this virus. Specifically, antiviral, inflammatory and immunomodulatory responses after DENV infection were investigated in human Müller cells *in vitro*. To emulate closer translation to clinical disease, primary human Müller cells and field isolates of DENV were used to characterise the interactions of this unique cell with DENV.

4.2 RESULTS

4.2.1 Susceptibility of the MIO-M1 human Müller cell line to infection with dengue virus

To determine the susceptibility of human Müller cells to infection with DENV, preliminary studies involved infecting the spontaneously immortalized human Müller cell line, MIO-M1,⁹⁵ with Mon601, a recombinant DENV serotype 2 from the New Guinea C strain.³⁴⁵ Confluent monolayers of MIO-M1 cells were infected with Mon601 across two experiments to determine (1) the optimal MOI and (2) the kinetics of infection in this cell line, and thus the most appropriate time to harvest the cells for use in molecular studies.

To determine the optimal MOI for further infections, confluent monolayers of MIO-M1 cells were infected with Mon601 at MOI of 1 and 5, mock-infected with heat-inactivated virus at MOI of 5, or treated with medium only, with 3 monolayers per condition. Cell monolayers were fixed with paraformaldehyde at 48 hpi for immunolabelling with anti-double-stranded (ds)RNA antibody, which demonstrated a productive infection of MIO-M1 cells at an MOI of 5 (Figure 4.2A-D). RNA was extracted from additional cells for analysis by RT-qPCR. This procedure showed higher viral copy numbers were present in MIO-M1 cells infected at MOI of 5 compared

to MOI of 1 ($p < 0.05$, two-tailed t-test) (Figure 4.2E). A plaque assay of supernatant from infected monolayers confirmed greater infection at MOI of 5 (6.30×10^4 pfu/mL) compared to MOI of 1 (7.33×10^3 pfu/mL).

To characterise the kinetics of DENV infection in human Müller cells, confluent monolayers of MIO-M1 cells were infected at MOI of 5, mock-infected with heat-inactivated virus at an MOI of 5, or left uninfected. At 24, 48 and 72 hpi, RNA was harvested. By RT-qPCR, viral RNA level was highest at 72 hours, but with variation across 4 replicates (Figure 4.2F). Imaging of cell monolayers by brightfield microscopy demonstrated a cytopathic effect – the term used in virology to indicate the effect of infection of cytolytic viruses on cells.^{346, 347} – in DENV-infected cells, with increased cell debris, rounded cell bodies and loss of cell confluence (Figure 4.3). Mock-infected and uninfected Müller cells showed no cytopathic effect, showing that inactivated virus particles were insufficient to cause macroscopic pathological changes. At 48 hours, the cytopathic effect was obvious, but it was more profound at 72 hours, when widespread cell death was pronounced. Given these observations, infections in subsequent experiments were conducted over 48 hours to ensure that the molecular profiles of cells reflected the response to active viral replication rather than progression to cell death.

Thus, preliminary experiments demonstrated robust infection of MIO-M1 cells with Mon601 at an MOI of 5, and 48 hours was an optimal period to study the molecular response to infection in these cells. Given that mock-infection with heat-inactivated virus generated similar results to non-infected monolayers, further infections were conducted using only medium-treated cells as a negative control.

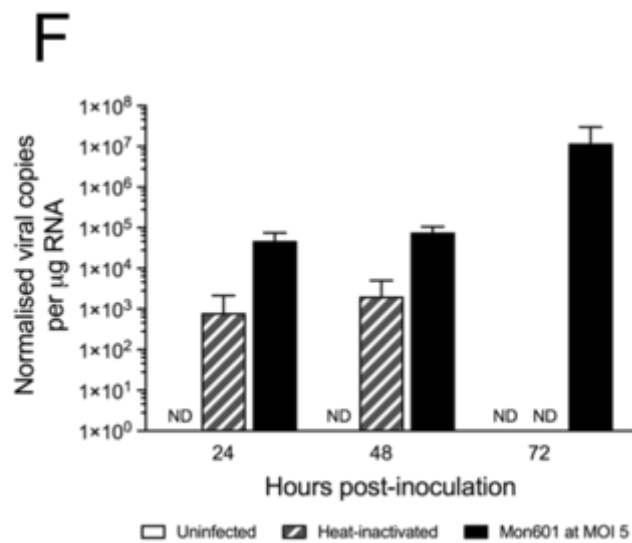
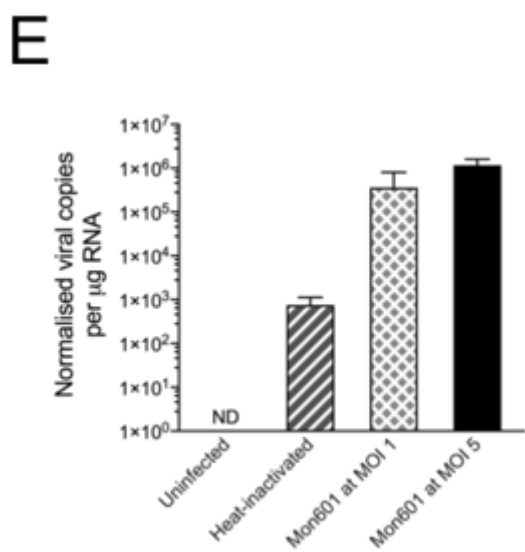
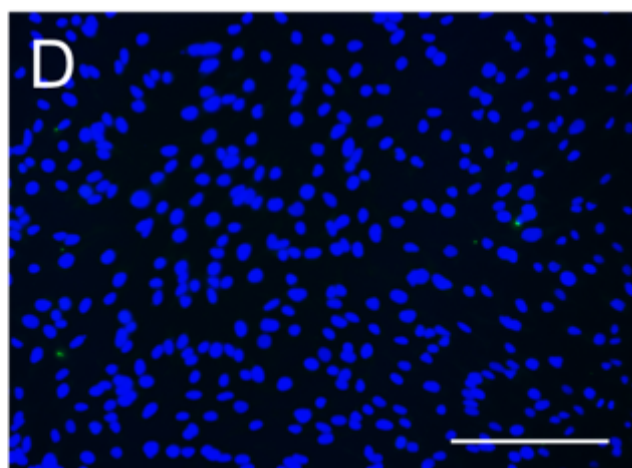
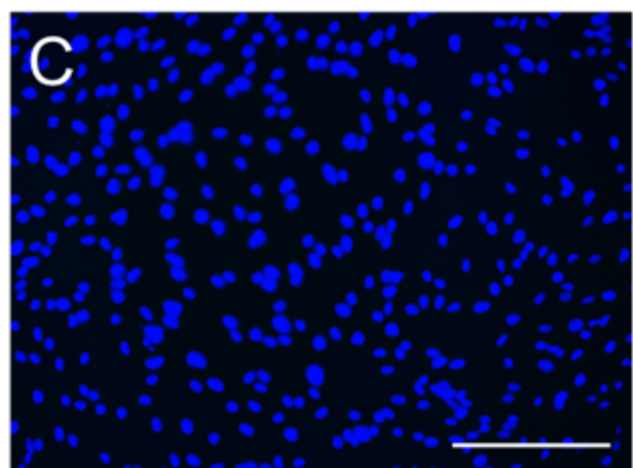
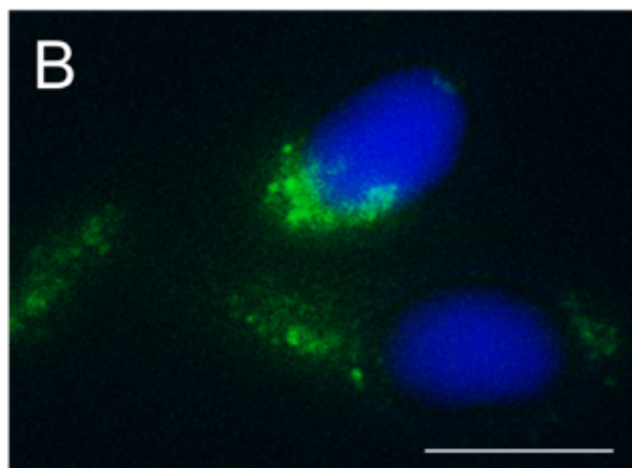
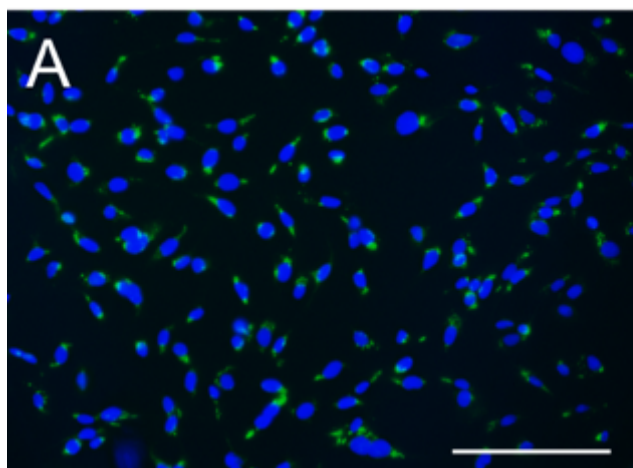


Figure 4.2: Infection of MIO-M1 human Müller cells with dengue virus

To determine the optimal MOI for further infections, confluent monolayers of MIO-M1 cells were infected with Mon601 at MOI of 1 and 5, mock-infected with heat-inactivated virus at MOI of 5, or treated with medium only, with 3 monolayers per condition. Fluorescent imaging of MIO-M1 cells at 48 hpi with Mon601 (A-C) at an MOI of 5, or (D) after treatment with medium alone; and after immunolabeling to detect (A, B, D) double-stranded RNA or (C) isotype-matched negative control antibody. Alexa Fluor 488 (green) with 4',6-diamidino-2-phenylindole (blue) nuclear counterstain. Scale bars 100 μm , except (B) = 10 μm . (E, F). Viral load of Mon601-infected MIO-M1 cells by RT-qPCR at (E) different viral inoculations at 48 hpi: at an MOI of 1 or 5, heat-inactivated virus at an MOI of 5, or medium only, and (F) different time points: 24, 48 and 72 hpi at an MOI of 5, heat-inactivated virus at an MOI of 5, or medium-only control. Genome copy number per μg RNA and normalized to reference genes, (E) glyceraldehyde-3-phosphate dehydrogenase or (F) ribosomal protein lateral stalk subunit P0. Error bars denote standard deviation, ND = no expression for at least half the replicates, n = 3-4 cultures per condition. Statistical analyses were not performed as some conditions had no expression of transcripts. Note logarithmic scale. **Abbreviations:** DENV = dengue virus, hpi = hours post-inoculation, MIO-M1 = Moorfields / Institute of Ophthalmology-Müller 1, MOI = multiplicity of infection, RNA = ribonucleic acid, RT-qPCR = quantitative reverse transcription polymerase chain reaction.

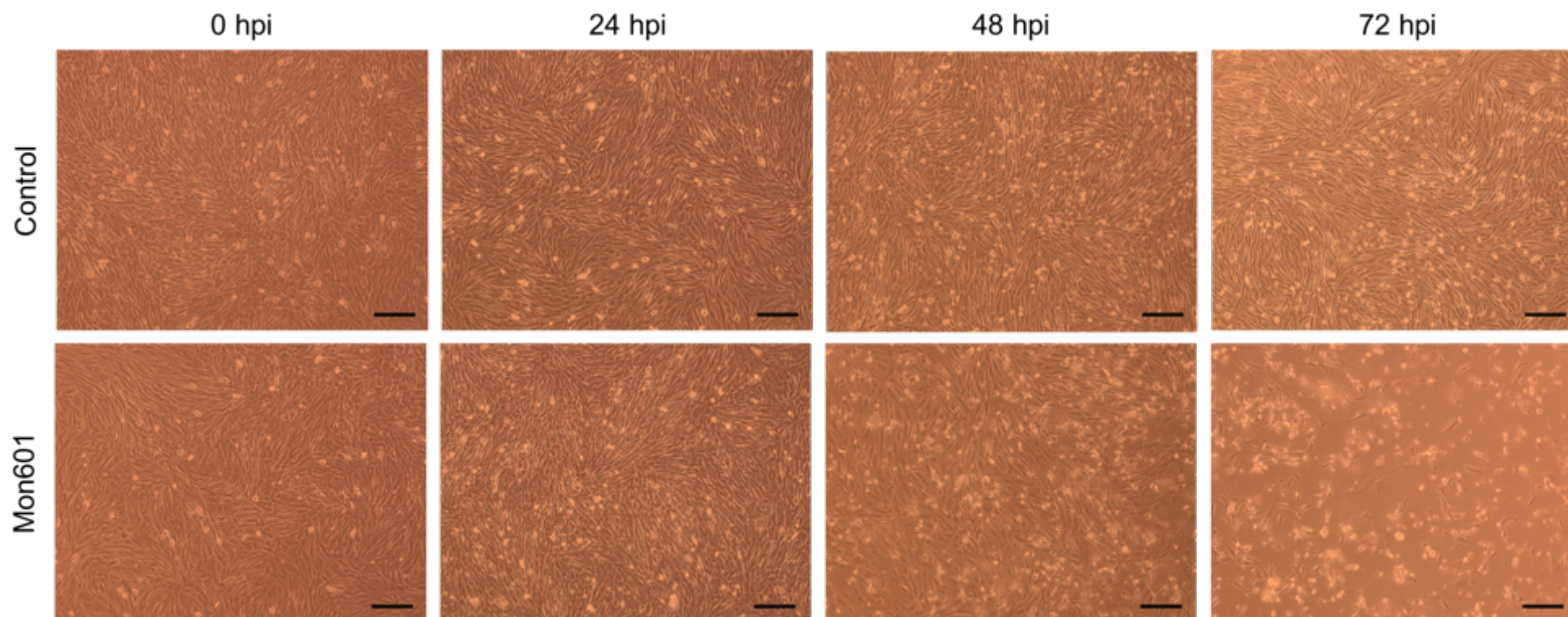


Figure 4.3: Infection of human Müller cells with Mon601

Preliminary infection studies were performed to determine the optimal MOI for further infections. Brightfield photomicrographs of Mon601-infected MIO-M1 cells at an MOI of 5, and medium-treated (control) MIO-M1 Müller cells. MIO-M1 cells treated with medium alone had a similar appearance to cells inoculated with heat-inactivated virus (not shown). Evaluated time points post-inoculation = 24, 48, 72 hpi. Scale bars = 100 μm , n = 4 cultures per condition. Representative images are shown. **Abbreviations:** hpi = hours post-inoculation, MIO-M1 = Moorfields / Institute of Ophthalmology-Müller 1, MOI = multiplicity of infection.

4.2.1.1 TYPE I INTERFERON RESPONSE IN DENGUE VIRUS-INFECTED MIO-M1 HUMAN MÜLLER CELLS

To determine the antiviral response of human Müller cells to infection with DENV, the expression of key molecules was quantified by RT-qPCR. Infection of MIO-M1 cells with Mon601 did not induce expression of IFN- β transcript (Figure 4.4A), and this observation was replicated in 3 experiments, which included kinetic studies of expression at 24, 48 and 72 hpi, and infections at MOI of 1 and an MOI of 5. To determine if this lack of type I IFN response was a function of the virus and observed in other cells of the eye, another ocular cell population was infected with Mon601 using the same experimental technique, and IFN- β transcript was measured from RNA of cell lysate by RT-qPCR. In contrast to MIO-M1 cells, the ARPE-19 human retinal pigment epithelial cell line²⁶² showed a robust IFN- β response by RT-qPCR compared to medium-only ARPE-19 cells ($p < 0.0001$), confirming that Mon601 can generate IFN- β in response to infection in other cells of the eye (Figure 4.4A).

Further investigation was undertaken to confirm that MIO-M1 cells did not produce IFN- β in response to DENV infection. Culture supernatant was collected from MIO-M1 cells at 24 and 48 hpi with Mon601 at an MOI of 5, or medium alone ($n = 3$ monolayers per condition). Supernatant samples were subjected to AlphaLISA®,³⁴⁸ a form of enzyme-linked immunosorbent assay to detect IFN- β protein. No IFN- β was found in supernatant from any sample, indicating levels below the minimum detection threshold of 9.6 pg/mL (data not shown), and consistent with RT-qPCR results.

To fully determine the type I IFN response of MIO-M1 cells in the context of DENV infection, expression of IFN- α , another component of the type I IFN response,³⁴⁹ was determined by RT-qPCR. Transcript expression of this cytokine also did not change in response to infection with DENV (Figure 4.4B). Similar results were obtained for the IFN-stimulated gene, eukaryotic translation initiation factor 2-alpha kinase 2 (EIF2AK2, also known as protein kinase dsRNA-

dependent (PKR)), but not ISG15, and radical S-adenosyl methionine domain containing 2 (RSAD2), which were significantly and highly upregulated in response to infection with DENV ($p < 0.0001$, Figure 4.4B). These data together show that although an antiviral response to DENV2 is generated in infected human Müller MIO-M1 cells, this response is characterized by a lack of the key antiviral cytokine, IFN- β , and driven through IFN- β independent pathways.

4.2.1.2 IMMUNE RESPONSES OF MIO-M1 HUMAN MÜLLER CELLS TO INFECTION WITH DENGUE VIRUS

To determine the immune response of human Müller MIO-M1 cells to infection with DENV, expression of molecular transcripts involved in inflammatory and immunomodulatory processes were determined by RT-qPCR. Monolayers of MIO-M1 cells were infected with Mon601 at an MOI of 5, or mock-infected, with 3-6 cultures per condition, and cells were lysed and RNA was extracted at 48 hours. Results generated across four experiments were consistent, and representative graphs are shown in Figure 4.5. The inflammatory response of MIO-M1 cells to infection with Mon601 was characterised by elevated expression of TNF- α , IL-1 β and IL-6 ($p < 0.01$) production compared to uninfected control cells (Figure 4.5A). Infected MIO-M1 cells also showed significantly increased expression of the transcripts encoding two immunomodulatory cell surface molecules, programmed death-ligand (PD-L)1 ($p < 0.0001$) and PD-L2 ($p < 0.0001$), but expression of the immunomodulatory cytokine, IL-10, was unchanged as a result of infection (Figure 4.5B). The immunomodulatory cell surface molecule, Fas ligand, was not detected by RT-qPCR in either infected or uninfected conditions (data not shown). Together, these data indicate that Mon601-infected human Müller MIO-M1 cells mount an immune response that is characterised by the induction of both pro-inflammatory and immunomodulatory molecules.

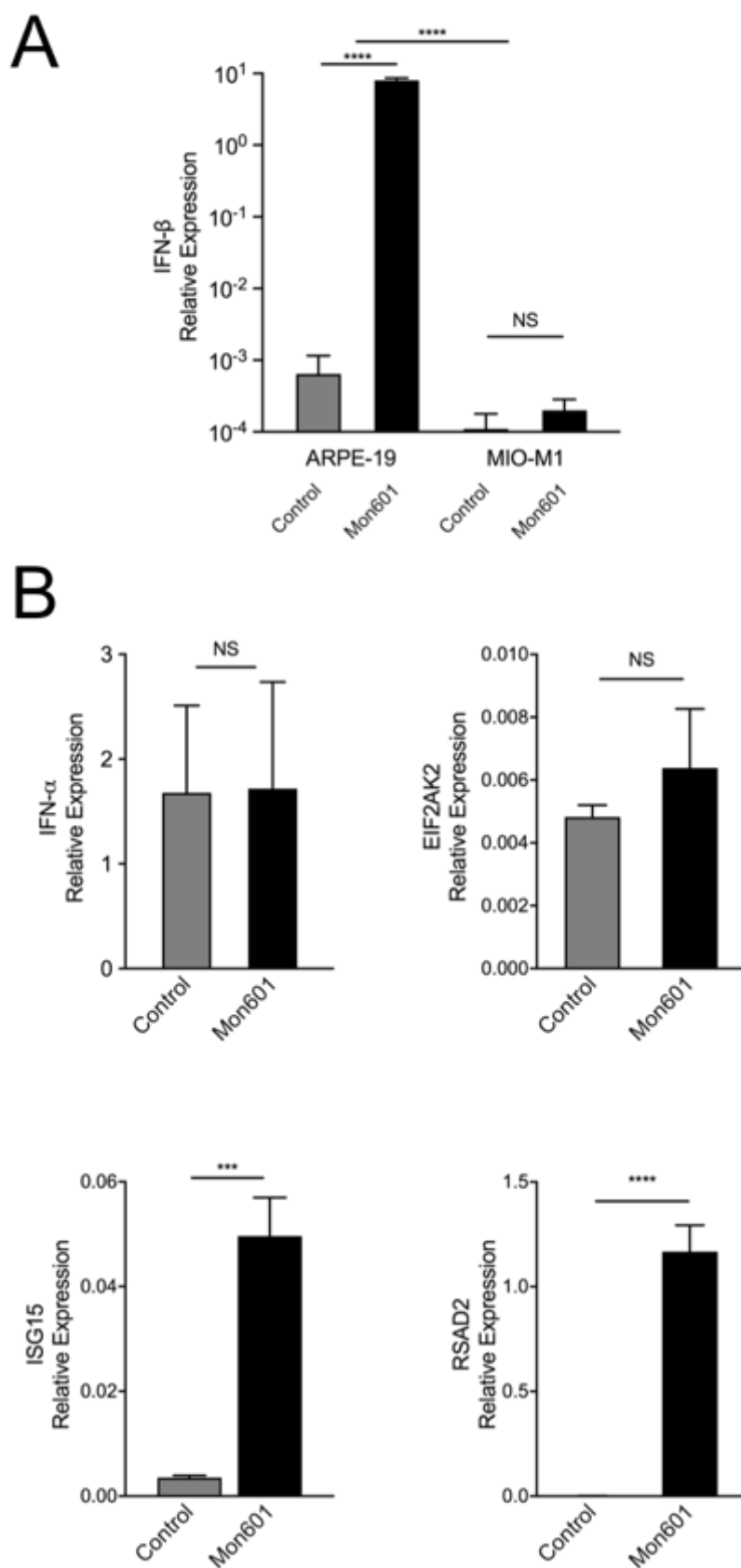


Figure 4.4: Type I interferon response to DENV infection in MIO-M1 human Müller cells

To determine the antiviral response of human Müller cells to infection with DENV, the expression of key molecules was quantified by RT-qPCR. Representative graphs from four experiments measuring expression of antiviral transcripts in Mon601-infected or media-treated (control) cell monolayers. (A). IFN- β expression in ARPE-19 and MIO-M1 cells at 48 hpi with Mon601 at an MOI of 5 ($p < 0.0001$). Note logarithmic scale. (B) Under the same conditions, MIO-M1 expression of IFN- α , EIF2AK2, ISG15, and RSAD2. Expression relative to reference genes, ribosomal protein lateral stalk subunit P0 and β -actin. Data analysed by (A) two-way ANOVA with Sidak multiple comparisons test (B) unpaired two-tailed t-test, with $n = 3-4$ cultures per condition. Error bars represent standard deviation, *** $p < 0.001$, **** $p < 0.0001$, NS not significant. Complete statistics are in Appendix F, Table 1 -3. **Abbreviations:** ANOVA = analysis of variance, DENV = dengue virus, EIF2AK2 = eukaryotic translation initiation factor 2-alpha kinase 2; hpi = hours post-inoculation, IFN = interferon, ISG15 = interferon-stimulated gene 15, MIO-M1 = Moorfields / Institute of Ophthalmology-Müller 1, MOI = multiplicity of infection, RNA = ribonucleic acid, RSAD2 = radical S-adenosyl methionine domain-containing 2; RT-qPCR = quantitative reverse transcription polymerase chain reaction.

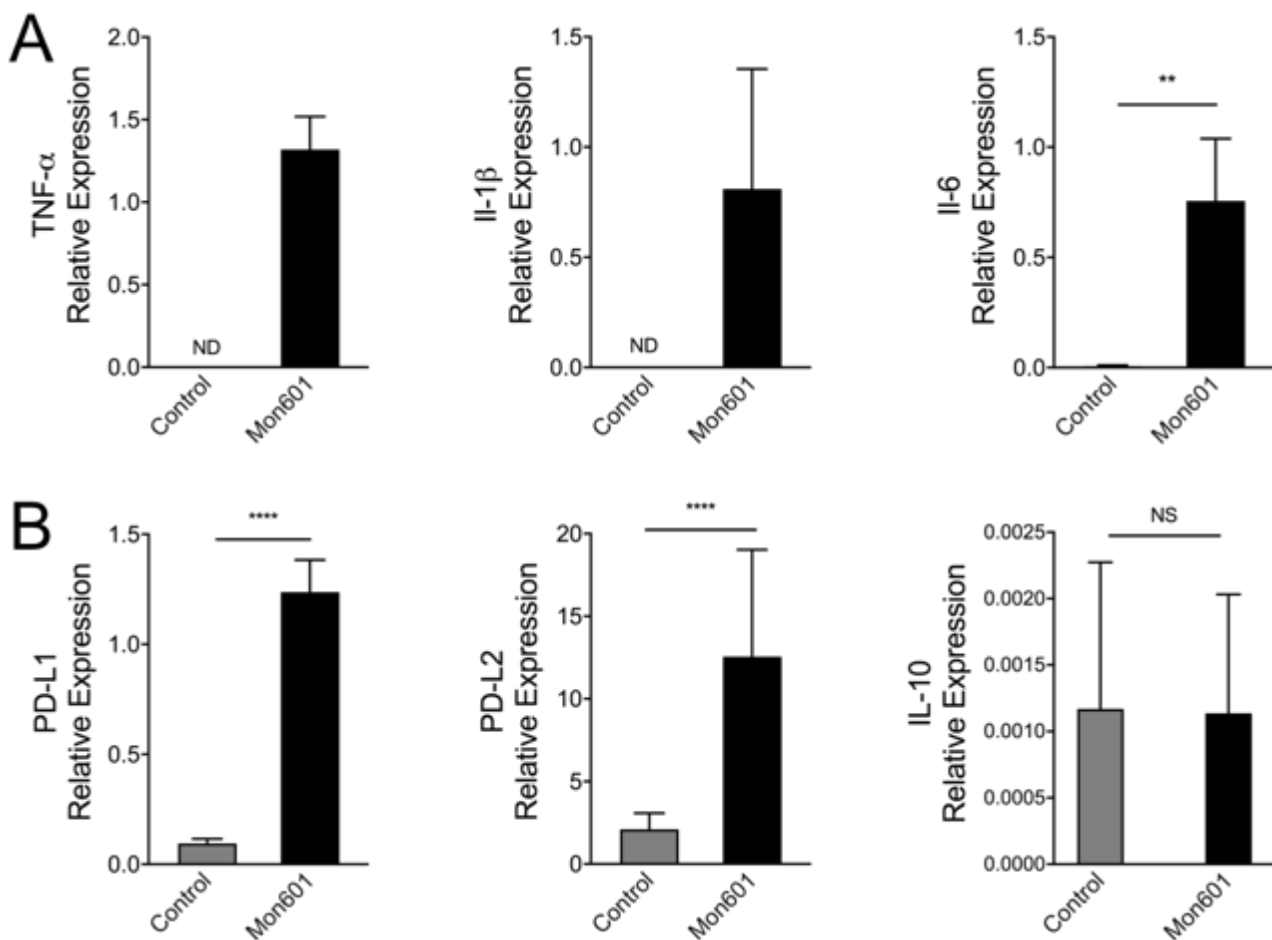


Figure 4.5: Immune response to dengue virus infection in MIO-M1 human Müller cells

To determine the immune response of human Müller cells to infection with DENV, the expression of key molecules was quantified by RT-qPCR. Representative graphs from 5 experiments measuring the (A) inflammatory and (B) immunomodulatory response by RT-qPCR in human Müller MIO-M1 cells 48 hours after inoculation with Mon601 at an MOI of 5, or medium-treated (control). Expression relative to reference genes, ribosomal protein lateral stalk subunit P0 and β -actin. Data were analysed by unpaired two-tailed t-test, with $n = 3-6$ cultures per condition. Error bars represent standard deviation, *** $p < 0.001$, ** $p < 0.01$, NS not significant, ND transcript expression not detected in at least half the replicates. Complete statistics are in Appendix F, Table 4. **Abbreviations:** hpi = hours post-inoculation, IL = interleukin, MIO-M1 = Moorfields / Institute of Ophthalmology-Müller 1, MOI = multiplicity of infection, PD-L = programmed death-ligand, RNA = ribonucleic acid, RT-qPCR = quantitative reverse transcription polymerase chain reaction.

4.2.2 Müller cell infection with field isolates of dengue virus

4.2.2.1 INFECTION OF MIO-M1 HUMAN MÜLLER CELLS WITH DENV FIELD ISOLATES

To reflect DENV infection with more fidelity and explore the effect of DENV strain and serotype on Müller cell response to infection, human Müller MIO-M1 cells were infected with viral isolates obtained from individuals with dengue, as well as the lab-adapted Mon601 recombinant strain. These DENV1 or DENV2 field isolates were collected during the 2004-2005 and 2007 epidemics in Singapore (Table 2.4). Confluent monolayers of MIO-M1 cells were infected at MOI of 5 with either Mon601 or one of 6 field isolates of DENV1 and DENV2, or treated with medium alone as negative control. At 48 hpi, monolayers were fixed in 4% paraformaldehyde and immunolabeled to detect the presence of dsRNA (Figure 4.6A). The dsRNA labelling was not detected in cells infected with DENV field isolates compared to infection with Mon601, as shown with isolate EHI0377Y04 (Figure 4.6A). Concordant with these results, the cytopathic effect in MIO-M1 cells infected with field isolates was minimal, as exemplified by isolate EHI0377Y04, in contrast to the obvious cytopathic effect induced by Mon601 (Figure 4.6B), and by RT-qPCR, viral RNA level was lower in cells infected with field isolates compared to Mon601 (Figure 4.7). A medium-treated control was included, from which no viral copies were detected. These data indicate that although the DENV field isolates were capable of infecting MIO-M1 cells, they did not replicate as well as Mon601 in these cells.

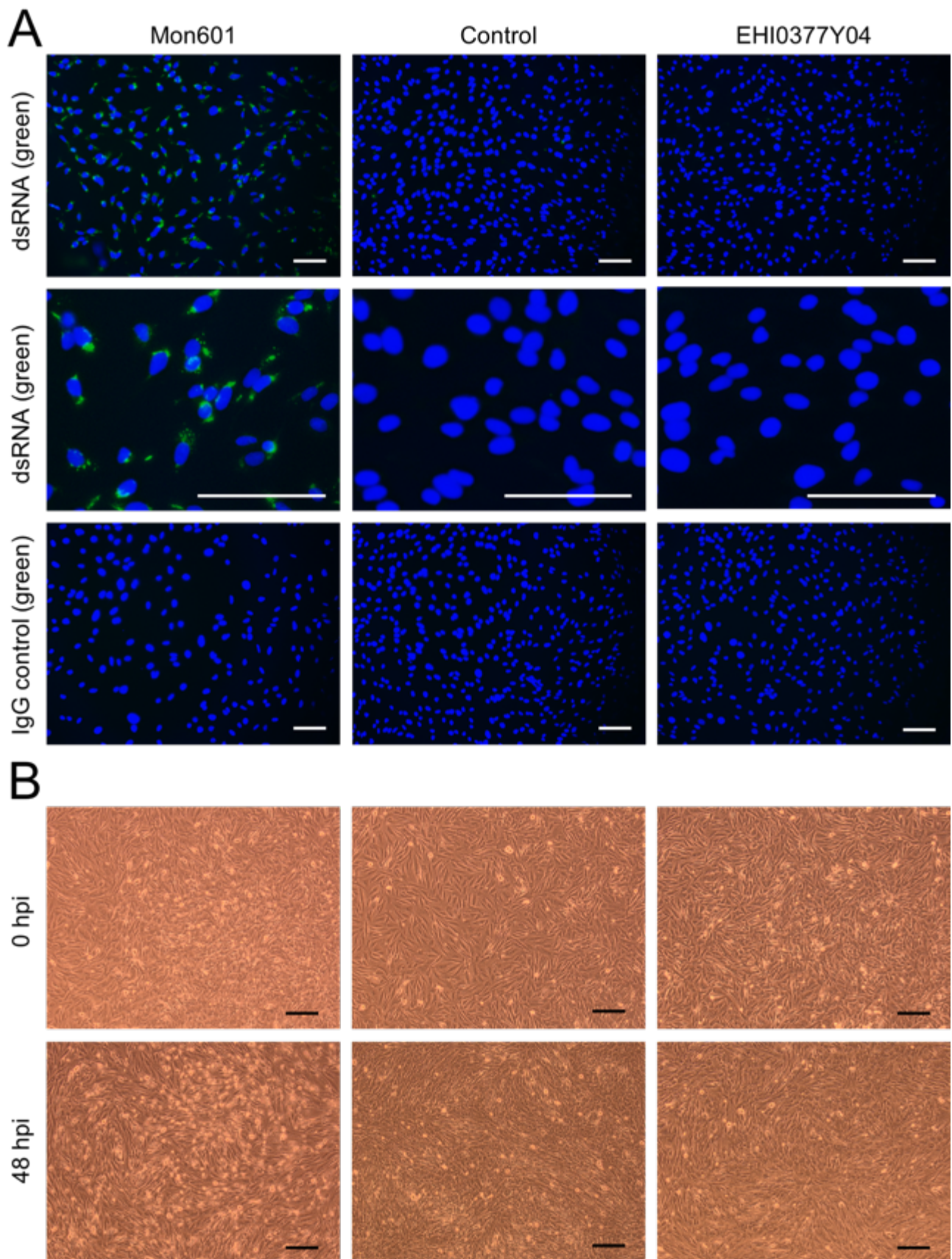


Figure 4.6: MIO-M1 human Müller cell infection with DENV field isolates

To reflect human DENV infection with more fidelity and explore the effect of DENV strain and serotype on Müller cell response to infection, human MIO-M1 cells were infected with laboratory-adapted Mon601 recombinant strain or one of 6 DENV field isolates (Table 2.4) at a MOI of 5, or with medium alone (control). Results for representative field isolate, EHI0377Y04, are displayed (A). Fluorescent photomicrographs showing cell monolayers at 48 hpi and immunolabelled for double-stranded (ds)RNA (green). Mon601-infected MIO-M1 Müller cells, but not cells infected with EHI0377Y04, stained positively for dsRNA, and no labelling was observed in uninfected cells or cells labelled with the negative control antibody. Primary antibody: J2 Mouse anti-dsRNA IgG2ak. Negative control: isotype-matched irrelevant mouse antibody. Secondary antibody: Alexa Fluor® 488 Goat anti-Mouse IgG (green). Nuclei counterstained with 4',6-diamidino-2-phenylindole (blue). (B). Brightfield photomicrographs demonstrating cytopathic effect at 48 hpi for Mon601-infected, medium-treated control, and representative field isolate, EHI0377Y04. All scale bars 100 µm. **Abbreviations:** hpi = hours post-inoculation, Ig = immunoglobulin, MIO-M1 = Moorfields / Institute of Ophthalmology-Müller 1, MOI = multiplicity of infection, dsRNA = double-stranded ribonucleic acid.

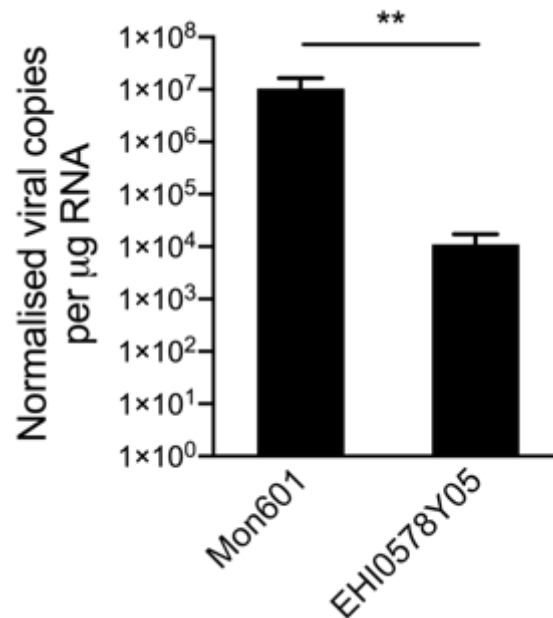


Figure 4.7: Viral RNA level of DENV-infected MIO-M1 human Müller cells

To demonstrate DENV infection with laboratory isolates of DENV on human Müller cells, human MIO-M1 cells were infected with laboratory-adapted Mon601 recombinant strain or one of 6 DENV field isolates. Human MIO-M1 cells were infected with Mon601 or one of 6 DENV field isolates (Table 2.4) at a MOI of 5. Results for representative field isolate, EHI0578Y05, is shown, and indicates that while the field isolates are capable of infecting MIO-M1 cells, they do not replicate as efficiently as the laboratory-adapted Mon601 strain. Virus was not detected in medium-treated control (not shown). Intracellular viral load by genome equivalents per μg of RNA and normalized to reference gene, ribosomal protein lateral stalk subunit P0. Error bars represent standard deviation, data analysed by two-tailed t test, ** $p < 0.01$. Note logarithmic scale. Complete statistics are in Appendix F, Table 5. **Abbreviations:** MIO-M1 = Moorfields / Institute of Ophthalmology-Müller 1, MOI = multiplicity of infection, RNA = ribonucleic acid.

To understand the antiviral and immune response of human Müller cells to infection with the DENV field isolates, transcript expression was measured by RT-qPCR. Monolayers of human Müller MIO-M1 cells were infected at an MOI of 5 with one of six DENV field isolates, Mon601, or were left uninfected, with six monolayers per condition. At 48 hpi, the key mediator of the type I IFN response, IFN- β , was not detected in any of the 48 samples, indicating an absence of expression of the antiviral cytokine both in the unstimulated state and in response to DENV infection. At 48 hpi, IFN- β was not detected and EIF2AK2 expression was not altered (data not shown). Again, expression of RSAD2 was increased significantly in all DENV-infected cells, with higher expression in DENV2 strain-infected monolayers (Mon601, EHI0377Y04 and EHI0578Y05, $p < 0.0001$) (Figure 4.8A).

The inflammatory transcripts, TNF- α , IL-1 β and IL-6, were not consistently detected in monolayers subjected to mock-infection with medium alone, but infection with all DENV isolates stimulated IL-6 expression, although notably higher levels were seen with DENV2 strains (Figure 4.8B). Infection with Mon601 induced production of TNF- α and IL-1 β RNA, and the EHI0578Y05 strain also stimulated expression of TNF- α RNA. Expression of the immunomodulatory transcript, PD-L1, was upregulated with infection with all DENV strains, and PD-L2 expression was especially high in Mon601-infected cells ($p < 0.001$, Figure 4.8C). The results show that differential immune responses of human Müller MIO-M1 were seen across infection with DENV1 and DENV2 strains. The DENV2 isolate EHI0578Y05, was used for further analysis since it showed the best replication and induction of immune responses

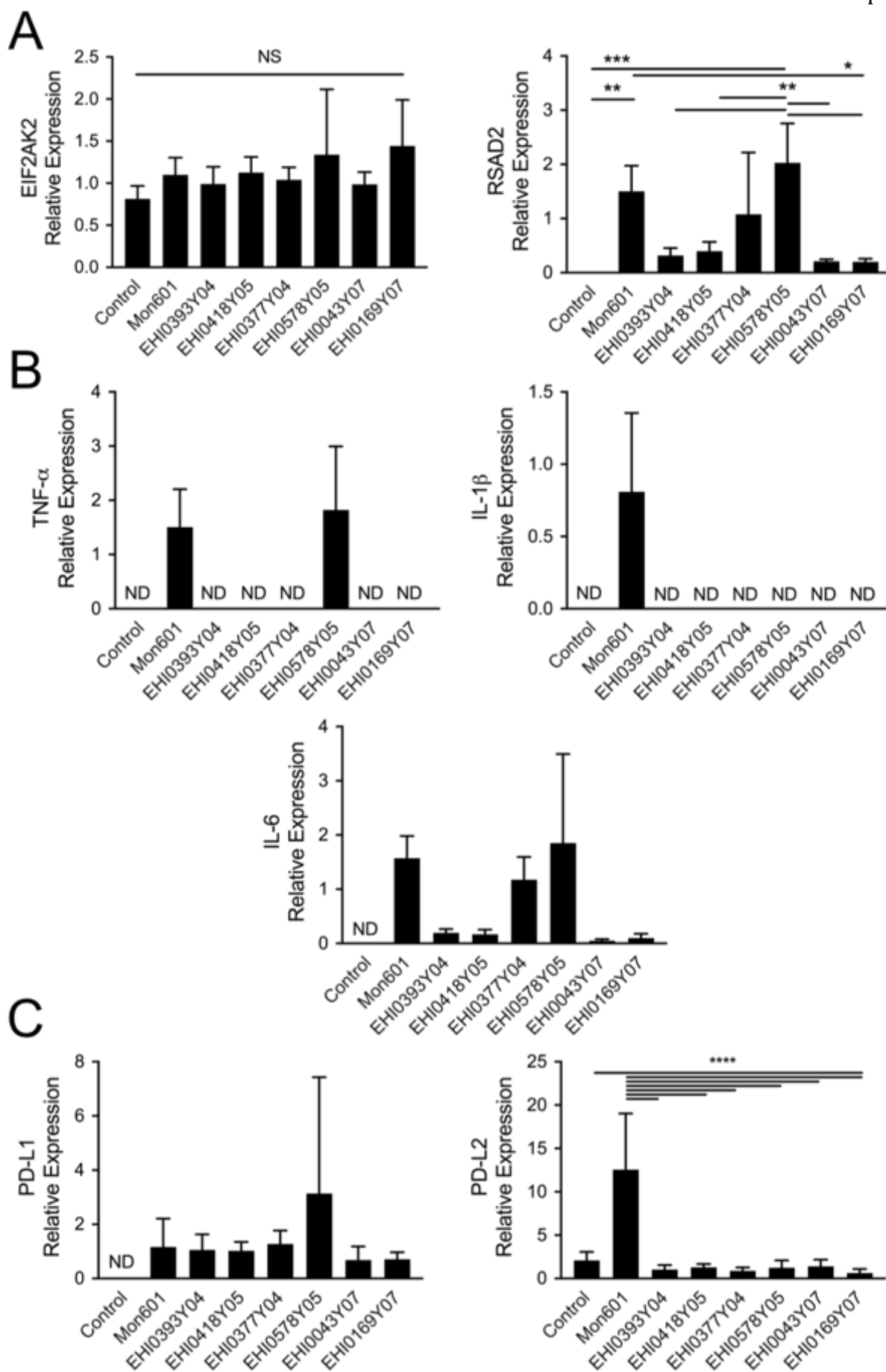


Figure 4.8: Molecular responses of MIO-M1 human Müller cells infected with DENV field isolates

To understand the antiviral and immune response of human Müller cells to infection with the DENV field isolates, transcript expression was measured by RT-qPCR. Human Müller MIO-M1 cells were infected with Mon601 or DENV field isolates (n=6 infections per condition) at an MOI of 5, and harvested at 48 hpi. Graphs showing expression of (A) anti-viral transcripts EIF2AK2 (p = 0.12) and RSAD2 (p < 0.0001); (B) inflammatory transcripts TNF- α , IL-1 β and IL-6; and (C) immunomodulatory transcripts PD-L1 and PD-L2 (p < 0.001). These results show that differential immune responses of human Müller MIO-M1 are seen across infection with DENV1 (EHI0393Y04, EHI0418Y05, EHI0043Y07, EHI0169Y07) and DENV2 (Mon601, EHI0377Y04, EHI0578Y05) strains. Expression relative to stable reference genes, ribosomal protein lateral stalk subunit P0 and β -actin. Error bars show standard deviation. Where transcript expression was present across all conditions, data were analysed by one-way ANOVA with Tukey multiple comparisons test. NS = not significant, * p < 0.05, ** p < 0.01, *** p < 0.001, **** p < 0.0001, ND = expression not detected in \geq 4 of 6 replicates. Complete statistical analysis is presented in Appendix F, Table 6. **Abbreviations:** ANOVA = analysis of variance, DENV = dengue virus, EIF2AK2 = eukaryotic translation initiation factor 2-alpha kinase 2, hpi = hours post-inoculation, IL = interleukin, MIO-M1 = Moorfields / Institute of Ophthalmology-Müller 1, MOI = multiplicity of infection, PD-L = programmed death-ligand, RNA = ribonucleic acid, RSAD2 = radical S-adenosyl methionine domain-containing 2, RT-qPCR = quantitative reverse transcription polymerase chain reaction, TNF- α = tumour necrosis factor-alpha.

4.2.3 Responses to dengue infection in primary Müller cells

4.2.3.1 INFECTION OF PRIMARY HUMAN MÜLLER CELLS WITH DENV

To more closely approximate *in vivo* responses of human Müller cells to DENV infection, primary human Müller cells were used to investigate molecular responses to infection with recombinant DENV2 Mon601 and the six DENV field isolates (Table 2.4). Primary human Müller cell isolates from eyes of three male cadaveric donors aged 68 to 82 years, obtained within a mean of 26 hours post-mortem, were used (Table 4.1); these cells were previously isolated by a published method by Dr Yuefang Ma and were passage 3 or less.³⁵⁰ The cultured cells had variable stellate or spindle morphology (Figure 4.9). To characterise these cell isolates prior to use in experiments, the cells were immunolabelled for several markers of cultured primary human Müller cells: glutamine synthetase (GS), an enzyme critical to glutamate processing and nitrogen metabolism,³⁵¹ and the intermediate filaments vimentin (VIM), and glial fibrillary acidic protein (GFAP).³³⁶ All cell isolates stained positively for these markers, in comparison with cells stained with negative control antibodies, consistent with a Müller cell phenotype (Figure 4.10).

Monolayers of primary human Müller cells were infected with Mon601 or representative field strain, EHI0578Y05 at a MOI of 5. At 48 hpi, the cytopathic effect varied across Müller isolates and DENV strains, and was most apparent for Müller cell isolate 3 following infection by Mon601 (Figure 4.11A). At this point, RNA was extracted from cells, or monolayers were fixed with 4% paraformaldehyde for immunolabelling. Viral load, as measured by RT-qPCR, reached higher levels in cell isolates infected with Mon601 compared with EHI0578Y05 (Figure 4.11B). Immunolabelling of dsRNA demonstrated greater infection of Müller isolate 2, with nearly all cells appearing infected (Figure 4.12), consistent with the results obtained by RT-qPCR.

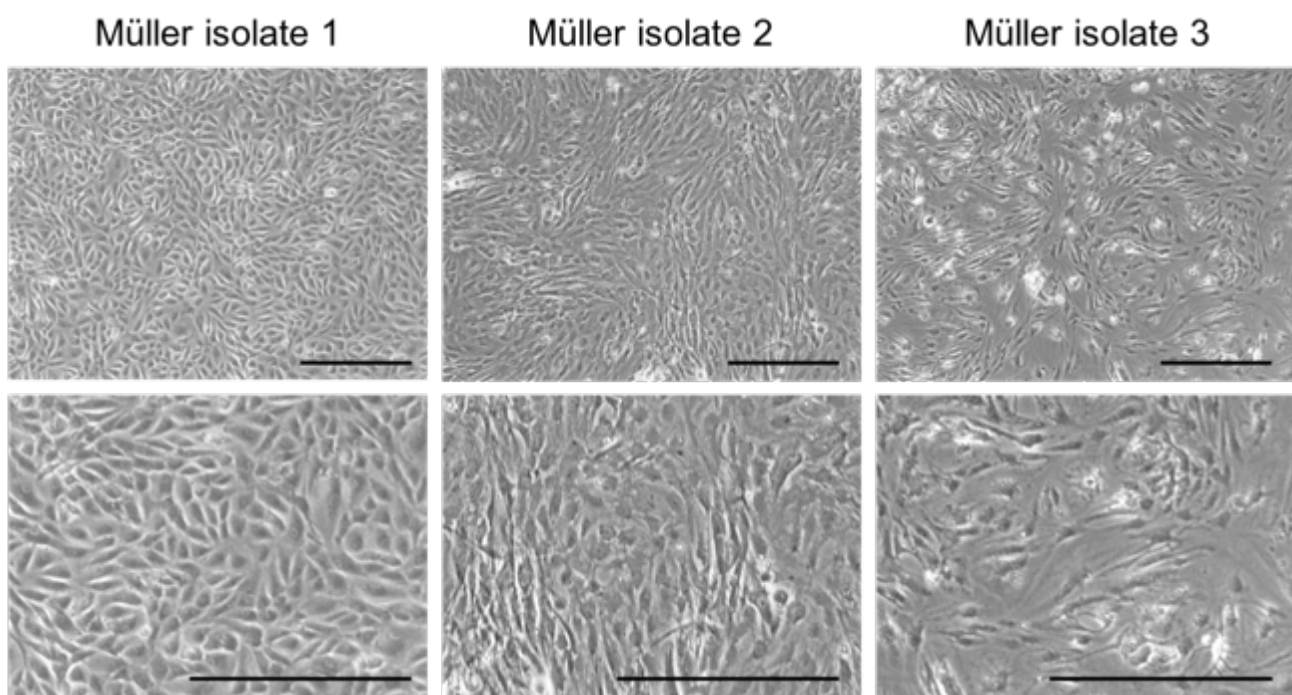


Figure 4.9: Human primary Müller cells

Photomicrographs of primary human Müller cell monolayers isolated from eyes of three male cadaveric donors. Scale bars 100 μm .

Table 4.1: Primary human Müller cell donors

Cell isolate number	Sex of donor	Age of donor at death	Time from death to cell isolation
Primary isolate 1	Male	68	24 hours
Primary isolate 2	Male	82	25 hours
Primary isolate 3	Male	71	31 hours

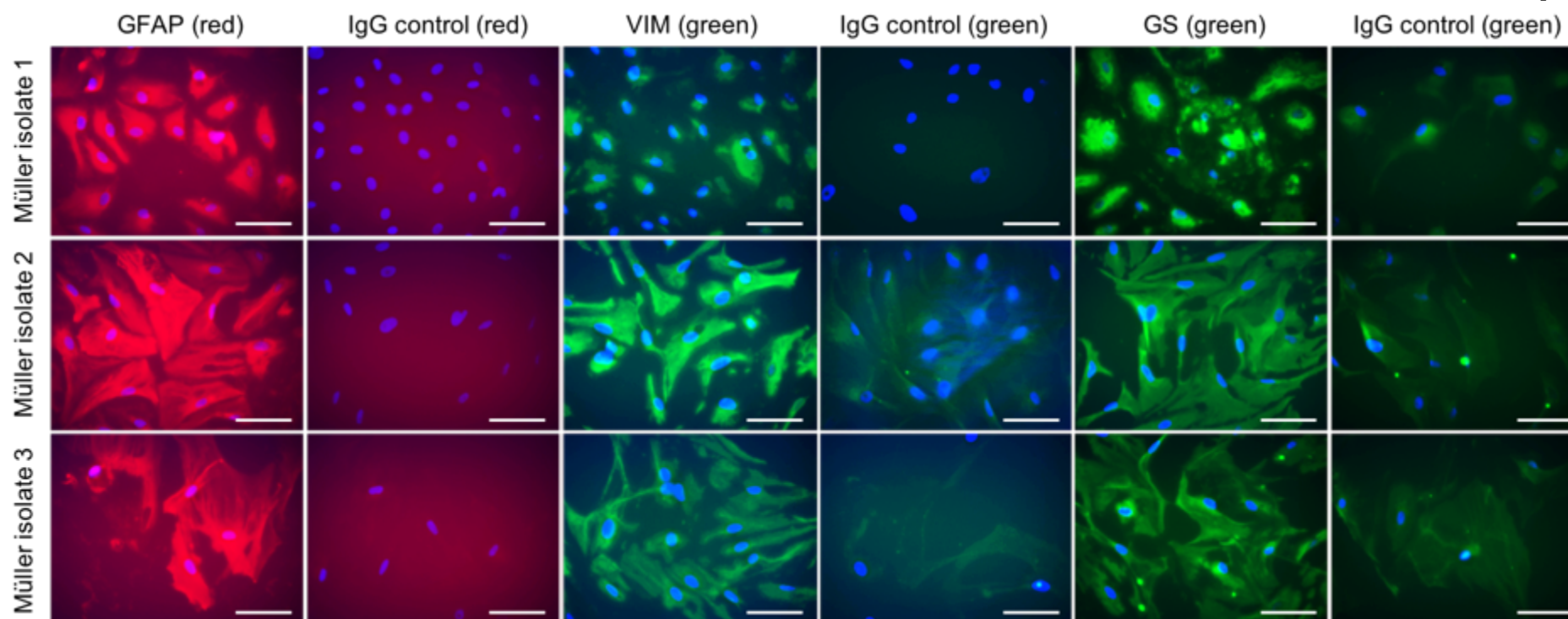


Figure 4.10: Expression of Müller cell markers in primary human Müller cell isolates

To characterise primary human Müller cell isolates prior to use in experiments, the cells were immunolabelled for markers of cultured primary human Müller cells. Fluorescent photomicrographs of human Müller cell monolayers immunolabelled for Müller cell markers: intermediate filaments glial fibrillary acidic protein (GFAP, red), vimentin (VIM, green), or glutamine synthetase (GS, green). Negative controls were labelled with species-matched polyclonal or monoclonal antibodies targeted to irrelevant antigens. Primary antibodies: sheep anti-GFAP IgG, mouse anti-VIM IgG1K, rabbit anti-GS IgG. Secondary antibodies: Alexa Fluor 594 donkey anti-sheep IgG (red), Alexa Fluor 488 goat anti-mouse (green), Alexa Fluor 488 goat anti-rabbit (green). Nuclei counterstained with 4',6-diamidino-2-phenylindole (blue). Scale bars 50 μm . **Abbreviations:** GFAP = glial fibrillary acidic protein, GS = glutamine synthetase, Ig = immunoglobulin, VIM = vimentin.

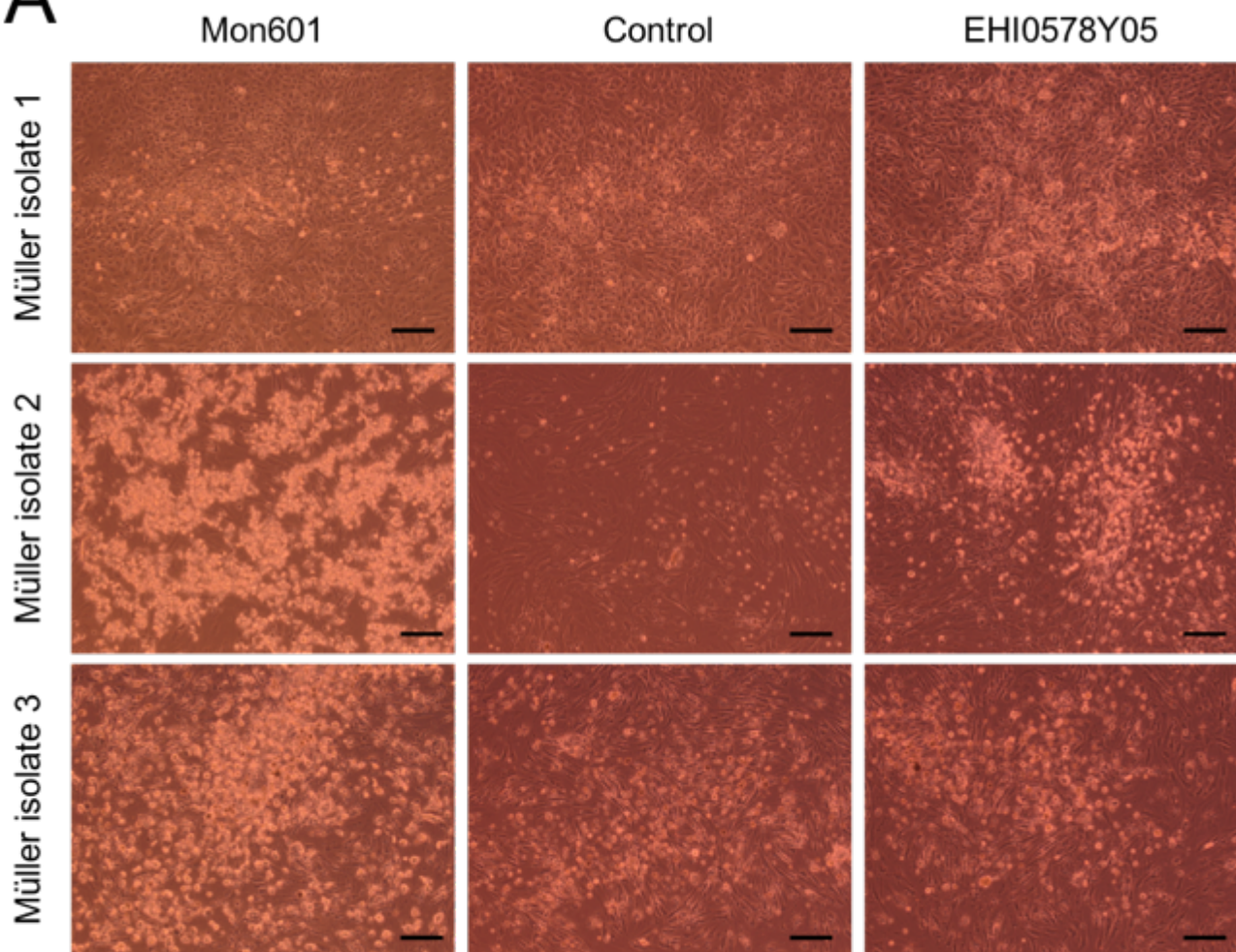
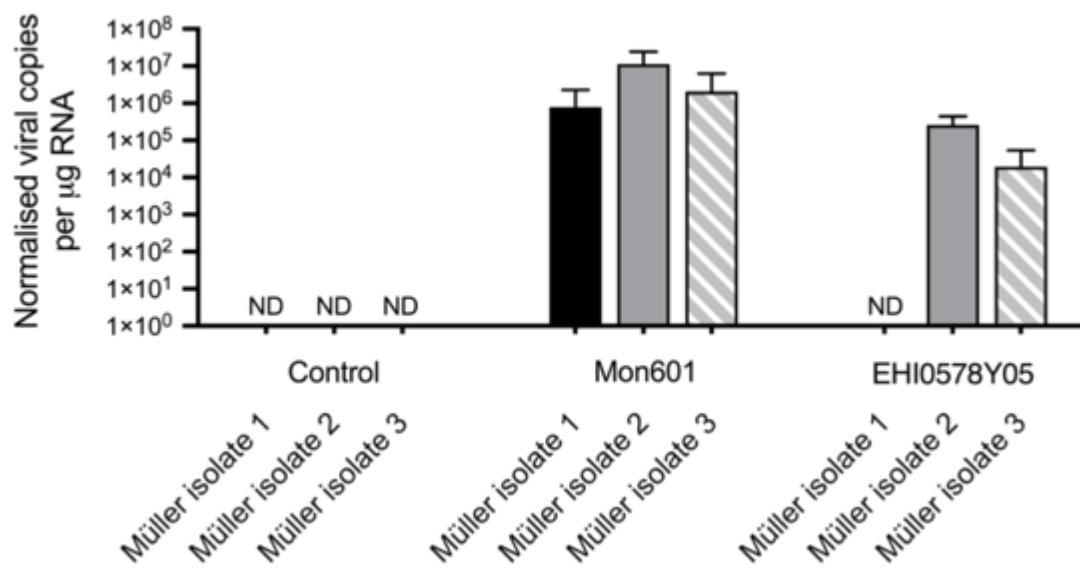
A**B**

Figure 4.11: Infection of primary human Müller cell infection with DENV

Monolayers of primary human Müller cells were infected with Mon601 or representative field strain, EHI0578Y05. (A). Brightfield images demonstrating cytopathic effect of primary human Müller cell isolates at 48 hpi with Mon601 strain or representative field strain, EHI0578Y05, at an MOI of 5. Scale bars 100 μm . (B) Quantification of viral genomes in primary Müller cell isolates by RT-qPCR at 48 hpi with Mon601 (M) or EHI0578Y05, at an MOI of 5, or control cells treated with medium alone. Expression normalised to reference gene, ribosomal protein lateral stalk subunit P0, n = 4 monolayers per condition. Error bars show standard deviation, ND = expression not detected in ≥ 3 of 4 replicates. Note logarithmic scale. **Abbreviations:** DENV = dengue virus, hpi = hours post-inoculation, MIO-M1 = Moorfields / Institute of Ophthalmology-Müller 1, MOI = multiplicity of infection, RNA = ribonucleic acid, RT-qPCR = quantitative reverse transcription polymerase chain reaction.

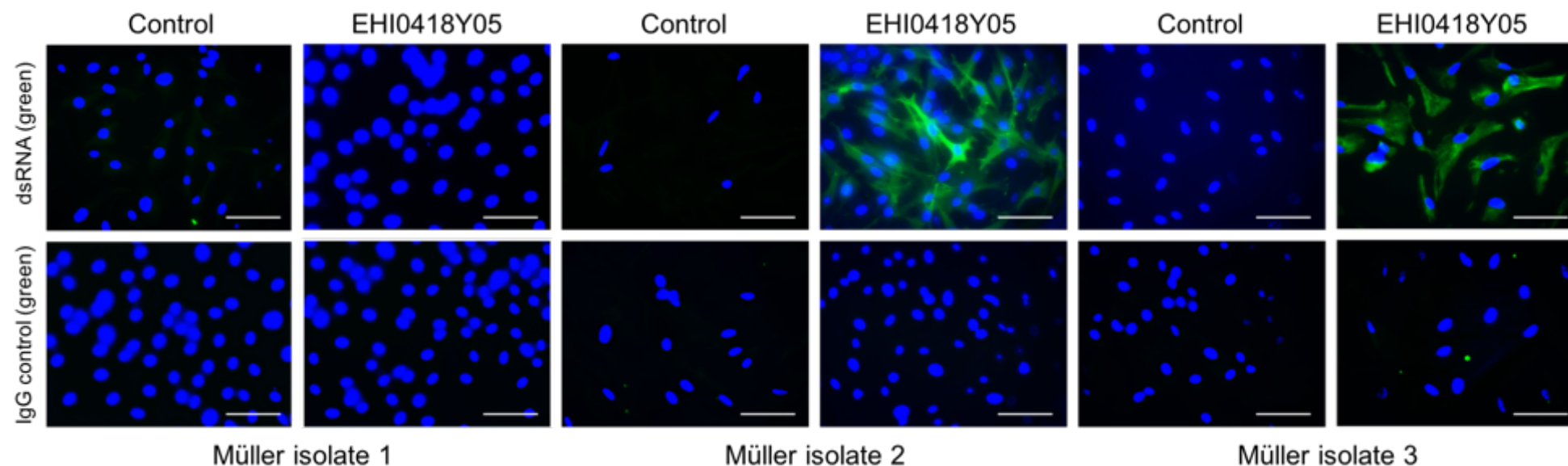


Figure 4.12: Primary Müller cell infection with DENV field isolates

Monolayers of primary human Müller cells were infected with Mon601 or representative field strain, EHI0578Y05. Fluorescent photomicrographs showing immunolabelling of double-stranded (ds)RNA (green) in primary human Müller isolates at 48 hpi with representative DENV field strain, EHI0418Y05 (DENV2, 2005), at an MOI of 5. Nuclei counterstained with 4',6-diamidino-2-phenylindole (blue). Müller isolates 2 and 3 show obvious presence of dsRNA in DENV-inoculated cells. Primary antibody: J2 Mouse anti-dsRNA IgG2ak, negative control: isotype-matched irrelevant mouse antibody. Secondary antibody: Alexa Fluor® 488 Goat anti-Mouse (green). Scale bars 100 μ m. **Abbreviations:** DENV = dengue virus, hpi = hours post-inoculation, Ig = immunoglobulin, MOI = multiplicity of infection, dsRNA = double-stranded ribonucleic acid.

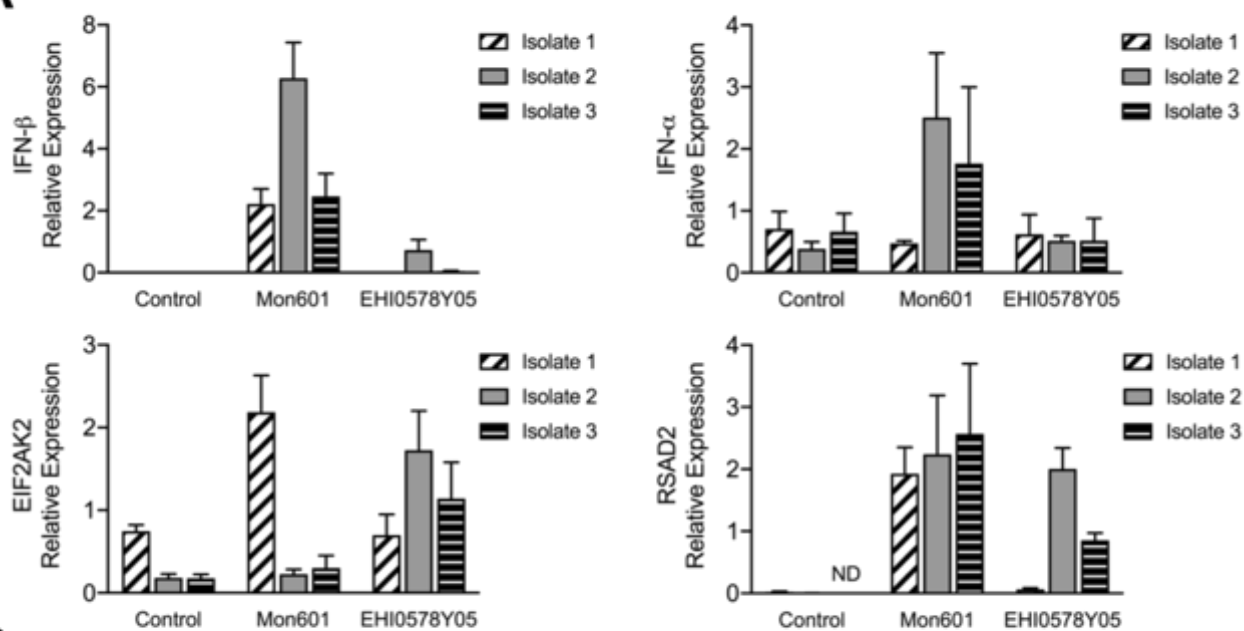
To investigate the molecular responses of the three primary human Müller cell isolates to DENV infection, analysis of transcript expression at 48 hpi was measured by RT-qPCR of extracted RNA. The innate response to infection was measured, and experimental conditions comprised control cells treated with medium alone, and cells infected with Mon601 or EHI0578Y05 field strain, both at MOI of 5. Firstly, the antiviral type I IFN response of Müller isolates to DENV infection was investigated (Figure 4.13A). In contrast to the lack of IFN- β induction in DENV-infected MIO-M1 cells, primary Müller cells expressed IFN- β mRNA in response to DENV infection, but the magnitude varied between Müller cell isolates. Expression of other components of the type I IFN pathway showed significant variation across cells, and by virus, and these molecules included IFN- α (df 4, mean squares 1.707, $F(4, 25) = 4.767$, $p < 0.01$) and EIF2AK2 (df 4, mean squares 2.487, $F(4, 27) = 31.39$, $p < 0.0001$). Interestingly, expression of EIFAK2 was higher for EHI0578Y05 compared to Mon601 infection in two Müller cell isolates, whereas expression was lower for EHI0578Y05 versus Mon601 infection in the third Müller cell isolate. The transcript RSAD2 had very low constitutive expression that was not detected in one Müller cell isolate, and higher induction in response to Mon601 than EHI0578Y05 infection. Because expression was not detected in one condition, statistical analysis could not be performed for this transcript.

Secondly, the inflammatory response of primary human Müller cells to infection with DENV was explored (Figure 4.13B). In two of three primary cell isolates, TNF- α was not expressed at baseline, but in one isolate, strong induction was seen following Mon601 infection and a modest induction after EHI0578Y05 infection. This same pattern of expression was observed for IL-6. Two-way ANOVA analysis conducted on IL-1 β transcript expression was significant for the interaction of infection status with primary Müller isolate (df 4, mean squares 12.51, $F(4, 25) = 7.490$, $p < 0.001$), and infection with Mon601 was the factor that most strongly influenced IL-1 β expression.

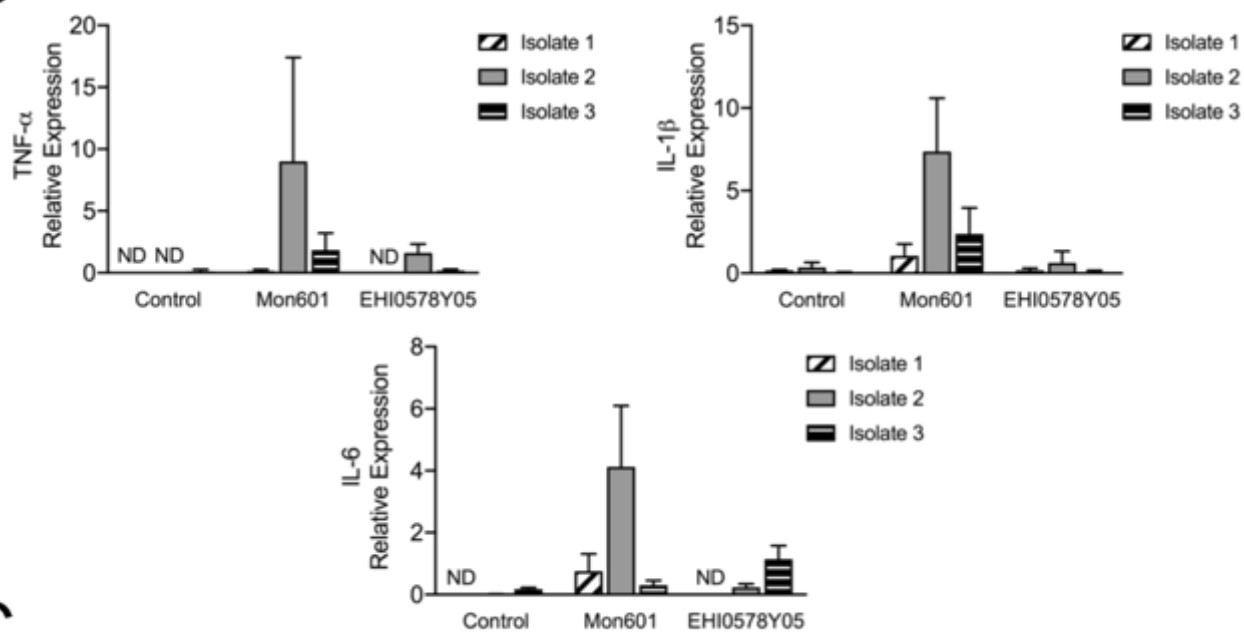
Finally, the immunomodulatory response to DENV infection was explored by measuring expression of PD-L1 and PD-L2 transcripts (Figure 4.13C). Infection with DENV resulted in increased expression of both PD-L1 (df 2, mean squares 11.94, $F(2, 27) = 26.36$, $p < 0.0001$) and PD-L2 (df 2, mean squares 2.895, $F(2, 27) = 13.87$, $p < 0.0001$), and PD-L1 expression was higher with Mon601 in comparison to EHI0578Y05. The influence of primary Müller isolate on transcript expression was smaller, with $p < 0.01$ for both PD-L1 (df 2, mean squares 3.117, $F(2, 27) = 6.880$) and PD-L2 (df 2, mean squares 1.341, $F(2, 27) = 6.427$). This showed that expression of immunomodulatory transcripts, PD-L1 and PD-L2, was influenced more by DENV infection than by individual cell isolates, and that patterns of increased expression in response to infection differed across donors.

In summary, primary human Müller cells mount a type I IFN response to infection with DENV, in contrast to MIO-M1 cells, and this response is characterised by expression of IFN- β , IFN- α , and IFN-stimulated genes. Inflammatory and immunomodulatory responses tended to be higher with Mon601 than EHI0578Y05 infection.

A



B



C

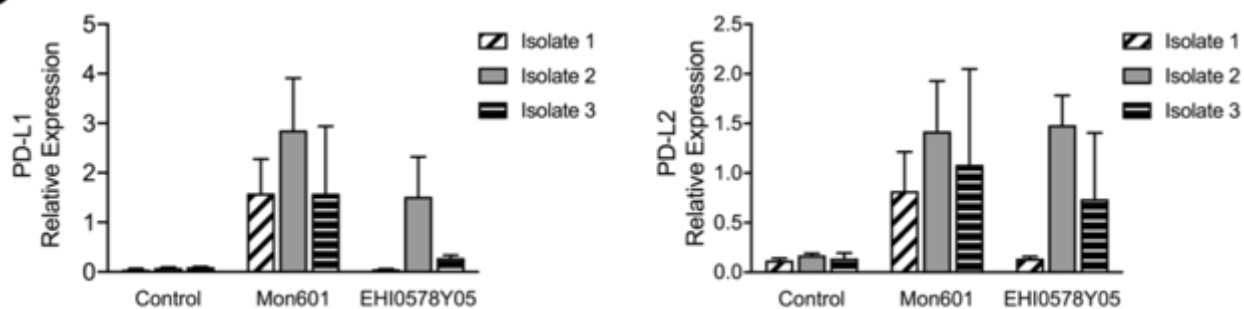


Figure 4.13: Responses of primary human Müller cell isolates to infection with DENV

To investigate the molecular responses of the three primary human Müller cell isolates to DENV infection, analysis of transcript expression at 48 hpi was measured by RT-qPCR. The antiviral, inflammatory, and immunomodulatory responses of Müller isolates to DENV infection were investigated. Graphs representing the expression of (A) anti-viral, (B) inflammatory and (C) immunomodulatory transcripts by RT-qPCR in primary human Müller cell isolates 48 hpi with either Mon601 or representative field isolate, EHI0578Y05, at an MOI of 5, or not infected. Expression relative to reference genes, ribosomal protein lateral stalk subunit P0 and β -actin. Statistics were performed where expression was above zero (i.e. this was not performed for RSAD2, TNF- α or IL-6, for which levels were undetectable for all conditions). Data were analysed by two-way ANOVA (see Table 4.2, and Appendix F, Tables 7-8). n = 4 cultures per condition. Error bars represent standard deviation. ND = expression not detected in ≥ 3 replicates. **Abbreviations:** ANOVA = analysis of variance, DENV = dengue virus, EIF2AK2 = eukaryotic translation initiation factor 2-alpha kinase 2, hpi = hours post-inoculation, IFN = interferon, IL = interleukin, MOI = multiplicity of infection, PD-L = programmed death-ligand, RNA = ribonucleic acid, RSAD2 = radical S-adenosyl methionine domain-containing 2, RT-qPCR = quantitative reverse transcription polymerase chain reaction, TNF- α = tumour necrosis factor-alpha.

Table 4.2: Two-way ANOVA of immune responses to DENV infection in Müller cells.

Gene	Interaction p-value		Infection factor* p-value		Cell isolate factor* p-value	
IFN- β	< 0.0001	****	< 0.0001	****	< 0.0001	****
IFN- α	0.0054	**	0.0004	***	0.1091	NS
EIFAK2	< 0.0001	****	< 0.0001	****	< 0.0001	****
IL-1 β	0.0004	***	< 0.0001	****	0.0006	***
PD-L1	0.1774	NS	< 0.0001	****	0.0038	**
PD-L2	0.1194	NS	< 0.0001	****	0.0052	**

*Infection factor refers to responses as a function of the infecting virus strain. Cell isolate factor refers to responses as a function of the cell isolate.

Abbreviations: ANOVA = analysis of variance, EIF2AK2 = eukaryotic translation initiation factor 2-alpha kinase 2; IFN- α = interferon alpha; IFN- β = interferon beta; IL-1 β = interleukin-1 beta; NS = not significant; PD-L1 = programmed death-ligand 1; PD-L2 = programmed death-ligand 1.

4.3 DISCUSSION

The work presented in this chapter represents the first reported investigation of DENV infection of human Müller cells, demonstrating Müller cell susceptibility to DENV infection, and providing a description of the Müller cell response to infection with DENV1 and DENV2 isolates. Initially infection was tested in human Müller MIO-M1 cells with the lab-adapted strain Mon601, and productive infection was demonstrated. The infection was characterised by a limited antiviral response that lacked components of the type I IFN pathway, including IFN- β , the key type I IFN. Immune responses generated with DENV infection included upregulation of the pro-inflammatory cytokines, TNF- α , IL-1 β and IL-6, which have also been documented in studies of Müller cells exposed to other infectious pathogens.⁹⁶ An immunomodulatory response to DENV infection was also seen, with increased expression of PD-L1 and PD-L2.

Follow-up experiments used DENV1 and DENV2 strains isolated from patients with dengue to infect MIO-M1 cells. Infection with these strains was relatively poor compared to Mon601 infection, but differential responses were seen across the two serotypes, with higher antiviral, inflammatory and immunomodulatory changes following exposure to DENV2 strains compared to DENV1. Primary human Müller cells isolated from cadaveric donor eyes were also infected with Mon601 and one representative field strain. In contrast to the MIO-M1 cell line, primary Müller cells expressed very low levels of IFN- β constitutively, and this antiviral cytokine was upregulated in the context of DENV infection. Other molecular components of the type I IFN response were also upregulated after DENV infection, namely IFN- α , and IFN-stimulated genes, EIF2AK2, ISG15 and

RSAD2, and these responses showed variation across individual cell isolates. These results suggest that *in vivo*, human retinal Müller cells are susceptible to infection and mount inflammatory and antiviral responses to DENV.

There have been no reports of DENV isolated from ocular fluid. In a case series of epidemic retinitis, the authors stated that aqueous humour in one patient with dengue was tested for DENV by RT-qPCR, and this returned a negative result.³⁵² In another series of posterior uveitis cases in Singapore, investigators found that DENV was the leading cause of infectious retinitis during dengue epidemics, and although the authors noted that PCR testing of ocular fluid was performed in cases of presumed infectious uveitis, they did not state whether there was specific testing for DENV.³⁵³ The only positive confirmation of DENV in ocular tissue was in a case report that described isolation of DENV3 from a corneal donor who died of a febrile illness. Virus was identified by RT-qPCR and plaque assay of corneal tissue suspension.³⁵⁴ Thus, there is no histopathological or laboratory confirmation of direct DENV infection of the human retina in clinical disease. In severe dengue, virus has been isolated from cerebrospinal fluid,³⁵⁵ and post-mortem studies have demonstrated DENV RNA, antigen and IgM antibodies in the brains of individuals with meningitis and encephalitis, indicating that the virus had crossed the BRB.³⁵⁶⁻³⁵⁹ In a mouse model of systemic DENV infection, inflammatory responses were observed in the eyes of infected AG129 mice.³⁶⁰ Thus, it is plausible that DENV might also cross the BRB.

The type I IFN response is the key human antiviral response, seen in DENV-infected human cells as well as in clinical dengue.³⁶¹⁻³⁶³ This work demonstrated that the antiviral response to DENV in primary, but not MIO-M1, human Müller cells is characterised by expression of its primary driver, IFN- β .³⁶⁴ This cytokine acts in an autocrine and paracrine fashion by engaging IFN α/β receptors on the cell surface, which ultimately activate IFN

regulatory factor 3, a transcription factor that drives expression of IFN-stimulated genes including RSAD2, EIF2AK2 and ISG15.³⁶⁵ Thus, infected Müller cells expressing IFN- β would also prime neighbouring retinal cell populations to switch to an antiviral state, and the Müller cell's strategic location at the inner BRB makes it one of the cell populations likely to be infected in the early stages of infection with vascular-borne pathogens. The cytokine, IFN- α , plays an overlapping and synergistic role in the type I IFN response and binds to the same IFN α/β receptors.³⁶⁶ In this work, IFN- α was upregulated in primary Müller cells in response to DENV infection.

Despite their name, some IFN-stimulated genes are also expressed independently of IFN- α and IFN- β .^{236, 367} This was demonstrated in the current work involving DENV-infected MIO-M1 cells. The IFN- β protein was not detected by Alpha-LISA[®] in infected or uninfected MIO-M1 cells, and transcript expression of IFN- α or EIF2AK2 was not altered with DENV infection. In contrast, increased expression of RSAD2 and ISG15 transcripts in these cells. Expression of these antiviral molecules through type I IFN-independent signalling pathways has been observed in viral infections,^{361, 368-374} The ISG15 molecule is an intrinsically multifunctional protein that is involved in diverse cell processes and plays a key role in the cellular innate immune response, acting as an extracellular cytokine, as well as enhancing intracellular antiviral pathways and binding to viral proteins.³⁷¹ Another broad-spectrum molecule, RSAD2 - known also as viperin, or virus inhibitory protein, endoplasmic reticulum-associated, interferon-inducible - is strongly expressed in response to diverse viral infections and inhibits early viral replication of DENV³⁷⁵ and other flaviviruses.^{370, 376}

In this work, alterations to expression of inflammatory molecules were observed in response to DENV infection of Müller cells. Increased expression of TNF- α , IL-1 β and IL-6

was seen predominantly with DENV2 infection, and at higher levels with Mon601 compared with DENV1/2 field isolates. Inflammation is a characteristic of murine infection with DENV,³⁶⁰ and high levels of circulating TNF- α and IL-1 β in patients are associated with severe dengue.^{377, 378} Retinopathy associated with DENV often presents with signs of posterior segment inflammation, and the spectrum of disease includes vasculitis and retinitis.³⁷⁹ Macular oedema, another feature of dengue retinopathy,^{193-196, 204, 209, 331, 380-385} represents breakdown of the BRB.³³⁷ The Müller cell performs an important role in controlling retinal fluid homeostasis,³³⁴ and direct infection of the cell could impair its function in this critical process, leading to excess fluid in the retinal interstitium with consequent macular oedema. Preliminary data assessed aquaporin 4 and inward-rectifier potassium channel 4.1 expression, but no conclusive changes were seen with DENV infection (data not shown). Potential avenues for further investigation could explore the effect of DENV infection on Müller cell fluid exchange.

The work presented in this chapter demonstrated molecular adjustments of components of immunomodulatory pathways. DENV-infected Müller cells showed increased expression of programmed death-ligands, PD-L1 and PD-L2. These ligands interact with programmed cell death protein 1 (PD-1) which is expressed on activated T-cells and other immune cells to form an inhibitory signal that prevents an excessive immune response by blocking production of pro-inflammatory cytokines.³⁸⁶ The PD-1/PD-L1 pathway also mediates immune responses to acute viral infection through suppression of T-cell-mediated tissue damage.³⁸⁷ Upregulation of PD-L1 has been seen in acute and chronic viral infections.³⁸⁸ Dendritic cells infected with DENV2 showed increased PD-L2 and decreased PD-L1 expression, expected to preferentially inhibit T-helper 1 effector cell responses.³⁸⁹ While expression of both PD-L1 and PD-L2 was induced with DENV

infection in this work, particularly high expression of PD-L2 was seen in MIO-M1 cells infected with DENV2 (Mon601). This was not reproduced in primary Müller cell infections, and may be a function of the unique MIO-M1 transcriptome.³⁹⁰ Müller cells may participate in ocular immune privilege through the expression of immunomodulatory genes PD-L1 and PD-L2, and other ocular cell populations also show expression of these ligands.³⁹¹

The *in vitro* work presented in this chapter showed responses of human Müller cells to infection with DENV1 and DENV2. In 2005, Singapore saw its highest rate of dengue on record, and this epidemic was characterised by a predominance of the DENV1 serotype, before a rapid shift to circulating DENV2 serotypes that tended to affect older people during the 2007 epidemic.^{392, 393} The prevalence of dengue retinopathy was assessed in cross-sectional studies conducted during these epidemics. In the 2005 epidemic, investigators reported that 10% of those hospitalised with dengue had maculopathy,¹⁹³ yet in 2007, no maculopathy was identified in any patient.¹⁹⁴ The predominant DENV serotype circulating in the 2005 epidemic in Singapore was DENV1, but all viral serotypes are endemic and circulate in Singapore,³⁹³ and patients with maculopathy were not tested for DENV serotype,¹⁹³ making any association with DENV1 merely speculative. The work in this chapter showed stronger responses to DENV2 compared to DENV1 infection. Severe dengue has been more closely associated with DENV2 compared to other serotypes,^{394, 395} but it is important to note the complexity of this disease, and that other factors influence dengue severity, including age, host genetics and prior DENV infection, which increases the risk of antibody-dependent enhancement and severe complications.¹⁷⁰

Previous work has concentrated on retinal pigment epithelial cells and retinal endothelial cells, and their participation in BRB function in DENV infection. One report detailed responses of primary human retinal pigment epithelial cells, retinal endothelial cells, and ARPE-19 cells infected with two strains of DENV2, and showed that infected endothelial cells increased their expression of cell adhesion molecules.²⁰⁵ Other investigators studied responses across different endothelial cell subpopulations and four DENV serotypes, including commercially-sourced primary human retinal endothelial cells. Researchers demonstrated loss of barrier function in retinal endothelial cells over time that was DENV serotype-dependent.²⁰⁷ Across all serotypes, DENV infection reduced endothelial cell membrane permeability that was greatest with DENV1 and DENV2, and a qualitative change in permeability in the early stage of infection was seen with DENV1. Effects on junctional molecules were not evaluated, but permeability changes were linked to the loss of cell-cell interactions, as well as their effect on cell membrane capacitance. The only other research of DENV-infected ocular cell populations involved DENV2 infection of primary retinal pigment epithelial cells as controls for systems biology comparison of the ZIKV transcriptome with other flaviviruses.²⁰⁶ In the context of DENV infection, retinal pigment epithelial and retinal endothelial cell function has been studied but other retinal cell populations, including Müller cells, had not been studied prior to this work.

In this work, human Müller cells were subjected to DENV infection with a lab-adapted isolate and six viral strains from dengue epidemics across 2 DENV serotypes. Induction of mRNA in response to infection tended to be stronger with DENV2 infection, which generated increased expression of inflammatory and antiviral transcripts. The DENV2 serotype also appeared to be more virulent than DENV1 across field isolates of the virus, based on intracellular levels achieved in the experiments. Taken together, these results

show tropism of DENV2 toward human Müller cells, and, in contrast to prior suggestion from studies from Singapore epidemics,¹⁹⁴ implicate this strain in DENV retinopathy. A stronger inflammatory response may generate more tissue pathology through inflammatory-mediated damage, and further investigations would be informative, including a wider assay of inflammatory and antiviral molecules, which could be achieved by RNA sequencing or multiplex cytokine analysis. By utilising whole mount retina in future infection studies, a more complete understanding of DENV infection in the context of a complex multi-cellular tissue could be gained.

Significant differences between primary isolates and cell lines are becoming apparent. Recent transcriptomic analysis of human retinal cell populations elegantly demonstrated that the MIO-M1 cell line forms a distinct cluster that bears more similarity to retinal astrocytes than primary human Müller cells.³⁹⁰ A curious finding in this research was the lack of a type I IFN response in DENV-infected MIO-M1 cells. This was unexpected, and had not been previously reported or measured in other viral infections of MIO-M1 cells.³⁹⁶ Validation of DENV infection in isolated primary human Müller cells confirmed that primary Müller cells do generate both IFN- β and IFN- α in response to infection with DENV. This is a significant finding that underscores the importance of using isolated human primary cells in research, as cell lines may generate idiosyncratic results that do not reflect *in vivo* biology.

Primary human Müller cells in this work displayed variation in terms of their cell phenotype and molecular responses to DENV infection, and biological and technical factors are likely to have contributed to these differences. Individuals differ in their responses to biological conditions, and this natural variation is also to be expected in cell culture. The cells of Müller isolate 1 had a higher growth rate and were more rounded in

comparison with isolates 2 and 3, which were more spindle-shaped. Investigators recently reported disparate human Müller cell phenotypes and transcriptomes that varied by retinal location.³¹⁰ Primary Müller cells isolated from the macula were morphologically distinct, displaying a spindle shape with a low cytoplasm-to-nucleus ratio, whereas peripheral Müller cells had relatively larger cell bodies with multiple cytoplasmic processes. These researchers also reported that cell populations initially retained their phenotypic differences in culture, but subsequently reverted to a phenotype more akin to that of the MIO-M1 Müller cell line.³¹⁰ Thus, phenotypic changes related to time in culture may have impacted results. Another technical source of variation included time from death to cell isolation (mean 27 hours, range 24-31 hours). The ideal cells to use for research into human disease would be as similar as possible to those of the adult *in vivo*, and a limitation of cell culture lies in the fact that cells from a complex tissue are isolated in order to study their biology, which may be different from native tissue. Alternative models for dengue retinopathy include genetically manipulated mice, such as the AG129 mouse, which lacks IFN α/β and IFN γ signalling.³⁶⁰ The advantage of an animal model lies in the ability to examine retinal tissue *in vivo*, but limitations include the fact that mice do not possess a macula which makes research on maculopathy challenging.

The research presented in this chapter represents first-in-field studies of human Müller cells in DENV infection. A limited number of molecules were examined in the response to infection, and this work could be expanded in a range of directions. Infecting more primary Müller cell isolates would allow a more complete picture of the spectrum of host cellular responses to infection. Further exploration of Müller cell function, especially in relation to fluid homeostasis and expression of aquaporins and potassium channels in

response to DENV infection could be first steps toward identifying mechanisms of dengue-associated maculopathy, and adjusting cell isolation techniques to harvest from the macula region of donor eyes would enable more fidelity to macular disease processes *in vivo*.

In summary, this work has demonstrated that human Müller cells mount an antiviral and immune response to DENV infection that is characterised by expression of pro-inflammatory cytokines, immunomodulatory molecules and the type I IFN response, and that this response varies across cell isolates and DENV serotype. This research provides a foundation and direction for future research efforts that will help us understand the pathogenesis of dengue retinopathy.

CHAPTER 5

Computational predictions of the biological effects of microRNA in *Ebola virus*-infected human retinal pigment epithelial cells

5.1	Introduction	185
5.2	Results.....	189
5.2.1	Small RNA dataset preparation by deep sequencing	189
5.2.2	Differential expression of microRNA	189
5.2.3	Gene target prediction of differentially expressed microRNA	194
5.2.4	Pathway analysis of gene targets of microRNA.....	196
5.2.5	Network analysis of miRNA-gene target interactions	199
5.3	Discussion.....	204

5.1 INTRODUCTION

Survivors of EVD suffer a chronic syndrome that carries a high burden of morbidity.^{34, 225, 229, 397} . Intraocular inflammation – termed uveitis – develops in 18 to 34% of Ebola survivors,^{228, 229} 40% of whom become blind.³⁴ Infectious *Zaire ebolavirus* (EBOV), one of 6 species of the Ebolavirus genus²¹² and the most virulent, has been isolated from intraocular fluid after resolution of viraemia in survivors.²²⁶ Retinal scars in these individuals indicate involvement of the retinal pigment epithelium (RPE), and are associated with uveitis.³⁴ The persistence of infective virus in immune privileged sites^{226, 234, 398} reflects the transition of viral replication from highly vascular organs such as the liver, lungs, and kidneys in the acute phase, to sites where chronic low-level immune surveillance is coupled with chronic low-level viral replication.^{237, 247}

Mechanisms of EBOV persistence in the eye are poorly understood.²²⁶ Ocular examination in the acute phase of EVD and histopathological studies of human ocular tissue have not been reported. Furthermore, ocular signs in EVD survivors have been documented in largely uncontrolled studies that make aetiological conclusions difficult, but uveitis, white cataract and retinal scars are characteristic findings.^{34, 227, 239} Attention was directed to the retinal pigment epithelial cell as a possible viral reservoir after the observation of pigmented retinal scars in an EVD survivor prior to the onset of florid uveitis, in which infective EBOV was isolated from ocular fluid.^{34, 226}

MicroRNAs (miRNAs) are short (18-22 nt) fragments of single-stranded RNA that bind the 3' untranslated region of messenger RNA, and directly suppress or indirectly activate gene expression (Figure 5.1). Because only a small (6-8 nt) “seed region” requires complementarity to permit binding, a single miRNA may have hundreds of potential

messenger RNA targets. Thus, miRNA play a complex regulatory role in cellular activity that varies by cell type and disease state.³⁹⁹ The roles of miRNAs in post-EVD uveitis are unstudied. The research presented in this chapter used small RNA sequencing (sRNA-Seq) to identify miRNA expression in EBOV-infected ARPE-19 human retinal pigment epithelial cells, and conducted *in silico* analyses to identify biological targets of, and molecular interactions with, these miRNAs. This work was published in BMC Research Notes (2019, Oct 1;12(1):639).⁴⁰⁰

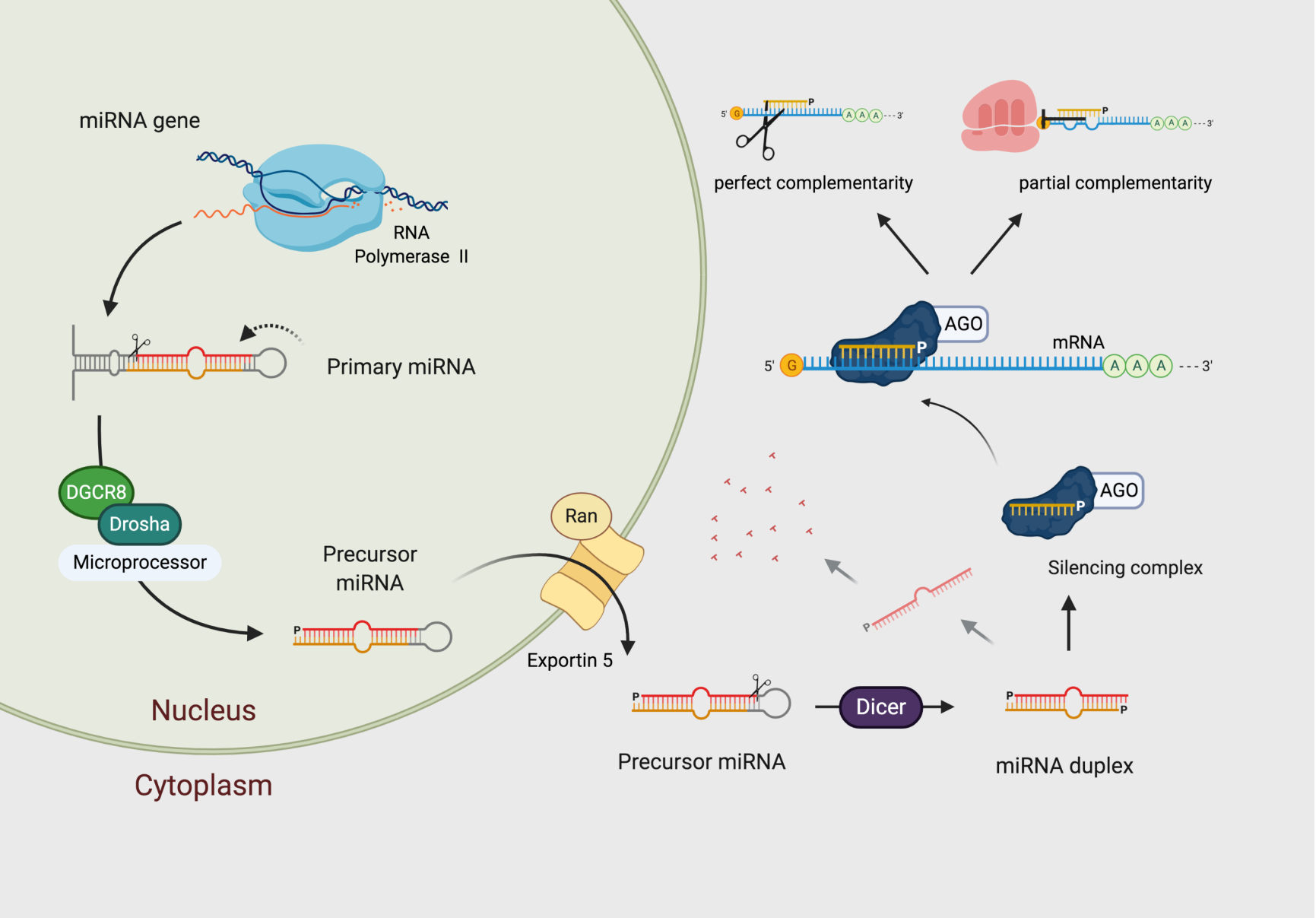


Figure 5.1: Processing and function of miRNA

MicroRNAs (miRNAs) are short (18-22 nt) fragments of single-stranded RNA that bind the 3' untranslated region of messenger RNA, and directly suppress or indirectly activate gene expression. In animals, canonical miRNAs are transcribed by RNA polymerase II to form a primary miRNA, which folds back on itself to form a hairpin loop. The microprocessor endonuclease complex (Drosha and DiGeorge syndrome chromosomal [or critical] region 8, DGCR8) cleaves both strands of the stem with a 2 bp offset to leave a ~60 bp precursor hairpin with a 5' cap (P). The precursor miRNA is transported out of the nucleus by Exportin 5 and Ras-related nuclear protein (Ran). In the cytoplasm, the pre-miRNA is further cleaved by Dicer to form a ~20 bp duplex with a 2-3 bp overhang at each end. The mature (yellow) strand of the duplex is loaded into the ArgonAUT protein to form a silencing complex while the other (red) strand is degraded. Inside the silencing complex, miRNA nucleotides 2-5 recognise complementary sequences on target RNA, and protein translation is repressed. If extensive pairing of the miRNA occurs, the RNA target is silenced by cleavage. Figure created at BioRender.com. **Abbreviations:** AGO = ArgonAUT protein, bp = base pairs, miRNA = micro RNA, RNA = ribonucleic acid.

5.2 RESULTS

5.2.1 Small RNA dataset preparation by deep sequencing

This work used miRNA extracted from total RNA that was generated in a separate experiment, in which the human retinal pigment epithelial cell line (ARPE-19) was infected in triplicate with EBOV at a multiplicity of infection of 1:5, or mock-infected.²³⁵ From 1 µg of total RNA per replicate isolated from cell lysate at 24 hours post-infection, small RNA was extracted, fragmented, and converted to a complementary DNA library by the Sequencing Facility at Flinders University. Sequencing yielded 1.61 to 3.88 x 10⁷ reads per replicate (Table 5.1). Filtering for a minimum size of 18 base pairs, 91% to 97% of adapter-trimmed sequences were mapped to the human genome. A total of 814 human miRNAs were identified. Multidimensional scaling (principal component analysis) showed clear separation between results for EBOV- and mock-infected human retinal pigment epithelial cells, indicating disparate miRNA expression profiles (Figure 5.2). Trimming statistics for RNA sequencing data generated for small RNA are available as [Additional File 1 at the publisher's site](#).⁴⁰⁰

5.2.2 Differential expression of microRNA

Defining differential expression by an adjusted p-value below 0.05, the abundance of 28 and 61 miRNAs was significantly increased or decreased, respectively, in EBOV-infected cells. Filtering more stringently for an adjusted p-value below 0.001 and log₂ fold-change

less than -1 or greater than +1,⁴⁰¹ 13 and 2 miRNAs were significantly increased or decreased (Table 5.2, and [Additional File 2 at publisher's site](#)).⁴⁰⁰

Reads were screened for complete matches to published EBOV miRNA-like sequences, allowing for three mismatches.²⁷⁶ Reads that did not map to the human genome included repetitive elements that aligned to multiple locations in the genome, as well as those that failed to correctly map to the human genome. The latter group included the consequences of technical errors of sequencing that were not resolved by quality controls, and foreign nucleic acid, including contaminants from serum,⁴⁰² and EBOV-derived miRNA. In this work, EBOV-miR-1-5p, EBOV-miR-T1-3p, EBOV-miR-T1-5p and EBOV-miR-T3-5p/T4-5p were identified in EBOV-infected human retinal pigment epithelial cells (Table 5.3, and [Additional File 4 at publisher's site](#)).⁴⁰⁰

Table 5.1: Trimming statistics

Trimming of sequencing data on small RNA extracted from ARPE-19 human retinal pigment epithelial cells at 24 hours after infection in triplicate with EBOV or mock infection. Sequencing yielded a total of 1.61 to 3.88 x 10⁷ reads per replicate. Filtering for a minimum size of 18 base pairs, 91 to 97% of trimmed sequences were mapped to the human genome.

Isolate	Total reads processed	Reads with adapters	Long reads	Reads written (passing filters)
EBOV 1	2.87 x 10 ⁷	2.83 x 10 ⁷ (98.6%)	1.51 x 10 ⁶ (5.3%)	2.72 x 10 ⁷ (94.7%)
EBOV 2	1.61 x 10 ⁷	1.57 x 10 ⁷ (97.6%)	0.50 x 10 ⁶ (3.1%)	1.56 x 10 ⁷ (96.9%)
EBOV 3	3.88 x 10 ⁷	3.81 x 10 ⁷ (98.2%)	1.30 x 10 ⁶ (3.4%)	3.75 x 10 ⁷ (96.6%)
Mock 1	2.14 x 10 ⁷	2.05 x 10 ⁷ (95.7%)	0.94 x 10 ⁶ (4.4%)	2.05 x 10 ⁷ (95.6%)
Mock 2	1.95 x 10 ⁷	1.92 x 10 ⁷ (98.7%)	1.42 x 10 ⁶ (7.3%)	1.81 x 10 ⁷ (92.7%)
Mock 3	2.30 x 10 ⁷	2.26 x 10 ⁷ (98.1%)	2.03 x 10 ⁶ (8.8%)	2.10 x 10 ⁷ (91.2%)

Abbreviations: EBOV = *Zaire* ebolavirus, RNA = ribonucleic acid.

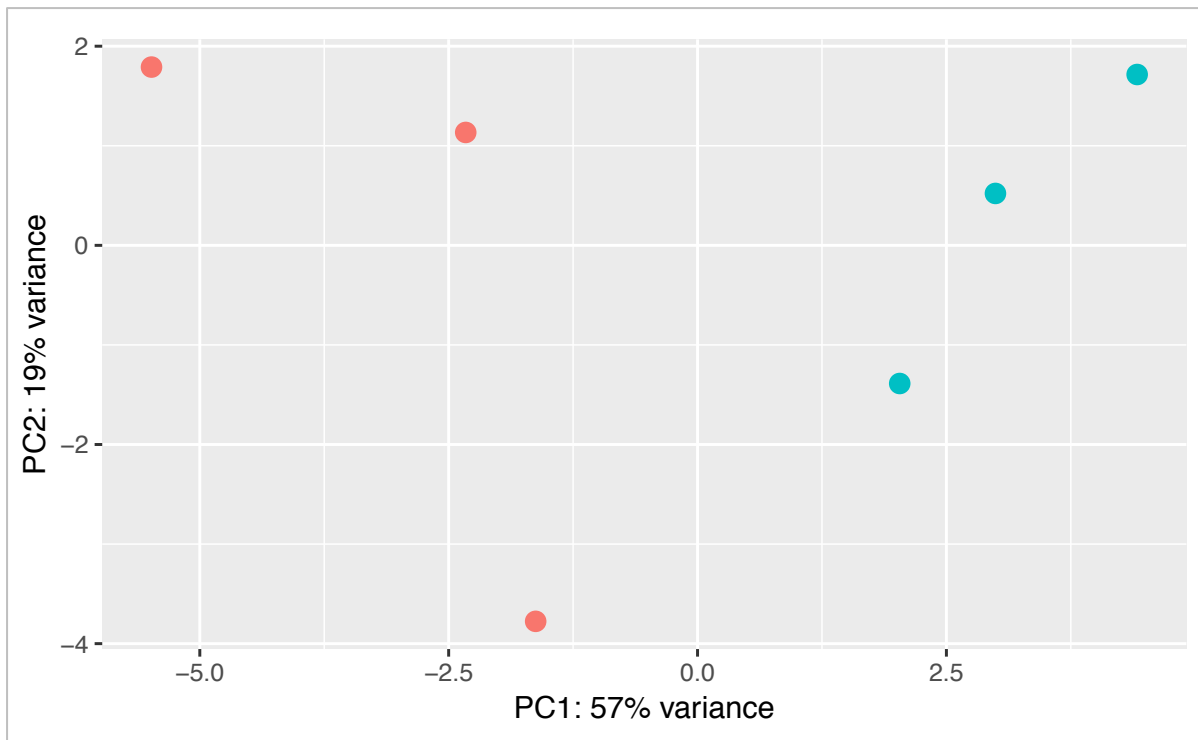


Figure 5.2: Multi-dimensional scaling

Graphic showing multidimensional scaling of miRNA expression in ARPE-19 human retinal pigment epithelial cells at 24 hours post-infection, showing clear separation between results for EBOV- and mock-infected human retinal pigment epithelial cells, indicating disparate miRNA expression profiles. Red spots indicate mock-infected samples and blue spots indicate EBOV-infected samples. Figure reprinted with permission under [Creative Commons Attribution 4.0 International License](#) from Oliver, G.F., Orang, A.V., Appukuttan, B. et al. Expression of microRNA in human retinal pigment epithelial cells following infection with Zaire ebolavirus. BMC Res Notes 12, 639 (2019). <https://doi.org/10.1186/s13104-019-4671-8> **Abbreviations:** EBOV = *Zaire ebolavirus*; microRNA = micro ribonucleic acid, PC = principal component.

Table 5.2: Differential expression of human miRNA

List of differentially expressed miRNAs isolated from EBOV- and mock-infected ARPE-19 human retinal pigment epithelial cells at 24 hours post-infection.

miRNA	log2 fold-change	Adjusted p-value
hsa-miR-3074-3p	-1.52	1.24 x 10⁻¹²
hsa-miR-27b-5p	-1.06	2.63 x 10⁻¹³
hsa-miR-101-5p	1.03	3.09 x 10⁻⁸
hsa-miR-33b-5p	1.04	8.18 x 10⁻⁵
hsa-miR-190a-3p	1.06	6.30 x 10⁻⁵
hsa-miR-1305	1.10	3.92 x 10⁻⁶
hsa-miR-130a-5p	1.19	3.15 x 10⁻⁵
hsa-miR-32-5p	1.21	2.39 x 10⁻⁶
hsa-miR-365a-5p	1.24	2.39 x 10⁻⁶
hsa-miR-100-3p	1.27	1.19 x 10⁻¹³
hsa-miR-33b-3p	1.33	7.05 x 10⁻¹⁰
hsa-miR-4521	1.37	2.63 x 10⁻¹³
hsa-miR-33a-5p	1.41	5.10 x 10⁻⁴
hsa-miR-29b-3p	1.47	2.24 x 10⁻⁸
hsa-miR-1307-5p	1.50	1.98 x 10⁻¹⁰

Abbreviations: EBOV = *Zaire ebolavirus*; hsa-miR = *Homo sapiens* (human) microRNA, miRNA = micro ribonucleic acid.

5.2.3 Gene target prediction of differentially expressed microRNA

Putative gene targets of the 15 highly differentially expressed human miRNAs in EBOV-infected ARPE-19 retinal pigment epithelial cells were identified. Given the inherent complexity of miRNA target prediction, the high rate of false-positive results, and the fact that no prediction tool outperforms others⁴⁰³ or applies the same assumptions to identify functional targets,⁴⁰⁴ three publicly-available online algorithms were used with stringent filters. Predictions yielded a total of 2,629 gene targets by Diana microT,^{280, 281} filtering with a threshold of 0.95; 1,799 genes by miRDB,²⁸³ with a threshold greater than 85; and 14,315 genes by TargetScan,²⁸² sorting on a total context score less than 0.15 ([available as Additional File 5 at publisher's site](#)).⁴⁰⁰ Target genes were also identified through interrogation of two publicly-available and experimentally-validated databases of molecular interactions with 'strong evidence', to identify 44 miRNA-gene interactions by miRecords and 9 miRNA-gene interactions by miRTarBase^{284, 285} ([available as Additional File 6 at publisher's site](#)).⁴⁰⁰ In all, a total of 1440 putative and validated human miRNA-target gene interactions in EBOV-infected human retinal pigment epithelial cells were identified ([available as Additional File 7 at publisher's site](#)).⁴⁰⁰

Table 5.3: Ebola virus-derived miRNA

Sequencing reads of cDNA derived from EBOV- and mock-infected human retinal pigment epithelial cells were screened against published sequences of putative Ebola virus-derived miRNA constructs. Asterisks identify EBOV miRNA found in EBOV-infected retinal pigment epithelial cells.

Published EBOV-derived miRNA	Sequence	Reads per replicate					
		1-24C	1-24E	2-24C	2-24E	3-24C	3-24E
EBOV-miR-1-3p	GCCACCATAGGACTTTTTCAAT	0	0	0	0	0	0
EBOV-miR-2-3p	TTATCCTTCTTGAATCCTGAGA	0	2	0	1	0	0
*EBOV-miR-T1-3p	TTCTTGAAAGTGGCGCAGTCA	0	2	0	1	0	13
*EBOV-miR-T1-5p	GGACAGTTTCCTTCTCATGCTT	0	1	0	1	0	2
EBOV-miR-T2-3p	TGTTTTTTCATTAACCTTCATC	0	0	0	0	0	0
EBOV-miR-T3-3p	TGTCCGTTCAACAGGGGATTGT	0	0	0	3	0	3
*EBOV-miR-T3-5p/T4-5p	ATCTTGACAGCAGGTCTGTCCG	0	3	0	3	0	2
EBOV-miR-T4-3p	CTGTCCGTTCAACAGGGGGTTG	0	0	0	3	0	3
EBOV-miR-VP-3p	TGCTTCATTAGCACTTTGGGGC	0	0	0	0	0	1
EBOV-miR-1-3p	AGATTAGGCCCAAGAGGCATT	0	0	0	0	0	0
*EBOV-miR-1-5p	ATTAATGCGGAGGTCTGATAAG	0	241	0	573	1	581

Abbreviations: C = control, cDNA = complementary deoxyribonucleic acid, E = *Zaire ebolavirus*; EBOV-miR = Ebolavirus micro ribonucleic acid.

5.2.4 Pathway analysis of gene targets of microRNA

Further analysis was undertaken to understand the effects of the 15 differentially expressed miRNA produced in human retinal pigment epithelial cells in response to infection with EBOV. The open-source bioinformatics platform Cytoscape (v.3.4.0) with the ClueGO (v.2.3.3) plugin^{287, 288} was used to explore biological pathways involving the set of miRNA-gene target pairs in EBOV-infected human retinal pigment epithelial cells. Highly enriched gene ontology (GO) categories^{286, 405} and Kyoto Encyclopedia of Genes and Genomes (KEGG)²⁸⁹ pathways were established for the target genes, based on numbers of genes represented within categories and pathways, and ranking of corrected p-values. A total of 223 pathways, including 179 molecular processes, 22 molecular functions and 22 KEGG categories, were enriched by the putative gene targets of differentially expressed miRNA, which were correlated with differential expression of mRNA from RNASeq analysis of the large RNA dataset.²³⁵ These pathways included regulation of cell signalling, phosphorylation, transcription, and protein modification, all of which are known to be involved in viral infection. The top biological processes, molecular functions and KEGG categories are displayed in Figure 5.3 (full list [available as Additional File 8 at publisher's site](#)).⁴⁰⁰

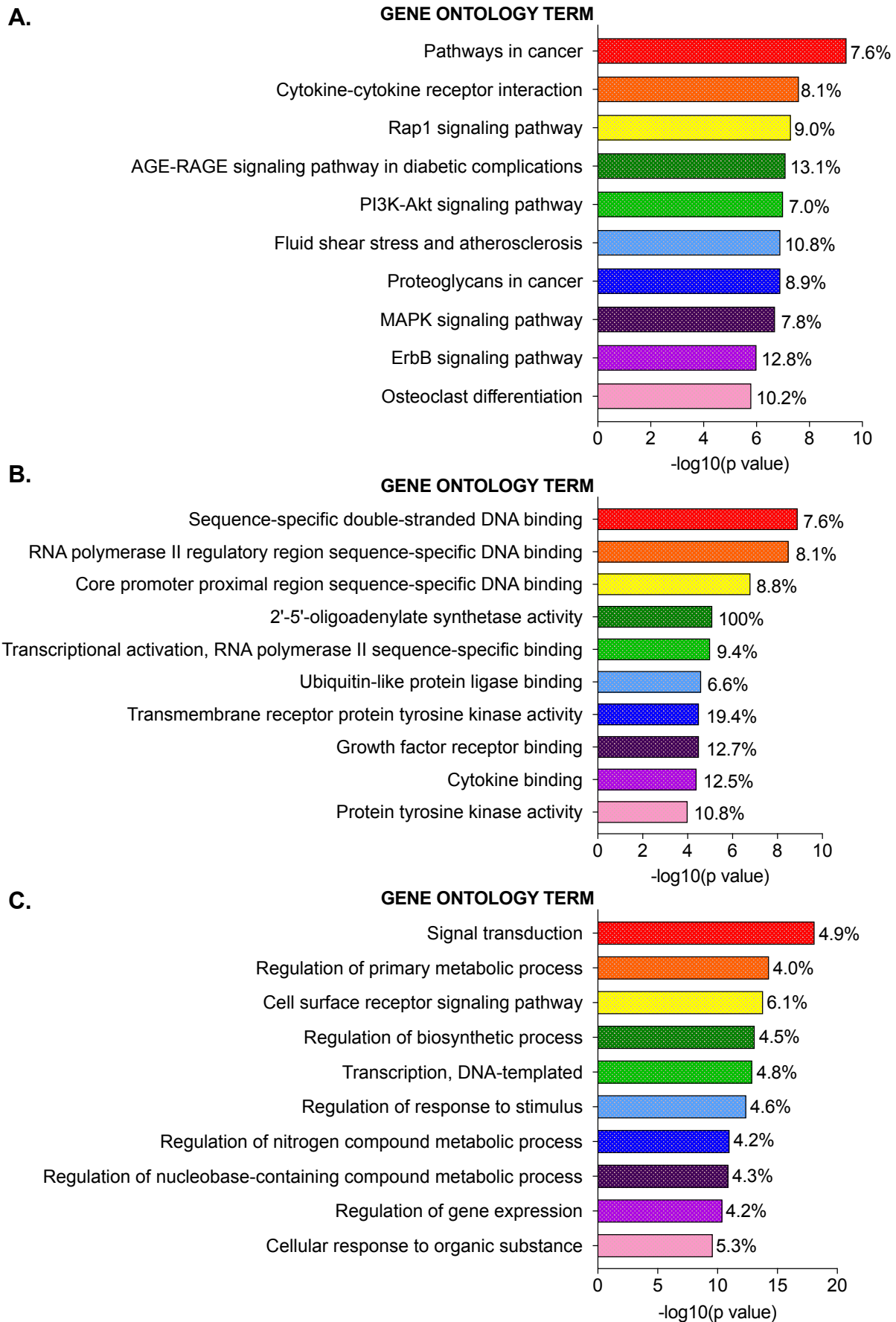
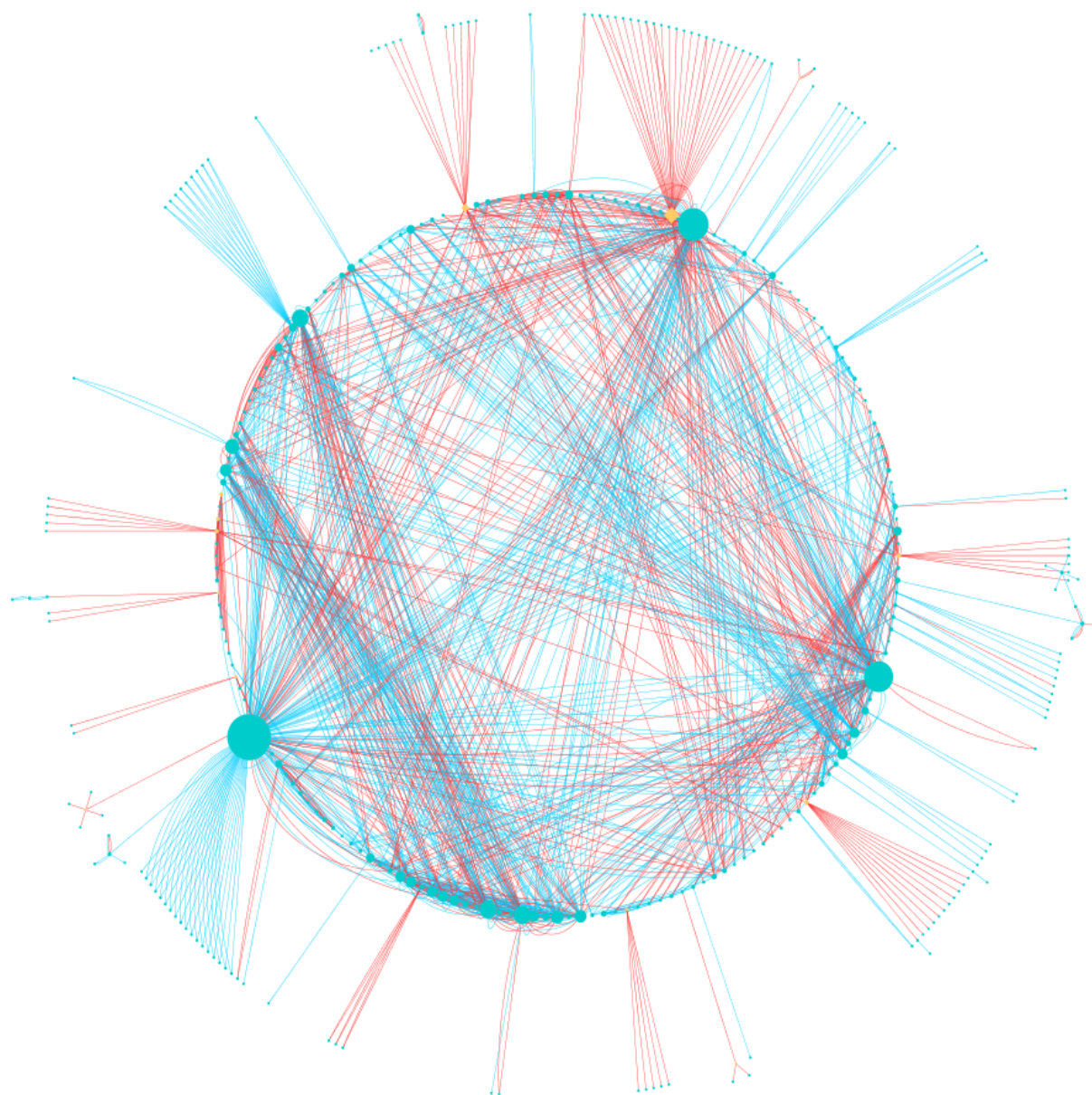


Figure 5.3: Pathway analysis of miRNA gene targets

To understand the effects of the 15 differentially expressed miRNA produced in human retinal pigment epithelial cells in response to infection with EBOV, the open-source bioinformatics platform, Cytoscape (v.3.4.0), was used to explore biological pathways involving the set of miRNA-gene target pairs in EBOV-infected human retinal pigment epithelial cells. Graphs showing enriched gene ontology categories – (A) biological process, (B) molecular function, and (C) KEGG pathways – in ARPE-19 human retinal pigment epithelial cells 24 hours after infection with EBOV. Percentages indicate proportion of known genes represented within the grouping. P-values calculated with Bonferroni adjustment. Figure modified and reprinted with permission under [Creative Commons Attribution 4.0 International License](https://creativecommons.org/licenses/by/4.0/) from Oliver, G.F., Orang, A.V., Appukuttan, B. et al. Expression of microRNA in human retinal pigment epithelial cells following infection with Zaire ebolavirus. BMC Res Notes 12, 639 (2019). <https://doi.org/10.1186/s13104-019-4671-8>. **Abbreviations:** EBOV = *Zaire ebolavirus*; KEGG = Kyoto Encyclopedia of Genes and Genomes, miRNA = micro ribonucleic acid.

5.2.5 Network analysis of miRNA-gene target interactions

In order to identify key molecules involved in EBOV infection of retinal pigment epithelial cells, network analysis of miRNA-gene target interactions was performed. Using the STRING Action dataset (v.9) within the CluePedia plugin (v.1.3.3),^{290, 291} and collating miRNA-gene pairs, a miRNA-based network was constructed from miRNA-predicted gene target lists, miRNA-validated target gene lists, anti-correlated expression patterns, and the differentially-expressed gene list. Interactions were demonstrated based on degree and identified the most highly connected genes and miRNAs. The most highly connected protein-coding genes and miRNA are displayed in graphic form (Figure 5.4) and as a table (Table 5.4). The molecular network constructed from the miRNA-target gene interactions included 363 highly connected molecules; the most connected molecule was LRRK2. The most highly connected miRNA was hsa-miR-190a ([full lists available as Additional Files 9 and 10 at publisher's site](#)).⁴⁰⁰



- molecule
- ◆ miRNA
- enhancement
- suppression

Figure 5.4: Host miRNA-gene target interactions

In order to identify key molecules involved in EBOV infection of retinal pigment epithelial cells, network analysis of miRNA-gene target interactions was performed. Using the STRING Action dataset (v.9) within the CluePedia plugin (v.1.3.3),^{290, 291} and collating miRNA-gene pairs, a miRNA-based network was constructed from miRNA-predicted gene target lists, miRNA-validated target gene lists, anti-correlated expression patterns, and the differentially-expressed gene list. Network of interactions between protein-coding gene targets and host miRNAs in EBOV-infected ARPE-19 human retinal pigment epithelial cells, with miRNAs indicated by yellow diamonds, molecules indicated by blue circles, and interactions that are promoting or inhibiting represented as blue or red lines, respectively. Size of circle or diamond is proportionate to the number of molecular interactions (degrees). Data is presented as a list in Table 5.4. Figure modified and reprinted with permission under [Creative Commons Attribution 4.0 International License](#) from Oliver, G.F., Orang, A.V., Appukuttan, B. et al. Expression of microRNA in human retinal pigment epithelial cells following infection with Zaire ebolavirus. BMC Res Notes 12, 639 (2019). <https://doi.org/10.1186/s13104-019-4671-8>. **Abbreviations:** EBOV = *Zaire ebolavirus*; miRNA = micro ribonucleic acid.

Table 5.4: Network connections

List of highly-connected protein-coding gene targets and miRNAs in EBOV-infected human retinal pigment epithelial cells. Data presented graphically in Figure 5.4.

Gene or miRNA	Description	Interactions
LRRK2	Leucine-rich repeat kinase 2	181
MAPK13	Mitogen-activated protein kinase 13	125
MAPK7	Mitogen- activated protein kinase 7	117
PRKCE	Protein kinase C epsilon	66
PRKCH	Protein kinase C eta	64
SGK494	Serum and glucocorticoid-inducible kinase 494	64
RND3	Rho family GTPase 3	52
DIRAS3	DIRAS family GTPase 3	44
RASD2	RASD family member 2	43
RASL11B	RAS like family 11 member B	43
PDGFRB	platelet derived growth factor receptor beta	37
ARHGEF3	Rho guanine nucleotide exchange factor 3	36
IQGAP2	IQ motif containing GTPase activating protein 2	36
ARL14	ADP ribosylation factor like GTPase 14	35
hsa-miR-190a	Human microRNA	58
hsa-miR-29b-3p	Human microRNA	25
hsa-miR-130a-5p	Human microRNA	17
hsa-miR-32-5p	Human microRNA	16
hsa-miR-33a-5p	Human microRNA	12
hsa-miR-33b-5p	Human microRNA	11

Gene or miRNA	Description	Interactions
hsa-miR-7-5p	Human microRNA	11
hsa-miR-33b-3p	Human microRNA	7
hsa-miR-1305	Human microRNA	6
hsa-miR-100-3p	Human microRNA	5
hsa-miR-19a-5p	Human microRNA	5
hsa-miR-101-5p	Human microRNA	4
hsa-miR-27b-5p	Human microRNA	3
hsa-miR-365a-5p	Human microRNA	1
hsa-miR-4521	Human microRNA	1

Abbreviations: miRNA = micro ribonucleic acid, EBOV = *Zaire ebolavirus*, has-miR = *homo sapiens* microRNA,

5.3 DISCUSSION

Zaire ebolavirus is a negative-sense RNA virus that is associated with uveitis and retinal pigment epithelial scarring in survivors of EVD.^{245, 247} This work identified human miRNAs produced in EBOV-infected retinal pigment epithelial cells, and computationally predicted associated gene targets, molecular interactions and biological processes that were concordant with gene transcript expression from the RNASeq dataset of the same infection. Viruses are known to manipulate the expression of host miRNAs in order to modify the cell phenotype and create an environment that supports viral replication.⁴⁰⁶ Human retinal pigment epithelial cells have been shown to make multiple molecular adjustments in response to infection with EBOV,²³⁵ and network analysis in the current work shows that miR-190a is central to this response. This highly-connected miRNA contributes to cell survival and latency in Epstein-Barr virus (EBV) infection by downregulating expression of tumour protein p53 inducible nuclear protein 1 and nuclear receptor subfamily 4 group A member 3 to prevent cell cycle arrest and apoptosis.⁴⁰⁷ A similar mechanism may be utilized by EBOV to contribute to latency within infected retinal pigment epithelial cells. Another highly-interacting miRNA found in the current work – miR-101 – prevents cell death in the context of herpes simplex virus type 1 infection,⁴⁰⁸ again pointing to the common strategy of viruses to promote survival and prolong the life of the host cell, which may contribute to the eye as a latent reservoir.

Another highly-connected miRNA in our analysis was miR-29b3p, which suppresses key immunological pathways by downregulating nuclear factor kappa-light-chain-enhancer of activated B cells (NF- κ B).⁴⁰⁹ This transcription factor plays an essential role in the antiviral type I IFN response. Multiple receptors – including TLRs and RIG-I – stimulate

NF- κ B, which activates transcription of IFN- β and IFN-stimulated genes. *Zaire ebolavirus* is known to profoundly inhibit the type I IFN response in monocytes and other cell populations through the action of two viral proteins – VP24 and VP35 – and suppression of RIG-I signalling.²⁵⁰ Prior work has demonstrated that EBOV-infected retinal pigment epithelial cells mount a type I IFN response;²³⁵ curiously, EBOV also may suppress this pathway through activation of miR-29b-3p. Other viruses use similar methods: the NF- κ B pathway is not activated in human retinal pigment epithelial cells infected with cytomegalovirus.⁴¹⁰ MicroRNA-29b is also activated in Japanese encephalitis virus infection, particularly in persons with neurological sequelae, and elevated serum levels may indicate severe disease.⁴¹¹

This work demonstrated that the molecule central to the miRNA-mediated response to EBOV infection is LRRK2, a ubiquitously-expressed kinase involved in wide-ranging cellular functions, including signal transduction pathways and direct protein interactions.⁴¹² Much interest was generated in this molecule due to its association with Parkinson's disease⁴¹³ and CNS inflammation,⁴¹⁴ but LRRK2 dysfunction is also implicated in other immune diseases, including systemic lupus erythematosus, Crohn's disease and inflammatory bowel disease.⁴¹² Evidence for involvement in cellular innate immunity is increasing, and LRRK2 has been shown to participate in pattern recognition of bacteria, phagocytosis regulation, and *Mycoplasma tuberculosis* control.⁴¹⁵

The role of LRRK2 in ocular inflammation has also been investigated. Researchers demonstrated that LRRK2-knockout mice had lower levels of experimental autoimmune uveitis,⁴¹⁶ and in another study of neurodegeneration, double-knockout-LRRK2 mice developed cataracts and died earlier.⁴¹⁷ It has also been shown that LRRK2 is a key regulator of the lysosomal system, and LRRK2 mutations result in the formation of large,

dysfunctional lysosomes.⁴¹⁸ Further research into the role of LRRK2 in EBOV infection of the eye may yield interesting results. After entering the host cell, EBOV utilizes endolysosomal trafficking to move through the cytoplasm, where it evades the immune system.⁴¹⁹ Two ocular complications strongly associated with EVD survivors are cataract and uveitis, and understanding the molecular mechanisms of LRRK2 in the pathogenesis of these sequelae may provide opportunities for therapeutic intervention. The next step could be to measure the effect of LRRK2 on EBOV replication in primary retinal pigment epithelial and iris pigment epithelial cell isolates from the same donors.

Network analysis of retinal pigment epithelial cells demonstrated the mitogen-activated protein kinases (MAPK) 13 and 7 were also highly involved in EBOV infection. These kinases have broad cellular functions. Investigators have reported that MAPK13 is a critical mediator of osteogenic differentiation of bone marrow-derived mesenchymal stem cells, and is directly inhibited by miR 23a-5p, which was not a miRNA identified as significantly involved in pathways in this work.⁴²⁰ In oncology research, MAPK13 has been shown to be involved in tumour initiation in a range of solid tumours, and is preferentially expressed in gynaecological cancer stem cells.⁴²¹ A number of studies implicate MAPK13 in cellular inflammatory pathways. In primary human keratinocytes⁴²² and microglia,⁴⁰¹ MAPK13 is associated with IL-1 β -induced inflammation. Further evidence for an association of MAPK13 with neuroinflammation was suggested in a bioinformatic study of retinal gene expression in a rat model of diabetic retinopathy.⁴²³ Interrogation of the role of MAPK13 in EBOV infection of human retinal pigment epithelial cells could involve gene knockdown of EBOV-infected and uninfected cells using small interfering RNA.

Mitogen-activated protein kinase 7, known also as extracellular signal-regulated kinase 5 (ERK5), is both a protein kinase and transcription factor that promotes acute cellular and systemic inflammation. In vascular endothelial cells and monocytes, MAPK7 promoted inflammation that was induced by broad stimuli, including TLR agonists and pro-inflammatory cytokines, such as TNF- α .⁴²⁴ The work in this chapter implicated MAPK7 as another key component of the cellular response to EBOV infection. Florid uveitis is a characteristic of clinical disease in EVD survivors, and destructive sequelae include retinal scars and white cataract, which are associated with visual impairment.³⁴ Small molecule MAPK7 kinase inhibitors have been developed for cancer therapeutics, and a recent inhibitor has been developed that blocks both kinase and non-kinase functions.⁴²⁵ Similar to MAPK13, gene knockdown experiments could be performed on retinal pigment epithelial cells and other ocular cell populations, with a view to better understanding the role of these kinases in EBOV infection retinal pigment epithelial cells.

Bioinformatics is an interdisciplinary field of science that develops software and tools to better understand biology. The field of sRNA-Seq is still being developed, and because of its inherent complexity, there are many sources of potential bias and error.⁴⁰⁴ A fundamental challenge of sRNA-Seq lies in the fact that in a biological system, the small 6-8 nt seed sequence of a given miRNA does not need to dock to its target with perfect complementarity. This means that one seed sequence could have many thousands of potential gene targets, and computational predictions may generate misleading results that must be interpreted with caution and validated experimentally.⁴²⁶ Therefore, the results presented in this work require further experimental validation, but provide direction for future studies.

Virus-infected cells may release extracellular vesicles containing host- and virus-derived miRNAs that modulate gene expression in uninfected neighbouring cells.⁴²⁷ In EBOV infection, secreted vesicles containing VP40 have been shown to stimulate apoptosis in uninfected monocytes and T cells, illustrating the intricate ways in which EBOV evades the immune system.⁴²⁸ Components of EBOV-associated extracellular vesicles also include viral NP protein, which strongly associates with both viral and host RNA.⁴²⁹ Whether miRNAs are found in EBOV-infected extracellular vesicles, and whether EBOV-infected retinal pigment epithelial cells release extracellular vesicles, is unstudied but plausible. Previous research has demonstrated that healthy human RPE secretes extracellular vesicles from both apical and basolateral aspects of the polarised cells,⁴³⁰ and retinal pigment epithelial cells under stress increase the release of these vesicles.⁴³¹ In the normal state, retinal pigment epithelial vesicles are likely involved in intercellular communication and lipid metabolism, and contain proteins, miRNAs and other nucleic acids.⁴³² The sRNA-Seq data in this work indicates that hsa-miR-27b-5p and hsa-miR-3074-3p are expressed at reduced levels in EBOV-infected human retinal pigment epithelial cells. Both of these miRNAs have been detected in next generation RNA sequencing of aqueous humour of healthy human eyes at levels higher than found in plasma, indicating local production.⁴³³ One cause of reduced expression of these miRNAs within retinal pigment epithelial cells could be active export from the RPE, and this could be investigated firstly by extracting miRNA from cell culture supernatant to determine the presence of these miRNAs.

While it was generally agreed that RNA viruses do not typically encode their own miRNA,⁴⁰⁶ this has become an increasingly contentious topic.⁴³⁴ In this work, analysis of EBOV-infected retinal pigment epithelial cells identified an EBOV-derived miRNA-like

structure, EBOV-miR-1-5p, which has also been described by several other investigator teams.^{276, 435} This virus-derived miRNA is an ortholog of the human miR-155, which is known to inhibit the expression of importin- α 5 and type I IFN signalling,⁴³⁶ and thus confer advantage to an infecting virus. Human miR-155 is also pro-inflammatory, and is upregulated in DENV infection.⁴³⁷ Molecular mimicry of human miR-155 has been demonstrated in other viral infections. The homologue kshv-miR-K12-11, identified in Kaposi's sarcoma-associated herpesvirus-infected B-cells, drives the cell to a state that avoids apoptosis and supports long-term viral latency.⁴³⁸ In the current work, several other EBOV-derived miRNAs were identified, but with very low read counts, suggesting reads were either spurious or had negligible biological activity. These data support the presence of EBOV-derived miRNA molecules, as also reported by other investigators,^{435, 436, 439, 440} but their function remains the subject of speculation. Recent work elegantly demonstrated that in EBOV infection of a human hepatocarcinoma-derived cell line (HepG2), mature EBOV-derived miRNA constructs are generated independent of the host endoribonuclease Dicer and the Argonaute component of the RNA-induced silencing complex (RISC).⁴⁴¹ Given this curious lack of association with host canonical miRNA machinery, the authors posited that EBOV-derived miRNA constructs might simply be "spandrels", or breakdown products of viral messenger RNA.

While this work has identified a pattern of miRNA expression in EBOV-infected human retinal pigment epithelial cells, it is unknown whether these changes would be seen in other ocular tissue types, or tissue from other immune-privileged sites such as the testes. Normal miRNA expression varies by tissue type,⁴⁴² and between ocular cell types,⁴⁴³ and thus the miRNA changes demonstrated with EBOV infection in retinal pigment epithelial cells may not be universal. This work studied EBOV infection in the ARPE-19 human

retinal pigment epithelial cell line, which is a well-characterized, robust model for studying RPE.²³⁵ While the findings of this work should provide some fidelity to an ocular infection in an EVD survivor, these human retinal pigment epithelial cells were studied in isolation, yet the intraocular environment includes multiple cell populations. However, this approach enables the study of gene expression in a key intraocular target cell for EBOV. The expression of miRNA was evaluated at one time-point post-infection. This time-point was selected as a previously published study demonstrated maximally-informative host cell responses to EBOV infection.²⁶²

This work provides new information about the potential post-transcriptional regulation of the human retinal pigment epithelial cell response to infection with EBOV. Key miRNAs in EBOV-infected retinal pigment epithelial cells were identified using sRNA-Seq, and through *in silico* analysis, multiple molecules that may be regulated in the retinal pigment epithelial response to infection were identified. Review of the biological targets of the 15 highly-induced or repressed miRNAs indicate a broad range of potential regulatory activities, including effects on innate and adaptive immune responses, cellular metabolism, cell cycle progression, apoptosis and autophagy in the host cells. Central to the response to EBOV infection, miR-190a and miR-101 may facilitate EBOV survival in RPE through prevention of apoptosis. Key molecules identified in the miRNA-driven response of retinal pigment epithelial cells – LRRK, MAPK13 and MAPK7 – are kinases known for their role in neuroinflammation.

Future experiments could identify the effect of knock-down of key components of the miRNA-driven molecular response to EBOV infection, with a view to identifying critical components of pathological pathways. Replication of these results in primary human retinal pigment epithelial cells, and at different time points post-infection would provide

a clearer picture of the response of the RPE to EBOV infection, and the mechanisms of latency within the eye in EVD survivors. Further molecular studies could be directed by initial experiments comparing EBOV infection with the non-pathogenic *Reston ebolavirus* strain, and co-culture of RPE with other components of the BRB, such as Müller cells. Development of a model of EBOV-associated uveitis would ultimately provide a platform by which to study therapeutic interventions that prevent blinding sequelae of EBOV infection.

CHAPTER 6

Ebola viral protein 35 and the type I interferon response in human retinal pigment epithelial cells

6.1	Introduction	213
6.2	Results.....	214
6.2.1	Restriction digest-based plasmid subcloning	214
6.2.2	Confirmation of plasmid structure	220
6.2.3	Confirmation of plasmid protein expression	220
6.2.4	Interferon- β expression in retinal pigment epithelial cells after treatment with Poly I:C .	221
6.2.4.1	<i>Primary human retinal pigment epithelial cell isolates</i>	224
6.2.5	Impact of Ebola protein 35 on interferon- β expression in retinal pigment epithelial cells	228
6.3	Discussion.....	236

6.1 INTRODUCTION

Those who survive EVD often suffer long-term sequelae and viral persistence at immune-privileged sites such as the eye. A hallmark of many *Ebolaviruses* is the ability to silence the type I IFN response, achieved largely through the actions of VP24 and VP35, which block IFN signalling and production, respectively.⁴⁴⁴⁻⁴⁵⁰ Previous research has demonstrated that EBOV-infected human RPE mounts a type I interferon (IFN) anti-viral response while maintaining immunomodulatory activity.²³⁵ Despite the upregulation of cellular antiviral pathways, EBOV replicated to high levels in infected ARPE-19 cells, indicating that the RPE may act as a reservoir for EBOV in the eye.

The VP35 protein has three main functions. It forms part of the viral replication and transcription enzyme complex,⁴⁵¹ facilitates viral particle assembly, and is a powerful inhibitor of type I IFN production.⁴⁴⁶ To antagonize the type I IFN system, VP35 works from the top of the signalling cascade to inhibit interactions at multiple junctures: by sequestering and disguising dsRNA from pattern recognition receptors,^{447, 452-454} by interacting with protein activator of the IFN-induced protein kinase (PACT), a protein that binds dsRNA and activates pattern recognition receptors,^{448, 450} and by inhibiting the phosphorylation and nuclear translocation of transcription factors (interferon regulatory factors 3 and 7 [IRF-3, IRF-7], and mitochondrial antiviral signalling protein, MAVS),^{446, 455} thus suppressing activation of the IFN- β promoter. The VP24 protein also contributes to EBOV virulence by interacting in a step common to both IFN- α/β and IFN- γ cascades, in which it inhibits karyopherin- α , an importin that transports phosphorylated signal transducer and activator of transcription (STAT)1 into the nucleus, consequently blocking transcriptional activation of IFN-stimulated genes.^{456, 457}

The role of the RPE in EBOV infection is incompletely understood. Researchers demonstrated that the human ARPE-19 cell line supported productive EBOV infection, and bioinformatic analysis of the host transcriptome of these infected cells implicated a strong type I IFN response.²³⁵ The fact that infected retinal pigment epithelial cells still produced IFN- β despite EBOV infection was unexpected, given profound IFN- β suppression observed in other infected cell populations such as dendritic cells⁴⁵⁸ and mononuclear phagocytes.²³⁶ The work presented in this chapter aimed to further investigate the type I IFN response of the retinal pigment epithelial cell to EBOV infection by focusing on the inhibitory action of VP35 on IFN- β production. In order to isolate the effect of VP35, a vector expressing VP35 was sub-cloned for transfection into human retinal pigment epithelial cells. The retinal pigment epithelial cell response to VP35 was measured by expression of IFN- β , the key cytokine of the type I IFN response. Additionally, in order to more closely model human disease, primary human retinal pigment epithelial isolates were used, in addition to the ARPE-19 cell line.

6.2 RESULTS

6.2.1 Restriction digest-based plasmid subcloning

In order to investigate retinal pigment epithelial cellular responses to VP35, a pCAGGS VP35 expression plasmid was produced using restriction digest-based subcloning (Figure 6.1). To create a control plasmid vector without an EBOV sequence insert (Fig. 6.1D), a double-digest using restriction enzymes XbaI and NheI was performed on a pCAGGS-FLAG-VP40 plasmid that was available in-house (Fig. 6.1A) to remove FLAG-VP40 sequence (Fig. 6.1C). Complementary ends of the purified pCAGGS vector backbone

(Fig. 6.1B) were ligated. This plasmid was transformed into competent *E. coli*, amplified in ampicillin-enriched broth and purified.

Taking advantage of presence of the FLAG sequence in the pCAGGS backbone, a pCAGGS-FLAG-VP35 plasmid (Fig. 6.1H) was generated by inserting the VP35 sequence into the pCAGGS-FLAG vector. First, VP35 was amplified from its pCAGGS vector (Fig. 6.1E) using ligation-mediated PCR with linker primers encoding NotI and NheI restriction sites. The purified gel product was digested with NotI and NheI restriction enzymes to create cohesive ends. The VP40 gene insert was excised from the pCAGGS-FLAG-VP40 vector (Fig. 6.1A) using the restriction enzymes NotI and NheI. Purified pCAGGS-FLAG vector (Fig. 6.1F), and the VP35 gene insert (Fig. 6.1G) were ligated (Fig. 6.1H) and transformed into competent *E. coli* cells in ampicillin-enriched broth. After amplification, plasmid DNA was extracted and purified. Figure 6.2 shows agarose gel photographs of electrophoresis products used to construct the plasmids.

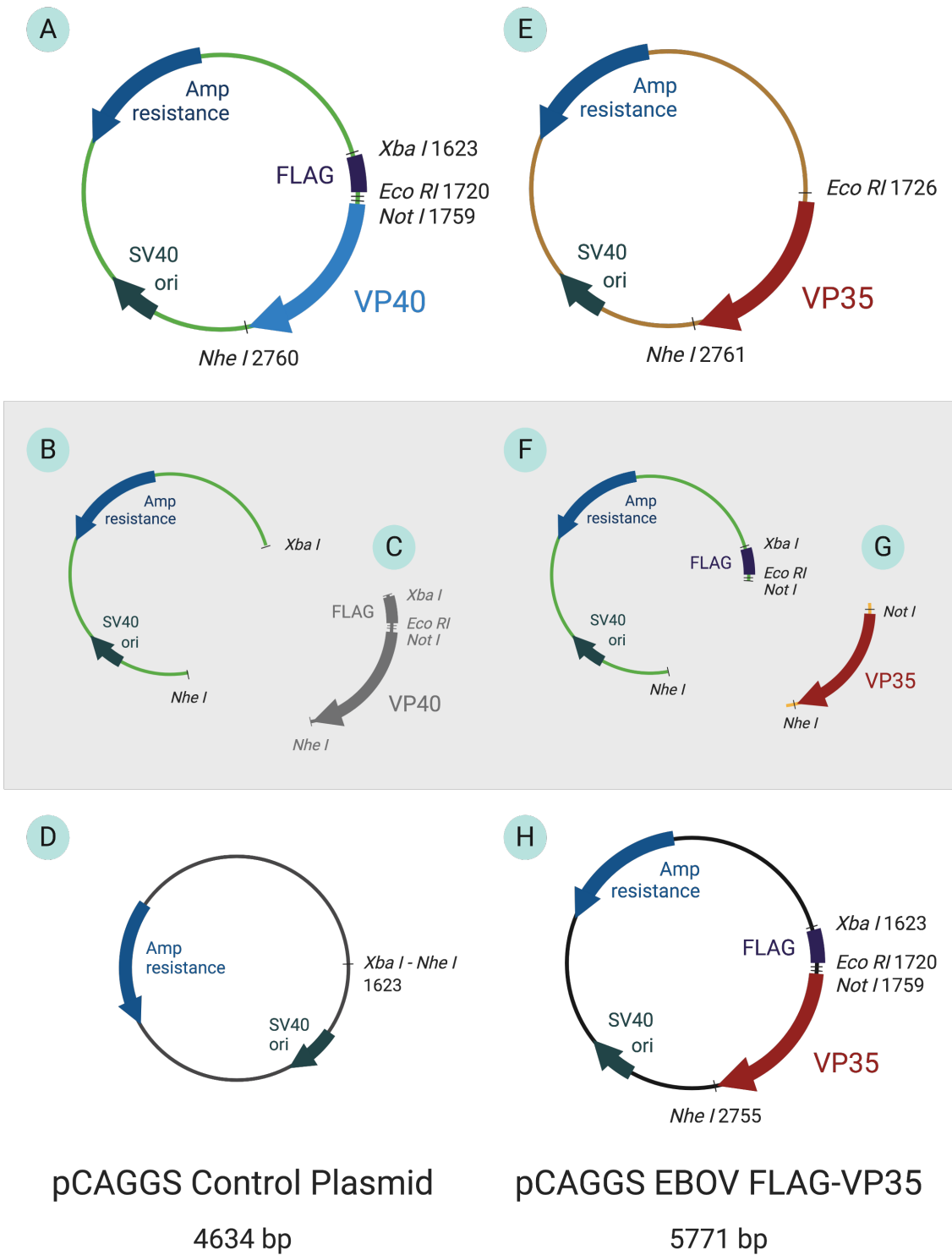


Figure 6.1: Construction of the pCAGGS-VP35 expression plasmid

In order to investigate retinal pigment epithelial cellular responses to VP35, a pCAGGS VP35 expression plasmid was produced using restriction digest-based subcloning. Vector products were generated by restriction digest-based subcloning to construct a plasmid expressing VP35 and FLAG, and a plasmid consisting of backbone alone. (A). Restriction enzymes XbaI and NheI were used to separate the pCAGGS backbone (B) from the FLAG-VP40 sequence insert (C). The sticky ends of pCAGGS were ligated to form a pCAGGS plasmid without an EBOV sequence insert (D). The pCAGGS-FLAG-VP40 plasmid (A) was cleaved at NotI and NheI sites, and the pCAGGS-VP35 vector (E) was amplified with ligation-mediated PCR to add the NotI restriction site. (F) pCAGGS backbone with FLAG® tag and VP35 with NotI site (G) were ligated to form pCAGGS FLAG-VP35 vector (H). Restriction enzyme sites in italics. Figure created in BioRender.com.

Abbreviations: Amp = ampicillin; bp = base pairs, EBOV = *Zaire ebolavirus*, SV40 ori = Simian Virus 40 origin of replication, VP = viral protein.

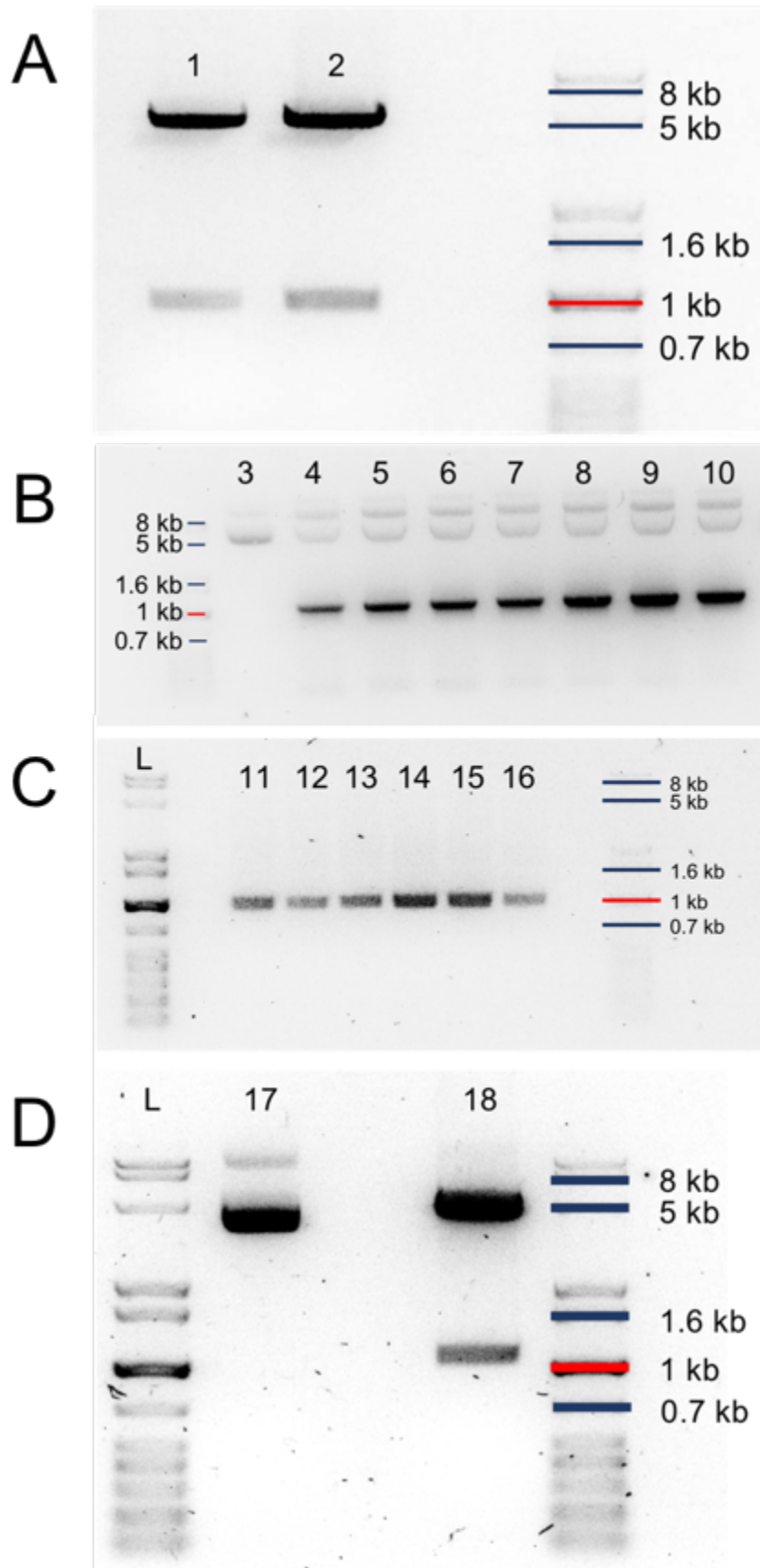


Figure 6.2: Sub-cloning DNA products

In order to investigate retinal pigment epithelial cellular responses to VP35, a pCAGGS VP35 expression plasmid was produced. Products were generated by restriction digest-based subcloning to construct a plasmid expressing VP35 and FLAG, and a plasmid consisting of backbone alone. UV-filtered photographs of 1% agarose gel, after electrophoresis of DNA products used to construct pCAGGS-FLAG-VP35 plasmid (A-C), and pCAGGS control plasmid without EBOV sequence insert (D). (A). Restriction endonucleases NotI and NheI were used to separate the 1001 bp VP40 gene insert from the 4738 bp pCAGGS-FLAG backbone (lanes 1 and 2). (B). Lane 3 shows neat pCAGGS-VP35 plasmid, and lanes 4 to 10 show ligation-mediated PCR products generated by touchdown PCR (annealing temperatures 58 to 68 °C) of VP35 gene with linker primers with expected product size of 1050 bp. Double bands at top of wells represent open circular (above) and supercoiled (below) plasmid conformations. (C). Purified VP35 product from (B) was digested with restriction endonucleases NotI and NheI to generate sticky ends (lanes 11 – 16) before ligation with 4738 bp pCAGGS-FLAG backbone generated in (A). (D). No-insert pCAGGS plasmid was generated by digesting neat pCAGGS-FLAG-VP40 plasmid (lane 17) with restriction endonucleases XbaI and NheI (lane 18) to generate a 4602 bp pCAGGS backbone and a 1137 bp FLAG-VP40 insert. The pCAGGS backbone was then ligated to form the pCAGGS control plasmid without EBOV sequence insert. Double bands at top of lane 17 represent open circular (above) and supercoiled (below) plasmid conformations. **Abbreviations:** bp = base pairs, DNA = deoxyribonucleic acid, EBOV = *Zaire ebolavirus*, L = ladder indicating molecular weight of DNA (GelPilot 1 kb Plus Ladder, Qiagen, cat. 239095), UV = ultraviolet, VP = viral protein.

6.2.2 Confirmation of plasmid structure

To check that the control pCAGGS vector did not contain the FLAG[®] tag or VP40 sequence, primers flanking the XbaI – NheI ligation site were designed, and PCR with gel purification yielded the expected product size, confirming successful excision of FLAG-VP40 insert. Sequencing of the region surrounding the XbaI and NheI sites was also performed as confirmation. To check the structure of the pCAGGS-FLAG-VP35 plasmid clone, single and double digests using restriction enzymes EcoRI and NheI were performed, and agarose gel electrophoresis demonstrated expected 1100 bp and 4600 bp fragments, confirming single copies of vector backbone and VP35 gene insert. This was corroborated by sequencing of the plasmid (Appendix G).

6.2.3 Confirmation of plasmid protein expression

To confirm plasmid expression of the VP35 and FLAG[®] tag protein products, chemiluminescent Western blot analysis was performed (Figure 6.3). Confluent monolayers of ARPE-19 cells were lipid-transfected with either pCAGGS plasmid without insert, pCAGGS-FLAG-VP35 or pCAGGS-FLAG-VP40. After 48 hours, total cell lysate was collected. Western blot detected FLAG[®] protein in lysate taken from cells transfected with pCAGGS-FLAG-VP35 or pCAGGS-FLAG-VP40, but not cells transfected with pCAGGS without insert, and VP35 protein in pCAGGS-FLAG-VP35 transfected cells, but not in pCAGGS-FLAG-VP40 or pCAGGS without insert. Additional bands seen in single lanes on the western blot of cell lysate with anti-VP35 antibody (Figure 6.3B) could represent

artefactual oligomerization of highly-concentrated VP35,⁴⁵⁹ but this was not pursued as the experiment had already confirmed the presence of VP35 protein.

6.2.4 Interferon- β expression in retinal pigment epithelial cells after treatment with Poly I:C

Polyriboinosinic:polyribocytidylic acid (Poly I:C) is a synthetic dsRNA molecule that potently stimulates TLR 3, RIG-I, and MDA5, pattern recognition receptors that initiate signalling pathways as part of the type I IFN response.^{460, 461} To determine (a) the kinetics of IFN- β production in human retinal pigment epithelial cells after administration of Poly I:C, and (b) whether lipid transfection was required for Poly I:C transfection in retinal pigment epithelial cells, confluent monolayers of ARPE-19 cells were treated with rhodamine fluorophore-conjugated Poly I:C, with and without Lipofectamine® 2000 transfection, or were left untreated, with 6 monolayers per condition. At 1 hour and 4 hours post-treatment, images were captured, and RNA was extracted from the cells. Expression of IFN- β transcript by RT-qPCR was measured to determine the optimal time point for harvesting cells in subsequent experiments.

Photomicrographs are displayed in Figure 6.4, and demonstrate Poly I:C-associated rhodamine fluorescence in cells subjected to lipid transfection at 4 hours. Minimal fluorescence was seen in Poly I:C and Lipofectamine® 2000-transfected cells at 1 hour, and in cells treated with Poly I:C alone after 4 hours.

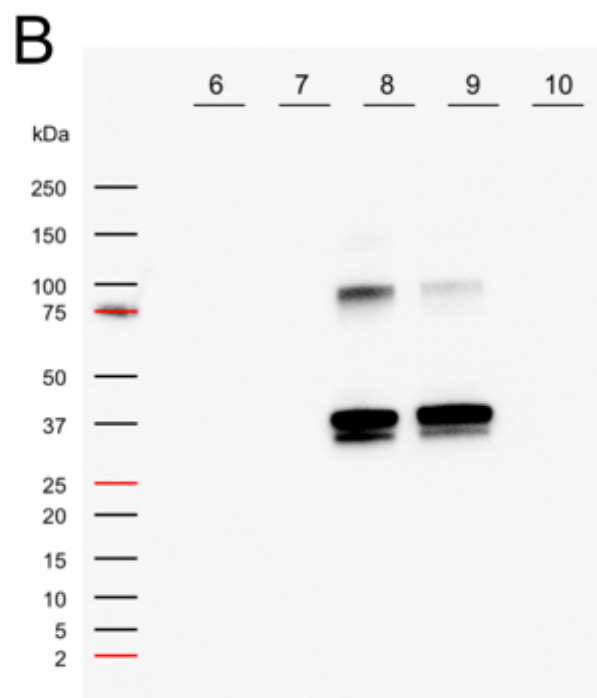
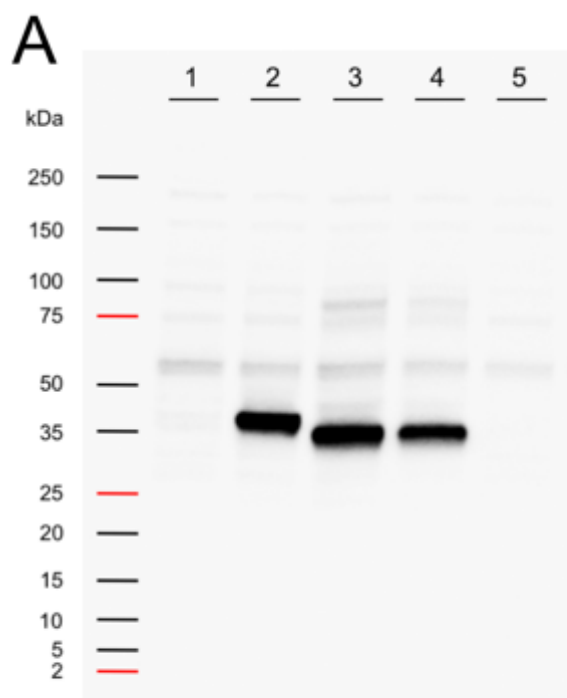


Figure 6.3: Western blots of protein lysate from transfected ARPE-19 cells

To confirm plasmid expression of the VP35 and FLAG® tag protein products, chemiluminescent Western blot analysis was performed. Confluent monolayers of ARPE-19 cells were lipid-transfected with plasmids and 48 hours later total cell protein was collected and quantified. Each well was loaded with 20 µg cell lysate. (A). Detection with mouse anti-FLAG antibody, and secondary anti-mouse immunoglobulin conjugated to horseradish peroxidase; (1) untransfected negative control, and cells transfected with (2) pCAGGS-FLAG-VP40 vector (expected product size 40 kDa), (3) and (4) cloned pCAGGS-FLAG-VP35 vectors (expected product size 35 kDa), (5) pCAGGS vector without an EBOV sequence insert. (B). Detection with mouse anti-VP35 and secondary anti-mouse immunoglobulin conjugated to HRP; (6) untransfected negative control, and cells transfected with (7) pCAGGS-FLAG-VP40 vector, (8) and (9) cloned pCAGGS-FLAG-VP35 vectors (expected product size 35 kDa), (10) pCAGGS vector without insert. Ladder indicates molecular weight of protein (Precision Plus Protein™ Dual Xtra Prestained Protein Standards, Bio-Rad, cat. 1610377). **Abbreviations:** Lipo = Lipofectamine, Poly I:C = polyriboinosinic:polyribocytidylic acid, VP = viral protein.

Expression of IFN- β transcripts was significantly elevated in Poly I:C and lipid-transfected cells at 4 hours ($p < 0.0001$, Figure 6.5), confirming that lipid transfection was required for adequate uptake of Poly I:C into retinal pigment epithelial cells, and for an increase in the expression of IFN- β transcript.

6.2.4.1 PRIMARY HUMAN RETINAL PIGMENT EPITHELIAL CELL ISOLATES

Primary retinal pigment epithelial cells were isolated from human eyes of three donors (two male and one female) between 29 and 37 hours after death (Table 6.1).

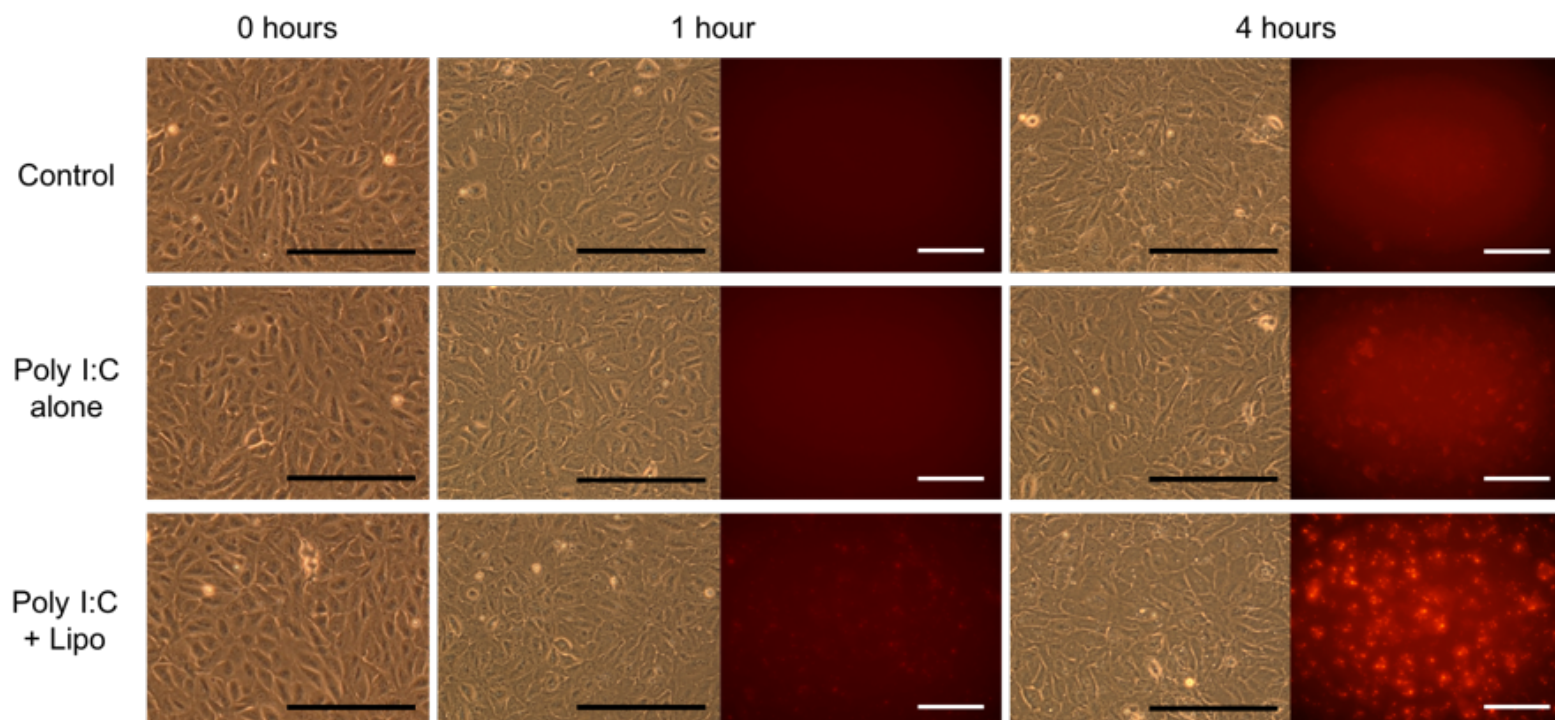


Figure 6.4: Treatment of ARPE-19 cells with Poly I:C

To determine whether lipid transfection was required for Poly I:C transfection in retinal pigment epithelial cells, confluent monolayers of ARPE-19 cells were treated with rhodamine fluorophore-conjugated Poly I:C, with and without Lipofectamine® 2000 transfection, or were left unmanipulated, with 6 monolayers per condition. At 1 and 4 hours post-treatment, brightfield photomicrographs were obtained, and fluorescence of rhodamine-conjugated Poly I:C was identified with a narrow-band excitation filter. No fluorescence was observed at 1 hour in cells treated with Poly I:C and Lipofectamine® 2000, but was strongly present at 4 hours, and after 4 hours some fluorescence could be seen in cells exposed to Poly I:C alone. Scale bars 100 μm . **Abbreviations:** Lipo = Lipofectamine, Poly I:C = polyriboinosinic:polyribocytidylic acid.

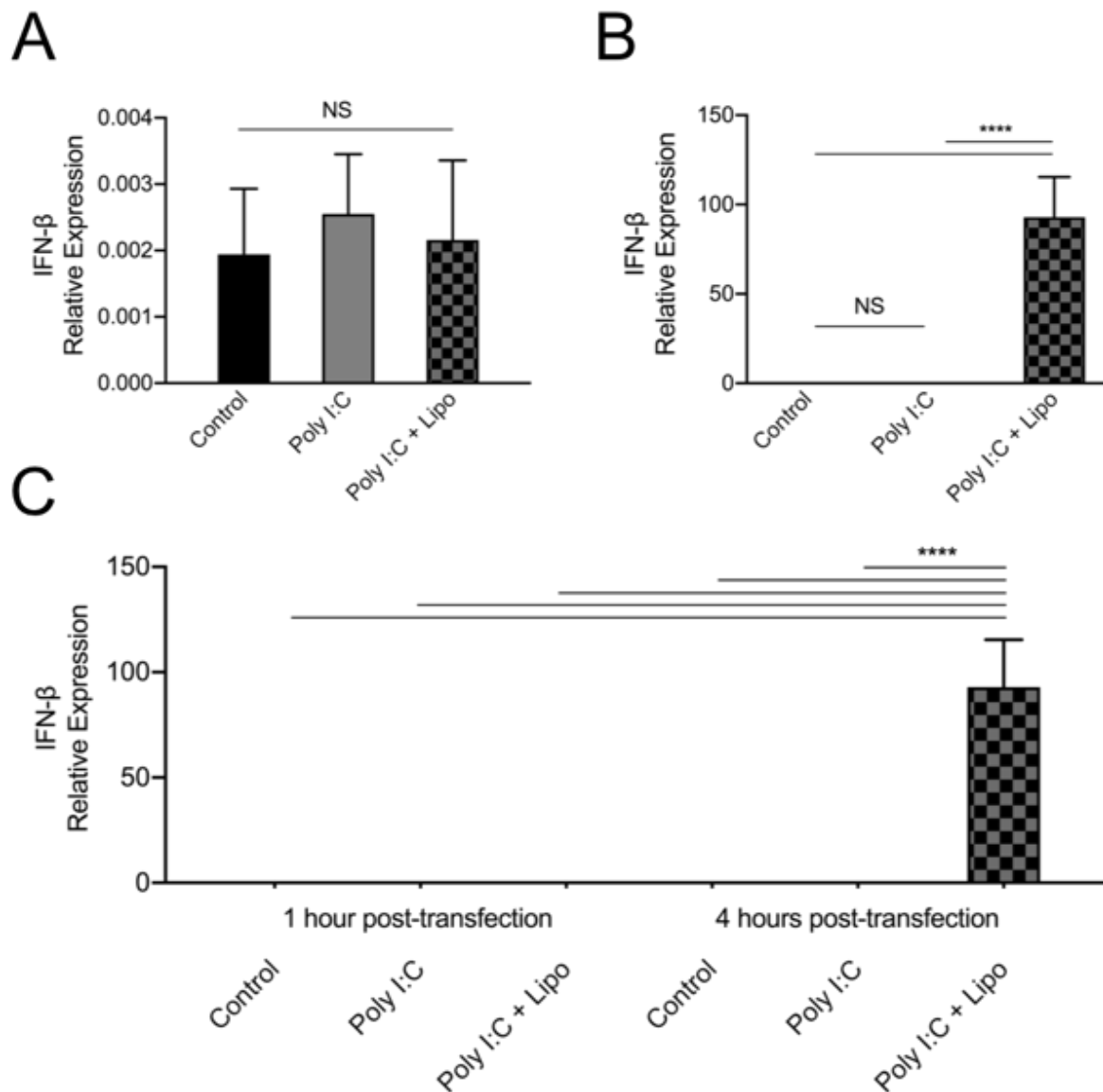


Figure 6.5: Poly I:C-induced IFN- β expression in ARPE-19 cells

To determine the kinetics of expression of IFN- β transcripts in Poly I:C and lipid-transfected cells monolayers of ARPE-19 cells were treated with Poly I:C, lipid-transfected with Poly I:C (Lipo), or left unmanipulated (Control). Expression of IFN- β transcript by RT-qPCR after (A) 1 hour ($p < 0.05$), and (B) 4 hours ($p > 0.0001$). (C). Composite results of (A) and (B) for comparison ($p > 0.0001$). Expression relative to stable reference genes ribosomal protein lateral stalk subunit P0 and β -actin, and over zero in all conditions. Error bars represent standard deviation, $n = 6$ monolayers per condition. Ordinary one-way ANOVA (A and B) and two-way ANOVA (C) with Tukey multiple comparisons test, **** $p < 0.0001$, NS not significant. **Abbreviations:** ANOVA = analysis of variance, IFN = interferon, Lipo = Lipofectamine, Poly I:C = polyriboinosinic:polyribocytidylic acid, RT-qPCR = quantitative reverse transcription polymerase chain reaction, VP35 = viral protein 35.

Table 6.1: Primary human retinal pigment epithelial cell isolates

Cell isolate number	Sex of donor	Age of donor at death	Time from death to cell isolation
Primary isolate 1	Male	50	37 hours
Primary isolate 2	Male	59	29 hours
Primary isolate 3	Female	65	35 hours

6.2.5 Impact of Ebola protein 35 on interferon- β expression in retinal pigment epithelial cells

To investigate the effect of VP35 on the type I IFN response in human retinal pigment epithelial cells, confluent monolayers of three primary human retinal pigment epithelial isolates and the ARPE-19 cell line were exposed to a VP35-encoding vector or a no-insert control pCAGGS vector with lipid transfection. After 48 hours, half the cells were Lipofectamine® 2000-transfected with rhodamine fluorophore-conjugated Poly I:C (n = 3 monolayers per condition). Four hours later, cells were photographed under a narrow band excitation filter, and RNA was extracted for RT-qPCR interrogation of IFN- β transcript expression. Cells stimulated with Poly I:C demonstrated strong fluorescence at 30 minutes and 4 hours after transfection (Figure 6.6). Cytotoxicity was observed under all conditions at 52 hours after plasmid transfection, and one primary isolate (3) demonstrated notably more cell loss, while the ARPE-19 cell line appeared the most resistant to the manipulation (Figure 6.7). These data demonstrated successful lipid transfection of Poly I:C in cells expressing pCAGGS plasmids.

To measure the type I IFN response in retinal pigment epithelial cells expressing VP35 protein, cell monolayers were harvested 4 hours after pattern recognition receptor stimulation with Poly I:C (and 52 hours after plasmid transfection). Cell lysate was collected for RNA extraction and cDNA synthesis, and IFN- β expression was determined by RT-qPCR against stable reference genes, ribosomal protein lateral stalk subunit P0 and β -actin (Figure 6.8). Regardless of which plasmid they were expressing, all cells simulated with Poly I:C showed increased IFN- β expression compared to cells treated with plasmid

alone, with the exception of primary isolate 3 (Figure 6.8C). Compared to no-insert plasmid-transfected cells, Poly I:C-stimulated cells expressing VP35 had lower transcript expression of IFN- β in isolates 1 and 2, while there was no difference between IFN- β expression in isolate 3 or the ARPE-19 cell line. The overall magnitude of IFN- β expression varied across cells, with more expression seen in primary isolate 1 and ARPE-19 cells. Primary isolate 3 had very low levels of IFN- β expression, and also showed the greatest cytotoxicity of all isolates (Figure 6.7). These results demonstrate that VP35 does not significantly reduce expression of IFN- β in the ARPE-19 cell line, which is consistent with published results.²³⁵ In contrast, VP35 antagonized production of IFN- β in primary retinal pigment epithelial cell isolates, with the exception of one primary isolate (3), which showed no difference in IFN- β expression with VP35 expression or Poly I:C stimulation.

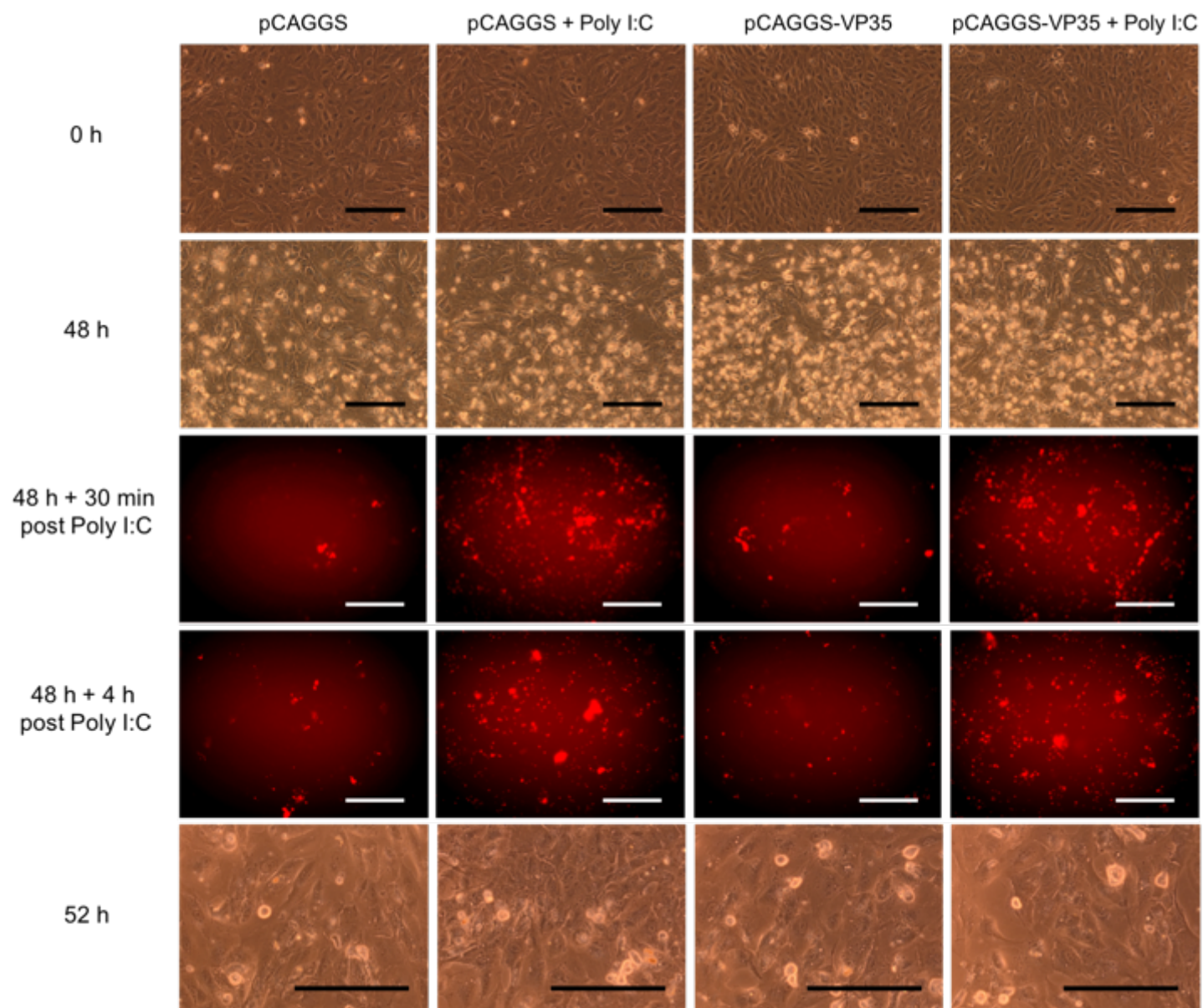


Figure 6.6: Stimulation of VP35-expressing ARPE-19 cells with Poly I:C

To investigate the effect of VP35 on the type I IFN response in human retinal pigment epithelial cells, confluent monolayers of three primary human retinal pigment epithelial isolates and the ARPE-19 cell line were exposed to a VP35-encoding vector or a no-insert control pCAGGS vector with lipid transfection. After 48 hours, half the cells were Lipofectamine® 2000-transfected with rhodamine fluorophore-conjugated Poly I:C (n = 3 monolayers per condition). Four hours later, cells were photographed under a narrow band excitation filter, and RNA was extracted for RT-qPCR interrogation of IFN- β transcript expression. Imaging 30 minutes and 4 hours later demonstrated rhodamine-related fluorescence in Poly I:C-stimulated cells, indicating successful lipid transfection of Poly I:C in cells expressing pCAGGS plasmid. Cell debris representing cytotoxicity is seen in all wells. Images for one representative primary cell isolate are displayed. Scale bars 100 μ m. **Abbreviations:** Poly I:C = polyriboinosinic:polyribocytidylic acid, VP35 = viral protein 35.

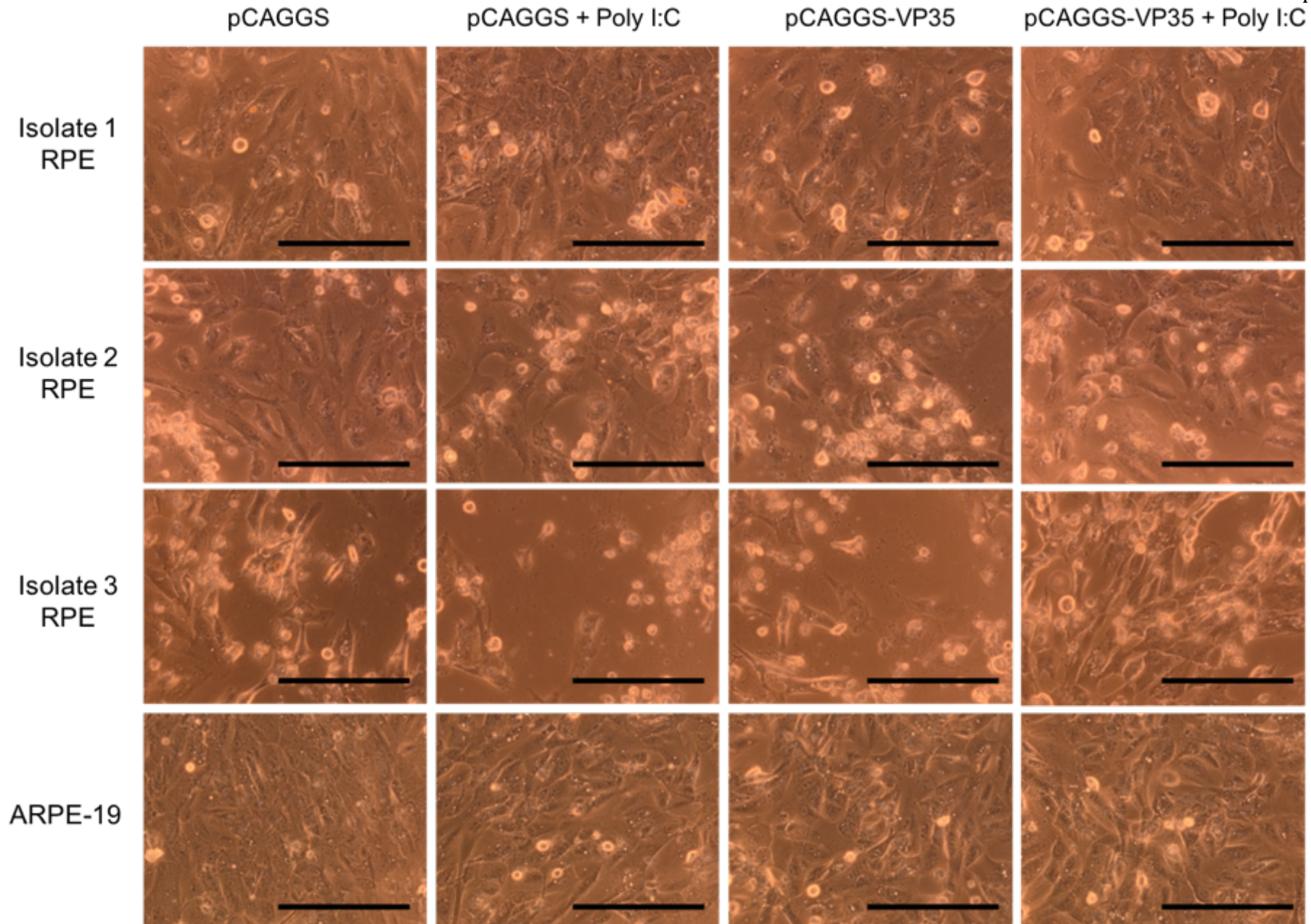


Figure 6.7: Cell toxicity after pCAGGS vector transfection and Poly I:C stimulation

In order to investigate the effect of VP35 on the type I IFN response in human retinal pigment epithelial cells, lipid transfection of Poly I:C in cells expressing pCAGGS plasmid was performed. Confluent monolayers of three primary human retinal pigment epithelial isolates and the ARPE-19 cell line were exposed to a VP35-encoding vector or a no-insert control pCAGGS vector with lipid transfection. After 48 hours, half the cells were Lipofectamine® 2000-transfected with rhodamine fluorophore-conjugated Poly I:C (n = 3 monolayers per condition). Four hours later, cells were photographed under a narrow band excitation filter, and RNA was extracted for RT-qPCR interrogation of IFN- β transcript expression. Confluent monolayers of human retinal pigment epithelial cells imaged 52 hours after lipid transfection with pCAGGS control plasmid or pCAGGS-VP35 plasmid. Cytotoxic changes are represented by loss of monolayer confluence and debris in the medium. Scale bars 100 μ m. **Abbreviations:** Poly I:C = polyriboinosinic:polyribocytidylic acid, RPE = retinal pigment epithelium, VP = viral protein.

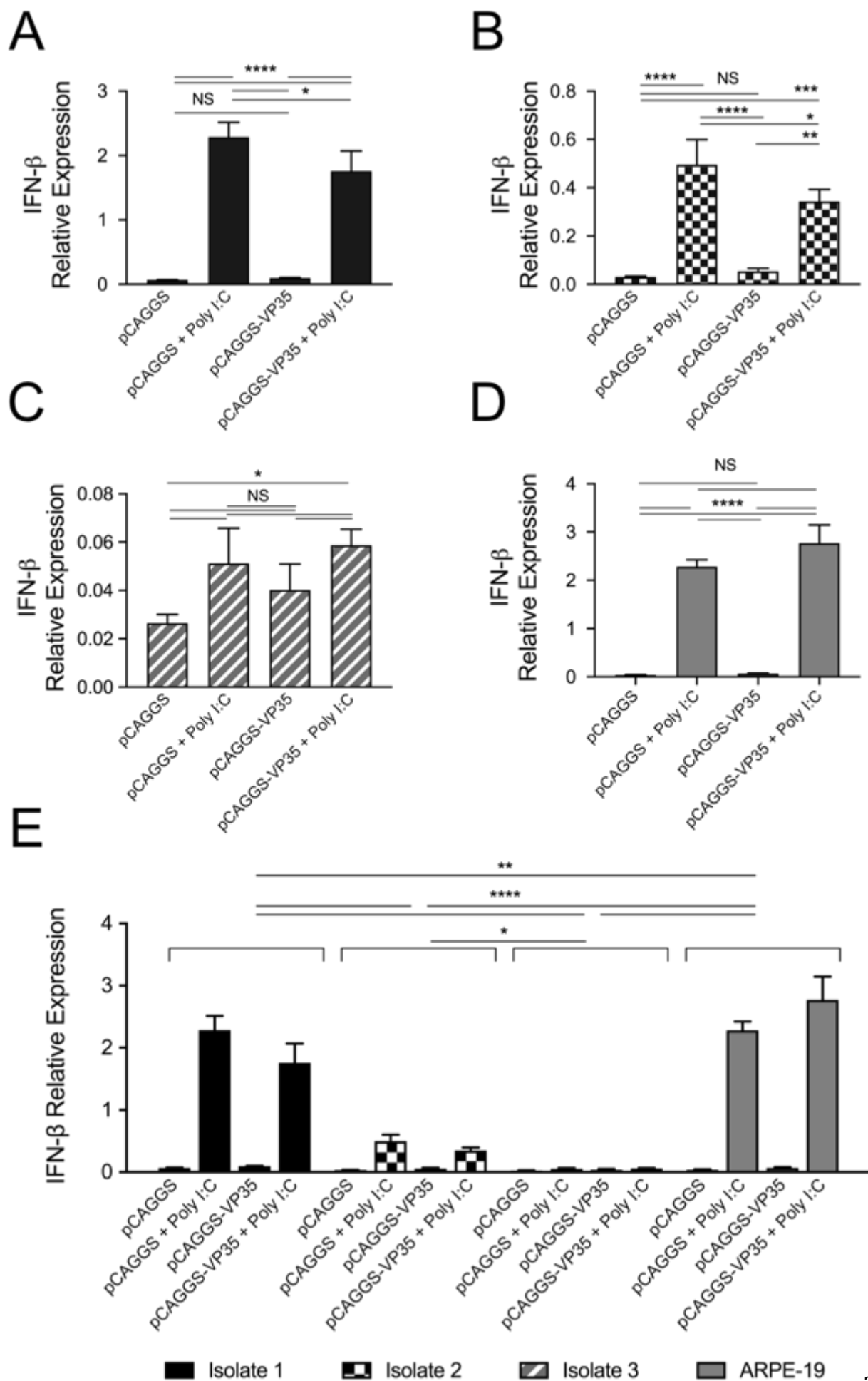


Figure 6.8: IFN- β production in VP35-expressing retinal pigment epithelial cells

To measure the type I IFN response in retinal pigment epithelial cells expressing VP35 protein, confluent monolayers of human retinal pigment epithelial cells were lipid-transfected with pCAGGS control plasmid or pCAGGS-VP35 plasmid. After 48 hours, half the samples underwent further lipid transfection with Poly I:C. At 52 hours, cells were harvested for RNA extraction and cDNA synthesis for RT-qPCR of IFN- β transcript, measured relative to reference genes RPLP0 and β -actin. Regardless of which plasmid they were expressing, all cells simulated with Poly I:C showed increased IFN- β expression compared to cells treated with plasmid alone, with the exception of isolate 3. Primary retinal pigment epithelial cell isolates (A) 1 ($p < 0.0001$), (B) 2 ($p < 0.0001$), (C) 3 ($p < 0.05$), and (D) ARPE-19 cells ($p < 0.0001$). (E). Composite graph of (A) to (D) ($p < 0.0001$). Graphs represent mean, and error bars indicate standard deviation. $N = 3$ monolayers per condition. Data analysed by ordinary one-way ANOVA (A) to (D), and two-way ANOVA (E). NS = not significant, * $p < 0.05$, ** $p < 0.01$, *** $p < 0.001$, **** $p < 0.0001$. **Abbreviations:** ANOVA = analysis of variance, cDNA = complementary deoxyribonucleic acid, IFN = interferon, Poly I:C = polyriboinosinic:polyribocytidylic acid, RPE = retinal pigment epithelium, RPLP0 = ribosomal protein lateral stalk subunit P0, RT-qPCR = quantitative reverse transcription polymerase chain reaction, VP = viral protein.

6.3 DISCUSSION

The EBOV protein, VP35, is a potent inhibitor of the host antiviral response through interactions with dsRNA, type I IFN signalling, host proteins, and RNA silencing mechanisms.⁴⁴⁵⁻⁴⁵⁰ In this work, a vector expressing FLAG-VP35 and a control plasmid vector lacking a viral sequence insert were sub-cloned and transfected into human retinal pigment epithelial cells, in order to investigate the effect of VP35 on production of IFN- β . In 2 of 3 primary human retinal pigment epithelial cell isolates, VP35-expressing cells exhibited reduced IFN- β expression as measured by RT-qPCR, but in one primary isolate, as in the ARPE-19 cell line, IFN- β expression was not influenced by VP35. These results demonstrate that in human retinal pigment epithelial cells, VP35 *can* inhibit production of IFN- β , a key component of the type I IFN response, and that this response may vary across donors.

The means by which VP35 represses the host immune response are diverse. Suppression of IFN regulatory factor 3 phosphorylation by VP35 directly inhibits transcriptional activation of type I signalling pathways.⁴⁴⁶ The VP35 protein can also evade pattern recognition receptor stimulation directly, by binding viral dsRNA,^{447, 448, 458} and indirectly through competitive inhibition by binding to PACT, a dsRNA-binding pattern recognition receptor agonist.⁴⁵⁰ Binding of VP35 also suppresses small interfering RNA-mediated gene silencing by host cells.⁴⁴⁹ Infection with EBOV suppresses the type I IFN response in most cell populations,²³⁶ yet some cell lines are reported to produce a strong IFN response to EBOV – specifically, ARPE-19²³⁵ and the 769p renal cell carcinoma cell line.⁴⁶² In this work, VP35 expression in Poly I:C-stimulated and unstimulated ARPE-19 cells did not alter expression of IFN- β .

The RPE is a highly-specialised monolayer of cells that forms the outer BRB, and is thus exposed to circulating pathogens. Survivors of EVD show signs of previous retinal pigment epithelial involvement in the form of retinal pigment epithelial scars,^{35, 238, 239} and nonhuman primates euthanised during acute lethal EVD demonstrate EBOV in the uveal tract,²³⁷ indicating that the RPE is exposed and likely infected by EBOV in the acute phase. The retinal pigment epithelial cell can be infected by a wide range of other RNA viruses. The flavivirus, West Nile virus, causes retinal infection and CNS complications by breaching the blood-brain and blood-retinal barriers.²⁷ Retinal pigment epithelial cells are easily infected by this virus, and mount an early IFN- β response that suppresses viral replication but which is circumvented by downstream inhibition of IFN- β signalling pathways.⁴⁶³ Retinal pigment epithelial cell infection with Zika, another flavivirus, generates florid infection and a type I IFN response coupled with robust inflammation and increased cell death, consistent with the atrophic changes in the RPE that are seen clinically.^{206, 396, 464-466}

In addition to its role in host antiviral defence, IFN- β also has immunomodulatory functions, and is approved by FDA as a treatment for multiple sclerosis.⁴⁶⁷ Researchers have shown that IFN- β inhibits the production of chemokine (C-X-C motif) ligand 9 and intercellular adhesion molecule 1 in Poly I:C-stimulated retinal pigment epithelial cells.⁴⁶⁸ During the acute phase of EVD, it is unknown whether circulating viral antigens or IFN- β stimulate the type I IFN response in uninfected RPE, but this would prime the cells to an antiviral state, as well as invoking immunomodulatory responses.

Although EBOV has been shown to profoundly suppress innate and adaptive immune responses in multiple cell populations, patients infected with EBOV show strong immune responses in the acute phase, as demonstrated by T-cell and B-cell activation, and have

sustained immune stimulation in convalescence, with activated T-cells circulating after plasma clearance of the virus, suggestive of ongoing antigenic stimulation.⁴⁶⁹ A study of rhesus monkey survivors at day 43 post-EVD identified infected CD68-positive cells in the vitreous, internal limiting membrane, uveal tract, and surrounding retinal vessels, implicating mononuclear phagocytes as EBOV reservoir cells within the eye.²³⁷ Perhaps ongoing antigenic stimulation of retinal pigment epithelial cells causes secretion of type I IFN and immunomodulatory molecules that suppress intraocular infection while low-grade viral replication occurs in monocytes, and this is held in balance until overt infection-induced inflammation manifests as uveitis. Latent ocular infection has been observed with other viruses such as cytomegalovirus, with RPE being the major site of persistent infection in hosts with a fully-competent immune system.²⁴⁴

A curious finding in this work was that ARPE-19 cells continued to produce IFN- β despite VP35 expression. Ebola virus works to counteract the type I IFN system in myriad ways, including inhibition of phosphorylation – and thus activation – of IRF-7, a transcription factor that induces expression of IFN- β .⁴⁵⁵ In contrast to primary human retinal pigment epithelial cells,²⁰⁶ the ARPE-19 cell line does not express IRF-7,²³⁵ and may have alternative pathways to IFN- β induction compared with primary retinal pigment epithelial cells. This work has highlighted differences in a widely-used RPE cell lines compared with primary isolates in their response to EBOV infection.

The effect of lipid transfection and plasmid expression on cell biology should be considered. While lipid transfection reagents are considered the gold standard for delivery of exogenous DNA,⁴⁷⁰ they can interfere with cell homeostasis, introduce off-target responses and stress cellular translational machinery. Permeabilization of the cell membrane induces cellular repair mechanisms requiring an influx of calcium ions into the

cell, which can trigger the apoptotic cascade.⁴⁷¹ In addition, Lipofectamine®-mediated transport can overwhelm the cell and increase the unfolded protein response and endoplasmic reticulum stress, also leading to apoptosis.⁴⁷² A recent study showed that Lipofectamine® transfection induced the type I IFN response through a mechanism dependent on IRF-3 and IRF-7, and that this was a cell-specific interaction.⁴⁷³ Whether lipid transfection stimulates this response in retinal pigment epithelial cells is unknown, but all cells were transfected at least once, so this was controlled by the experimental design.

The transition from extracellular plasmid DNA to intracellular protein is a multistep process involving a raft of physical and biochemical barriers.⁴⁷⁴ Plasmid DNA represents large cargo that, by virtue of its phosphate groups, carries a strongly negative charge.⁴⁷⁵ The cell membrane is also negatively charged, and to overcome electrostatic repulsion, a cationic liposome-based vehicle is often used to enable cell entry.⁴⁷⁶ Once inside the cell, plasmid DNA must (1) avoid active intracellular transport, which results in DNA degradation, (2) avoid entrapment and destruction within lysosomal compartments, and (3) escape the endosome, cross a congested cytoplasm rich in endonucleases, and enter the nucleus.⁴⁷⁰ Plasmids used in this work have a molecular weight of at least 200 kDa and must traverse a nuclear envelope that only allows passive diffusion of molecules less than 70 kDa in size.⁴⁷⁵ All of these factors can influence the transfection efficiency of a plasmid.

Variation in IFN- β expression and cytotoxicity between retinal pigment epithelial cell isolates was seen, and could be influenced by a number of factors. Firstly, the cells were all isolated at different points in time, and the time between death and isolation varied. Also, donor age and sex varied across isolates. Cytotoxic changes were greatest with

isolate 3, and these cells produced the least amount of IFN- β , and did not measurably respond to VP35. It would be useful to clarify whether these differences were influenced by technical aspects or if they were entirely due to biological variation.

While technical aspects of this experiment could be optimised, further investigations should draw on this work. More extensive kinetic studies of the primary retinal pigment epithelial cell transcriptome would provide a better picture of the characteristics of the type I IFN response to EBOV. While only IFN- β was studied in these experiments, this was appropriate as it is the primary driver of the type I IFN response. Infection of primary iris and retinal pigment epithelial cell isolates from the same donors, exposing retinal pigment epithelial cells to IFN- β prior to infection, or co-culture with infected monocytes could be future directions for research.

In summary, the work in this chapter has demonstrated that in simulated infection, VP35 inhibits expression of IFN- β in some – but not all – human retinal pigment epithelial cell populations. Viral inhibition of the type I IFN response means that RPE is vulnerable to EBOV infection and may provide a route of entry to the eye in the acute phase of EVD, and may contribute to post-Ebola uveitis, which is characterised by infective EBOV with florid inflammation in EVD survivors. This work simulated EBOV infection and studied the effect of VP35 in isolation. Given the differences in type I IFN response seen between ARPE-19 and primary retinal pigment epithelial cells in this work, the effect of intact EBOV infection of primary human retinal pigment epithelial cells remains an open question. Further investigation into the type I IFN response to EBOV in these cells would help clarify the characteristics of the response and further inform understanding of the mechanisms of viral persistence in the eye.

CHAPTER 7

Discussion

This thesis describes original studies that identify and address knowledge gaps relating to the mechanisms of retinal pathology caused by three intracellular zoonoses: *T. gondii* (an apicomplexan parasite), DENV (an arboviral flavivirus) and EBOV (a filovirus). These disparate organisms can all cause vision-threatening uveitis in infected humans. To better understand the mechanisms of disease pathology, this research used a range of techniques to study the retina at the tissue, cellular, and molecular level, *in vivo*, in real-time, and *in vitro*. Diverse approaches were taken, employing research methods that involved cell culture, bioinformatic processes, and clinical imaging tools.

This thesis advances the body of knowledge of retinal infections on many fronts. Chapter 3 presents an original and thorough portrayal of the spectrum of retinal tissue changes resulting from infection with *T. gondii* and identifies signs that are characteristic of TRC and indicate poor visual prognosis. This represents the largest study of TRC by SD-OCT, and is useful for the treating clinician. The potential involvement of Müller glial cells in DENV infection is investigated in Chapter 4 and describes the first published work on human Müller cells in DENV infection. Through the use of immortalised and primary

human Müller cells in culture, this work details the molecular responses to DENV infection. This work is the first to demonstrate the lack of a type I IFN response to infection in the human Müller cell line, MIO-M1, an original and significant contribution to the field. Chapter 5 describes an *in silico* analysis of miRNA responses of retinal pigment epithelial cells to EBOV. Aside from RNA sequencing data that has been previously reported,²³⁵ there are no other studies of EBOV infection of ocular cell populations. Mechanistic studies of the interplay between EBOV and the type I IFN response in retinal pigment epithelial cells are described in Chapter 6 and use advanced molecular techniques to effectively study the effect of VP35 on molecular responses. The work on EBOV infection of the RPE represents first-in-field experiments and provides avenues for further research on this emerging retinal infection.

To demonstrate pathological changes to retinal tissue in *T. gondii* infection, SD-OCT scans of a large cohort of individuals with active retinochoroiditis were examined. To understand the response of human Müller cells to infection in dengue, the immortalised MIO-M1 human Müller cell line and human primary Müller cell isolates were infected with DENV strains. To isolate the effect of EBOV on the type I IFN response of human retinal pigment epithelial cells, a plasmid expressing VP35 was transfected into the ARPE-19 cell line and human retinal pigment epithelial cell isolates. To understand the global processes involved in miRNA signalling in EBOV infection of human retinal pigment epithelial cells, bioinformatic processes were utilized to predict pathways and networks based on miRNA expression in infected ARPE-19 cells.

Zoonotic diseases are poorly understood, continuously emerging and difficult to study. These infections disproportionately arise in countries with limited research capacity and are not usually a research priority in highly-resourced nations. In the case of neglected

diseases such dengue,⁴⁷⁷ ocular complications were not recognised as being associated with infection until population-based studies were performed on hospital inpatients approximately 15 years ago.¹⁹³ These studies would be difficult to replicate for dangerous pathogens such as EBOV. High-level biosafety infrastructure shrinks the global pool of researchers, and exposure risk to healthcare workers limits clinical examination in the acute phase of infection to what is absolutely necessary, contraindicates post-mortem examination⁴⁷⁸ and delays surgery,²⁴⁵ decreasing opportunities to study these diseases. These zoonoses also tend to occur with epidemic spread, which places extreme demands on health systems and often subordinates basic science research. Despite significant and fundamental knowledge gaps, neglected infectious diseases, such as toxoplasmosis, receive little attention and remain highly prevalent in many countries, including Australia,⁵⁸ and ocular toxoplasmosis manifesting as TRC represents a significant cause of blindness in many parts of the world.

Regional susceptibility to different diseases within the retina is well known,⁴⁷⁹ and variation in retinal pathology was explored in this thesis. In the SD-OCT studies of TRC, macular (zone 1) pathology, such as oedema and epiretinal membrane, was demonstrated in the presence of peripheral (zone 2) necrotising retinitis. Transcriptomic research has demonstrated geographic variation in gene expression within cell groups in retinal tissue.^{308, 480-482} Human Müller cells located at the macula rely disproportionately on serine biosynthesis to combat oxidative stress, and dysfunction of this pathway may contribute to macular disease.³¹⁰ Further understanding of topographical variation could shed light on mechanisms of infection, such as why foveolitis occurs in DENV infection, and why retinal necrosis is more likely to occur at the macula in *T. gondii* infection. These

research questions could be addressed by infecting cell populations isolated from different regions of the retina, or infecting wholemount retinal tissue.

Various aspects of the human immune response to infection were addressed in this thesis, and inflammatory responses were seen across infections with all three pathogens. Widespread signs of ocular inflammation in the vitreous, retina and choroid were evident by SD-OCT imaging of active TRC. Müller cells mounted an inflammatory response to DENV infection that was characterised by upregulation of pro-inflammatory cytokines. Bioinformatic analysis of miRNA-driven pathways in EBOV-infected retinal pigment epithelial cells identified leucine-rich repeat kinase 2 (LRRK2) as the most highly involved molecule in EBOV-infected retinal pigment epithelial cells. Central to the host response to infection, LRRK is strongly associated with neuroinflammatory diseases and experimental autoimmune uveitis.^{414, 416} Mitogen-activated protein kinases (MAPK) 13 and 7 were also highly involved in EBOV infection and are associated with neuroinflammation. Collateral damage to retinal tissue from the effects of the inflammatory response to infection are a significant cause of blindness, and augmenting this response may mitigate tissue damage. Further investigation into the role of LRRK2 in EBOV infection may yield therapeutic targets for the treatment of post-Ebola uveitis.

A challenge for all retinal research is a lack of readily-available human retinal tissue. The unacceptable risk-to-benefit ratio of acquiring retinal biopsies demands indirect and surrogate means to understand pathogenic mechanisms. Biological markers – or “biomarkers” – are objective, quantifiable signs that demonstrate biological or pathological processes.⁴⁸³ While clinical signs, the proprietary biomarker of medicine, have been used for centuries, systems biology is at the forefront in generating biomarkers from the “-omics” fields.⁴⁸⁴ Identifying non-invasive biomarkers that indicate disease in

poorly-accessible tissue is appealing, and plasma biomarkers of ocular disease have been investigated in diseases such as age-related macular degeneration.⁴⁸⁵ However, access to these tests will be limited in poorly-resourced areas, where infectious diseases are more prevalent. Given the optical function of the eye, clinical imaging tools, such as SD-OCT, are especially suited to the study of retinal disease, and provide real-time, *in vivo* information about tissue changes. This work demonstrated a range of indicators of retinal tissue damage in TRC, and identified retinal hyporeflective spaces or signal voids as a sign associated with a poor visual prognosis. This latter observation is expected to be useful to the practising ophthalmologist.

Cell lines provide a homogenous, easily manipulatable model in which to study biological processes,⁴⁸⁶ but research conclusions may not perfectly translate to human systems, as it is presumed that the biology of a cell in culture is representative of its tissue of origin. Technical and biological factors are being increasingly recognised as sources of uncontrolled variation in experiments,⁴⁸⁷ including misidentification and cross-contamination of cell lines.⁴⁸⁸ Cells can demonstrate genetic⁴⁸⁹ and phenotypic⁴⁹⁰ variation that is influenced by culture conditions. Some culture medium formulations contain molecules that bind cellular hormone receptors, inducing different effects depending on brand and batch of medium and cell sex.⁴⁹¹ Hormonal interactions aside, human cells in culture demonstrate sexual dimorphism through differential expression of thousands of genes involved in wide-ranging biological processes, and in responses to cytokines and growth factors.^{492, 493} Cultured cells of similar origin and age show similar responses in normal conditions, but display sexual dimorphism in response to cellular stress, with female cells displaying more resilience.⁴⁹⁴ Sexual dimorphism has been demonstrated in apoptotic and cytotoxic responses of neural cell populations.⁴⁹⁵ The

ARPE-19 cell line is male;²⁶² the MIO-M1 cell line is female;⁹⁵ primary human Müller cells used in this thesis were isolated from males; and the primary human retinal pigment epithelial cell isolates were prepared from both male and female donors. Differences between primary cells and cell lines were found in all experiments. Whether cell sex contributed to this variation was not studied, but presents an intriguing possibility.

Differences between cell lines and isolated primary human cells are being increasingly recognized at a molecular level. Recent advances in RNA sequencing have seen the development of transcriptome libraries representing cell populations of complex tissues.³⁹⁰ Transcriptome analysis of the neural retinal cell populations of three post-mortem donor eyes by single cell RNA sequencing demonstrated 18 distinct cell populations, and noted differences in gene transcription of Müller cells when compared to the MIO-M1 cell line.⁹⁵ In this work, three of four chapters involved data gained from cell lines, and two chapters demonstrated different results with isolated human primary cells. Moving beyond the single cell, other models involving human retinal cells involve co-culture with leukocytes, and sophisticated systems such as a recently-described *in vitro* model of the BRB of a mixed-culture of human retinal endothelial cells, pericytes and astrocytes.⁴⁹⁶ Further complexity can be added by organoid models.⁴⁹⁷ Cell-pathogen interactions are complex, and this complexity is compounded by the intricacy of the surrounding tissue. This was elegantly demonstrated in a cerebral organoid model containing neurons and astrocytes, whereby inflammatory responses to DENV infection were only elicited when microglial populations were present.⁴⁹⁸ Thus, intact human retinal tissue may be superior for the study of retinal infections. Whole mount *ex vivo* human retina has been used to demonstrate *T. gondii* migration and cellular tropism.³⁰⁹ This could be an avenue for further studies of DENV retinopathy.

Animal models are appealing for the study of complex interactions in complex tissue, but come with caveats. The appropriate animal model may differ depending on which aspect of infection is being studied and by what means.^{499,500} A wide range of animal models have been used to study *T. gondii*, EBOV, and DENV infections.^{350,501-504} Artificial manipulation of the animal host may be required to induce disease in EBOV infection, and can be achieved with models including mice that do not express critical genes in immune pathways, such as A129 mice that lack type I IFN receptors, or “humanised mice” that express human genes or contain human cells or tissue.⁵⁰⁵ Non-human primates are preferred due to their similarity to humans and fidelity to the human manifestations of disease, as only non-human primates have a macula,⁵⁰⁶ but the cost, scale, ethics and harm-benefit analysis is usually too high for this research to be undertaken.⁵⁰⁰ Despite their complexity,⁵⁰⁷ *in vitro* and *in silico* methods of retinal and infectious disease research that reduce the use of experimental animals continue to gain traction.⁵⁰⁸

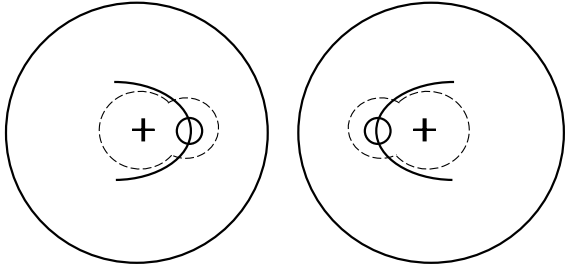
Zoonoses are extremely difficult to eliminate, and scientists will continue to direct research efforts to new and emerging infectious diseases. To this end, utilizing available research tools will enable a better understanding of the fundamental mechanisms of host-pathogen interactions within the retina. Biomarker research represents opportunities to utilize big data to generate tools that will continue to increase the clinician’s ability to provide earlier diagnosis, personalised prognostication, and targeted therapeutic invention to improve outcomes for zoonotic retinal infections. This thesis presents a body of work that identifies mechanisms of retinal damage by serious and neglected pathogens. Inflammation appears to be one of the primary characteristics of retinal damage in these infections. The host response to these pathogens is the critical factor that determines the outcome, be it overwhelming infection with retinal necrosis and tissue destruction, or

collateral damage of bystander tissue due to severe inflammation. Understanding the factors that modify the host-pathogen relationship will create opportunities for therapeutic interventions of these potentially blinding diseases.

APPENDICES

Appendix A: Spectral-domain optical coherence tomography data collection sheet.....	250
Appendix B: Manufacturer headquarters.....	253
Appendix C: Primary cell isolation	256
Appendix D: Primer sequences used for quantitative reverse transcription polymerase chain reaction	259
Appendix E: Viral quantification	262
Appendix F: Statistical analyses in Chapter 4.....	263
Appendix G: pCAGGS-FLAG-VP35 sequencing	272

**APPENDIX A: SPECTRAL-DOMAIN OPTICAL
COHERENCE TOMOGRAPHY DATA COLLECTION
SHEET**

PATIENT ID						SAVE IMAGE							
Zone 1: macula extending 3000 µm from fovea (i.e. ETDRS grid), plus 1500 µm from disc margin.						<input type="checkbox"/> SCANS OF MACULA BUT NOT LESION							
 <p>WEEK F/UP</p> <p>ETDRS central subfield volume (mm³, using 1, 3, 6 mm grid)</p>						OCT DATE							
						C		P		C		P	
RIGHT		LEFT		THICKNESS @ lesion ILM > base RPE (µm)		0							
Zone 1	Zone 2	Zone 1	Zone 2	Zone 1: 3000 µm from fovea (outside ETDRS grid), plus 1500 µm from disc margin.	SRF								
MACULAR changes if ZONE TWO lesion						N/A	1	1	1	1	1	1	1
						NO	2	2	2	2	2	2	2
						YES	3	3	3	3	3	3	3
ERM ^A / macular schisis ^B / lamellar hole ^C							1	1	1	1	1	1	1
VMT ^A / FTMH ^B							2	2	2	2	2	2	2
intraretinal fluid – IPL-INL ^A / OPL-ONL ^B / outer ^C / CMO ^D							3	3	3	3	3	3	3
large hyper-r dots vitreous ^A / ILM ^B / retina ^C							4	4	4	4	4	4	4
subretinal fluid							5	5	5	5	5	5	5
RPE thickening ^A / discontinuity ^B / other ^C							6	6	6	6	6	6	6
pachychoroid > 300 µm ^A / other ^B							7	7	7	7	7	7	7
POSTERIOR HYALOID						CANNOT GRADE	1	1	1	1	1	1	1
						ATTACHED	2	2	2	2	2	2	2
						VMA	3	3	3	3	3	3	3
						VMT	4	4	4	4	4	4	4
						localized / partial PVD	5	5	5	5	5	5	5
						PVD across OCT scan	6	6	6	6	6	6	6
EXPANDED PVD ON FOLLOW-UP						YES	-	-	1	1	1	1	1
VITREOUS HYPER-REFLECTIVITY						NONE / NORMAL	1	1	1	1	1	1	1
						DENSE: can't grade retina	2	2	2	2	2	2	2
						VITRITIS	3	3	3	3	3	3	3
						VITRITIS plus SUB-HYALOID	4	4	4	4	4	4	4
						VITREOSCHISIS	1	1	1	1	1	1	1
						HYALOID THICKENING at lesion	1	1	1	1	1	1	1
						ERM at lesion	1	1	1	1	1	1	1

HYPER-REFLECTIVE DEPOSITS	CANNOT GRADE	1	1	1	1		
	ILM	2	2	2	2		
	LARGEST DIAMETER: _____ μm						
	HYALOID only (if PVD)	3	3	3	3		
	HYALOID and ILM (if PVD)	4	4	4	4		
FATE OF DEPOSITS	SMALLER	-	1	1	1		
	ABSORBED INTO RETINA	-	1	1	1		
FLUID LOCATION	CANNOT GRADE	1	1	1	1	1	1
	NONE	2	2	2	2	2	2
	INTRARETINAL - DIFFUSE	3	3	3	3	3	3
	INTRARETINAL - CYSTOID	4	4	4	4	4	4
	*INTRARETINAL - ONL	5	5	5	5	5	5
	SUBRETINAL	6	6	6	6	6	6
LAMINATION	CANNOT GRADE	1	1	1	1	1	1
	NORMAL	2	2	2	2	2	2
	DISORGANIZED – inner ^A / outer ^B	3	3	3	3	3	3
	ABSENT – HYPER-R / TISSUE LOSS	4	4	4	4	4	4
RETINAL HYPER-REFLECTIVITY	CANNOT GRADE	1	1	1	1	1	1
	NONE	2	2	2	2	2	2
	LOCALIZED inner ^A / outer ^B	3	3	3	3	3	3
	FULL THICKNESS	4	4	4	4	4	4
	*ONL VERTICAL STRIPS	5	5	5	5	5	5
	RETINAL HYPOREFLECTIVITY / NECROSIS	1	1	1	1	1	1
RETINAL THICKNESS	CANNOT GRADE	1	1	1	1	1	1
	THINNING	2	2	2	2	2	2
	THICKENED	3	3	3	3	3	3
	LOSS OF TISSUE	4	4	4	4	4	4
RPE	CANNOT GRADE	1	1	1	1	1	1
	ATROPHY	2	2	2	2	2	2
	NORMAL	3	3	3	3	3	3
	THICKENED	4	4	4	4	4	4
RPE POSITION	ELEVATED	1	1	1	1	1	1
	DETACHMENT	2	2	2	2	2	2
CHOROID	CANNOT GRADE	1	1	1	1	1	1
	NORMAL	2	2	2	2	2	2
	SHADOWING / HYPO-R	3	3	3	3	3	3
	HYPER-RE (RPE ATROPHY)	4	4	4	4	4	4
PACHYCHOROID	THICKENED	1	1	1	1		
	CANNOT GRADE	2	2	2	2		
LOSS OF SEPTAE	LOSS SEPTAE	1	1	1	1		
	CANNOT GRADE	2	2	2	2		

APPENDIX B: MANUFACTURER HEADQUARTERS

- Abacus ALS, Brisbane, Australia
- Adelab Scientific, Thebarton, Australia
- Adobe, San Jose, CA
- American Type Culture Collection, Manassas, VA
- BD Biosciences, Franklin Lakes, NJ
- Beckman Coulter Life Sciences, Brea, CA
- Benchmark Scientific, Edison, NJ
- BioAir Solutions, Voorhees, NJ
- Bio-Rad Laboratories, Hercules, CA
- BioScientific, Sydney, Australia
- Bovogen Biologicals, Keilor East, Australia
- Canon, Toyko, Japan
- GeneWorks, Thebarton, Australia
- Gibco – a Thermo Fisher Scientific brand
- GraphPad Software, San Diego, CA

- Heidelberg Engineering, Heidelberg, Germany
- Illumina, San Diego, CA
- Invitrogen – a Thermo Fisher Scientific brand
- InvivoGen, San Diego, CA
- Kerafast, Boston, MA
- Lonza, Basel, Switzerland
- Medshop, Preston, Australia
- Merck, Darmstadt, Germany
- Merck Millipore, Burlington, MA (now part of MilliporeSigma)
- New England BioLabs, Ipswich, MA
- Olympus, Tokyo, Japan
- Panasonic Healthcare, Tokyo, Japan
- PerkinElmer, Waltham, MA
- Qiagen, Hilden, Germany
- Raytek, Boronia, Australia
- R&D Systems, Minneapolis, MN
- Roche Life Sciences, Penzberg, Germany
- Sage Science, Beverley, MA

- Scicons, Szirák, Hungary
- Sci-Ed Software, Westminster, CO
- Sheldon Manufacturing, Cornelius, OR
- Sigma-Aldrich, St Louis, MO (now part of MiliporeSigma)
- Thermo Fisher Scientific, Waltham, MA (acquired Life Technologies)
- Tuttnauer, Breda, Netherlands
- VWR International, Radnor, PA

APPENDIX C: PRIMARY CELL ISOLATION

Primary cell isolation was performed by Dr Yuefang Ma.

PRIMARY HUMAN RETINAL PIGMENT EPITHELIAL CELL ISOLATION

Sheets of retinal pigment epithelium (RPE) and choroid were dissected from human cadaver eye cups and placed into 6 cm dishes (Sigma-Aldrich, cat. CLS430166) with 2% FBS in PBS. Sheets were washed with 2% FBS in PBS, and digested in 0.5 mg/mL of collagenase IA (Sigma-Aldrich, cat. C9891) and collagenase IV solution (Sigma-Aldrich, cat. C5138) for 35 minutes at 37 °C and 5% CO₂. The enzyme solution was removed, and sheets were washed with 2% FBS in PBS before RPE was gently dissected from the choroid under a microscope. Sheets were placed in a 15 mL tube and centrifuged at 280 x *g* and RT for 1 minute on the Allegra X-12R Centrifuge (Beckman Coulter).

Supernatant was removed and the pellet re-suspended in 3 mL of 2% FBS in PBS before 3 mL of 10% sucrose medium (Sigma-Aldrich, cat. S0389) was layered on top of the solution. The tube was incubated at RT for 10 minutes and the top precipitate was removed before centrifugation again at 10 x *g* for 5 min. Cells were washed with 2% FBS in PBS and further centrifuged at 10 x *g* for 5 min. Supernatant was discarded and cells resuspended in RPE medium by gentle pipetting. Cells were plated in a dish, checked under the microscope, and incubated overnight. Cells with morphology that suggested another phenotype were removed with a pipette tip and cell monolayers were washed with PBS before medium was replaced. Primary retinal pigment epithelial cells used in the experiments were passage 2.

PRIMARY HUMAN RETINAL PIGMENT EPITHELIAL CELL MEDIUM

Cells were cultured in 1:1 Dulbecco's modified Eagle's medium:Ham's nutrient mixture F-12 (DMEM: F12, Thermo Fisher Scientific, cat. 10565) and minimum essential medium Eagle (MEM, Sigma-Aldrich, cat. 11140050), supplemented with FBS (initially at 10%, then reduced to 2% after 2 days, 1x N1 Medium Supplement (Sigma-Aldrich, cat. N6530), 0.25 mg/mL taurine (Sigma-Aldrich, cat. T0625), 0.02 mg/mL hydrocortisone (Sigma-Aldrich, cat. H0396), 0.013 ng/mL 3,3',5-Triiodo-L-thyronine sodium salt (Sigma-Aldrich, cat. T6397), 1x MEM Non-Essential Amino Acids Solution (Thermo Fisher Scientific, cat. 11140-050), 1x GlutaMAX™ Supplement and 100 U/mL penicillin-100 µg/mL streptomycin and incubated.

PRIMARY HUMAN MÜLLER CELL ISOLATION

To isolate human Müller cells, retina was dissected from posterior eye cups, washed with PBS and 2% FBS until clean, cut into small pieces and gently homogenized using a 1 mL pipette. The tissue homogenate was digested for 10 minutes with 0.5 mg/mL dispase I (Sigma-Aldrich, cat. 4942086001) at 37 °C and 5% CO₂. After further pipetting, the cell suspension was strained through 100 µm pores into a 50 mL centrifuge tube. Cells were pelleted by centrifugation at 280 x *g* and RT for 5 min, then resuspended in medium, plated into a 10 cm dish (Sigma-Aldrich, cat. CLS430167), and incubated. Medium was replaced on day 5, then weekly. Cell monolayers were sub-cultured to 1:3 once confluent, and frozen in liquid nitrogen or used for experiments. Primary Müller cells used in these experiments were passage 2.

PRIMARY HUMAN MÜLLER CELL MEDIUM

Cells were cultured in DMEM with 10% FBS, 1x GlutaMAX™ (Thermo Fisher Scientific, cat. 35050061), 1x NEAA, 1 mM sodium pyruvate (Thermo Fisher Scientific, cat. 11360070) and 100 U/mL penicillin-100 µg/mL streptomycin (Thermo Fisher Scientific, cat. 15140-122).

APPENDIX D: PRIMER SEQUENCES USED FOR QUANTITATIVE REVERSE TRANSCRIPTION POLYMERASE CHAIN REACTION

Primer sequences used in this thesis with GenBank® nucleic acid sequence database identification (release 238.0),⁵⁰⁹ provided by the National Center for Biotechnology Information (NCBI).⁵¹⁰

Transcript	Species		Primer sequences	Source	GenBank® ID	Expected product size (bp)
MG1 and MG2	Mycoplasma	FWD REV	5'-GGG AGC AAA CAG GAT TAG ATA CCC T-3' 5'-TGC ACC ATC TGT CAC TCT GTT AAC CTG-3'	Sigma-Aldrich	EU596508.1	269
Pan-DENV	Dengue	FWD REV	5'-CTA TGC TAA GCT TGA GCC CCG TC-3' 5'-CGG ATC CTC TAG AAC CTG TTG-3'	GeneWorks	KP188543.1	400
IFN- α	Human	FWD REV	5'-CAA GGT TCA GAG TCA CCC ATC-3' 5'-CAG AGA GCA GCT TGA CTT GCA-3'	GeneWorks	AB578886.1	120
IFN- β	Human	FWD REV	5'-AAA CTC ATG AGC AGT CTG CA-3' 5'-AGG AGA TCT TCA GTT TCG GAG G-3'	GeneWorks	EF064725.1	168
ISG15	Human	FWD REV	5'-GAG AGG CAG CGA ACT CAT CT-3' 5'-AGC ATC TTC ACC GTC AGG TC-3'	GeneWorks	AH001495.2	231

Transcript	Species	Primer sequences		Source	GenBank® ID	Expected product size (bp)
RSAD2	Human	FWD REV	5'-TGA CGG AAC AGA TCA AAG CA-3' 5'-GCA CCA AGC AGG ACA CTT CT-3'	GeneWorks	DQ891977.2	174
TNF- α	Human	FWD REV	5'-TCT CGA ACC CCG AGT GAC AA-3' 5'-TGA AGA GGA CCT GGG AGT AG-3'	GeneWorks	MH180383.1	482
IL-1 β	Human	FWD REV	5'-TGA CCT GAG CAC CTT CTT TC-3' 5'-CAG CTG TAG AGT GGG CTT ATC-3'	GeneWorks	NM_000576.3	331
IL-6	Human	FWD REV	5'-ATG AAC TCC TTC TCC ACA AGC GC-3' 5'-GAA GAG CCC TCA GGC TGG ACT G-3'	GeneWorks	NM_000600	628
IL-10	Human	FWD REV	5'-GTG ATG CCC CAA GCT GAG A-3' 5'-GCA TCT GGC AAC CCT ACA ACA AG-3'	GeneWorks	AF043333.1	138
PD-L1	Human	FWD REV	5'-ACG CAT TTA CTG TCA CGG TTC C-3' 5'-GAC TTC GGC CTT GGG GTA GC-3'	GeneWorks	AK314567.1	446
PD-L2	Human	FWD REV	5'-CAA CTT GGC TGC TTC ACA TTT T-3' 5'-TGT GGT GAC AGG TCT TTT TGT TGT-3'	GeneWorks	BC113680.1	137
FASL	Human	FWD REV	5'-GGG TGG ACT GGG GTG GCC TAT-3' 5'-GGA TTG GGC CTG GGG ATG TTT CA-3'	GeneWorks	AY858799.1	126

Transcript	Species	Primer sequences	Source	GenBank® ID	Expected product size (bp)
RPLP0	Human	FWD 5'-GCA GCA TCT ACA ACC CTG AA-3' REV 5'-GCA GAT GGA TCA GCC AAG AA-3'	Sigma-Aldrich	NM_001002.4	235
β-Actin	Human	FWD 5'-TCA AGA TCA TTG CTC CTC CTG AG-3' REV 5'-ACA TCT GCT GGA AGG TGG ACA-3'	GeneWorks	NM_001101.5	87
GAPDH	Human	FWD 5'-AGC TGA ACG GGA AGC TCA CTG G-3' REV 5'-GGA GTG GGT GTC GCT GTT GAA GTC-3'	Sigma-Aldrich	NM_001357943.2	209

Abbreviations: bp = base pairs, DENV = dengue virus, EIF2AK2 = eukaryotic translation initiation factor 2-alpha kinase 2, FWD = forward, FASL = Fas ligand, GAPDH = glyceraldehyde-3-phosphate dehydrogenase, IFN = interferon, IL = interleukin, ISG = interferon-stimulated gene, PD-L = programmed death-ligand, REV = reverse, RNA = ribonucleic acid, RPLP0 = ribosomal protein lateral stalk subunit P0, RSAD2 = radical S-adenosyl methionine domain-containing 2, TNF-α = tumour necrosis factor-alpha.

APPENDIX E: VIRAL QUANTIFICATION

Viral strains were propagated and quantified by Ms Abby Dawson. Viral titre of Mon601 stocks were determined by plaque assay of Vero cells using neutral red overlay and expressed in plaque-forming units (pfu)/mL. The six DENV field isolates were not amenable to quantification by plaque assay as Vero cells infected with these isolates did not form plaques. Instead, stocks were quantified by RT-qPCR to Mon601 pfu-equivalent units. Supernatant stocks of known pfu from Mon601-infected C6/36 cells were RNA-extracted (High Pure Viral Nucleic Acid Kit, Roche Life Sciences cat. 1185874001), and a Mon601 pfu:RNA ratio was calculated. Equivalent Mon601 genomes per pfu were calculated for all DENV field isolates based on RNA quantity, and viral stocks were quantified by Mon601-pfu/mL units and stored in 1 mL aliquots at -80 °C ahead of use in the experiments.

APPENDIX F: STATISTICAL ANALYSES IN CHAPTER 4

Appendix F, Table 1: Two-way ANOVA for Figure 4.4A

Transcript	Source of variation	df	Mean squares	F ratio	P-value	
IFN- β	Interaction	1	63.73	F (1, 12) = 615.6	< 0.0001	****
	Infection status	1	63.73	F (1, 12) = 615.6	< 0.0001	****
	Cell line	1	63.75	F (1, 12) = 615.7	< 0.0001	****

Abbreviations: ANOVA = analysis of variance, df = degrees of freedom, F = F statistic, IFN = interferon.

Appendix F, Table 2: Sidak's multiple comparisons for Figure 4.4A

Control -Mon601	Mean Difference	95% CI of difference	Adjusted P-value	
ARPE-19	-7.983	-8.564 to -7.402	< 0.0001	****
MIO-M1	-0.00009	-0.5810 to 0.5808	> 0.9999	NS

Abbreviations: CI = confidence interval, MIO-M1 = Moorfields / Institute of Ophthalmology-Müller 1, NS = not significant.

Appendix F, Table 3: Two-tailed unpaired t-test for Figure 4.4B

Transcript	Interaction	P-value	t, df	95% CI
IFN- α	Mon601 v control	0.9542	NS t=0.05984, df=6	-1.569 to 1.648
EIF2AK2	Mon601 v control	0.2323	NS t=1.407, df=4	-0.001519 to 0.004639
RSAD2	Mon601 v control	< 0.0001	**** t=18.38, df=6	1.010 to 1.321
ISG15	Mon601 v control	0.0004	*** t=10.88, df=4	0.03435 to 0.05787

Abbreviations: CI = confidence interval, df = degrees of freedom, EIFAK2 = eukaryotic translation initiation factor 2-alpha kinase 2, F = F statistic, IFN = interferon, IL = interleukin, ISG15 = interferon-stimulated gene 15, NS = not significant, PD-L = programmed death-ligand, RSAD2 = radical S-adenosyl methionine domain-containing 2, t = t statistic, TNF- α = tumour necrosis factor-alpha.

Appendix F, Table 4: Two-tailed unpaired t-test for Figure 4.5

Transcript	Interaction	P-value		t, df	95% CI
IL-6	Mon601 v control	0.0018	**	t=5.307, df=6	0.4042 to 1.096
PD-L1	Mon601 v control	<0.0001	****	t=15.48, df=6	0.9619 to 1.323
PD-L2	Mon601 v control	0.0073	**	t=3.568, df=8	3.698 to 17.21
IL-10	Mon601 v control	0.9695	NS	t=0.04062, df=4	-0.002312 to 0.002245

Transcripts TNF- α and IL-1 β had no expression in at least half the replicates for at least one condition, precluding statistical analysis. **Abbreviations:** CI = confidence interval, df = degrees of freedom, EIFAK2 = eukaryotic translation initiation factor 2-alpha kinase 2, F = F statistic, IFN = interferon, IL = interleukin, NS = not significant, PD-L = programmed death-ligand, RSAD2 = radical S-adenosyl methionine domain-containing 2, t = t statistic, TNF- α = tumour necrosis factor-alpha.

Appendix F, Table 5: Two-tailed unpaired t-test for Figure 4.7

Transcript	Interaction	P-value	t, df	95% CI
DENV	Mon601 v. EHI0578Y05	0.0045	** t=3.911, df=8	10649 to 41254

Abbreviations: CI = confidence interval, DENV = dengue virus, df = degrees of freedom, t = t statistic.

Appendix F, Table 6: One-way ANOVA for Figure 4.8

Transcript	P-value		F ratio
EIF2AK2	0.1145	NS	F (7, 40) = 1.798
RSAD2	0.0221	*	F (3, 18) = 4.100
PD-L2	<0.0001	****	F (7, 35) = 15.77

Transcripts TNF- α , IL-1 β , IL-6 and PD-L1 had no expression in at least half the replicates for at least one condition, precluding statistical analyses. **Abbreviations:** ANOVA = analysis of variance, CI = confidence interval, df = degrees of freedom, EIFAK2 = eukaryotic translation initiation factor 2-alpha kinase 2, F = F statistic, IFN = interferon, IL = interleukin, NS = not significant, PD-L = programmed death-ligand, RSAD2 = radical S-adenosyl methionine domain-containing 2, t = t statistic, TNF- α = tumour necrosis factor-alpha.

Appendix F, Table 7: Two-way ANOVA for Figure 4.13

Transcript	Source of variation	df	Mean squares	F ratio	P-value	
IFN- β	Interaction	4	5.903	F (4, 27) = 23.98	<0.0001	****
	Infection status	2	49.81	F (2, 27) = 202.3	<0.0001	****
	Cell population	2	9.626	F (2, 27) = 39.10	<0.0001	****
IFN- α	Interaction	4	1.707	F (4, 25) = 4.767	0.0054	**
	Infection status	2	3.971	F (2, 25) = 11.09	0.0004	***
	Cell population	2	0.8681	F (2, 25) = 2.424	0.1091	NS
EIFAK2	Interaction	4	2.487	F (4, 27) = 31.39	<0.0001	****
	Infection status	2	2.085	F (2, 27) = 26.32	<0.0001	****
	Cell population	2	1.452	F (2, 27) = 18.33	<0.0001	****
IL-1 β	Interaction	4	12.51	F (4, 25) = 7.490	0.0004	***
	Infection status	2	43.35	F (2, 25) = 25.96	<0.0001	****
	Cell population	2	16.87	F (2, 25) = 10.10	0.0006	***
PD-L1	Interaction	4	0.7738	F (4, 27) = 1.708	0.1774	NS
	Infection status	2	11.94	F (2, 27) = 26.36	<0.0001	****
	Cell population	2	3.117	F (2, 27) = 6.880	0.0038	**
PD-L2	Interaction	4	0.4222	F (4, 27) = 2.023	0.1194	NS
	Infection status	2	2.895	F (2, 27) = 13.87	<0.0001	****
	Cell population	2	1.341	F (2, 27) = 6.427	0.0052	**

Transcripts RSAD2, TNF- α and IL-6 had no expression in at least half the replicates for at least one condition, precluding statistical analyses. **Abbreviations:** ANOVA = analysis of variance, CI = confidence interval, df = degrees of freedom, EIFAK2 = eukaryotic translation initiation factor 2-alpha kinase 2, F = F statistic, IFN = interferon, IL = interleukin, NS = not significant, PD-L = programmed death-ligand, RSAD2 = radical S-adenosyl methionine domain-containing 2, t = t statistic, TNF- α = tumour necrosis factor-alpha.

Appendix F, Table 8: Tukey's multiple comparisons test for Figure 4.13

Transcript expression of 3 primary human Müller cell isolates was calculated by two-way ANOVA, where data were complete.

Transcript	Müller cell	Tukey's multiple comparisons test	Mean Difference	95% CI of difference	Adjusted P-value	
IFN- β	Isolate 1	Control vs. Mon601	-2.213	-3.083 to -1.343	< 0.0001	****
		Control vs. EHI0578Y05	0.0000225	-0.8699 to 0.8699	> 0.9999	NS
		Mon601 vs. EHI0578Y05	2.213	1.343 to 3.083	< 0.0001	****
	Isolate 2	Control vs. Mon601	-6.279	-7.149 to -5.409	< 0.0001	****
		Control vs. EHI0578Y05	-0.7311	-1.601 to 0.1388	0.1121	NS
		Mon601 vs. EHI0578Y05	5.548	4.678 to 6.417	< 0.0001	****
	Isolate 3	Control vs. Mon601	-2.464	-3.334 to -1.594	< 0.0001	****
		Control vs. EHI0578Y05	-0.04949	-0.9194 to 0.8204	0.9891	NS
		Mon601 vs. EHI0578Y05	2.414	1.544 to 3.284	< 0.0001	****
IFN- α	Isolate 1	Control vs. Mon601	0.2319	-0.8222 to 1.286	0.8484	NS
		Control vs. EHI0578Y05	0.08615	-0.9679 to 1.140	0.9774	NS
		Mon601 vs. EHI0578Y05	-0.1458	-1.200 to 0.9083	0.9368	NS
	Isolate 2	Control vs. Mon601	-2.121	-3.175 to -1.067	0.0001	***
		Control vs. EHI0578Y05	-0.1277	-1.266 to 1.011	0.9579	NS
		Mon601 vs. EHI0578Y05	1.993	0.8549 to 3.132	0.0006	***
	Isolate 3	Control vs. Mon601	-1.102	-2.240 to 0.03676	0.0592	NS
		Control vs. EHI0578Y05	0.1449	-0.9936 to 1.283	0.9462	NS
		Mon601 vs. EHI0578Y05	1.247	0.1926 to 2.301	0.0182	*
EIFAK2	Isolate 1	Control vs. Mon601	-1.441	-1.934 to -0.9474	< 0.0001	****
		Control vs. EHI0578Y05	0.04673	-0.4467 to 0.5402	0.9701	NS
		Mon601 vs. EHI0578Y05	1.488	0.9941 to 1.981	< 0.0001	****
	Isolate 2	Control vs. Mon601	-0.04375	-0.5372 to 0.4497	0.9737	NS
		Control vs. EHI0578Y05	-1.546	-2.039 to -1.052	< 0.0001	****
		Mon601 vs. EHI0578Y05	-1.502	-1.995 to -1.008	< 0.0001	****
	Isolate 3	Control vs. Mon601	-0.124	-0.6175 to 0.3694	0.8087	NS
		Control vs. EHI0578Y05	-0.9641	-1.458 to -0.4707	0.0001	***
		Mon601 vs. EHI0578Y05	-0.8401	-1.334 to -0.3466	0.0007	***
IL-1 β	Isolate 1	Control vs. Mon601	-0.8771	-3.335 to 1.581	0.6523	NS
		Control vs. EHI0578Y05	-0.007699	-2.466 to 2.451	> 0.9999	NS
		Mon601 vs. EHI0578Y05	0.8694	-1.406 to 3.145	0.6135	NS
	Isolate 2	Control vs. Mon601	-7.01	-9.286 to -4.734	< 0.0001	****
		Control vs. EHI0578Y05	-0.2814	-2.740 to 2.177	0.9562	NS
		Mon601 vs. EHI0578Y05	6.729	4.271 to 9.187	< 0.0001	****

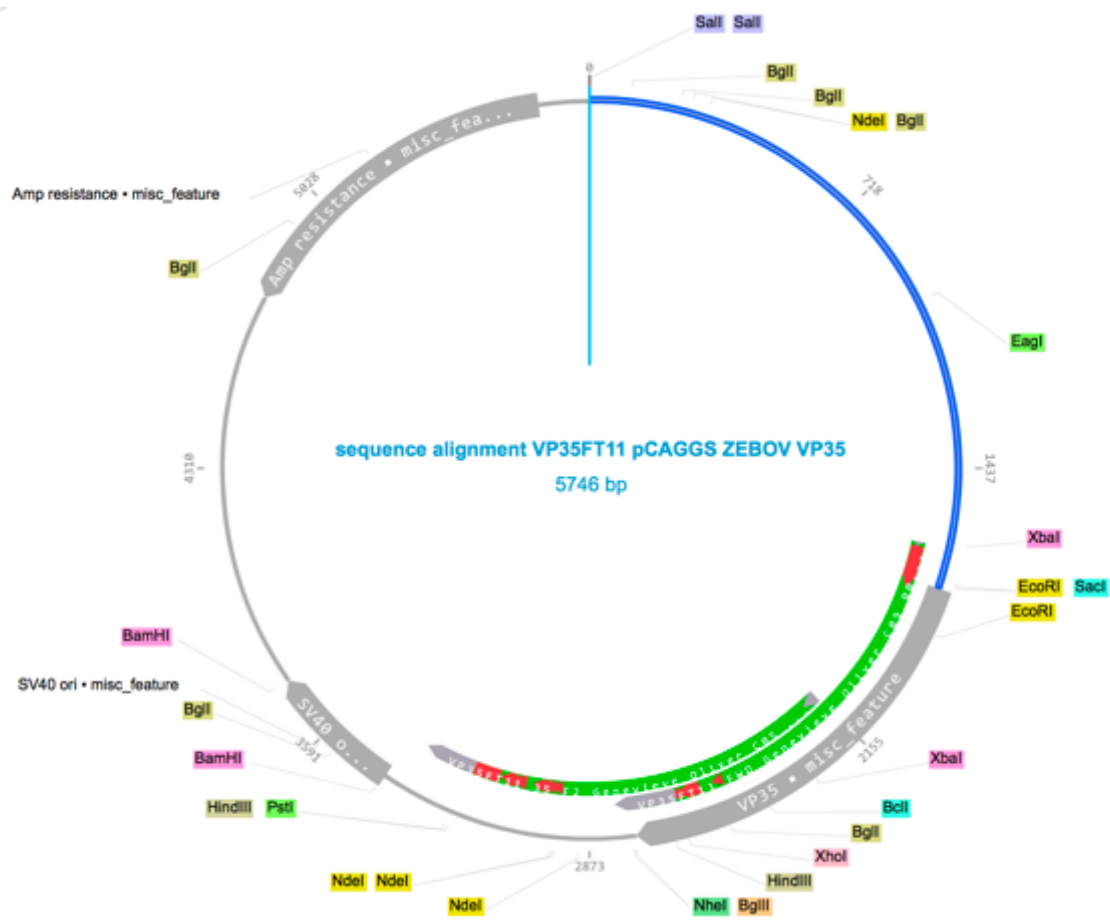
Transcript	Müller cell	Tukey's multiple comparisons test	Mean Difference	95% CI of difference	Adjusted P-value	
	Isolate 3	Control vs. Mon601	-2.33	-4.606 to -0.05372	0.0441	*
		Control vs. EHI0578Y05	-0.03724	-2.313 to 2.239	0.9991	NS
		Mon601 vs. EHI0578Y05	2.292	0.01649 to 4.568	0.0481	*
PD-L1	Isolate 1	Control vs. Mon601	-1.537	-2.717 to -0.3569	0.0088	**
		Control vs. EHI0578Y05	-0.00495	-1.185 to 1.175	> 0.9999	NS
		Mon601 vs. EHI0578Y05	1.532	0.3519 to 2.712	0.0091	**
	Isolate 2	Control vs. Mon601	-2.78	-3.960 to -1.599	< 0.0001	****
		Control vs. EHI0578Y05	-1.438	-2.618 to -0.2578	0.0146	*
		Mon601 vs. EHI0578Y05	1.342	0.1616 to 2.522	0.0235	*
	Isolate 3	Control vs. Mon601	-1.486	-2.666 to -0.3061	0.0114	*
		Control vs. EHI0578Y05	-0.1865	-1.367 to 0.9936	0.9191	NS
		Mon601 vs. EHI0578Y05	1.3	0.1196 to 2.480	0.0287	*
PD-L2	Isolate 1	Control vs. Mon601	-0.6998	-1.501 to 0.1011	0.0955	NS
		Control vs. EHI0578Y05	-0.01936	-0.8202 to 0.7815	0.998	NS
		Mon601 vs. EHI0578Y05	0.6804	-0.1204 to 1.481	0.1073	NS
	Isolate 2	Control vs. Mon601	-1.25	-2.051 to -0.4489	0.0018	**
		Control vs. EHI0578Y05	-1.312	-2.113 to -0.5109	0.0011	**
		Mon601 vs. EHI0578Y05	-0.06204	-0.8629 to 0.7388	0.9799	NS
	Isolate 3	Control vs. Mon601	-0.9441	-1.745 to -0.1432	0.0184	*
		Control vs. EHI0578Y05	-0.5986	-1.399 to 0.2023	0.1719	NS
		Mon601 vs. EHI0578Y05	0.3455	-0.4553 to 1.146	0.5406	NS

Transcripts RSAD2, TNF- α and IL-6 had no expression in at least half the replicates for at least one condition, precluding statistical analyses. **Abbreviations:** ANOVA = analysis of variance, CI = confidence interval, df = degrees of freedom, EIFAK2 = eukaryotic translation initiation factor 2-alpha kinase 2, F = F statistic, IFN = interferon, IL = interleukin, NS = not significant, PD-L = programmed death-ligand, t = t statistic.

APPENDIX G: PCAGGS-FLAG-VP35 SEQUENCING

Sequencing of pCAGGS-FLAG-VP35 plasmid was performed. Using the Basic Local Alignment Search Tool (BLAST) at the National Center for Biotechnology Information (NCBI) website,^{269, 270} 100% alignment to *Zaire ebolavirus* was confirmed. The FLAG sequence is underlined in blue, and VP35 sequence is displayed in red:

GATTATAAAGATGACGATGATAAAGCGGCCGC**ATGACAACTAGAACAAGGGCAGGGGCCA**
TACTGCGGCCACGACTCAAACGACAGAATGCCAGGCCCTGAGCTTTCGGGCTGGATCTC
TGAGCAGCTAATGACCGGAAGAATTCCTGTAAGCGACATCTTCTGTGATATTGAGAACA
ATCCAGGATTATGCTACGCATCCCAAATGCAACAAACGAAGCCAAACCCGAAGACGCGCA
ACAGTCAAACCCAAACGGACCCAATTTGCAATCATAGTTTTGAGGAGGTAGTACAAACA
TTGGCTTCATTGGCTACTGTTGTGCAACAACAAACCATCGCATCAGAATCATTAGAACAA
CGCATTACGAGTCTTGAGAATGGTCTAAAGCCAGTTTATGATATGGCAAAAACAATCTC
CTCATTGAACAGGGTTTTGTGCTGAGATGGTTGCAAAATATGATCTTCTGGTGATGACAA
CCGGTCGGGCAACAGCAACCGCTGCGGCAACTGAGGCTTATTGGGCCGAACATGGTCAAC
CACCACCTGGACCATCACTTTATGAAGAAAGTTCGATTTCGGGGTAAGATTGAATCTAGA
GATGAGACCGTCCCTCAAAGTGTTAGGGAGGCATTCAACAATCTAAACAGTACCACTTCA
CTAACTGAGGAAAATTTTGGGAAACCTGACATTTTCGGCAAAGGATTTGAGAAACATTAT
GTATGATCACTTGCCTGGTTTTGGAACTGCTTTCACCAATTAGTACAAGTGATTTGTA
AATTGGGAAAAGATAGCAACTCATTGGACATCATTCATGCTGAGTTCAGGCCAGCCTG
GCTGAAGGAGACTCTCCTCAATGTGCCCTAATTCAAATTACAAAAGAGTTCCAATCTTC
CAAGATGCTGCTCCACCTGTCATCCACATCCGCTCTCGAGGTGACATTCCTCCGAGCTTGCC
AGAAAAGCTTGCGTCCAGTCCCACCATCGCCCAAGATTGATCGAGGTTGGGTATGTGTTT
TTCAGCTTCAAGATGGTAAACACTTGGACTCAAATTTGAGCTAGCAGATCTTTTCCC
TCTGCCAAAATTATGGGGACATCATGAAGCCCCTTGAGC



Appendix G Figure 1: Plasmid sequencing

Cloned pCAGGS-FLAG-VP35 (green arcs) alongside original pCAGGS-VP35 plasmid to demonstrate VP35 sequence alignment. Green indicates sequence match, and red indicates mismatch. Diagram created in Genome Compiler (v. 2.2, Twist Bioscience, San Francisco, CA)

REFERENCES

1. Mandl JN, Ahmed R, Barreiro LB, Daszak P, Epstein JH, Virgin HW, Feinberg MB. Reservoir host immune responses to emerging zoonotic viruses. *Cell*. 2015;160(1-2):20-35.
2. Rouse BT, Sehrawat S. Immunity and immunopathology to viruses: what decides the outcome? *Nat Rev Immunol*. 2010;10(7):514-26.
3. Jones KE, Patel NG, Levy MA, Storeygard A, Balk D, Gittleman JL, Daszak P. Global trends in emerging infectious diseases. *Nature*. 2008;451(7181):990-3.
4. Garcia-Sastre A, Richt JA. Editorial overview: Emerging viruses: interspecies transmission: Expect the unexpected. *Curr Opin Virol*. 2019;34:iii-vi.
5. Institute of Medicine Committee on Emerging Microbial Threats to Health. In: Lederberg J, Shope RE, Oaks SC, Jr., editors. *Emerging Infections: Microbial Threats to Health in the United States*. Washington (DC): National Academies Press (US) Copyright 1992 by the National Academy of Sciences. All rights reserved.; 1992.
6. Lloyd-Smith JO, George D, Pepin KM, Pitzer VE, Pulliam JR, Dobson AP, Hudson PJ, Grenfell BT. Epidemic dynamics at the human-animal interface. *Science*. 2009;326(5958):1362-7.
7. Giesecke J, Stag IH. The truth about PHEICs. *Lancet*. 2019.
8. Pierson TC, Diamond MS. The continued threat of emerging flaviviruses. *Nat Microbiol*. 2020;5(6):796-812.
9. Girard M, Nelson CB, Picot V, Gubler DJ. Arboviruses: A global public health threat. *Vaccine*. 2020;38(24):3989-94.
10. Pandit PS, Doyle MM, Smart KM, Young CCW, Drape GW, Johnson CK. Predicting wildlife reservoirs and global vulnerability to zoonotic Flaviviruses. *Nat Commun*. 2018;9(1):5425.

11. Guzman MG, Gubler DJ, Izquierdo A, Martinez E, Halstead SB. Dengue infection. *Nat Rev Dis Primers*. 2016;2:16055.
12. Katzelnick LC, Coloma J, Harris E. Dengue: knowledge gaps, unmet needs, and research priorities. *Lancet Infect Dis*. 2017;17(3):e88-e100.
13. Bhatt S, Gething PW, Brady OJ, Messina JP, Farlow AW, Moyes CL, Drake JM, Brownstein JS, Hoen AG, Sankoh O, Myers MF, George DB, Jaenisch T, Wint GR, Simmons CP, Scott TW, Farrar JJ, Hay SI. The global distribution and burden of dengue. *Nature*. 2013;496(7446):504-7.
14. Messina JP, Brady OJ, Golding N, Kraemer MUG, Wint GRW, Ray SE, Pigott DM, Shearer FM, Johnson K, Earl L, Marczak LB, Shirude S, Davis Weaver N, Gilbert M, Velayudhan R, Jones P, Jaenisch T, Scott TW, Reiner RC, Jr., Hay SI. The current and future global distribution and population at risk of dengue. *Nat Microbiol*. 2019;4(9):1508-15.
15. Fontenille D, Powell JR. From Anonymous to Public Enemy: How Does a Mosquito Become a Feared Arbovirus Vector? *Pathogens*. 2020;9(4).
16. Guarner J, Hale GL. Four human diseases with significant public health impact caused by mosquito-borne flaviviruses: West Nile, Zika, dengue and yellow fever. *Semin Diagn Pathol*. 2019;36(3):170-6.
17. Faria NR, Kraemer MUG, Hill SC, Goes de Jesus J, Aguiar RS, Iani FCM, Xavier J, Quick J, du Plessis L, Dellicour S, Theze J, Carvalho RDO, Baele G, Wu CH, Silveira PP, Arruda MB, Pereira MA, Pereira GC, Lourenco J, Obolski U, Abade L, Vasylyeva TI, Giovanetti M, Yi D, Weiss DJ, Wint GRW, Shearer FM, Funk S, Nikolay B, Fonseca V, Adelino TER, Oliveira MAA, Silva MVF, Sacchetto L, Figueiredo PO, Rezende IM, Mello EM, Said RFC, Santos DA, Ferraz ML, Brito MG, Santana LF, Menezes MT, Brindeiro RM, Tanuri A, Dos Santos FCP, Cunha MS, Nogueira JS, Rocco IM, da Costa AC, Komninakis SCV, Azevedo V, Chieppe AO, Araujo ESM, Mendonca MCL, Dos Santos CC, Dos Santos CD, Mares-Guia AM, Nogueira RMR, Sequeira PC, Abreu RG, Garcia MHO, Abreu AL, Okumoto O, Kroon EG, de Albuquerque CFC, Lewandowski K, Pullan ST, Carroll M, de Oliveira T, Sabino EC, Souza RP, Suchard MA, Lemey P,

- Trindade GS, Drumond BP, Filippis AMB, Loman NJ, Cauchemez S, Alcantara LCJ, Pybus OG. Genomic and epidemiological monitoring of yellow fever virus transmission potential. *Science*. 2018;361(6405):894-9.
18. Fagbami AH. Zika virus infections in Nigeria: virological and seroepidemiological investigations in Oyo State. *J Hyg (Lond)*. 1979;83(2):213-9.
 19. Simpson DI. Zika Virus Infection in Man. *Trans R Soc Trop Med Hyg*. 1964;58:335-8.
 20. Duffy MR, Chen TH, Hancock WT, Powers AM, Kool JL, Lanciotti RS, Pretrick M, Marfel M, Holzbauer S, Dubray C, Guillaumot L, Griggs A, Bel M, Lambert AJ, Laven J, Kosoy O, Panella A, Biggerstaff BJ, Fischer M, Hayes EB. Zika virus outbreak on Yap Island, Federated States of Micronesia. *N Engl J Med*. 2009;360(24):2536-43.
 21. Cao-Lormeau VM, Blake A, Mons S, Lastere S, Roche C, Vanhomwegen J, Dub T, Baudouin L, Teissier A, Larre P, Vial AL, Decam C, Choumet V, Halstead SK, Willison HJ, Musset L, Manuguerra JC, Despres P, Fournier E, Mallet HP, Musso D, Fontanet A, Neil J, Ghawche F. Guillain-Barre Syndrome outbreak associated with Zika virus infection in French Polynesia: a case-control study. *Lancet*. 2016;387(10027):1531-9.
 22. Franca GV, Schuler-Faccini L, Oliveira WK, Henriques CM, Carmo EH, Pedi VD, Nunes ML, Castro MC, Serruya S, Silveira MF, Barros FC, Victora CG. Congenital Zika virus syndrome in Brazil: a case series of the first 1501 livebirths with complete investigation. *Lancet*. 2016;388(10047):891-7.
 23. de Oliveira WK, de Franca GVA, Carmo EH, Duncan BB, de Souza Kuchenbecker R, Schmidt MI. Infection-related microcephaly after the 2015 and 2016 Zika virus outbreaks in Brazil: a surveillance-based analysis. *Lancet*. 2017;390(10097):861-70.
 24. Satterfield-Nash A, Kotzky K, Allen J, Bertolli J, Moore CA, Pereira IO, Pessoa A, Melo F, Santelli A, Boyle CA, Peacock G. Health and Development at Age 19-24 Months of 19 Children Who Were Born with Microcephaly and Laboratory Evidence of

- Congenital Zika Virus Infection During the 2015 Zika Virus Outbreak - Brazil, 2017. *MMWR Morb Mortal Wkly Rep.* 2017;66(49):1347-51.
25. Rasmussen SA, Jamieson DJ, Honein MA, Petersen LR. Zika Virus and Birth Defects--Reviewing the Evidence for Causality. *N Engl J Med.* 2016;374(20):1981-7.
 26. Alvarado MG, Schwartz DA. Zika Virus Infection in Pregnancy, Microcephaly, and Maternal and Fetal Health: What We Think, What We Know, and What We Think We Know. *Arch Pathol Lab Med.* 2017;141(1):26-32.
 27. Hasbun R, Garcia MN, Kellaway J, Baker L, Salazar L, Woods SP, Murray KO. West Nile Virus Retinopathy and Associations with Long Term Neurological and Neurocognitive Sequelae. *PLoS One.* 2016;11(3):e0148898.
 28. Wang P, Zhang R. Chikungunya Virus and (Re-) Emerging Alphaviruses. *Viruses.* 2019;11(9).
 29. Tsetsarkin KA, Vanlandingham DL, McGee CE, Higgs S. A single mutation in chikungunya virus affects vector specificity and epidemic potential. *PLoS Pathog.* 2007;3(12):e201.
 30. Lee JH, Agarwal A, Mahendradas P, Lee CS, Gupta V, Pavesio CE, Agrawal R. Viral posterior uveitis. *Surv Ophthalmol.* 2017;62(4):404-45.
 31. Wang LF, Anderson DE. Viruses in bats and potential spillover to animals and humans. *Curr Opin Virol.* 2019;34:79-89.
 32. Rojas M, Monsalve DM, Pacheco Y, Acosta-Ampudia Y, Ramirez-Santana C, Ansari AA, Gershwin ME, Anaya JM. Ebola virus disease: An emerging and re-emerging viral threat. *J Autoimmun.* 2020;106:102375.
 33. World Health Organization. Ebola virus disease [webpage]. 2020 [updated 11/05/2020; cited 2020 10 May]. Available from: https://www.who.int/health-topics/ebola#tab=tab_1.

34. Shantha JG, Crozier I, Hayek BR, Bruce BB, Gargu C, Brown J, Fankhauser J, Yeh S. Ophthalmic Manifestations and Causes of Vision Impairment in Ebola Virus Disease Survivors in Monrovia, Liberia. *Ophthalmology*. 2017;124(2):170-7.
35. Yeh S, Varkey JB, Crozier I. Persistent Ebola Virus in the Eye. *N Engl J Med*. 2015;373(20):1982-3.
36. Clark DV, Kibuuka H, Millard M, Wakabi S, Lukwago L, Taylor A, Eller MA, Eller LA, Michael NL, Honko AN, Olinger GG, Jr., Schoepp RJ, Hepburn MJ, Hensley LE, Robb ML. Long-term sequelae after Ebola virus disease in Bundibugyo, Uganda: a retrospective cohort study. *Lancet Infect Dis*. 2015;15(8):905-12.
37. Lindsay DS, Dubey JP. Toxoplasmosis in wild and domestic animals. In: Weiss LM, Kim K, editors. *Toxoplasma gondii*: Academic Press; 2020. p. 293-320.
38. Montoya JG, Liesenfeld O. Toxoplasmosis. *Lancet*. 2004;363(9425):1965-76.
39. Findal G, Barlinn R, Sandven I, Stray-Pedersen B, Nordbo SA, Samdal HH, Vainio K, Dudman SG, Jenum PA. Toxoplasma prevalence among pregnant women in Norway: a cross-sectional study. *Apmis*. 2015;123(4):321-5.
40. Lopes AP, Dubey JP, Darde ML, Cardoso L. Epidemiological review of Toxoplasma gondii infection in humans and animals in Portugal. *Parasitology*. 2014;141(13):1699-708.
41. Hofhuis A, van Pelt W, van Duynhoven YT, Nijhuis CD, Mollema L, van der Klis FR, Havelaar AH, Kortbeek LM. Decreased prevalence and age-specific risk factors for Toxoplasma gondii IgG antibodies in The Netherlands between 1995/1996 and 2006/2007. *Epidemiol Infect*. 2011;139(4):530-8.
42. Mustafa M, Fathy F, Mirghani A, Mohamed MA, Muneer MS, Ahmed AE, Ali MS, Omer RA, Siddig EE, Mohamed NS, Abd Elkareem AM. Prevalence and risk factors profile of seropositive Toxoplasmosis gondii infection among apparently immunocompetent Sudanese women. *BMC Res Notes*. 2019;12(1):279.

43. Wam EC, Sama LF, Ali IM, Ebile WA, Aghangu LA, Tume CB. Seroprevalence of *Toxoplasma gondii* IgG and IgM antibodies and associated risk factors in women of child-bearing age in Njinikom, NW Cameroon. *BMC Res Notes*. 2016;9(1):406.
44. Daryani A, Sarvi S, Aarabi M, Mizani A, Ahmadpour E, Shokri A, Rahimi MT, Sharif M. Seroprevalence of *Toxoplasma gondii* in the Iranian general population: a systematic review and meta-analysis. *Acta Trop*. 2014;137:185-94.
45. Mosawi SH, Zarghona Z, Dalimi A, Jokelainen P, Safa AH, Mohammadi MR, Javanmardi E, Basirat MB. Particularly neglected in countries with other challenges: High *Toxoplasma gondii* seroprevalence in pregnant women in Kabul, Afghanistan, while a low proportion know about the parasite. *PLoS One*. 2019;14(10):e0223585.
46. Markovich MP, Shohat T, Riklis I, Avni R, Yujelevski-Rozenblit D, Bassal R, Cohen D, Rorman E. Seroepidemiology of *Toxoplasma gondii* infection in the Israeli population. *Epidemiol Infect*. 2014;142(1):149-55.
47. Zhou Q, Wang Q, Shen H, Zhang Y, Zhang S, Li X, Acharya G. Seroepidemiological map of *Toxoplasma gondii* infection and associated risk factors in preconception period in China: A nationwide cross-sectional study. *J Obstet Gynaecol Res*. 2018;44(6):1134-9.
48. Singh S, Munawwar A, Rao S, Mehta S, Hazarika NK. Serologic prevalence of *Toxoplasma gondii* in Indian women of child bearing age and effects of social and environmental factors. *PLoS Negl Trop Dis*. 2014;8(3):e2737.
49. Iddawela D, Vithana SMP, Ratnayake C. Seroprevalence of toxoplasmosis and risk factors of *Toxoplasma gondii* infection among pregnant women in Sri Lanka: a cross sectional study. *BMC Public Health*. 2017;17(1):930.
50. Karunajeewa H, Siebert D, Hammond R, Garland S, Kelly H. Seroprevalence of varicella zoster virus, parvovirus B19 and *Toxoplasma gondii* in a Melbourne obstetric population: implications for management. *Aust N Z J Obstet Gynaecol*. 2001;41(1):23-8.

51. Morris A, Croxson M. Serological evidence of *Toxoplasma gondii* infection among pregnant women in Auckland. *N Z Med J*. 2004;117(1189):U770.
52. Dubey JP, Verma SK, Villena I, Aubert D, Geers R, Su C, Lee E, Forde MS, Krecek RC. Toxoplasmosis in the Caribbean islands: literature review, seroprevalence in pregnant women in ten countries, isolation of viable *Toxoplasma gondii* from dogs from St. Kitts, West Indies with report of new *T. gondii* genetic types. *Parasitol Res*. 2016;115(4):1627-34.
53. Jones JL, Kruszon-Moran D, Elder S, Rivera HN, Press C, Montoya JG, McQuillan GM. *Toxoplasma gondii* Infection in the United States, 2011-2014. *Am J Trop Med Hyg*. 2018;98(2):551-7.
54. Dubey JP, Lago EG, Gennari SM, Su C, Jones JL. Toxoplasmosis in humans and animals in Brazil: high prevalence, high burden of disease, and epidemiology. *Parasitology*. 2012;139(11):1375-424.
55. Wang T, Han Y, Pan Z, Wang H, Yuan M, Lin H. Seroprevalence of *Toxoplasma gondii* infection in blood donors in mainland China: a systematic review and meta-analysis. *Parasite*. 2018;25:36.
56. Rai SK, Matsumura T, Ono K, Abe A, Hirai K, Rai G, Sumi K, Kubota K, Uga S, Shrestha HG. High *Toxoplasma* seroprevalence associated with meat eating habits of locals in Nepal. *Asia Pac J Public Health*. 1999;11(2):89-93.
57. Messier V, Levesque B, Proulx JF, Rochette L, Libman MD, Ward BJ, Serhir B, Couillard M, Ogden NH, Dewailly E, Hubert B, Dery S, Barthe C, Murphy D, Dixon B. Seroprevalence of *Toxoplasma gondii* among Nunavik Inuit (Canada). *Zoonoses Public Health*. 2009;56(4):188-97.
58. Molan A, Nosaka K, Hunter M, Wang W. Seroprevalence and associated risk factors of *Toxoplasma gondii* infection in a representative Australian human population: The Busselton health study. *Clinical Epidemiology and Global Health*. 2020;8(3):808-14.

59. Wilking H, Thamm M, Stark K, Aebischer T, Seeber F. Prevalence, incidence estimations, and risk factors of *Toxoplasma gondii* infection in Germany: a representative, cross-sectional, serological study. *Sci Rep*. 2016;6:22551.
60. Villena I, Ancelle T, Delmas C, Garcia P, Brezin AP, Thulliez P, Wallon M, King L, Goulet V, Toxosurv n, National Reference Centre for T. Congenital toxoplasmosis in France in 2007: first results from a national surveillance system. *Euro Surveill*. 2010;15(25).
61. Rougier S, Montoya JG, Peyron F. Lifelong Persistence of *Toxoplasma* Cysts: A Questionable Dogma? *Trends Parasitol*. 2017;33(2):93-101.
62. Dubey JP, Hill DE, Jones JL, Hightower AW, Kirkland E, Roberts JM, Marcet PL, Lehmann T, Vianna MC, Miska K, Sreekumar C, Kwok OC, Shen SK, Gamble HR. Prevalence of viable *Toxoplasma gondii* in beef, chicken, and pork from retail meat stores in the United States: risk assessment to consumers. *J Parasitol*. 2005;91(5):1082-93.
63. Dubey JP. *Toxoplasma gondii* oocyst survival under defined temperatures. *J Parasitol*. 1998;84(4):862-5.
64. Bosch-Driessen LE, Berendschot TT, Ongkosuwito JV, Rothova A. Ocular toxoplasmosis: clinical features and prognosis of 154 patients. *Ophthalmology*. 2002;109(5):869-78.
65. Singh S, Kumar A. Ocular Manifestations of Emerging Flaviviruses and the Blood-Retinal Barrier. *Viruses*. 2018;10(10).
66. Manangeeswaran M, Kielczewski JL, Sen HN, Xu BC, Ireland DDC, McWilliams IL, Chan CC, Caspi RR, Verthelyi D. ZIKA virus infection causes persistent chorioretinal lesions. *Emerg Microbes Infect*. 2018;7(1):96.
67. Furtado JM, Esposito DL, Klein TM, Teixeira-Pinto T, da Fonseca BA. Uveitis Associated with Zika Virus Infection. *N Engl J Med*. 2016;375(4):394-6.
68. Zin OA, Medina FMC, da Costa DS, Barcaui HS, Belfort R, Jr. Retinal maculopathy in an adult with yellow fever. *Lancet Infect Dis*. 2019;19(2):216.

69. Brandao-de-Resende C, Cunha LHM, Oliveira SL, Pereira LS, Oliveira JGF, Santos TA, Vasconcelos-Santos DV. Characterization of Retinopathy Among Patients With Yellow Fever During 2 Outbreaks in Southeastern Brazil. *JAMA Ophthalmol*. 2019.
70. Oliver GF, Carr JM, Smith JR. Emerging infectious uveitis: Chikungunya, dengue, Zika and Ebola: A review. *Clin Exp Ophthalmol*. 2019;47(3):372-80.
71. Gomez-Marin JE, de-la-Torre A. Ocular disease due to *Toxoplasma gondii*. In: Weiss LM, Kim K, editors. *Toxoplasma gondii*: Academic Press; 2020. p. 229-91.
72. Quinn N, Csincsik L, Flynn E, Curcio CA, Kiss S, Sadda SR, Hogg R, Peto T, Lengyel I. The clinical relevance of visualising the peripheral retina. *Prog Retin Eye Res*. 2019;68:83-109.
73. McMenamin PG, Saban DR, Dando SJ. Immune cells in the retina and choroid: Two different tissue environments that require different defenses and surveillance. *Prog Retin Eye Res*. 2019;70:85-98.
74. Lakkaraju A, Umapathy A, Tan LX, Daniele L, Philp NJ, Boesze-Battaglia K, Williams DS. The cell biology of the retinal pigment epithelium. *Prog Retin Eye Res*. 2020:100846.
75. Reichenbach A, Bringmann A. Glia of the human retina. *Glia*. 2020;68(4):768-96.
76. Strauss O. The retinal pigment epithelium in visual function. *Physiol Rev*. 2005;85(3):845-81.
77. Murakami Y, Ishikawa K, Nakao S, Sonoda KH. Innate immune response in retinal homeostasis and inflammatory disorders. *Prog Retin Eye Res*. 2020;74:100778.
78. Niederkorn JY. The Eye Sees Eye to Eye With the Immune System: The 2019 Proctor Lecture. *Invest Ophthalmol Vis Sci*. 2019;60(13):4489-95.
79. Mochizuki M, Sugita S, Kamoi K. Immunological homeostasis of the eye. *Prog Retin Eye Res*. 2013;33:10-27.

80. Spadoni I, Fornasa G, Rescigno M. Organ-specific protection mediated by cooperation between vascular and epithelial barriers. *Nat Rev Immunol.* 2017;17(12):761-73.
81. Niederkorn JY, Stein-Streilein J. History and physiology of immune privilege. *Ocul Immunol Inflamm.* 2010;18(1):19-23.
82. Nasirudeen AM, Wong HH, Thien P, Xu S, Lam KP, Liu DX. RIG-I, MDA5 and TLR3 synergistically play an important role in restriction of dengue virus infection. *PLoS Negl Trop Dis.* 2011;5(1):e926.
83. Liang Z, Wu S, Li Y, He L, Wu M, Jiang L, Feng L, Zhang P, Huang X. Activation of Toll-like receptor 3 impairs the dengue virus serotype 2 replication through induction of IFN-beta in cultured hepatoma cells. *PLoS One.* 2011;6(8):e23346.
84. Uno N, Ross TM. Dengue virus and the host innate immune response. *Emerg Microbes Infect.* 2018;7(1):167.
85. Chan YK, Gack MU. Viral evasion of intracellular DNA and RNA sensing. *Nat Rev Microbiol.* 2016;14(6):360-73.
86. Chow KT, Gale M, Jr., Loo YM. RIG-I and Other RNA Sensors in Antiviral Immunity. *Annu Rev Immunol.* 2018;36:667-94.
87. Yarovinsky F. Innate immunity to *Toxoplasma gondii* infection. *Nat Rev Immunol.* 2014;14(2):109-21.
88. Safronova A, Araujo A, Camanzo ET, Moon TJ, Elliott MR, Beiting DP, Yarovinsky F. Alarmin S100A11 initiates a chemokine response to the human pathogen *Toxoplasma gondii*. *Nat Immunol.* 2019;20(1):64-72.
89. Miller FC, Coburn PS, Huzzatul MM, LaGrow AL, Livingston E, Callegan MC. Targets of immunomodulation in bacterial endophthalmitis. *Prog Retin Eye Res.* 2019;73:100763.
90. Sasai M, Yamamoto M. Innate, adaptive, and cell-autonomous immunity against *Toxoplasma gondii* infection. *Exp Mol Med.* 2019;51(12):1-10.

91. Zhang Y, He J, Zheng H, Huang S, Lu F. Association of TREM-1, IL-1beta, IL-33/ST2, and TLR Expressions With the Pathogenesis of Ocular Toxoplasmosis in Mouse Models on Different Genetic Backgrounds. *Front Microbiol.* 2019;10:2264.
92. Zhu W, Li J, Pappoe F, Shen J, Yu L. Strategies Developed by *Toxoplasma gondii* to Survive in the Host. *Front Microbiol.* 2019;10:899.
93. Kumar MV, Nagineni CN, Chin MS, Hooks JJ, Detrick B. Innate immunity in the retina: Toll-like receptor (TLR) signaling in human retinal pigment epithelial cells. *J Neuroimmunol.* 2004;153(1-2):7-15.
94. Stewart EA, Wei R, Branch MJ, Sidney LE, Amoaku WM. Expression of Toll-like receptors in human retinal and choroidal vascular endothelial cells. *Exp Eye Res.* 2015;138:114-23.
95. Limb GA, Salt TE, Munro PM, Moss SE, Khaw PT. In vitro characterization of a spontaneously immortalized human Müller cell line (MIO-M1). *Invest Ophthalmol Vis Sci.* 2002;43(3):864-9.
96. Kumar A, Shamsuddin N. Retinal Müller glia initiate innate response to infectious stimuli via toll-like receptor signaling. *PLoS One.* 2012;7(1):e29830.
97. Sauter MM, Kolb AW, Brandt CR. Toll-like receptors 4, 5, 6 and 7 are constitutively expressed in non-human primate retinal neurons. *J Neuroimmunol.* 2018;322:26-35.
98. Fercher AF. Optical coherence tomography - development, principles, applications. *Z Med Phys.* 2010;20(4):251-76.
99. Huang D, Swanson EA, Lin CP, Schuman JS, Stinson WG, Chang W, Hee MR, Flotte T, Gregory K, Puliafito CA, et al. Optical coherence tomography. *Science.* 1991;254(5035):1178-81.
100. Drexler W, Fujimoto JG. State-of-the-art retinal optical coherence tomography. *Prog Retin Eye Res.* 2008;27(1):45-88.

101. Swanson EA, Izatt JA, Hee MR, Huang D, Lin CP, Schuman JS, Puliafito CA, Fujimoto JG. In vivo retinal imaging by optical coherence tomography. *Opt Lett*. 1993;18(21):1864-6.
102. Sull AC, Vuong LN, Price LL, Srinivasan VJ, Gorczynska I, Fujimoto JG, Schuman JS, Duker JS. Comparison of spectral/Fourier domain optical coherence tomography instruments for assessment of normal macular thickness. *Retina*. 2010;30(2):235-45.
103. Li DQ, Choudhry N. The future of retinal imaging. *Curr Opin Ophthalmol*. 2020;31(3):199-206.
104. Wieser W, Biedermann BR, Klein T, Eigenwillig CM, Huber R. Multi-megahertz OCT: High quality 3D imaging at 20 million A-scans and 4.5 GVoxels per second. *Opt Express*. 2010;18(14):14685-704.
105. Makita S, Hong Y, Yamanari M, Yatagai T, Yasuno Y. Optical coherence angiography. *Opt Express*. 2006;14(17):7821-40.
106. Cuenca N, Ortuno-Lizaran I, Pinilla I. Cellular Characterization of OCT and Outer Retinal Bands Using Specific Immunohistochemistry Markers and Clinical Implications. *Ophthalmology*. 2018;125(3):407-22.
107. Burns SA, Elsner AE, Sapoznik KA, Warner RL, Gast TJ. Adaptive optics imaging of the human retina. *Prog Retin Eye Res*. 2019;68:1-30.
108. Lehmann T, Marcet PL, Graham DH, Dahl ER, Dubey JP. Globalization and the population structure of *Toxoplasma gondii*. *Proc Natl Acad Sci U S A*. 2006;103(30):11423-8.
109. Elmore SA, Jones JL, Conrad PA, Patton S, Lindsay DS, Dubey JP. *Toxoplasma gondii*: epidemiology, feline clinical aspects, and prevention. *Trends Parasitol*. 2010;26(4):190-6.
110. Dubey JP. The history and life cycle of *Toxoplasma gondii*. In: Weiss LM, Kim K, editors. *Toxoplasma gondii*: Academic Press; 2020. p. 1-19.

111. McLeod R, Cohen W, Dovgin S, Finkelstein L, Boyer KM. Human *Toxoplasma* infection. In: Weiss LM, Kim K, editors. *Toxoplasma gondii*: Academic Press; 2020. p. 117-227.
112. Dubey JP, Lindsay DS, Speer CA. Structures of *Toxoplasma gondii* tachyzoites, bradyzoites, and sporozoites and biology and development of tissue cysts. *Clin Microbiol Rev.* 1998;11(2):267-99.
113. Gras L, Gilbert RE, Wallon M, Peyron F, Cortina-Borja M. Duration of the IgM response in women acquiring *Toxoplasma gondii* during pregnancy: implications for clinical practice and cross-sectional incidence studies. *Epidemiol Infect.* 2004;132(3):541-8.
114. Greigert V, Di Foggia E, Filisetti D, Villard O, Pfaff AW, Sauer A, Candolfi E. When biology supports clinical diagnosis: review of techniques to diagnose ocular toxoplasmosis. *Br J Ophthalmol.* 2019;103(7):1008-12.
115. Bigna JJ, Tochie JN, Tounouga DN, Bekolo AO, Ymele NS, Youda EL, Sime PS, Nansseu JR. Global, regional, and country seroprevalence of *Toxoplasma gondii* in pregnant women: a systematic review, modelling and meta-analysis. *Sci Rep.* 2020;10(1):12102.
116. Bowie WR, King AS, Werker DH, Isaac-Renton JL, Bell A, Eng SB, Marion SA. Outbreak of toxoplasmosis associated with municipal drinking water. The BC *Toxoplasma* Investigation Team. *Lancet.* 1997;350(9072):173-7.
117. Silveira C, Muccioli C, Holland GN, Jones JL, Yu F, de Paulo A, Belfort R, Jr. Ocular Involvement Following an Epidemic of *Toxoplasma gondii* Infection in Santa Isabel do Ivaí, Brazil. *Am J Ophthalmol.* 2015;159(6):1013-21 e3.
118. Holland GN. Ocular toxoplasmosis: a global reassessment. Part I: epidemiology and course of disease. *Am J Ophthalmol.* 2003;136(6):973-88.
119. Glasner PD, Silveira C, Kruszon-Moran D, Martins MC, Burnier Junior M, Silveira S, Camargo ME, Nussenblatt RB, Kaslow RA, Belfort Junior R. An unusually high

- prevalence of ocular toxoplasmosis in southern Brazil. *Am J Ophthalmol.* 1992;114(2):136-44.
120. Elbaz H, Schulz A, Ponto KA, Nickels S, Pfeiffer N, Mirshahi A, Peto T. Posterior segment eye lesions: prevalence and associations with ocular and systemic parameters: results from the Gutenberg Health Study. *Graefes Arch Clin Exp Ophthalmol.* 2019;257(10):2127-35.
 121. Abu EK, Boampong JN, Amoabeng JK, Ilechie AA, Kyei S, Owusu-Ansah A, Boadi-Kusi SB, Amoani B, Ayi I. Epidemiology of Ocular Toxoplasmosis in Three Community Surveys in the Central Region of Ghana, West Africa. *Ophthalmic Epidemiol.* 2016;23(1):14-9.
 122. Hou JH, Patel SS, Farooq AV, Qadir AA, Tessler HH, Goldstein DA. Decline in Ocular Toxoplasmosis over 40 Years at a Tertiary Referral Practice in the United States. *Ocul Immunol Inflamm.* 2018;26(4):577-83.
 123. Pavesio CE, Lightman S. *Toxoplasma gondii* and ocular toxoplasmosis: pathogenesis. *Br J Ophthalmol.* 1996;80(12):1099-107.
 124. Aleixo AL, Curi AL, Benchimol EI, Amendoeira MR. Toxoplasmic Retinochoroiditis: Clinical Characteristics and Visual Outcome in a Prospective Study. *PLoS Negl Trop Dis.* 2016;10(5):e0004685.
 125. Holland GN, Engstrom RE, Jr., Glasgow BJ, Berger BB, Daniels SA, Sidikaro Y, Harmon JA, Fischer DH, Boyer DS, Rao NA, et al. Ocular toxoplasmosis in patients with the acquired immunodeficiency syndrome. *Am J Ophthalmol.* 1988;106(6):653-67.
 126. de-la-Torre A, Gomez-Marin J. Disease of the Year 2019: Ocular Toxoplasmosis in HIV-infected Patients. *Ocul Immunol Inflamm.* 2020:1-9.
 127. Lie S, Vieira BR, Arruda S, Simoes M, Ashander LM, Furtado JM, Smith JR. Molecular Basis of The Retinal Pigment Epithelial Changes That Characterize The Ocular Lesion in Toxoplasmosis. *Microorganisms.* 2019;7(10).

128. Rothova A, Meenken C, Buitenhuis HJ, Brinkman CJ, Baarsma GS, Boen-Tan TN, de Jong PT, Klaassen-Broekema N, Schweitzer CM, Timmerman Z, et al. Therapy for ocular toxoplasmosis. *Am J Ophthalmol.* 1993;115(4):517-23.
129. Pradhan E, Bhandari S, Gilbert RE, Stanford M. Antibiotics versus no treatment for toxoplasma retinochoroiditis. *Cochrane Database Syst Rev.* 2016(5):CD002218.
130. Jasper S, Vedula SS, John SS, Horo S, Sepah YJ, Nguyen QD. Corticosteroids as adjuvant therapy for ocular toxoplasmosis. *Cochrane Database Syst Rev.* 2017;1:CD007417.
131. Holland GN. Ocular toxoplasmosis: a global reassessment. Part II: disease manifestations and management. *Am J Ophthalmol.* 2004;137(1):1-17.
132. London NJ, Hovakimyan A, Cubillan LD, Siverio CD, Jr., Cunningham ET, Jr. Prevalence, clinical characteristics, and causes of vision loss in patients with ocular toxoplasmosis. *Eur J Ophthalmol.* 2011;21(6):811-9.
133. Yates WB, Chiong F, Zagora S, Post JJ, Wakefield D, McCluskey P. Ocular Toxoplasmosis in a Tertiary Referral Center in Sydney Australia-Clinical Features, Treatment, and Prognosis. *Asia Pac J Ophthalmol (Phila).* 2019;8(4):280-4.
134. Scherrer J, Iliev ME, Halberstadt M, Kodjikian L, Garweg JG. Visual function in human ocular toxoplasmosis. *Br J Ophthalmol.* 2007;91(2):233-6.
135. Wilder HC. Toxoplasma chorioretinitis in adults; a preliminary study of forty-one cases diagnosed by microscopic examination. *AMA Arch Ophthalmol.* 1952;47(4):425.
136. Wilder HC. Toxoplasma chorioretinitis in adults. *AMA Arch Ophthalmol.* 1952;48(2):127-36.
137. Miyamoto C, Mattos Neto RB, Cesare SD, Belfort Junior R, Burnier MN, Jr. Use of CD25 as an immunohistochemical marker for acquired ocular toxoplasmosis. *Arq Bras Oftalmol.* 2010;73(5):443-6.

138. Zscheile FP. Recurrent Toxoplasmic Retinitis with Weakly Positive Methylene Blue Dye Test. *Arch Ophthalmol*. 1964;71:645-8.
139. Cerutti A, Blanchard N, Besteiro S. The Bradyzoite: A Key Developmental Stage for the Persistence and Pathogenesis of Toxoplasmosis. *Pathogens*. 2020;9(3).
140. Waldman BS, Schwarz D, Wadsworth MH, 2nd, Saeij JP, Shalek AK, Lourido S. Identification of a Master Regulator of Differentiation in *Toxoplasma*. *Cell*. 2020;180(2):359-72.e16.
141. Watts E, Zhao Y, Dhara A, Eller B, Patwardhan A, Sinai AP. Novel Approaches Reveal that *Toxoplasma gondii* Bradyzoites within Tissue Cysts Are Dynamic and Replicating Entities In Vivo. *MBio*. 2015;6(5):e01155-15.
142. Pernas L. mSphere of Influence: Finding a Direction-How Do Mitochondria Know Where To Go? *mSphere*. 2019;4(4).
143. Chimelli L. A morphological approach to the diagnosis of protozoal infections of the central nervous system. *Patholog Res Int*. 2011;2011:290853.
144. Nicholson DH, Wolchok EB. Ocular toxoplasmosis in an adult receiving long-term corticosteroid therapy. *Arch Ophthalmol*. 1976;94(2):248-54.
145. Friedman AH. The retinal lesions of the acquired immune deficiency syndrome. *Trans Am Ophthalmol Soc*. 1984;82:447-91.
146. Johnston RL, Tufail A, Lightman S, Luthert PJ, Pavesio CE, Cooling RJ, Charteris D. Retinal and choroidal biopsies are helpful in unclear uveitis of suspected infectious or malignant origin. *Ophthalmology*. 2004;111(3):522-8.
147. Belfort RN, Rasmussen S, Kherani A, Lodha N, Williams G, Fernandes BF, Burnier MN, Jr. Bilateral progressive necrotizing retinochoroiditis in an immunocompromised patient: histopathological diagnosis. *Acta Ophthalmol*. 2010;88(5):614-5.

148. Bottos J, Miller RH, Belfort RN, Macedo AC, Group UT, Belfort R, Jr., Grigg ME. Bilateral retinochoroiditis caused by an atypical strain of *Toxoplasma gondii*. *Br J Ophthalmol*. 2009;93(11):1546-50.
149. Imai H, Azumi A, Nagai T, Yamamoto H, Negi A, Ohbayashi C. A case of ocular toxoplasmosis: direct proof of the protozoan infection by retinal biopsy. *Retin Cases Brief Rep*. 2008;2(1):76-9.
150. Moshfeghi DM, Dodds EM, Couto CA, Santos CI, Nicholson DH, Lowder CY, Davis JL. Diagnostic approaches to severe, atypical toxoplasmosis mimicking acute retinal necrosis. *Ophthalmology*. 2004;111(4):716-25.
151. Parke DW, 2nd, Font RL. Diffuse toxoplasmic retinochoroiditis in a patient with AIDS. *Arch Ophthalmol*. 1986;104(4):571-5.
152. Rao NA, Font RL. Toxoplasmic retinochoroiditis: electron-microscopic and immunofluorescence studies of formalin-fixed tissue. *Arch Ophthalmol*. 1977;95(2):273-7.
153. Singer MA, Hagler WS, Grossniklaus HE. *Toxoplasma gondii* retinochoroiditis after liver transplantation. *Retina*. 1993;13(1):40-5.
154. Yeo JH, Jakobiec FA, Iwamoto T, Richard G, Kreissig I. Opportunistic toxoplasmic retinochoroiditis following chemotherapy for systemic lymphoma. A light and electron microscopic study. *Ophthalmology*. 1983;90(8):885-98.
155. Greven CM, Teot LA. Cytologic identification of *Toxoplasma gondii* from vitreous fluid. *Arch Ophthalmol*. 1994;112(8):1086-8.
156. Crosson JN, Laird PW, Grossniklaus HE, Hendrick AM. *Toxoplasma* chorioretinitis diagnosed by histopathology in a patient with AIDS. *Retin Cases Brief Rep*. 2015;9(2):162-3.
157. Heinemann MH, Gold JM, Maisel J. Bilateral toxoplasma retinochoroiditis in a patient with acquired immune deficiency syndrome. *Retina*. 1986;6(4):224-7.

158. Kharel Sitaula R, Joshi SN, Sah R, Khadka S, Khatri Kc A, Pokharel BM. Toxoplasma gondii bradyzoites and tachyzoites isolation from vitreous of atypical necrotizing retinitis. *J Ophthalmic Inflamm Infect*. 2018;8(1):8.
159. Adan A, Sole M, Mateo C, Jean AS, Alforja S. Cytologic identification of Toxoplasma gondii from subretinal aspirate. *Acta Ophthalmol*. 2012;90(4):392-3.
160. Nijhawan R, Bansal R, Gupta N, Beke N, Kulkarni P, Gupta A. Intraocular cysts of toxoplasma gondii in patients with necrotizing retinitis following periocular/intraocular triamcinolone injection. *Ocul Immunol Inflamm*. 2013;21(5):396-9.
161. Fowler SC, Capiz-Correa DR, Grossniklaus HE, Shadowen RD, Reichstein DA. Ocular Toxoplasmosis Mimicking Choroidal Metastasis From Colorectal Adenocarcinoma. *Journal of VitreoRetinal Diseases*. 2018;2(6):384-7.
162. Jacobs L, Fair JR, Bickerton JH. Adult ocular toxoplasmosis; report of a parasitologically proved case. *AMA Arch Ophthalmol*. 1954;52(1):63-71.
163. Moorthy RS, Smith RE, Rao NA. Progressive ocular toxoplasmosis in patients with acquired immunodeficiency syndrome. *Am J Ophthalmol*. 1993;115(6):742-7.
164. Goldenberg D, Goldstein M, Loewenstein A, Habet-Wilner Z. Vitreal, retinal, and choroidal findings in active and scarred toxoplasmosis lesions: a prospective study by spectral-domain optical coherence tomography. *Graefes Arch Clin Exp Ophthalmol*. 2013;251(8):2037-45.
165. Grossniklaus HE, Specht CS, Allaire G, Leavitt JA. Toxoplasma gondii retinochoroiditis and optic neuritis in acquired immune deficiency syndrome. Report of a case. *Ophthalmology*. 1990;97(10):1342-6.
166. Hogan MJ, Zweigart PA, Lewis A. Recovery of toxoplasma from a human eye. *AMA Arch Ophthalmol*. 1958;60(4 Part 1):548-54.
167. Smith TJ, Brandt WE, Swanson JL, McCown JM, Buescher EL. Physical and biological properties of dengue-2 virus and associated antigens. *J Virol*. 1970;5(4):524-32.

168. Zhang X, Sheng J, Plevka P, Kuhn RJ, Diamond MS, Rossmann MG. Dengue structure differs at the temperatures of its human and mosquito hosts. *Proc Natl Acad Sci U S A*. 2013;110(17):6795-9.
169. Kuhn RJ, Zhang W, Rossmann MG, Pletnev SV, Corver J, Lenches E, Jones CT, Mukhopadhyay S, Chipman PR, Strauss EG, Baker TS, Strauss JH. Structure of dengue virus: implications for flavivirus organization, maturation, and fusion. *Cell*. 2002;108(5):717-25.
170. Wilder-Smith A, Ooi EE, Horstick O, Wills B. Dengue. *Lancet*. 2019;393(10169):350-63.
171. Glasner DR, Puerta-Guardo H, Beatty PR, Harris E. The Good, the Bad, and the Shocking: The Multiple Roles of Dengue Virus Nonstructural Protein 1 in Protection and Pathogenesis. *Annu Rev Virol*. 2018;5(1):227-53.
172. Zeidler JD, Fernandes-Siqueira LO, Barbosa GM, Da Poian AT. Non-Canonical Roles of Dengue Virus Non-Structural Proteins. *Viruses*. 2017;9(3).
173. Aguirre S, Luthra P, Sanchez-Aparicio MT, Maestre AM, Patel J, Lamothe F, Fredericks AC, Tripathi S, Zhu T, Pintado-Silva J, Webb LG, Bernal-Rubio D, Solovyov A, Greenbaum B, Simon V, Basler CF, Mulder LC, Garcia-Sastre A, Fernandez-Sesma A. Dengue virus NS2B protein targets cGAS for degradation and prevents mitochondrial DNA sensing during infection. *Nat Microbiol*. 2017;2:17037.
174. Yacoub S, Mongkolsapaya J, Sreaton G. Recent advances in understanding dengue. *F1000Res*. 2016;5.
175. Begum F, Das S, Mukherjee D, Ray U. Hijacking the Host Immune Cells by Dengue Virus: Molecular Interplay of Receptors and Dengue Virus Envelope. *Microorganisms*. 2019;7(9).
176. Tremblay N, Freppel W, Sow AA, Chatel-Chaix L. The Interplay between Dengue Virus and the Human Innate Immune System: A Game of Hide and Seek. *Vaccines (Basel)*. 2019;7(4).

177. World Health Organization. Dengue guidelines, for diagnosis, treatment, prevention and control: World Health Organization; 2009.
178. Low GK, Ogston SA, Yong MH, Gan SC, Chee HY. Global dengue death before and after the new World Health Organization 2009 case classification: A systematic review and meta-regression analysis. *Acta Trop.* 2018;182:237-45.
179. World Health Organization. Dengue and severe dengue 2017 [cited 2017 20 October]. Available from: <http://www.who.int/mediacentre/factsheets/fs117/en/>.
180. Zeng Z, Zhan J, Chen L, Chen H, Cheng S. Global, regional, and national dengue burden from 1990 to 2017: A systematic analysis based on the global burden of disease study 2017. *EClinicalMedicine.* 2021;32:100712.
181. Messina JP, Brady OJ, Scott TW, Zou C, Pigott DM, Duda KA, Bhatt S, Katzelnick L, Howes RE, Battle KE, Simmons CP, Hay SI. Global spread of dengue virus types: mapping the 70 year history. *Trends Microbiol.* 2014;22(3):138-46.
182. Sabin AB. Research on dengue during World War II. *Am J Trop Med Hyg.* 1952;1(1):30-50.
183. Halstead SB, Nimmannitya S, Yamarat C, Russell PK. Hemorrhagic fever in Thailand; recent knowledge regarding etiology. *Jpn J Med Sci Biol.* 1967;20 Suppl:96-103.
184. Halstead S. Recent advances in understanding dengue. *F1000Res.* 2019;8.
185. Neufeldt CJ, Cortese M, Acosta EG, Bartenschlager R. Rewiring cellular networks by members of the Flaviviridae family. *Nat Rev Microbiol.* 2018;16(3):125-42.
186. Halstead SB, Dans LF. Dengue infection and advances in dengue vaccines for children. *Lancet Child Adolesc Health.* 2019;3(10):734-41.
187. Gill W. Ocular symptoms in dengue based on analysis of 1241 cases *Arch Ophthalmol.* 1928;57:628-38.

188. Weymann MF. Some cases of ocular complication during an epidemic of dengue fever. *American Journal of Ophthalmology*. 1929;12(8):708.
189. Weymann MF. The ocular complications of dengue fever during the last epidemic in Greece. *American Journal of Ophthalmology*. 1929;12(8):708.
190. Richardson S. Ocular Symptoms and Complications Observed in Dengue. *Trans Am Ophthalmol Soc*. 1933;31:450-77.
191. Teoh S, Chan DP, Nah G, Rajagopalan R, Laude A, Ang B, Barkham T, Chee CK, Lim TH, Goh KY. A Re-Look at Ocular Complications in Dengue Fever and Dengue Haemorrhagic Fever. *Dengue Bulletin WHO Regional Office for South-East Asia*. 2006;30:184-90.
192. Bacsal KE, Chee SP, Cheng CL, Flores JV. Dengue-associated maculopathy. *Arch Ophthalmol*. 2007;125(4):501-10.
193. Su DH, Bacsal K, Chee SP, Flores JV, Lim WK, Cheng BC, Jap AH, Dengue Maculopathy Study G. Prevalence of dengue maculopathy in patients hospitalized for dengue fever. *Ophthalmology*. 2007;114(9):1743-7.
194. Chee E, Sims JL, Jap A, Tan BH, Oh H, Chee SP. Comparison of prevalence of dengue maculopathy during two epidemics with differing predominant serotypes. *Am J Ophthalmol*. 2009;148(6):910-3.
195. Teoh SC, Chee CK, Laude A, Goh KY, Barkham T, Ang BS, Eye Institute Dengue-related Ophthalmic Complications W. Optical coherence tomography patterns as predictors of visual outcome in dengue-related maculopathy. *Retina*. 2010;30(3):390-8.
196. Li M, Zhang X, Ji Y, Ye B, Wen F. Acute Macular Neuroretinopathy in Dengue Fever: Short-term Prospectively Followed Up Case Series. *JAMA Ophthalmol*. 2015;133(11):1329-33.
197. Bhavsar KV, Lin S, Rahimy E, Joseph A, Freund KB, Sarraf D, Cunningham ET, Jr. Acute macular neuroretinopathy: A comprehensive review of the literature. *Surv Ophthalmol*. 2016;61(5):538-65.

198. Munk MR, Jampol LM, Cunha Souza E, de Andrade GC, Esmaili DD, Sarraf D, Fawzi AA. New associations of classic acute macular neuroretinopathy. *Br J Ophthalmol*. 2016;100(3):389-94.
199. Aggarwal K, Agarwal A, Katoch D, Sharma M, Gupta V. Optical coherence tomography angiography features of acute macular neuroretinopathy in dengue fever. *Indian J Ophthalmol*. 2017;65(11):1235-8.
200. Tan CS, Teoh SC, Chan DP, Wong IB, Lim TH. Dengue retinopathy manifesting with bilateral vasculitis and macular oedema. *Eye (Lond)*. 2007;21(6):875-7.
201. Koundanya VV, Chowdhary N, Agarwal M, Katre P. Secondary dengue retinitis with associated occlusive retinal vasculitis. *J Ophthalmic Inflamm Infect*. 2019;9(1):7.
202. Goldhardt R, Patel H, Davis JL. Acute Posterior Multifocal Placoid Pigment Epitheliopathy Following Dengue Fever: A New Association for an Old Disease. *Ocul Immunol Inflamm*. 2016;24(6):610-4.
203. Tan MH, Tan PE, Wong EN, Chen FK. Structure and function correlation in a patient with dengue-associated maculopathy. *Clin Exp Ophthalmol*. 2014;42(5):504-7.
204. Chia A, Luu CD, Mathur R, Cheng B, Chee SP. Electrophysiological findings in patients with dengue-related maculopathy. *Arch Ophthalmol*. 2006;124(10):1421-6.
205. Carr JM, Ashander LM, Calvert JK, Ma Y, Aloia A, Bracho GG, Chee SP, Appukuttan B, Smith JR. Molecular Responses of Human Retinal Cells to Infection with Dengue Virus. *Mediators Inflamm*. 2017;2017:3164375.
206. Singh PK, Khatri I, Jha A, Preto CD, Spindler KR, Arumugaswami V, Giri S, Kumar A, Bhasin MK. Determination of system level alterations in host transcriptome due to Zika virus (ZIKV) Infection in retinal pigment epithelium. *Sci Rep*. 2018;8(1):11209.
207. Soe HJ, Khan AM, Manikam R, Samudi Raju C, Vanhoutte P, Sekaran SD. High dengue virus load differentially modulates human microvascular endothelial barrier function during early infection. *J Gen Virol*. 2017;98(12):2993-3007.

208. Zhu S, Luo H, Liu H, Ha Y, Mays ER, Lawrence RE, Winkelmann E, Barrett AD, Smith SB, Wang M, Wang T, Zhang W. p38MAPK plays a critical role in induction of a pro-inflammatory phenotype of retinal Müller cells following Zika virus infection. *Antiviral Res.* 2017;145:70-81.
209. Agarwal A, Aggarwal K, Dogra M, Kumar A, Akella M, Katoch D, Bansal R, Singh R, Gupta V, Group OS. Dengue-Induced Inflammatory, Ischemic Foveolitis and Outer Maculopathy: A Swept-Source Imaging Evaluation. *Ophthalmol Retina.* 2019;3(2):170-7.
210. Messaoudi I, Amarasinghe GK, Basler CF. Filovirus pathogenesis and immune evasion: insights from Ebola virus and Marburg virus. *Nat Rev Microbiol.* 2015;13(11):663-76.
211. Kuhn JH, Amarasinghe GK, Basler CF, Bavari S, Bukreyev A, Chandran K, Crozier I, Dolnik O, Dye JM, Formenty PBH, Griffiths A, Hewson R, Kobinger GP, Leroy EM, Muhlberger E, Netesov capital En CiCtCiReCoCvCcESCiCeCgCiCsi, Palacios G, Palyi B, Paweska JT, Smither SJ, Takada A, Towner JS, Wahl V, Ictv Report C. ICTV Virus Taxonomy Profile: Filoviridae. *J Gen Virol.* 2019;100(6):911-2.
212. Goldstein T, Anthony SJ, Gbakima A, Bird BH, Bangura J, Tremeau-Bravard A, Belaganahalli MN, Wells HL, Dhanota JK, Liang E, Grodus M, Jangra RK, DeJesus VA, Lasso G, Smith BR, Jambai A, Kamara BO, Kamara S, Bangura W, Monagin C, Shapira S, Johnson CK, Saylor K, Rubin EM, Chandran K, Lipkin WI, Mazet JAK. The discovery of Bombali virus adds further support for bats as hosts of ebolaviruses. *Nat Microbiol.* 2018;3(10):1084-9.
213. Martell HJ, Masterson SG, McGreig JE, Michaelis M, Wass MN. Is the Bombali virus pathogenic in humans? *Bioinformatics.* 2019;35(19):3553-8.
214. Kuhn JH, Adachi T, Adhikari NKJ, Arribas JR, Bah IE, Bausch DG, Bhadelia N, Borchert M, Brantsaeter AB, Brett-Major DM, Burgess TH, Chertow DS, Chute CG, Cieslak TJ, Colebunders R, Crozier I, Davey RT, de Clerck H, Delgado R, Evans L, Fallah M, Fischer WA, 2nd, Fletcher TE, Fowler RA, Grunewald T, Hall A, Hewlett A, Hoepelman AIM, Houlihan CF, Ippolito G, Jacob ST, Jacobs M, Jakob R, Jacquerioz

- FA, Kaiser L, Kalil AC, Kamara RF, Kapetshi J, Klenk HD, Kobinger G, Kortepeter MG, Kraft CS, Kratz T, Bosa HSK, Lado M, Lamontagne F, Lane HC, Lobel L, Lutwama J, Lyon GM, 3rd, Massaquoi MBF, Massaquoi TA, Mehta AK, Makuma VM, Murthy S, Musoke TS, Muyembe-Tamfum JJ, Nakyeyune P, Nanclares C, Nanyunja M, Nsio-Mbeta J, O'Dempsey T, Paweska JT, Peters CJ, Piot P, Rapp C, Renaud B, Ribner B, Sabeti PC, Schieffelin JS, Slenczka W, Soka MJ, Sprecher A, Strong J, Swanepoel R, Uyeki TM, van Herp M, Vetter P, Wohl DA, Wolf T, Wolz A, Wurie AH, Yoti Z. New filovirus disease classification and nomenclature. *Nat Rev Microbiol.* 2019;17(5):261-3.
215. Misasi J, Sullivan NJ. Camouflage and misdirection: the full-on assault of ebola virus disease. *Cell.* 2014;159(3):477-86.
216. Basler CF, Krogan NJ, Leung DW, Amarasinghe GK. Virus and host interactions critical for filoviral RNA synthesis as therapeutic targets. *Antiviral Res.* 2019;162:90-100.
217. Jacob ST, Crozier I, Fischer WA, 2nd, Hewlett A, Kraft CS, Vega MA, Soka MJ, Wahl V, Griffiths A, Bollinger L, Kuhn JH. Ebola virus disease. *Nat Rev Dis Primers.* 2020;6(1):13.
218. Uyeki TM, Mehta AK, Davey RT, Jr., Liddell AM, Wolf T, Vetter P, Schmiedel S, Grunewald T, Jacobs M, Arribas JR, Evans L, Hewlett AL, Brantsaeter AB, Ippolito G, Rapp C, Hoepelman AI, Gutman J, Working Group of the USECNoCMoEVDpitUS, Europe. Clinical Management of Ebola Virus Disease in the United States and Europe. *N Engl J Med.* 2016;374(7):636-46.
219. Group PIW, Multi-National PIIST, Davey RT, Jr., Dodd L, Proschan MA, Neaton J, Neuhaus Nordwall J, Koopmeiners JS, Beigel J, Tierney J, Lane HC, Fauci AS, Massaquoi MBF, Sahr F, Malvy D. A Randomized, Controlled Trial of ZMapp for Ebola Virus Infection. *N Engl J Med.* 2016;375(15):1448-56.
220. van Griensven J, Edwards T, de Lamballerie X, Semple MG, Gallian P, Baize S, Horby PW, Raoul H, Magassouba N, Antierens A, Lomas C, Faye O, Sall AA, Fransen K, Buyze J, Ravinetto R, Tiberghien P, Claeys Y, De Crop M, Lynen L, Bah EI, Smith PG,

- Delamou A, De Weggheleire A, Haba N, Ebola-Tx C. Evaluation of Convalescent Plasma for Ebola Virus Disease in Guinea. *N Engl J Med*. 2016;374(1):33-42.
221. Samai M, Seward JF, Goldstein ST, Mahon BE, Lisk DR, Widdowson MA, Jalloh MI, Schrag SJ, Idriss A, Carter RJ, Dawson P, Kargbo SAS, Leigh B, Bawoh M, Legardy-Williams J, Deen G, Carr W, Callis A, Lindblad R, Russell JBW, Petrie CR, Fombah AE, Kargbo B, McDonald W, Jarrett OD, Walker RE, Gargiullo P, Bash-Taqi D, Gibson L, Fofanah AB, Schuchat A, Team SS. The Sierra Leone Trial to Introduce a Vaccine Against Ebola: An Evaluation of rVSVG-ZEBOV-GP Vaccine Tolerability and Safety During the West Africa Ebola Outbreak. *J Infect Dis*. 2018;217(suppl_1):S6-S15.
222. Clarke DK, Xu R, Matassov D, Latham TE, Ota-Setlik A, Gerardi CS, Luckay A, Witko SE, Hermida L, Higgins T, Tremblay M, Sciotto-Brown S, Chen T, Egan MA, Rusnak JM, Ward LA, Eldridge JH. Safety and immunogenicity of a highly attenuated rVSVN4CT1-EBOVGP1 Ebola virus vaccine: a randomised, double-blind, placebo-controlled, phase 1 clinical trial. *Lancet Infect Dis*. 2020;20(4):455-66.
223. World Health Organization. Sierra Leone: Helping the Ebola survivors turn the page [webpage]. 2014 [cited 2018 19 June]. Available from: <http://www.who.int/features/2014/post-ebola-syndrome/en/>.
224. Vetter P, Kaiser L, Schibler M, Ciglenecki I, Bausch DG. Sequelae of Ebola virus disease: the emergency within the emergency. *Lancet Infect Dis*. 2016;16(6):e82-e91.
225. Epstein L, Wong KK, Kallen AJ, Uyeki TM. Post-Ebola Signs and Symptoms in U.S. Survivors. *N Engl J Med*. 2015;373(25):2484-6.
226. Varkey JB, Shantha JG, Crozier I, Kraft CS, Lyon GM, Mehta AK, Kumar G, Smith JR, Kainulainen MH, Whitmer S, Stroher U, Uyeki TM, Ribner BS, Yeh S. Persistence of Ebola Virus in Ocular Fluid during Convalescence. *N Engl J Med*. 2015;372(25):2423-7.
227. Hereth-Hebert E, Bah MO, Etard JF, Sow MS, Resnikoff S, Fardeau C, Toure A, Ouendeno AN, Sagnon IC, March L, Izard S, Lama PL, Barry M, Delaporte E,

- Postebogui Study G. Ocular Complications in Survivors of the Ebola Outbreak in Guinea. *Am J Ophthalmol.* 2017;175:114-21.
228. Mattia JG, Vandy MJ, Chang JC, Platt DE, Dierberg K, Bausch DG, Brooks T, Conteh S, Crozier I, Fowler RA, Kamara AP, Kang C, Mahadevan S, Mansaray Y, Marcell L, McKay G, O'Dempsey T, Parris V, Pinto R, Rangel A, Salam AP, Shantha J, Wolfman V, Yeh S, Chan AK, Mishra S. Early clinical sequelae of Ebola virus disease in Sierra Leone: a cross-sectional study. *Lancet Infect Dis.* 2016;16(3):331-8.
229. Tiffany A, Vetter P, Mattia J, Dayer JA, Bartsch M, Kasztura M, Sterk E, Tijerino AM, Kaiser L, Ciglenecki I. Ebola Virus Disease Complications as Experienced by Survivors in Sierra Leone. *Clin Infect Dis.* 2016;62(11):1360-6.
230. Kibadi K, Mupapa K, Kuvula K, Massamba M, Ndaberey D, Muyembe-Tamfum JJ, Bwaka MA, De Roo A, Colebunders R. Late ophthalmologic manifestations in survivors of the 1995 Ebola virus epidemic in Kikwit, Democratic Republic of the Congo. *J Infect Dis.* 1999;179 Suppl 1:S13-4.
231. Steptoe PJ, Scott JT, Harding SP, Beare NAV, Semple MG, Vandy MJ, Sahr F. Ocular Complications in Survivors of the Ebola Outbreak in Guinea. *Am J Ophthalmol.* 2017;181:180.
232. Larsen T, Stevens EL, Davis KJ, Geisbert JB, Daddario-DiCaprio KM, Jahrling PB, Hensley LE, Geisbert TW. Pathologic findings associated with delayed death in nonhuman primates experimentally infected with Zaire Ebola virus. *J Infect Dis.* 2007;196 Suppl 2:S323-8.
233. Alves DA, Honko AN, Kortepeter MG, Sun M, Johnson JC, Lugo-Roman LA, Hensley LE. Necrotizing Scleritis, Conjunctivitis, and Other Pathologic Findings in the Left Eye and Brain of an Ebola Virus-Infected Rhesus Macaque (*Macaca mulatta*) With Apparent Recovery and a Delayed Time of Death. *J Infect Dis.* 2016;213(1):57-60.
234. Jacobs M, Rodger A, Bell DJ, Bhagani S, Cropley I, Filipe A, Gifford RJ, Hopkins S, Hughes J, Jabeen F, Johannessen I, Karageorgopoulos D, Lackenby A, Lester R, Liu RS, MacConnachie A, Mahungu T, Martin D, Marshall N, Mepham S, Orton R, Palmarini M, Patel M, Perry C, Peters SE, Porter D, Ritchie D, Ritchie ND, Seaton RA,

- Sreenu VB, Templeton K, Warren S, Wilkie GS, Zambon M, Gopal R, Thomson EC. Late Ebola virus relapse causing meningoencephalitis: a case report. *Lancet*. 2016;388(10043):498-503.
235. Smith JR, Todd S, Ashander LM, Charitou T, Ma Y, Yeh S, Crozier I, Michael MZ, Appukuttan B, Williams KA, Lynn DJ, Marsh GA. Retinal Pigment Epithelial Cells are a Potential Reservoir for Ebola Virus in the Human Eye. *Transl Vis Sci Technol*. 2017;6(4):12.
236. Speranza E, Connor JH. Host Transcriptional Response to Ebola Virus Infection. *Vaccines (Basel)*. 2017;5(3).
237. Zeng X, Blancett CD, Koistinen KA, Schellhase CW, Bearss JJ, Radoshitzky SR, Honnold SP, Chance TB, Warren TK, Froude JW, Cashman KA, Dye JM, Bavari S, Palacios G, Kuhn JH, Sun MG. Identification and pathological characterization of persistent asymptomatic Ebola virus infection in rhesus monkeys. *Nat Microbiol*. 2017;2:17113.
238. Steptoe PJ, Momorie F, Fornah AD, Komba SP, Emsley E, Scott JT, Harding SP, Vandy MJ, Sahr F, Beare NAV, Semple MG. Multimodal Imaging and Spatial Analysis of Ebola Retinal Lesions in 14 Survivors of Ebola Virus Disease. *JAMA Ophthalmol*. 2018;136(6):689-93.
239. Steptoe PJ, Momorie F, Fornah AD, Komba P, Emsley E, Scott JT, Williams SJ, Harding SP, Vandy MJ, Sahr F, Beare NAV, Semple MG. Evolving Longitudinal Retinal Observations in a Cohort of Survivors of Ebola Virus Disease. *JAMA Ophthalmol*. 2020.
240. Moysidis SN, Koullisis N, Ameri H, Matsunaga D, Yi J, Isozaki VL, Kashani AH, Olmos de Koo LC. Multimodal Imaging of Geographic Areas of Retinal Darkening. *Retin Cases Brief Rep*. 2015;9(4):347-51.
241. Chen X, Liang M. Changes in Dark without Pressure. *Ophthalmol Retina*. 2018;2(10):1077.

242. Chang MY, McBeath JB, McCannel CA, McCannel TA. 'Shadow sign' in congenital hypertrophy of the retinal pigment epithelium of young myopic pigmented patients. *Eye (Lond)*. 2016;30(1):160-3.
243. Fawzi AA, Nielsen JS, Mateo-Montoya A, Somkijrungrroj T, Li HK, Gonzales J, Mauget-Faysse M, Jampol LM. Multimodal imaging of white and dark without pressure fundus lesions. *Retina*. 2014;34(12):2376-87.
244. Voigt V, Andoniou CE, Schuster IS, Oszmiana A, Ong ML, Fleming P, Forrester JV, Degli-Esposti MA. Cytomegalovirus establishes a latent reservoir and triggers long-lasting inflammation in the eye. *PLoS Pathog*. 2018;14(5):e1007040.
245. Shantha JG, Mattia JG, Goba A, Barnes KG, Ebrahim FK, Kraft CS, Hayek BR, Hartnett JN, Shaffer JG, Schieffelin JS, Sandi JD, Momoh M, Jalloh S, Grant DS, Dierberg K, Chang J, Mishra S, Chan AK, Fowler R, O'Dempsey T, Kaluma E, Hendricks T, Reiners R, Reiners M, Gess LA, K ON, Kamara S, Wurie A, Mansaray M, Acharya NR, Liu WJ, Bavari S, Palacios G, Teshome M, Crozier I, Farmer PE, Uyeki TM, Bausch DG, Garry RF, Vandy MJ, Yeh S. Ebola Virus Persistence in Ocular Tissues and Fluids (EVICT) Study: Reverse Transcription-Polymerase Chain Reaction and Cataract Surgery Outcomes of Ebola Survivors in Sierra Leone. *EBioMedicine*. 2018;30:217-24.
246. Steptoe PJ, Scott JT, Baxter JM, Parkes CK, Dwivedi R, Czanner G, Vandy MJ, Momorie F, Fornah AD, Komba P, Richards J, Sahr F, Beare NAV, Semple MG. Novel Retinal Lesion in Ebola Survivors, Sierra Leone, 2016. *Emerg Infect Dis*. 2017;23(7):1102-9.
247. Forrester JV. Ebola virus and persistent chronic infection: when does replication cease? *Ann Transl Med*. 2018;6(Suppl 1):S39.
248. Basler CF, Amarasinghe GK. Evasion of interferon responses by Ebola and Marburg viruses. *J Interferon Cytokine Res*. 2009;29(9):511-20.
249. Martines RB, Ng DL, Greer PW, Rollin PE, Zaki SR. Tissue and cellular tropism, pathology and pathogenesis of Ebola and Marburg viruses. *J Pathol*. 2015;235(2):153-74.

250. Edwards MR, Liu G, Mire CE, Sureshchandra S, Luthra P, Yen B, Shabman RS, Leung DW, Messaoudi I, Geisbert TW, Amarasinghe GK, Basler CF. Differential Regulation of Interferon Responses by Ebola and Marburg Virus VP35 Proteins. *Cell Rep.* 2016;14(7):1632-40.
251. Kuming BS, Kokoris N. Uveal involvement in Marburg virus disease. *Br J Ophthalmol.* 1977;61(4):265-6.
252. Gear JS, Cassel GA, Gear AJ, Trappler B, Clausen L, Meyers AM, Kew MC, Bothwell TH, Sher R, Miller GB, Schneider J, Koornhof HJ, Gomperts ED, Isaacson M, Gear JH. Outbreak of Marburg virus disease in Johannesburg. *Br Med J.* 1975;4(5995):489-93.
253. Cooper TK, Sword J, Johnson JC, Bonilla A, Hart R, Liu DX, Bernbaum JG, Cooper K, Jahrling PB, Hensley LE. New Insights Into Marburg Virus Disease Pathogenesis in the Rhesus Macaque Model. *J Infect Dis.* 2018;218(suppl_5):S423-S33.
254. Ashander LM, Appukuttan B, Ma Y, Gardner-Stephen D, Smith JR. Targeting Endothelial Adhesion Molecule Transcription for Treatment of Inflammatory Disease: A Proof-of-Concept Study. *Mediators Inflamm.* 2016;2016:7945848.
255. Dal Ponte S, Burguez D, Andrioli G. Outbreak of Toxoplasmosis in the City of Santa Maria, Brazil. *Prehospital and Disaster Medicine.* 2019;34(s1):s74-s.
256. Group PIS, Sneller MC, Reilly C, Badio M, Bishop RJ, Eghrari AO, Moses SJ, Johnson KL, Gayedyu-Dennis D, Hensley LE, Higgs ES, Nath A, Tuznik K, Varughese J, Jensen KS, Dighero-Kemp B, Neaton JD, Lane HC, Fallah MP. A Longitudinal Study of Ebola Sequelae in Liberia. *N Engl J Med.* 2019;380(10):924-34.
257. Heeney JL. Ebola: Hidden reservoirs. *Nature.* 2015;527(7579):453-5.
258. Passos ADC, Bollela VR, Furtado JMF, Lucena MM, Bellissimo-Rodrigues F, Paula JS, Melo LVL, Rodrigues MLV. Prevalence and risk factors of toxoplasmosis among adults in a small Brazilian city. *Rev Soc Bras Med Trop.* 2018;51(6):781-7.
259. Butler NJ, Furtado JM, Winthrop KL, Smith JR. Ocular toxoplasmosis II: clinical features, pathology and management. *Clin Exp Ophthalmol.* 2013;41(1):95-108.

260. Holland GN, Buhles WC, Jr., Mastre B, Kaplan HJ. A controlled retrospective study of ganciclovir treatment for cytomegalovirus retinopathy. Use of a standardized system for the assessment of disease outcome. UCLA CMV Retinopathy. Study Group. Arch Ophthalmol. 1989;107(12):1759-66.
261. Australia. S. Safety in laboratories Part 3: Microbiological safety and containment, AS/NZS 2243.3:2010 Standards Australia; 2010 [6th:[Available from: https://infostore.saiglobal.com/en-au/Standards/AS-NZS-2243-3-2010-117305_SAIG_AS_AS_273922/].
262. Dunn KC, Aotaki-Keen AE, Putkey FR, Hjelmeland LM. ARPE-19, a human retinal pigment epithelial cell line with differentiated properties. Exp Eye Res. 1996;62(2):155-69.
263. Ammerman NC, Beier-Sexton M, Azad AF. Growth and maintenance of Vero cell lines. Curr Protoc Microbiol. 2008;Appendix 4:Appendix 4E.
264. Igarashi A. Isolation of a Singh's Aedes albopictus cell clone sensitive to Dengue and Chikungunya viruses. J Gen Virol. 1978;40(3):531-44.
265. The National Health and Medical Research Council tARCatAV-CC. National Statement on Ethical Conduct in Human Research (Publication E72). Commonwealth of Australia, Canberra: National Health and Medical Research Council; 2015. Available from: www.nhmrc.gov.au/guidelines/publications/e72.
266. National Health and Medical Research Council ARCaUA. Australian Code for Responsible Conduct of Research (Publication R41). Commonwealth of Australia, Canberra: National Health and Medical Research Council; 2018. Available from: www.nhmrc.gov.au/guidelines/publications/r41.
267. Roth JS, Lee TD, Cheff DM, Gosztyla ML, Asawa RR, Danchik C, Michael S, Simeonov A, Klumpp-Thomas C, Wilson KM, Hall MD. Keeping It Clean: The Cell Culture Quality Control Experience at the National Center for Advancing Translational Sciences. SLAS Discov. 2020;25(5):491-7.

268. Pryor MJ, Carr JM, Hocking H, Davidson AD, Li P, Wright PJ. Replication of dengue virus type 2 in human monocyte-derived macrophages: comparisons of isolates and recombinant viruses with substitutions at amino acid 390 in the envelope glycoprotein. *Am J Trop Med Hyg.* 2001;65(5):427-34.
269. Geer LY, Marchler-Bauer A, Geer RC, Han L, He J, He S, Liu C, Shi W, Bryant SH. The NCBI BioSystems database. *Nucleic Acids Res.* 2010;38(Database issue):D492-6.
270. National Center for Biotechnology Information NLoMU. Basic Local Alignment Search Tool (BLAST) Bethesda (MD): National Library of Medicine (US), National Center for Biotechnology Information; [Available from: <https://blast.ncbi.nlm.nih.gov/Blast.cgi>].
271. Martin M. Cutadapt removes adapter sequences from high-throughput sequencing reads. 2011. 2011;17(1):3.
272. Harrow J, Frankish A, Gonzalez JM, Tapanari E, Diekhans M, Kokocinski F, Aken BL, Barrell D, Zadissa A, Searle S, Barnes I, Bignell A, Boychenko V, Hunt T, Kay M, Mukherjee G, Rajan J, Despacio-Reyes G, Saunders G, Steward C, Harte R, Lin M, Howald C, Tanzer A, Derrien T, Chrast J, Walters N, Balasubramanian S, Pei B, Tress M, Rodriguez JM, Ezkurdia I, van Baren J, Brent M, Haussler D, Kellis M, Valencia A, Reymond A, Gerstein M, Guigo R, Hubbard TJ. GENCODE: the reference human genome annotation for The ENCODE Project. *Genome Res.* 2012;22(9):1760-74.
273. Kozomara A, Griffiths-Jones S. miRBase: annotating high confidence microRNAs using deep sequencing data. *Nucleic Acids Res.* 2014;42(Database issue):D68-73.
274. Anders S, Pyl PT, Huber W. HTSeq--a Python framework to work with high-throughput sequencing data. *Bioinformatics.* 2015;31(2):166-9.
275. Love MI, Huber W, Anders S. Moderated estimation of fold change and dispersion for RNA-seq data with DESeq2. *Genome Biol.* 2014;15(12):550.
276. Duy J, Honko AN, Altamura LA, Bixler SL, Wollen-Roberts S, Wauquier N, O'Hearn A, Mucker EM, Johnson JC, Shamblin JD, Zelko J, Botto MA, Bangura J, Coomber M,

- Pitt ML, Gonzalez JP, Schoepp RJ, Goff AJ, Minogue TD. Virus-encoded miRNAs in Ebola virus disease. *Sci Rep*. 2018;8(1):6480.
277. Edgar R, Domrachev M, Lash AE. Gene Expression Omnibus: NCBI gene expression and hybridization array data repository. *Nucleic Acids Res*. 2002;30(1):207-10.
278. Barrett T, Wilhite SE, Ledoux P, Evangelista C, Kim IF, Tomashevsky M, Marshall KA, Phillippy KH, Sherman PM, Holko M, Yefanov A, Lee H, Zhang N, Robertson CL, Serova N, Davis S, Soboleva A. NCBI GEO: archive for functional genomics data sets-update. *Nucleic Acids Res*. 2013;41(Database issue):D991-5.
279. National Center for Biotechnology Information NLoMU. Gene Expression Omnibus (GEO) Bethesda (MD): National Library of Medicine (US), National Center for Biotechnology Information; [Available from: <https://www.ncbi.nlm.nih.gov/geo/query/acc.cgi>].
280. Paraskevopoulou MD, Georgakilas G, Kostoulas N, Vlachos IS, Vergoulis T, Reczko M, Filippidis C, Dalamagas T, Hatzigeorgiou AG. DIANA-microT web server v5.0: service integration into miRNA functional analysis workflows. *Nucleic Acids Res*. 2013;41(Web Server issue):W169-73.
281. Reczko M, Maragkakis M, Alexiou P, Grosse I, Hatzigeorgiou AG. Functional microRNA targets in protein coding sequences. *Bioinformatics*. 2012;28(6):771-6.
282. Agarwal V, Bell GW, Nam JW, Bartel DP. Predicting effective microRNA target sites in mammalian mRNAs. *Elife*. 2015;4.
283. Wong N, Wang X. miRDB: an online resource for microRNA target prediction and functional annotations. *Nucleic Acids Res*. 2015;43(Database issue):D146-52.
284. Xiao F, Zuo Z, Cai G, Kang S, Gao X, Li T. miRecords: an integrated resource for microRNA-target interactions. *Nucleic Acids Res*. 2009;37(Database issue):D105-10.
285. Chou CH, Chang NW, Shrestha S, Hsu SD, Lin YL, Lee WH, Yang CD, Hong HC, Wei TY, Tu SJ, Tsai TR, Ho SY, Jian TY, Wu HY, Chen PR, Lin NC, Huang HT, Yang TL, Pai CY, Tai CS, Chen WL, Huang CY, Liu CC, Weng SL, Liao KW, Hsu WL, Huang HD.

- miRTarBase 2016: updates to the experimentally validated miRNA-target interactions database. *Nucleic Acids Res.* 2016;44(D1):D239-47.
286. Ashburner M, Ball CA, Blake JA, Botstein D, Butler H, Cherry JM, Davis AP, Dolinski K, Dwight SS, Eppig JT, Harris MA, Hill DP, Issel-Tarver L, Kasarskis A, Lewis S, Matese JC, Richardson JE, Ringwald M, Rubin GM, Sherlock G. Gene ontology: tool for the unification of biology. The Gene Ontology Consortium. *Nat Genet.* 2000;25(1):25-9.
287. Shannon P, Markiel A, Ozier O, Baliga NS, Wang JT, Ramage D, Amin N, Schwikowski B, Ideker T. Cytoscape: a software environment for integrated models of biomolecular interaction networks. *Genome Res.* 2003;13(11):2498-504.
288. Bindea G, Mlecnik B, Hackl H, Charoentong P, Tosolini M, Kirilovsky A, Fridman WH, Pages F, Trajanoski Z, Galon J. ClueGO: a Cytoscape plug-in to decipher functionally grouped gene ontology and pathway annotation networks. *Bioinformatics.* 2009;25(8):1091-3.
289. Kanehisa M, Goto S. KEGG: kyoto encyclopedia of genes and genomes. *Nucleic Acids Res.* 2000;28(1):27-30.
290. Bindea G, Galon J, Mlecnik B. CluePedia Cytoscape plugin: pathway insights using integrated experimental and in silico data. *Bioinformatics.* 2013;29(5):661-3.
291. Szklarczyk D, Franceschini A, Kuhn M, Simonovic M, Roth A, Minguetz P, Doerks T, Stark M, Muller J, Bork P, Jensen LJ, von Mering C. The STRING database in 2011: functional interaction networks of proteins, globally integrated and scored. *Nucleic Acids Res.* 2011;39(Database issue):D561-8.
292. Orefice JL, Costa RA, Scott IU, Calucci D, Orefice F. Spectral optical coherence tomography findings in patients with ocular toxoplasmosis and active satellite lesions (MINAS Report 1). *Acta Ophthalmol.* 2013;91(1):e41-7.
293. Freitas-Neto CA, Cao JH, Orefice JL, Costa RA, Orefice F, Lee J, Payal A, Foster CS. Increased Submacular Choroidal Thickness in Active, Isolated, Extramacular Toxoplasmosis. *Ophthalmology.* 2016;123(1):222-4.e1.

294. Ouyang Y, Li F, Shao Q, Heussen FM, Keane PA, Stubiger N, Sadda SR, Pleyer U. Subretinal fluid in eyes with active ocular toxoplasmosis observed using spectral domain optical coherence tomography. *PLoS One*. 2015;10(5):e0127683.
295. Ouyang Y, Pleyer U, Shao Q, Keane PA, Stubiger N, Jousseaume AM, Sadda SR, Heussen FM. Evaluation of cystoid change phenotypes in ocular toxoplasmosis using optical coherence tomography. *PLoS One*. 2014;9(2):e86626.
296. Diniz B, Regatieri C, Andrade R, Maia A. Evaluation of spectral domain and time domain optical coherence tomography findings in toxoplasmic retinochoroiditis. *Clin Ophthalmol*. 2011;5:645-50.
297. Ammar F, Mahjoub A, Ben Abdesslam N, Knani L, Ghorbel M, Mahjoub H. Spectral optical coherence tomography findings in patients with ocular toxoplasmosis: A case series study. *Ann Med Surg (Lond)*. 2020;54:125-8.
298. FDA-NIH Biomarker Working Group. BEST (Biomarkers E, and other Tools) Resource [Internet]. Diagnostic Biomarker. Silver Spring (MD). Food and Drug Administration (US); National Institutes of Health (US). 2016- [cited 2020 April 16]. Available from: <https://preview.ncbi.nlm.nih.gov/books/NBK402285/>
299. FDA-NIH Biomarker Working Group. BEST (Biomarkers E, and other Tools) Resource [Internet]. . Monitoring Biomarker. Silver Spring (MD): Food and Drug Administration (US); National Institutes of Health (US). 2016 [updated 2016 Dec 22]. Available from: <https://preview.ncbi.nlm.nih.gov/books/NBK402282/>
300. Saito M, Barbazetto IA, Spaide RF. Intravitreal cellular infiltrate imaged as punctate spots by spectral-domain optical coherence tomography in eyes with posterior segment inflammatory disease. *Retina*. 2013;33(3):559-65.
301. Guagnini AP, De Potter P, Levecq L, Kozyreff A. Atypical spherical deposition on vitreoretinal interface associated with toxoplasmic chorioretinitis. *Graefes Arch Clin Exp Ophthalmol*. 2007;245(1):158-60.

302. Invernizzi A, Agarwal AK, Ravera V, Mapelli C, Riva A, Staurenghi G, McCluskey PJ, Viola F. Comparing optical coherence tomography findings in different aetiologies of infectious necrotising retinitis. *Br J Ophthalmol*. 2018;102(4):433-7.
303. Sogawa T, Hashida N, Sawa M, Nishida K. Rare Association of Perivascular Granulomatous Lesions in a Patient with Acute Retinal Necrosis. *Case Rep Ophthalmol*. 2015;6(3):373-9.
304. Auer C, Bernasconi O, Herbort CP. Indocyanine green angiography features in toxoplasmic retinochoroiditis. *Retina*. 1999;19(1):22-9.
305. Margolis R, Spaide RF. A Pilot Study of Enhanced Depth Imaging Optical Coherence Tomography of the Choroid in Normal Eyes. *American Journal of Ophthalmology*. 2009;147(5):811-5.
306. Spaide RF, Koizumi H, Pozonni MC. Enhanced Depth Imaging Spectral-Domain Optical Coherence Tomography. *American Journal of Ophthalmology*. 2008;146(4):496-500.
307. Azevedo MH, Moura GL, Camilo EN, Muccioli C, Arantes TE. Visual function and macular architecture in patients with inactive zone 2 and 3 toxoplasmic retinochoroiditis. *Arq Bras Oftalmol*. 2015;78(5):273-7.
308. Whitmore SS, Wagner AH, DeLuca AP, Drack AV, Stone EM, Tucker BA, Zeng S, Braun TA, Mullins RF, Scheetz TE. Transcriptomic analysis across nasal, temporal, and macular regions of human neural retina and RPE/choroid by RNA-Seq. *Exp Eye Res*. 2014;129:93-106.
309. Furtado JM, Ashander LM, Mohs K, Chipps TJ, Appukuttan B, Smith JR. *Toxoplasma gondii* migration within and infection of human retina. *PLoS One*. 2013;8(2):e54358.
310. Zhang T, Zhu L, Madigan MC, Liu W, Shen W, Cherepanoff S, Zhou F, Zeng S, Du J, Gillies MC. Human macular Müller cells rely more on serine biosynthesis to combat oxidative stress than those from the periphery. *Elife*. 2019;8.

311. Arantes TE, Silveira C, Holland GN, Muccioli C, Yu F, Jones JL, Goldhardt R, Lewis KG, Belfort R, Jr. Ocular Involvement Following Postnatally Acquired *Toxoplasma gondii* Infection in Southern Brazil: A 28-Year Experience. *Am J Ophthalmol.* 2015;159(6):1002-12 e2.
312. Ajamil-Rodanes S, Luis J, Bourkiza R, Girling B, Rees A, Cosgrove C, Pavesio C, Westcott M. Ocular toxoplasmosis: phenotype differences between toxoplasma IgM positive and IgM negative patients in a large cohort. *Br J Ophthalmol.* 2020.
313. Meyaard L, Schuitemaker H, Miedema F. T-cell dysfunction in HIV infection: anergy due to defective antigen-presenting cell function? *Immunol Today.* 1993;14(4):161-4.
314. Eagle RC, Jr. Optical Coherence Tomography: Clinicopathologic Correlations - The 2016 Gordon K. Klintworth Lecture. *Ocul Oncol Pathol.* 2018;4(4):203-12.
315. Adigun R, Basit H, Murray J. Necrosis, Cell (Liquefactive, Coagulative, Caseous, Fat, Fibrinoid, and Gangrenous). *StatPearls. Treasure Island (FL): StatPearls Publishing LLC.; 2020.*
316. van der Meer FJ, Faber DJ, Aalders MC, Poot AA, Vermes I, van Leeuwen TG. Apoptosis- and necrosis-induced changes in light attenuation measured by optical coherence tomography. *Lasers Med Sci.* 2010;25(2):259-67.
317. Yu S, Pang CE, Gong Y, Freund KB, Yannuzzi LA, Rahimy E, Lujan BJ, Tabandeh H, Cooney MJ, Sarraf D. The spectrum of superficial and deep capillary ischemia in retinal artery occlusion. *Am J Ophthalmol.* 2015;159(1):53-63.e1-2.
318. Tonnus W, Meyer C, Paliege A, Belavgeni A, von Massenhausen A, Bornstein SR, Hugo C, Becker JU, Linkermann A. The pathological features of regulated necrosis. *J Pathol.* 2019;247(5):697-707.
319. Huang Y, Wang S, Guo Q, Kessel S, Rubinoff I, Chan LL, Li P, Liu Y, Qiu J, Zhou C. Optical Coherence Tomography Detects Necrotic Regions and Volumetrically Quantifies Multicellular Tumor Spheroids. *Cancer Res.* 2017;77(21):6011-20.

320. Alwassia AA, Cho H, Adhi M, Duker JS, Baurnal CR. Sequential optical coherence tomography images of retinal necrosis in acute ocular toxoplasmosis. *Retin Cases Brief Rep.* 2013;7(1):98-101.
321. Invernizzi A, Agarwal A, Ravera V, Oldani M, Staurenghi G, Viola F. Optical Coherence Tomography Findings In Cytomegalovirus Retinitis: A Longitudinal Study. *Retina.* 2018;38(1):108-17.
322. Song HB, Jung BK, Kim JH, Lee YH, Choi MH, Kim JH. Investigation of tissue cysts in the retina in a mouse model of ocular toxoplasmosis: distribution and interaction with glial cells. *Parasitol Res.* 2018;117(8):2597-605.
323. McMenamin PG, Dutton GN, Hay J, Cameron S. The ultrastructural pathology of congenital murine toxoplasmic retinochoroiditis. Part I: The localization and morphology of *Toxoplasma* cysts in the retina. *Exp Eye Res.* 1986;43(4):529-43.
324. Wilson JD, Foster TH. Characterization of lysosomal contribution to whole-cell light scattering by organelle ablation. *J Biomed Opt.* 2007;12(3):030503.
325. Kurup SP, Khan S, Gill MK. Spectral domain optical coherence tomography in the evaluation and management of infectious retinitis. *Retina.* 2014;34(11):2233-41.
326. Yashiro S, Nishijima T, Yamamoto Y, Sekine Y, Yoshida-Hata N, Iida T, Oka S. Spectral domain optical coherence tomography and fundus autofluorescence findings in cytomegalovirus retinitis in HIV-infected patients. *Jpn J Ophthalmol.* 2018;62(3):373-89.
327. Jain A, Anantharaman G, Gopalakrishnan M, Narayanan S. Sequential optical coherence tomography images of early acute retinal necrosis. *Indian J Ophthalmol.* 2020;68(3):520-2.
328. Massuda A, Hone T, Leles FAG, de Castro MC, Atun R. The Brazilian health system at crossroads: progress, crisis and resilience. *BMJ Glob Health.* 2018;3(4):e000829.
329. Ishihara K, Hangai M, Kita M, Yoshimura N. Acute Vogt-Koyanagi-Harada disease in enhanced spectral-domain optical coherence tomography. *Ophthalmology.* 2009;116(9):1799-807.

330. Roy RN. Affections of the Eye Following Dengue. *Ind Med Gaz.* 1873;8(2):42-3.
331. Chan DP, Teoh SC, Tan CS, Nah GK, Rajagopalan R, Prabhakaragupta MK, Chee CK, Lim TH, Goh KY. Ophthalmic complications of dengue. *Emerg Infect Dis.* 2006;12(2):285-9.
332. Kapoor HK, Bhai S, John M, Xavier J. Ocular manifestations of dengue fever in an East Indian epidemic. *Can J Ophthalmol.* 2006;41(6):741-6.
333. Syrbe S, Kuhrt H, Gartner U, Habermann G, Wiedemann P, Bringmann A, Reichenbach A. Müller glial cells of the primate foveola: An electron microscopical study. *Exp Eye Res.* 2018;167:110-7.
334. Reichenbach A, Bringmann A. New functions of Müller cells. *Glia.* 2013;61(5):651-78.
335. Toft-Kehler AK, Skytt DM, Kolko M. A Perspective on the Müller Cell-Neuron Metabolic Partnership in the Inner Retina. *Mol Neurobiol.* 2018;55(6):5353-61.
336. Vecino E, Rodriguez FD, Ruzafa N, Pereiro X, Sharma SC. Glia-neuron interactions in the mammalian retina. *Prog Retin Eye Res.* 2016;51:1-40.
337. Spaide RF. Retinal Vascular Cystoid Macular Edema: Review And New Theory. *Retina.* 2016;36(10):1823-42.
338. Xu L, Ruan G, Dai H, Liu AC, Penn J, McMahon DG. Mammalian retinal Müller cells have circadian clock function. *Mol Vis.* 2016;22:275-83.
339. Zhao Z, Yang M, Azar SR, Soong L, Weaver SC, Sun J, Chen Y, Rossi SL, Cai J. Viral Retinopathy in Experimental Models of Zika Infection. *Invest Ophthalmol Vis Sci.* 2017;58(10):4355-65.
340. Rochet E, Appukuttan B, Ma Y, Ashander LM, Smith JR. Expression of Long Non-Coding RNAs by Human Retinal Müller Glial Cells Infected with Clonal and Exotic Virulent *Toxoplasma gondii*. *Noncoding RNA.* 2019;5(4).
341. Geller SF, Ge PS, Visel M, Greenberg KP, Flannery JG. Functional promoter testing using a modified lentiviral transfer vector. *Mol Vis.* 2007;13:730-9.

342. Klimczak RR, Koerber JT, Dalkara D, Flannery JG, Schaffer DV. A novel adeno-associated viral variant for efficient and selective intravitreal transduction of rat Müller cells. *PLoS One*. 2009;4(10):e7467.
343. Kumar A, Pandey RK, Miller LJ, Singh PK, Kanwar M. Müller glia in retinal innate immunity: a perspective on their roles in endophthalmitis. *Crit Rev Immunol*. 2013;33(2):119-35.
344. Mursalin MH, Coburn PS, Livingston E, Miller FC, Astley R, Flores-Mireles AL, Callegan MC. Bacillus S-Layer-Mediated Innate Interactions During Endophthalmitis. *Front Immunol*. 2020;11:215.
345. Gualano RC, Pryor MJ, Cauchi MR, Wright PJ, Davidson AD. Identification of a major determinant of mouse neurovirulence of dengue virus type 2 using stably cloned genomic-length cDNA. *J Gen Virol*. 1998;79 (Pt 3):437-46.
346. Heaton NS. Revisiting the concept of a cytopathic viral infection. *PLoS Pathog*. 2017;13(7):e1006409.
347. McCormick KD, Liu S, Jacobs JL, Marques ET, Jr., Sluis-Cremer N, Wang T. Development of a robust cytopathic effect-based high-throughput screening assay to identify novel inhibitors of dengue virus. *Antimicrob Agents Chemother*. 2012;56(6):3399-401.
348. Bielefeld-Sevigny M. AlphaLISA immunoassay platform- the "no-wash" high-throughput alternative to ELISA. *Assay Drug Dev Technol*. 2009;7(1):90-2.
349. Miorin L, Maestre AM, Fernandez-Sesma A, Garcia-Sastre A. Antagonism of type I interferon by flaviviruses. *Biochem Biophys Res Commun*. 2017;492(4):587-96.
350. Smith JR, Ashander LM, Ma Y, Rochet E, Furtado JM. Model Systems for Studying Mechanisms of Ocular Toxoplasmosis. *Methods Mol Biol*. 2020;2071:297-321.
351. Pfeiffer RL, Marc RE, Jones BW. Müller Cell Metabolic Signatures: Evolutionary Conservation and Disruption in Disease. *Trends Endocrinol Metab*. 2020;31(4):320-9.

352. Kawali A, Mahendradas P, Mohan A, Mallavarapu M, Shetty B. Epidemic Retinitis. *Ocul Immunol Inflamm.* 2018;1-7.
353. Mi H, Ho SL, Lim WK, Wong EP, Teoh SC. Trends in Patterns of Posterior Uveitis and Panuveitis in a Tertiary Institution in Singapore. *Ocul Immunol Inflamm.* 2015;23(4):329-38.
354. Janani MK, Durgadevi P, Padmapriya J, Malathi J, Kulandai LT, Rao Madhavan HN. First Report on Detection of Dengue Virus in the Donor Cornea. *Cornea.* 2018;37(12):1586-9.
355. Carod-Artal FJ, Wichmann O, Farrar J, Gascón J. Neurological complications of dengue virus infection. *Lancet Neurol.* 2013;12(9):906-19.
356. Araújo F, Nogueira R, Araújo Mde S, Perdigão A, Cavalcanti L, Brilhante R, Rocha M, Vilar DF, Holanda SS, Braga Dde M, Sidrim J. Dengue in patients with central nervous system manifestations, Brazil. *Emerg Infect Dis.* 2012;18(4):677-9.
357. Vieira M, Costa CHN, Linhares ADC, Borba AS, Henriques DF, Silva E, Tavares FN, Batista FMA, Guimarães HCL, Martins LC, Monteiro TAF, Cruz ACR, Azevedo R, Vasconcelos P. Potential role of dengue virus, chikungunya virus and Zika virus in neurological diseases. *Mem Inst Oswaldo Cruz.* 2018;113(11):e170538.
358. Salomão N, Rabelo K, Basílio-de-Oliveira C, Basílio-de-Oliveira R, Geraldo L, Lima F, Dos Santos F, Nuovo G, Oliveira ERA, Paes M. Fatal Dengue Cases Reveal Brain Injury and Viral Replication in Brain-Resident Cells Associated with the Local Production of Pro-Inflammatory Mediators. *Viruses.* 2020;12(6).
359. Ramos C, Sanchez G, Pando RH, Baquera J, Hernandez D, Mota J, Ramos J, Flores A, Llausas E. Dengue virus in the brain of a fatal case of hemorrhagic dengue fever. *J Neurovirol.* 1998;4(4):465-8.
360. Norbury AJ, Calvert JK, Al-Shujairi WH, Cabezas-Falcon S, Tang V, Ong LC, Alonso SL, Smith JR, Carr JM. Dengue virus infects the mouse eye following systemic or intracranial infection and induces inflammatory responses. *J Gen Virol.* 2020;101(1):79-85.

361. Diamond MS, Harris E. Interferon inhibits dengue virus infection by preventing translation of viral RNA through a PKR-independent mechanism. *Virology*. 2001;289(2):297-311.
362. Diamond MS, Roberts TG, Edgil D, Lu B, Ernst J, Harris E. Modulation of Dengue virus infection in human cells by alpha, beta, and gamma interferons. *J Virol*. 2000;74(11):4957-66.
363. Talarico LB, Byrne AB, Amarilla S, Lovera D, Vázquez C, Chamorro G, Acosta PL, Ferretti A, Caballero MT, Arbo A, Polack FP. Characterization of type I interferon responses in dengue and severe dengue in children in Paraguay. *J Clin Virol*. 2017;97:10-7.
364. McNab F, Mayer-Barber K, Sher A, Wack A, O'Garra A. Type I interferons in infectious disease. *Nat Rev Immunol*. 2015;15(2):87-103.
365. Ivashkiv LB, Donlin LT. Regulation of type I interferon responses. *Nat Rev Immunol*. 2014;14(1):36-49.
366. Ng CT, Mendoza JL, Garcia KC, Oldstone MB. Alpha and Beta Type 1 Interferon Signaling: Passage for Diverse Biologic Outcomes. *Cell*. 2016;164(3):349-52.
367. Schneider WM, Chevillotte MD, Rice CM. Interferon-stimulated genes: a complex web of host defenses. *Annu Rev Immunol*. 2014;32:513-45.
368. Ashley CL, Abendroth A, McSharry BP, Slobedman B. Interferon-Independent Innate Responses to Cytomegalovirus. *Front Immunol*. 2019;10:2751.
369. Mlcochova P, Winstone H, Zuliani-Alvarez L, Gupta RK. TLR4-Mediated Pathway Triggers Interferon-Independent G0 Arrest and Antiviral SAMHD1 Activity in Macrophages. *Cell Rep*. 2020;30(12):3972-80.e5.
370. Lindqvist R, Kurhade C, Gilthorpe JD, Överby AK. Cell-type- and region-specific restriction of neurotropic flavivirus infection by viperin. *Journal of Neuroinflammation*. 2018;15(1):80.

371. Dzimianski JV, Scholte FEM, Bergeron E, Pegan SD. ISG15: It's Complicated. *J Mol Biol.* 2019;431(21):4203-16.
372. Freitas BT, Scholte FEM, Bergeron É, Pegan SD. How ISG15 combats viral infection. *Virus Res.* 2020:198036.
373. Helbig KJ, Beard MR. The role of viperin in the innate antiviral response. *J Mol Biol.* 2014;426(6):1210-9.
374. Stirnweiss A, Ksienzyk A, Klages K, Rand U, Grashoff M, Hauser H, Kröger A. IFN regulatory factor-1 bypasses IFN-mediated antiviral effects through viperin gene induction. *J Immunol.* 2010;184(9):5179-85.
375. Helbig KJ, Carr JM, Calvert JK, Wati S, Clarke JN, Eyre NS, Narayana SK, Fiches GN, McCartney EM, Beard MR. Viperin is induced following dengue virus type-2 (DENV-2) infection and has anti-viral actions requiring the C-terminal end of viperin. *PLoS Negl Trop Dis.* 2013;7(4):e2178.
376. Van der Hoek KH, Eyre NS, Shue B, Khantisitthiporn O, Glab-Ampi K, Carr JM, Gartner MJ, Jolly LA, Thomas PQ, Adikusuma F, Jankovic-Karasoulos T, Roberts CT, Helbig KJ, Beard MR. Viperin is an important host restriction factor in control of Zika virus infection. *Sci Rep.* 2017;7(1):4475.
377. Arias J, Valero N, Mosquera J, Montiel M, Reyes E, Larreal Y, Alvarez-Mon M. Increased expression of cytokines, soluble cytokine receptors, soluble apoptosis ligand and apoptosis in dengue. *Virology.* 2014;452-453:42-51.
378. Tuyen TT, Viet NT, Hang NT, Giang NT, Anh DD, Anh DT, Hung HV, Quyet D, Toan NL, Cam TD, Tong HV. Pro-Inflammatory Cytokines Are Modulated in Vietnamese Patients with Dengue Fever. *Viral Immunol.* 2020.
379. Ng AW, Teoh SC. Dengue eye disease. *Surv Ophthalmol.* 2015;60(2):106-14.
380. Lim WK, Mathur R, Koh A, Yeoh R, Chee SP. Ocular manifestations of dengue fever. *Ophthalmology.* 2004;111(11):2057-64.

381. Chang PE, Cheng CL, Asok K, Fong KY, Chee SP, Tan CK. Visual disturbances in dengue fever: an answer at last? *Singapore Med J.* 2007;48(3):e71-3.
382. Tan SY, Kumar G, Surrun SK, Ong YY. Dengue maculopathy: a case report. *Travel Med Infect Dis.* 2007;5(1):62-3.
383. Gupta S, Das D. Subhyaloid haemorrhage in dengue fever. *J Indian Med Assoc.* 2013;111(9):623-4.
384. Yamamoto K, Takahashi H, Kanno M, Noda Y, Fujino Y. Changes in parafoveal retinal thickness and subfoveal choroidal thickness in a patient with dengue fever-associated maculopathy. *J Ophthalmic Inflamm Infect.* 2013;3(1):63.
385. Ooi KG, Inglis H, Paramanathan N, Downie JA, Hennessy MP. Dengue Fever-Associated Maculopathy and Panuveitis in Australia. *Case Rep Ophthalmol Med.* 2016;2016:5704695.
386. Wang X, Wu M, Cao Y, Zhang Z, Guo F, Li X, Zhang Y. Exploring the role of programmed cell death protein 1 and its ligand 1 in eye diseases. *Crit Rev Clin Lab Sci.* 2019;56(1):18-32.
387. Schönrich G, Raftery MJ. The PD-1/PD-L1 Axis and Virus Infections: A Delicate Balance. *Front Cell Infect Microbiol.* 2019;9:207.
388. Jubel JM, Barbati ZR, Burger C, Wirtz DC, Schildberg FA. The Role of PD-1 in Acute and Chronic Infection. *Front Immunol.* 2020;11:487.
389. Nightingale ZD, Patkar C, Rothman AL. Viral replication and paracrine effects result in distinct, functional responses of dendritic cells following infection with dengue 2 virus. *J Leukoc Biol.* 2008;84(4):1028-38.
390. Lukowski SW, Lo CY, Sharov AA, Nguyen Q, Fang L, Hung SS, Zhu L, Zhang T, Grunert U, Nguyen T, Senabouth A, Jabbari JS, Welby E, Sowden JC, Waugh HS, Mackey A, Pollock G, Lamb TD, Wang PY, Hewitt AW, Gillies MC, Powell JE, Wong RC. A single-cell transcriptome atlas of the adult human retina. *Embo j.* 2019;38(18):e100811.

391. Yang W, Li H, Chen PW, Alizadeh H, He Y, Hogan RN, Niederkorn JY. PD-L1 expression on human ocular cells and its possible role in regulating immune-mediated ocular inflammation. *Invest Ophthalmol Vis Sci.* 2009;50(1):273-80.
392. Ler TS, Ang LW, Yap GS, Ng LC, Tai JC, James L, Goh KT. Epidemiological characteristics of the 2005 and 2007 dengue epidemics in Singapore - similarities and distinctions. *Western Pac Surveill Response J.* 2011;2(2):24-9.
393. Rajarethinam J, Ang LW, Ong J, Ycasas J, Hapuarachchi HC, Yap G, Chong CS, Lai YL, Cutter J, Ho D, Lee V, Ng LC. Dengue in Singapore from 2004 to 2016: Cyclical Epidemic Patterns Dominated by Serotypes 1 and 2. *Am J Trop Med Hyg.* 2018;99(1):204-10.
394. Vaughn DW, Green S, Kalayanarooj S, Innis BL, Nimmannitya S, Suntayakorn S, Endy TP, Raengsakulrach B, Rothman AL, Ennis FA, Nisalak A. Dengue viremia titer, antibody response pattern, and virus serotype correlate with disease severity. *J Infect Dis.* 2000;181(1):2-9.
395. Fried JR, Gibbons RV, Kalayanarooj S, Thomas SJ, Srikiatkachorn A, Yoon IK, Jarman RG, Green S, Rothman AL, Cummings DA. Serotype-specific differences in the risk of dengue hemorrhagic fever: an analysis of data collected in Bangkok, Thailand from 1994 to 2006. *PLoS Negl Trop Dis.* 2010;4(3):e617.
396. Roach T, Alcendor DJ. Zika virus infection of cellular components of the blood-retinal barriers: implications for viral associated congenital ocular disease. *Journal of Neuroinflammation.* 2017;14(1):43.
397. Jagadesh S, Sevalie S, Fatoma R, Sesay F, Sahr F, Faragher B, Semple MG, Fletcher TE, Weigel R, Scott JT. Disability Among Ebola Survivors and Their Close Contacts in Sierra Leone: A Retrospective Case-Controlled Cohort Study. *Clin Infect Dis.* 2018;66(1):131-3.
398. Deen GF, Broutet N, Xu W, Knust B, Sesay FR, McDonald SLR, Ervin E, Marrinan JE, Gaillard P, Habib N, Liu H, Liu W, Thorson AE, Yamba F, Massaquoi TA, James F, Ariyaratnam A, Ross C, Bernstein K, Coursier A, Klens J, Carino M, Wurie AH, Zhang Y, Dumbuya MS, Abad N, Idriss B, Wi T, Bennett SD, Davies T, Ebrahim FK, Meites

- E, Naidoo D, Smith SJ, Ongpin P, Malik T, Banerjee A, Erickson BR, Liu Y, Liu Y, Xu K, Brault A, Durski KN, Winter J, Sealy T, Nichol ST, Lamunu M, Bangura J, Landoulsi S, Jambai A, Morgan O, Wu G, Liang M, Su Q, Lan Y, Hao Y, Formenty P, Stroher U, Sahr F. Ebola RNA Persistence in Semen of Ebola Virus Disease Survivors - Final Report. *N Engl J Med.* 2017;377(15):1428-37.
399. Drury RE, O'Connor D, Pollard AJ. The Clinical Application of MicroRNAs in Infectious Disease. *Front Immunol.* 2017;8:1182.
400. Oliver GF, Orang AV, Appukuttan B, Marri S, Michael MZ, Marsh GA, Smith JR. Expression of microRNA in human retinal pigment epithelial cells following infection with Zaire ebolavirus. *BMC Res Notes.* 2019;12(1):639.
401. Swaroop S, Sengupta N, Suryawanshi AR, Adlakha YK, Basu A. HSP60 plays a regulatory role in IL-1beta-induced microglial inflammation via TLR4-p38 MAPK axis. *Journal of Neuroinflammation.* 2016;13:27.
402. Wei Z, Batagov AO, Carter DR, Krichevsky AM. Fetal Bovine Serum RNA Interferes with the Cell Culture derived Extracellular RNA. *Sci Rep.* 2016;6:31175.
403. Quillet A, Saad C, Ferry G, Anouar Y, Vergne N, Lecroq T, Dubessy C. Improving Bioinformatics Prediction of microRNA Targets by Ranks Aggregation. *Front Genet.* 2019;10:1330.
404. Witwer KW, Halushka MK. Toward the promise of microRNAs - Enhancing reproducibility and rigor in microRNA research. *RNA Biol.* 2016;13(11):1103-16.
405. The Gene Ontology Consortium. The Gene Ontology Resource: 20 years and still GOing strong. *Nucleic Acids Res.* 2019;47(D1):D330-D8.
406. Bernier A, Sagan SM. The Diverse Roles of microRNAs at the Host(-)Virus Interface. *Viruses.* 2018;10(8).
407. Cramer EM, Shao Y, Wang Y, Yuan Y. miR-190 is upregulated in Epstein-Barr Virus type I latency and modulates cellular mRNAs involved in cell survival and viral reactivation. *Virology.* 2014;464-465:184-95.

408. Cokaric Brdovcak M, Zubkovic A, Jurak I. Herpes Simplex Virus 1 Deregulation of Host MicroRNAs. *Noncoding RNA*. 2018;4(4).
409. Liston A, Papadopoulou AS, Danso-Abeam D, Dooley J. MicroRNA-29 in the adaptive immune system: setting the threshold. *Cell Mol Life Sci*. 2012;69(21):3533-41.
410. Cinatl J, Jr., Margraf S, Vogel JU, Scholz M, Cinatl J, Doerr HW. Human cytomegalovirus circumvents NF-kappa B dependence in retinal pigment epithelial cells. *J Immunol*. 2001;167(4):1900-8.
411. Baluni M, Ghildiyal S, Singh D, Himanshu Reddy D, Kumar R, Dhole TN. Increased serum microRNA-29b expression and bad recovery in Japanese encephalitis virus infected patients; A new component to improve the disease recovery. *J Neuroimmunol*. 2018;323:56-61.
412. Price A, Manzoni C, Cookson MR, Lewis PA. The LRRK2 signalling system. *Cell Tissue Res*. 2018;373(1):39-50.
413. Madureira M, Connor-Robson N, Wade-Martins R. "LRRK2: Autophagy and Lysosomal Activity". *Front Neurosci*. 2020;14:498.
414. Puccini JM, Marker DF, Fitzgerald T, Barbieri J, Kim CS, Miller-Rhodes P, Lu SM, Dewhurst S, Gelbard HA. Leucine-rich repeat kinase 2 modulates neuroinflammation and neurotoxicity in models of human immunodeficiency virus 1-associated neurocognitive disorders. *J Neurosci*. 2015;35(13):5271-83.
415. Wallings RL, Tansey MG. LRRK2 regulation of immune-pathways and inflammatory disease. *Biochem Soc Trans*. 2019;47(6):1581-95.
416. Wandu WS, Tan C, Ogbeifun O, Vistica BP, Shi G, Hinshaw SJ, Xie C, Chen X, Klinman DM, Cai H, Gery I. Leucine-Rich Repeat Kinase 2 (*Lrrk2*) Deficiency Diminishes the Development of Experimental Autoimmune Uveitis (EAU) and the Adaptive Immune Response. *PLoS One*. 2015;10(6):e0128906.

417. Giaime E, Tong Y, Wagner LK, Yuan Y, Huang G, Shen J. Age-Dependent Dopaminergic Neurodegeneration and Impairment of the Autophagy-Lysosomal Pathway in LRRK-Deficient Mice. *Neuron*. 2017;96(4):796-807 e6.
418. Henry AG, Aghamohammadzadeh S, Samaroo H, Chen Y, Mou K, Needle E, Hirst WD. Pathogenic LRRK2 mutations, through increased kinase activity, produce enlarged lysosomes with reduced degradative capacity and increase ATP13A2 expression. *Hum Mol Genet*. 2015;24(21):6013-28.
419. Grimm C, Butz E, Chen CC, Wahl-Schott C, Biel M. From mucopolidosis type IV to Ebola: TRPML and two-pore channels at the crossroads of endo-lysosomal trafficking and disease. *Cell Calcium*. 2017;67:148-55.
420. Ren G, Sun J, Li MM, Zhang YD, Li RH, Li YM. MicroRNA-23a-5p regulates osteogenic differentiation of human bone marrow-derived mesenchymal stem cells by targeting mitogen-activated protein kinase-13. *Mol Med Rep*. 2018;17(3):4554-60.
421. Yasuda K, Hirohashi Y, Kuroda T, Takaya A, Kubo T, Kanaseki T, Tsukahara T, Hasegawa T, Saito T, Sato N, Torigoe T. MAPK13 is preferentially expressed in gynecological cancer stem cells and has a role in the tumor-initiation. *Biochem Biophys Res Commun*. 2016;472(4):643-7.
422. Fenini G, Grossi S, Gehrke S, Beer HD, Satoh TK, Contassot E, French LE. The p38 Mitogen-Activated Protein Kinase Critically Regulates Human Keratinocyte Inflammasome Activation. *J Invest Dermatol*. 2018;138(6):1380-90.
423. Zhao W, Wang D, Zhao J, Zhao W. Bioinformatic analysis of retinal gene function and expression in diabetic rats. *Exp Ther Med*. 2017;14(3):2485-92.
424. Wilhelmsen K, Xu F, Farrar K, Tran A, Khakpour S, Sundar S, Prakash A, Wang J, Gray NS, Hellman J. Extracellular signal-regulated kinase 5 promotes acute cellular and systemic inflammation. *Sci Signal*. 2015;8(391):ra86.
425. Lochhead PA, Tucker JA, Tatum NJ, Wang J, Oxley D, Kidger AM, Johnson VP, Cassidy MA, Gray NS, Noble MEM, Cook SJ. Paradoxical activation of the protein

- kinase-transcription factor ERK5 by ERK5 kinase inhibitors. *Nat Commun.* 2020;11(1):1383.
426. Wright C, Rajpurohit A, Burke EE, Williams C, Collado-Torres L, Kimos M, Brandon NJ, Cross AJ, Jaffe AE, Weinberger DR, Shin JH. Comprehensive assessment of multiple biases in small RNA sequencing reveals significant differences in the performance of widely used methods. *BMC Genomics.* 2019;20(1):513.
427. Zomer A, Vendrig T, Hopmans ES, van Eijndhoven M, Middeldorp JM, Pegtel DM. Exosomes: Fit to deliver small RNA. *Commun Integr Biol.* 2010;3(5):447-50.
428. Pleet ML, DeMarino C, Lepene B, Aman MJ, Kashanchi F. The Role of Exosomal VP40 in Ebola Virus Disease. *DNA Cell Biol.* 2017;36(4):243-8.
429. Pleet ML, DeMarino C, Stonier SW, Dye JM, Jacobson S, Aman MJ, Kashanchi F. Extracellular Vesicles and Ebola Virus: A New Mechanism of Immune Evasion. *Viruses.* 2019;11(5).
430. Klingeborn M, Stamer WD, Bowes Rickman C. Polarized Exosome Release from the Retinal Pigmented Epithelium. *Adv Exp Med Biol.* 2018;1074:539-44.
431. Klingeborn M, Dismuke WM, Bowes Rickman C, Stamer WD. Roles of exosomes in the normal and diseased eye. *Prog Retin Eye Res.* 2017;59:158-77.
432. van der Merwe Y, Steketee MB. Extracellular Vesicles: Biomarkers, Therapeutics, and Vehicles in the Visual System. *Curr Ophthalmol Rep.* 2017;5(4):276-82.
433. Wecker T, Hoffmeier K, Plotner A, Gruning BA, Horres R, Backofen R, Reinhard T, Schlunck G. MicroRNA Profiling in Aqueous Humor of Individual Human Eyes by Next-Generation Sequencing. *Invest Ophthalmol Vis Sci.* 2016;57(4):1706-13.
434. Aguado LC, tenOever B. RNA virus building blocks-miRNAs not included. *PLoS Pathog.* 2018;14(5):e1006963.
435. Teng Y, Wang Y, Zhang X, Liu W, Fan H, Yao H, Lin B, Zhu P, Yuan W, Tong Y, Cao W. Systematic Genome-wide Screening and Prediction of microRNAs in EBOV During the 2014 Ebolavirus Outbreak. *Sci Rep.* 2015;5:9912.

436. Liu Y, Sun J, Zhang H, Wang M, Gao GF, Li X. Ebola virus encodes a miR-155 analog to regulate importin- α 5 expression. *Cell Mol Life Sci.* 2016;73(19):3733-44.
437. Aloia AL, Abraham AM, Bonder CS, Pitson SM, Carr JM. Dengue Virus-Induced Inflammation of the Endothelium and the Potential Roles of Sphingosine Kinase-1 and MicroRNAs. *Mediators Inflamm.* 2015;2015:509306.
438. Dahlke C, Maul K, Christalla T, Walz N, Schult P, Stocking C, Grundhoff A. A microRNA encoded by Kaposi sarcoma-associated herpesvirus promotes B-cell expansion in vivo. *PLoS One.* 2012;7(11):e49435.
439. Liang H, Zhou Z, Zhang S, Zen K, Chen X, Zhang C. Identification of Ebola virus microRNAs and their putative pathological function. *Sci China Life Sci.* 2014;57(10):973-81.
440. Hsu PC, Chiou BH, Huang CM. On revealing the gene targets of Ebola virus microRNAs involved in the human skin microbiome. *PeerJ.* 2018;6:e4138.
441. Prasad AN, Ronk AJ, Widen SG, Wood TG, Basler CF, Bukreyev A. Ebola Virus Produces Discrete Small Noncoding RNAs Independently of the Host MicroRNA Pathway Which Lack RNA Interference Activity in Bat and Human Cells. *J Virol.* 2020;94(6).
442. Liang Y, Ridzon D, Wong L, Chen C. Characterization of microRNA expression profiles in normal human tissues. *BMC Genomics.* 2007;8:166.
443. Xu S. microRNA expression in the eyes and their significance in relation to functions. *Prog Retin Eye Res.* 2009;28(2):87-116.
444. Woolsey C, Menicucci AR, Cross RW, Luthra P, Agans KN, Borisevich V, Geisbert JB, Mire CE, Fenton KA, Jankeel A, Anand S, Ebihara H, Geisbert TW, Messaoudi I, Basler CF. A VP35 Mutant Ebola Virus Lacks Virulence but Can Elicit Protective Immunity to Wild-Type Virus Challenge. *Cell Rep.* 2019;28(12):3032-46 e6.
445. Basler CF, Wang X, Mühlberger E, Volchkov V, Paragas J, Klenk H-D, García-Sastre A, Palese P. The Ebola virus VP35 protein functions as a type I IFN antagonist. *Proceedings of the National Academy of Sciences.* 2000;97(22):12289-94.

446. Basler CF, Mikulasova A, Martinez-Sobrido L, Paragas J, Muhlberger E, Bray M, Klenk HD, Palese P, Garcia-Sastre A. The Ebola virus VP35 protein inhibits activation of interferon regulatory factor 3. *J Virol.* 2003;77(14):7945-56.
447. Cardenas WB, Loo YM, Gale M, Jr., Hartman AL, Kimberlin CR, Martinez-Sobrido L, Saphire EO, Basler CF. Ebola virus VP35 protein binds double-stranded RNA and inhibits alpha/beta interferon production induced by RIG-I signaling. *J Virol.* 2006;80(11):5168-78.
448. Feng Z, Cerveny M, Yan Z, He B. The VP35 protein of Ebola virus inhibits the antiviral effect mediated by double-stranded RNA-dependent protein kinase PKR. *J Virol.* 2007;81(1):182-92.
449. Haasnoot J, de Vries W, Geutjes EJ, Prins M, de Haan P, Berkhout B. The Ebola virus VP35 protein is a suppressor of RNA silencing. *PLoS Pathog.* 2007;3(6):e86.
450. Luthra P, Ramanan P, Mire CE, Weisend C, Tsuda Y, Yen B, Liu G, Leung DW, Geisbert TW, Ebihara H, Amarasinghe GK, Basler CF. Mutual antagonism between the Ebola virus VP35 protein and the RIG-I activator PACT determines infection outcome. *Cell Host Microbe.* 2013;14(1):74-84.
451. Zhu L, Gao T, Yang W, Liu Y, Liu X, Hu Y, Jin Y, Li P, Xu K, Zou G, Zhao L, Cao R, Zhong W, Xia X, Cao C. Ebola virus replication is regulated by the phosphorylation of viral protein VP35. *Biochem Biophys Res Commun.* 2020;521(3):687-92.
452. Prins KC, Delpeut S, Leung DW, Reynard O, Volchkova VA, Reid SP, Ramanan P, Cardenas WB, Amarasinghe GK, Volchkov VE, Basler CF. Mutations abrogating VP35 interaction with double-stranded RNA render Ebola virus avirulent in guinea pigs. *J Virol.* 2010;84(6):3004-15.
453. Leung DW, Prins KC, Borek DM, Farahbakhsh M, Tufariello JM, Ramanan P, Nix JC, Helgeson LA, Otwinowski Z, Honzatko RB, Basler CF, Amarasinghe GK. Structural basis for dsRNA recognition and interferon antagonism by Ebola VP35. *Nat Struct Mol Biol.* 2010;17(2):165-72.

454. Dilley KA, Voorhies AA, Luthra P, Puri V, Stockwell TB, Lorenzi H, Basler CF, Shabman RS. The Ebola virus VP35 protein binds viral immunostimulatory and host RNAs identified through deep sequencing. *PLoS One*. 2017;12(6):e0178717.
455. Prins KC, Cardenas WB, Basler CF. Ebola virus protein VP35 impairs the function of interferon regulatory factor-activating kinases IKKepsilon and TBK-1. *J Virol*. 2009;83(7):3069-77.
456. Reid SP, Leung LW, Hartman AL, Martinez O, Shaw ML, Carbonnelle C, Volchkov VE, Nichol ST, Basler CF. Ebola virus VP24 binds karyopherin alpha1 and blocks STAT1 nuclear accumulation. *J Virol*. 2006;80(11):5156-67.
457. Xu W, Edwards MR, Borek DM, Feagins AR, Mittal A, Alinger JB, Berry KN, Yen B, Hamilton J, Brett TJ, Pappu RV, Leung DW, Basler CF, Amarasinghe GK. Ebola virus VP24 targets a unique NLS binding site on karyopherin alpha 5 to selectively compete with nuclear import of phosphorylated STAT1. *Cell Host Microbe*. 2014;16(2):187-200.
458. Yen B, Mulder LC, Martinez O, Basler CF. Molecular basis for ebolavirus VP35 suppression of human dendritic cell maturation. *J Virol*. 2014;88(21):12500-10.
459. Zinzula L, Nagy I, Orsini M, Weyher-Stingl E, Bracher A, Baumeister W. Structures of Ebola and Reston Virus VP35 Oligomerization Domains and Comparative Biophysical Characterization in All Ebolavirus Species. *Structure*. 2019;27(1):39-54 e6.
460. Alexopoulou L, Holt AC, Medzhitov R, Flavell RA. Recognition of double-stranded RNA and activation of NF-kappaB by Toll-like receptor 3. *Nature*. 2001;413(6857):732-8.
461. Matsumoto M, Seya T. TLR3: interferon induction by double-stranded RNA including poly(I:C). *Adv Drug Deliv Rev*. 2008;60(7):805-12.
462. Kuzmin IV, Schwarz TM, Ilinykh PA, Jordan I, Ksiazek TG, Sachidanandam R, Basler CF, Bukreyev A. Innate Immune Responses of Bat and Human Cells to Filoviruses: Commonalities and Distinctions. *J Virol*. 2017;91(8).

463. Cinatl J, Jr., Michaelis M, Fleckenstein C, Bauer G, Kabickova H, Scholz M, Rabenau HF, Doerr HW. West Nile virus infection induces interferon signalling in human retinal pigment epithelial cells. *Invest Ophthalmol Vis Sci.* 2006;47(2):645-51.
464. Henry CR, Al-Attar L, Cruz-Chacon AM, Davis JL. Chorioretinal Lesions Presumed Secondary to Zika Virus Infection in an Immunocompromised Adult. *JAMA Ophthalmol.* 2017;135(4):386-9.
465. Salinas S, Erkilic N, Damodar K, Moles JP, Fournier-Wirth C, Van de Perre P, Kalatzis V, Simonin Y. Zika Virus Efficiently Replicates in Human Retinal Epithelium and Disturbs Its Permeability. *J Virol.* 2017;91(3).
466. Singh PK, Guest JM, Kanwar M, Boss J, Gao N, Juzych MS, Abrams GW, Yu FS, Kumar A. Zika virus infects cells lining the blood-retinal barrier and causes chorioretinal atrophy in mouse eyes. *JCI Insight.* 2017;2(4):e92340.
467. Schwid SR, Panitch HS. Full results of the Evidence of Interferon Dose-Response-European North American Comparative Efficacy (EVIDENCE) study: a multicenter, randomized, assessor-blinded comparison of low-dose weekly versus high-dose, high-frequency interferon beta-1a for relapsing multiple sclerosis. *Clin Ther.* 2007;29(9):2031-48.
468. Hooks JJ, Nagineni CN, Hooper LC, Hayashi K, Detrick B. IFN-beta provides immuno-protection in the retina by inhibiting ICAM-1 and CXCL9 in retinal pigment epithelial cells. *J Immunol.* 2008;180(6):3789-96.
469. McElroy AK, Akondy RS, Davis CW, Ellebedy AH, Mehta AK, Kraft CS, Lyon GM, Ribner BS, Varkey J, Sidney J, Sette A, Campbell S, Stroher U, Damon I, Nichol ST, Spiropoulou CF, Ahmed R. Human Ebola virus infection results in substantial immune activation. *Proc Natl Acad Sci U S A.* 2015;112(15):4719-24.
470. Cardarelli F, Digiacoimo L, Marchini C, Amici A, Salomone F, Fiume G, Rossetta A, Gratton E, Pozzi D, Caracciolo G. The intracellular trafficking mechanism of Lipofectamine-based transfection reagents and its implication for gene delivery. *Sci Rep.* 2016;6:25879.

471. Brock DJ, Kondow-McConaghy HM, Hager EC, Pellois JP. Endosomal Escape and Cytosolic Penetration of Macromolecules Mediated by Synthetic Delivery Agents. *Bioconjug Chem.* 2019;30(2):293-304.
472. Li Z, Zhang C, Wang Z, Shen J, Xiang P, Chen X, Nan J, Lin Y. Lipofectamine 2000/siRNA complexes cause endoplasmic reticulum unfolded protein response in human endothelial cells. *J Cell Physiol.* 2019;234(11):21166-81.
473. Guo X, Wang H, Li Y, Leng X, Huang W, Ma Y, Xu T, Qi X. Transfection reagent Lipofectamine triggers type I interferon signaling activation in macrophages. *Immunol Cell Biol.* 2019;97(1):92-6.
474. Bai H, Lester GMS, Petishnok LC, Dean DA. Cytoplasmic transport and nuclear import of plasmid DNA. *Biosci Rep.* 2017;37(6).
475. Upadhyaya A, Sangave PC. Hydrophobic and electrostatic interactions between cell penetrating peptides and plasmid DNA are important for stable non-covalent complexation and intracellular delivery. *J Pept Sci.* 2016;22(10):647-59.
476. Dalby B, Cates S, Harris A, Ohki EC, Tilkins ML, Price PJ, Ciccarone VC. Advanced transfection with Lipofectamine 2000 reagent: primary neurons, siRNA, and high-throughput applications. *Methods.* 2004;33(2):95-103.
477. Horstick O, Tozan Y, Wilder-Smith A. Reviewing dengue: still a neglected tropical disease? *PLoS Negl Trop Dis.* 2015;9(4):e0003632.
478. Prescott J, Bushmaker T, Fischer R, Miazgowicz K, Judson S, Munster VJ. Postmortem stability of Ebola virus. *Emerg Infect Dis.* 2015;21(5):856-9.
479. Bird AC, Bok D. Why the macula? *Eye (Lond).* 2018;32(5):858-62.
480. Tian L, Kazmierkiewicz KL, Bowman AS, Li M, Curcio CA, Stambolian DE. Transcriptome of the human retina, retinal pigmented epithelium and choroid. *Genomics.* 2015;105(5-6):253-64.
481. Voigt AP, Mulfaul K, Mullin NK, Flamme-Wiese MJ, Giacalone JC, Stone EM, Tucker BA, Scheetz TE, Mullins RF. Single-cell transcriptomics of the human retinal

- pigment epithelium and choroid in health and macular degeneration. *Proc Natl Acad Sci U S A*. 2019;116(48):24100-7.
482. Liang Q, Dharmat R, Owen L, Shakoor A, Li Y, Kim S, Vitale A, Kim I, Morgan D, Liang S, Wu N, Chen K, DeAngelis MM, Chen R. Single-nuclei RNA-seq on human retinal tissue provides improved transcriptome profiling. *Nat Commun*. 2019;10(1):5743.
483. Strimbu K, Tavel JA. What are biomarkers? *Curr Opin HIV AIDS*. 2010;5(6):463-6.
484. Bravo-Merodio L, Williams JA, Gkoutos GV, Acharjee A. -Omics biomarker identification pipeline for translational medicine. *J Transl Med*. 2019;17(1):155.
485. Lambert NG, ElShelmani H, Singh MK, Mansergh FC, Wride MA, Padilla M, Keegan D, Hogg RE, Ambati BK. Risk factors and biomarkers of age-related macular degeneration. *Prog Retin Eye Res*. 2016;54:64-102.
486. Kaur G, Dufour JM. Cell lines: Valuable tools or useless artifacts. *Spermatogenesis*. 2012;2(1):1-5.
487. Lee SK. Sex as an important biological variable in biomedical research. *BMB Rep*. 2018;51(4):167-73.
488. Huang Y, Liu Y, Zheng C, Shen C. Investigation of Cross-Contamination and Misidentification of 278 Widely Used Tumor Cell Lines. *PLoS One*. 2017;12(1):e0170384.
489. Ben-David U, Siranosian B, Ha G, Tang H, Oren Y, Hinohara K, Strathdee CA, Dempster J, Lyons NJ, Burns R, Nag A, Kugener G, Cimini B, Tsvetkov P, Maruvka YE, O'Rourke R, Garrity A, Tubelli AA, Bandopadhyay P, Tsherniak A, Vazquez F, Wong B, Birger C, Ghandi M, Thorner AR, Bittker JA, Meyerson M, Getz G, Beroukhim R, Golub TR. Genetic and transcriptional evolution alters cancer cell line drug response. *Nature*. 2018;560(7718):325-30.
490. Samuel W, Jaworski C, Postnikova OA, Kutty RK, Duncan T, Tan LX, Poliakov E, Lakkaraju A, Redmond TM. Appropriately differentiated ARPE-19 cells regain phenotype and gene expression profiles similar to those of native RPE cells. *Mol Vis*. 2017;23:60-89.

491. De Souza Santos R, Frank AP, Palmer BF, Clegg DJ. Sex and media: Considerations for cell culture studies. *Altex*. 2018;35(4):435-40.
492. Lorenz M, Koschate J, Kaufmann K, Kreye C, Mertens M, Kuebler WM, Baumann G, Gossing G, Marki A, Zakrzewicz A, Miéville C, Benn A, Horbelt D, Wratil PR, Stangl K, Stangl V. Does cellular sex matter? Dimorphic transcriptional differences between female and male endothelial cells. *Atherosclerosis*. 2015;240(1):61-72.
493. Shah K, McCormack CE, Bradbury NA. Do you know the sex of your cells? *Am J Physiol Cell Physiol*. 2014;306(1):C3-18.
494. Penaloza C, Estevez B, Orlanski S, Sikorska M, Walker R, Smith C, Smith B, Lockshin RA, Zakeri Z. Sex of the cell dictates its response: differential gene expression and sensitivity to cell death inducing stress in male and female cells. *Faseb j*. 2009;23(6):1869-79.
495. Du L, Bayir H, Lai Y, Zhang X, Kochanek PM, Watkins SC, Graham SH, Clark RS. Innate gender-based proclivity in response to cytotoxicity and programmed cell death pathway. *J Biol Chem*. 2004;279(37):38563-70.
496. Fresta CG, Fidilio A, Caruso G, Caraci F, Giblin FJ, Leggio GM, Salomone S, Drago F, Bucolo C. A New Human Blood-Retinal Barrier Model Based on Endothelial Cells, Pericytes, and Astrocytes. *Int J Mol Sci*. 2020;21(5).
497. Lidgerwood GE, Hewitt AW, Pébay A. Human pluripotent stem cells for the modelling of diseases of the retina and optic nerve: toward a retina in a dish. *Curr Opin Pharmacol*. 2019;48:114-9.
498. Abreu CM, Gama L, Krasemann S, Chesnut M, Odwin-Dacosta S, Hogberg HT, Hartung T, Pamies D. Microglia Increase Inflammatory Responses in iPSC-Derived Human BrainSpheres. *Front Microbiol*. 2018;9:2766.
499. Swearingen JR. Choosing the right animal model for infectious disease research. *Animal Model Exp Med*. 2018;1(2):100-8.
500. Colby LA, Quenee LE, Zitzow LA. Considerations for Infectious Disease Research Studies Using Animals. *Comp Med*. 2017;67(3):222-31.

501. Bente DA, Rico-Hesse R. Models of dengue virus infection. *Drug Discov Today Dis Models.* 2006;3(1):97-103.
502. Chan KW, Watanabe S, Kavishna R, Alonso S, Vasudevan SG. Animal models for studying dengue pathogenesis and therapy. *Antiviral Res.* 2015;123:5-14.
503. Coronel-Ruiz C, Gutierrez-Barbosa H, Medina-Moreno S, Velandia-Romero ML, Chua JV, Castellanos JE, Zapata JC. Humanized Mice in Dengue Research: A Comparison with Other Mouse Models. *Vaccines (Basel).* 2020;8(1).
504. St Claire MC, Ragland DR, Bollinger L, Jahrling PB. Animal Models of Ebolavirus Infection. *Comp Med.* 2017;67(3):253-62.
505. Spengler JR, Prescott J, Feldmann H, Spiropoulou CF. Human immune system mouse models of Ebola virus infection. *Curr Opin Virol.* 2017;25:90-6.
506. Picaud S, Dalkara D, Marazova K, Goureau O, Roska B, Sahel JA. The primate model for understanding and restoring vision. *Proc Natl Acad Sci U S A.* 2019;116(52):26280-7.
507. Grunert U, Martin PR. Cell types and cell circuits in human and non-human primate retina. *Prog Retin Eye Res.* 2020:100844.
508. Chesnut M, Muñoz LS, Harris G, Freeman D, Gama L, Pardo CA, Pamies D. In vitro and in silico Models to Study Mosquito-Borne Flavivirus Neuropathogenesis, Prevention, and Treatment. *Front Cell Infect Microbiol.* 2019;9:223.
509. National Center for Biotechnology Information NLoMU. Genetic Sequence Data Bank (GenBank) Bethesda (MD): National Library of Medicine (US), National Center for Biotechnology Information; [Release 238.0:[Available from: <https://www.ncbi.nlm.nih.gov/genbank/>].
510. Sayers EW, Beck J, Brister JR, Bolton EE, Canese K, Comeau DC, Funk K, Ketter A, Kim S, Kimchi A, Kitts PA, Kuznetsov A, Lathrop S, Lu Z, McGarvey K, Madden TL, Murphy TD, O'Leary N, Phan L, Schneider VA, Thibaud-Nissen F, Trawick BW, Pruitt KD, Ostell J. Database resources of the National Center for Biotechnology Information. *Nucleic Acids Res.* 2020;48(D1):D9-d16.